DOT/FAA/TC-23/50

Federal Aviation Administration
William J. Hughes Technical Center
Aviation Research Division
Atlantic City International Airport
New Jersey 08405

Small Unmanned Aircraft System for Pavement Inspection

August 2023

Final Report

U.S. Department of Transportation
Federal Aviation Administration

NOTICE

Technical Report Documentation Page

1. Report No.	2. Government Accession No.	3. Recipient's Catalog No.
DOT/FAA/TC-23/50		

4. Title and Subtitle	5. Report Date
SMALL UNMANNED AIRCRAFT SYSTEM FOR PAVEMENT INSPECTION	August 2023
	6. Performing Organization Code

7. Author(s)	8. Performing Organization Report No.
Dr. Md Abdullah All Sourav, Dr. Halil Ceylan, Dr. Colin Brooks, David Peshkin, Dr. Sunghwan Kim, Rick Dobson, Chris Cook, Dr. Masrur Mahedi, and Abby Jenkins	

9. Performing Organization Name and Address	10. Work Unit No. (TRAIS)
Department of Civil, Construction and Environmental Engineering (CCEE) Iowa State University Ames, IA 50011	11. Contract or Grant No.

12. Sponsoring Agency Name and Address	13. Type of Report and Period Covered
U.S. Department of Transportation Federal Aviation Administration Airport Engineering Division 800 Independence Ave., SW Washington, DC 20591	Final Report
	14. Sponsoring Agency Code AAS-110

15. Supplementary Notes

The Federal Aviation Administration Aviation Research Division CORs were Mr. Mike DiPilato and Mr. Matthew Brynick.

16. Abstract

Airport pavements require routine maintenance, upgrading, and rehabilitation to reach or exceed their design period. While pavement distresses caused by environmental conditions cannot be prevented, early and routine maintenance work can minimize the deterioration. The current practice for airport pavement inspections relies on time-consuming visual surveys and manual interpretation of reports and sketches prepared by inspectors in the field.

Recently, the use of small Unmanned Aircraft Systems (sUAS) has attracted attention as an option for performing cost-effective and efficient pavement inspections. In this study, the research team deployed several sUAS at different altitudes at six airports in Michigan, Illinois, Iowa, and New Jersey from December 2020 to November 2021. Red, green, and blue (RGB) optical orthophotos, Digital Elevation Models (DEMs), hillshades from DEMs, and thermal orthophotos collected using several sUAS at different altitudes were analyzed for their usefulness in airfield distress detection. The results showed that RGB optical data could detect as many as 13 Portland cement concrete (PCC) pavement distresses out of 14 available in this study and 6 out of 9 asphalt concrete (AC) pavement distresses available on the airports. Similarly, DEMs were found to be useful for confirming the location of distresses with elevation change, such as faulting in PCC pavement and shoving in AC pavement. In addition, thermal orthophotos showed potential to detect crack-based distresses. Based on the data analysis, RGB orthophoto resolution of 1.5 millimeters per pixel (mm/pix), DEM resolution of 6 mm/pix, and thermal orthophoto resolution of 30 mm/pix or higher were recommended for airfield pavement distress detection and rating.

This research also concluded that sUAS-based PCI inspection not only detects and rates a number of airfield pavement distresses, but also provides PCI values close to the foot-on-ground traditional PCI inspection value. Recommendations on sUAS data collection plan development, safe and efficient data collection, data processing, data analysis, and the process of incorporating sUAS-based PCI inspection to complement traditional PCI inspections are discussed in detail.

17. Key Words	18. Distribution Statement
Small Unmanned Aircraft Systems, Uncrewed, Drones, Airport Pavements, Pavement Management Program, Cracks, Pavement Condition Index	This document is available to the U.S. public through the National Technical Information Service (NTIS), Springfield, Virginia 22161. This document is also available from the Federal Aviation Administration William J. Hughes Technical Center at actlibrary.tc.faa.gov.

19. Security Classif. (of this report)	20. Security Classif. (of this page)	21. No. of Pages	22. Price
Unclassified	Unclassified	252	

ACKNOWLEDGEMENTS

The authors gratefully acknowledge the Federal Aviation Administration for supporting this study. The authors would like to thank the project technical points of contact, Mike DiPilato and Matthew Brynick, for their invaluable guidance, support, and direction during this study. Special thanks are expressed to Grosse Ile Municipal Airport managers, Michael Duker and Janel Macnee; Custer Airport manager, Dan Diesing; Coles County Memorial Airport manager, Andrew Fearn; Boone Municipal Airport manager, Dale Farnham; Perry Municipal Airport manager, Jonathan Walter; and Cape May Airport manager, Thomas Berry for their full support during data collection. The authors would like to express their sincere gratitude to Yongsung Koh, Robin Valle, Md Jibon, Ankita Mandelia, Vanessa Barber, Ben Hart, Julie Carter, Abby Jenkins, Kyle Potvin, Peter-Paul Dzwilewski, Trent Montgomery, Katie Gauthier, and other team members from Iowa State University, Michigan Tech Research Institute, and Applied Pavement Technology, Inc., who assisted with data collection and organization. We also would like to express our gratitude to Adam Shover and William H. Smith from General Dynamics Information Technology, Inc., for their kind assistance for efficient sUAS data collection.

TABLE OF CONTENTS

APPENDICES

LIST OF FIGURES

LIST OF TABLES

LIST OF ACRONYMS

3D	Three-dimensional
1H2	Effingham County Memorial Airport
AAC	Asphalt overlay over asphalt concrete
AC	Asphalt concrete
AIP	Airport Improvement Program
APTech	Applied Pavement Technology, Inc.
ARB	Ann Arbor Municipal Airport
ASR	Alkali-silica reaction
ASTM	American Society for Testing and Materials
ATC	Air traffic control
AWM	Ames Municipal Airport
BNW	Boone Municipal Airport
°C	degrees Celcius
CMI	University of Illinois Willard Airport
DEM	Digital Elevation Model
DJI	Da-Jiang Innovations
DNV	Vermilion Regional Airport
DOT	Department of Transportation
FAA	Federal Aviation Administration
FBO	Fixed-base operator
FLIR	Forward-looking infrared
FOG	Foot-on-ground
FOV	Field of view
GCP	Ground control point
GIS	Geographic Information System
GNSS	Global Navigation Satellite System
GPS	Global Positioning System
GRVD	Grooved
IKV	Ankeny Regional Airport
JYM	Hillsdale Municipal Airport
km	kilometers
km/h	kilometers per hour
L&T	Longitudinal and transverse
LiDAR	Light detection and ranging
LTD	Longitudinal, transverse, and diagonal
m	Meter
M2EA	Mavic 2 Enterprise Advanced
MDOT	Michigan Department of Transportation
MIW	Marshalltown Municipal Airport
mm	Millimeter
mm/pix	Millimeter per pixel
MnDOT	Minnesota Department of Transportation
mp	Megapixel
MTO	Coles County Memorial Airport
MTRI	Michigan Tech Research Institute

nm	nanometers
NOTAM	Notice to Air Mission
OEB	Branch County Memorial
ONZ	Grosse Ile Municipal Airport
PCC	Portland cement concrete
PCI	Pavement Condition Index
PFC	Porous friction course
PMP	Pavement Management Program
PPK	Post-processed kinematic
PRO	Perry Municipal Airport
RGB	Red, green, and blue
RTK	Real-time kinematic
RW	Runway
SfM	Structure from Motion
SU	Sample unit
sUAS	Small unmanned/uncrewed aircraft system
TTF	Custer Airport
UAV	Unmanned aircraft vehicle
UAVSI	UAV Systems International
UNCON	Uncontrolled airport (No tower)
UNGRVD	Ungrooved
VTOL	Vertical takeoff and landing
WWD	Cape May Airport

EXECUTIVE SUMMARY

Airport pavements require routine maintenance, upgrading, and rehabilitation to reach or exceed their design period. While pavement distresses caused by environmental conditions cannot be prevented, early and routine maintenance work can minimize the deterioration. To determine the need for timely interventions, the current practice for airport pavement inspections relies on visual surveys and manual interpretation of reports and sketches prepared by inspectors in the field to quantify pavement conditions using the Pavement Condition Index (PCI) method as outlined in American Society for Testing and Materials (ASTM) document, ASTM D5340-20. The procedure is time-consuming and costly, and the assessment of a pavement branch (i.e., apron, taxiway, and runway) is completed by selecting and inspecting sample units within a pavement section, which has the potential to miss distresses of concern.

Recently, the use of small Unmanned (alternatively referred to as Uncrewed) Aircraft Systems (sUAS) has attracted attention as an option for performing cost-effective and efficient pavement inspections, among many other applications which are mostly proof-of-concept demonstrations involving various types of sUAS platforms, sensors, and procedures under previous and newer sUAS regulations. In this study, the research team deployed several sUAS at different altitudes at six airports in Michigan, Illinois, Iowa, and New Jersey from December 2020 to November 2021. Red, green, and blue (RGB) (natural color) optical orthophotos, Digital Elevation Models (DEMs), hillshades from DEMs, and thermal orthophotos collected using several sUAS at different altitudes were analyzed for their usefulness in airfield distress detection. The results showed that RGB optical data could detect as many as 13 Portland cement concrete (PCC) pavement distresses out of 14 available in this study and 6 out of 9 asphalt concrete (AC) pavement distresses available on the airports. Similarly, DEMs were found to be useful for confirming the location of distresses with elevation change, such as faulting in PCC pavement and shoving in AC pavement. The hillshades helped with visually interpreting elevation differences, including finding their locations. In addition, thermal orthophotos showed potential to detect crack-based distresses. Based on the data analysis, the following minimum resolutions (in millimeters per pixel [mm/pix]) were recommended for airfield pavement distress detection and rating: RGB orthophotos of 1.5 mm/pix, DEMs of 6 mm/pix, and thermal orthophotos of 30 mm/pix or better (higher).

This research also concluded that sUAS-based PCI inspection not only detects and rates a number of airfield pavement distresses but also provides PCI values close to the foot-on-ground (FOG) traditional PCI inspection values. Recommendations on sUAS data collection plan development, data collection, data processing, data analysis, and the process of incorporating sUAS-based PCI inspection to complement traditional PCI inspections are discussed in detail.

1. INTRODUCTION

The U.S. Federal Aviation Administration (FAA) airport pavement design procedure is based on a minimum of 20 years of design life, considering regular maintenance and repair works. Over time, pavements deteriorate due to climatic/environmental factors, traffic loading, differential subgrade movements, and maintenance practices. To reach 20 years of life or more, airport pavements require routine maintenance, upgrading, and rehabilitation. The most effective way to preserve airport pavement is to establish and implement a maintenance program, and Airport Improvement Program (AIP) grants require many airports to develop and sustain an effective maintenance program. According to the FAA, the early detection and repair of distresses are essential aspects of preserving airport pavements (FAA, 2014). If pavements are not routinely maintained during the early stages of deterioration, severe distresses requiring costly and extensive repairs will develop. While pavement distresses caused by environmental conditions cannot be prevented, early and routine maintenance work can minimize the deterioration. The airport authorities should adopt effective and timely pavement inspection techniques to ensure the structural integrity, riding quality, and safety of the airport users. The current practice for airport pavement inspections relies on visual surveys and manual interpretation of reports and sketches prepared by inspectors in the field to quantify pavement conditions using the Pavement Condition Index (PCI) method as outlined in the American Society for Testing and Materials (ASTM) document, ASTM D5340-20, *Standard Test Method for Airport Pavement Condition Index Surveys* (ASTM International, 2020). The procedure is time-consuming and costly, and, thus, the assessment of a pavement branch (i.e., apron, taxiway, and runway) is completed by selecting and inspecting sample units within a pavement section. For a network-level survey, the overall PCI of a pavement section is based on the inspection results of selected sample units rather than a complete inspection of 100 percent of the pavement.

Recently, the use of small Unmanned (also referred to as Uncrewed) Aircraft Systems (sUAS) has attracted attention as an option for performing cost-effective and efficient pavement inspections, among many other applications (Vidyadharan et al., 2017). In recent years, several attempts have been made both by the industry and airport operators to use sUAS for conducting various types of pavement imaging and inspection of airports, among other infrastructure. These activities have included proof-of-concept demonstrations involving various types of sUAS platforms, sensors, and procedures under previous and newer sUAS regulations. Many researchers have demonstrated the potential of at least partly automated pavement distress detection using high-resolution sUAS optical imagery (Airsight, 2020a, 2020b; Inzerillo, DiMino, & Roberts, 2018; Romero-Chambi et al., 2020; Tan & Li, 2019). Inzerillo et al. (2018) showed the capabilities of high-resolution sUAS-integrated and stand-alone photogrammetric sensors to accurately identify distresses on roadway pavement on a large scale.

In this study, the research team deployed several sUAS at different altitudes at six airports in Michigan, Illinois, Iowa, and New Jersey from December 2020 to November 2021. sUAS data of different types were collected from these airports and processed to create red, green, and blue (RGB) or "natural color" orthophotos, Digital Elevation Models (DEMs), hillshades derived from DEMs, and thermal orthophotos. Sourav et al. (2022a) discussed some of the lessons learned from these data collections, processing, and field demonstrations. This report describes additional lessons learned about platforms, sensors, data collection methods, data processing, and data analysis from these challenges. In addition, the research team made a set of observations about the

data and processed results based on the deployment of different sUAS and the use of collected data in airfield pavement distress detection and rating. A summary of the observations and additional conclusions are provided in this report. The sUAS-collected RGB data were found to be useful in detecting crack-based distresses in airfield pavement, which has been described in detail with supporting figures (Sourav et al., 2022b). DEM and RGB data were already used for detecting joint deal damage, spalling, pop-outs, scaling, alkali-silica reaction (ASR), and patching in Portland cement concrete (PCC) pavement (Sourav et al., 2022c). However, this report evaluates the use of RGB, DEM, and thermal data not only in PCC pavement but also asphalt concrete (AC) pavement distress detection. This report also illustrates how sUAS technologies and different data types can be used to meet airport pavement evaluation requirements. Another primary objective of this research is to develop recommended processes and procedures for using sUAS to complement current methods of airport Pavement Management Program (PMP) inspections and to evaluate various types of sUAS platforms and sensors that will lead to recommended minimum specifications required for consistently safe, reliable, and effective sUAS-assisted airport PMP inspections. This report also illustrates how sUAS technologies and different data types can be used to meet airport pavement evaluation requirements. It also focuses on the ability of technologies to generate a PCI or partial PCI, which can be helpful in assisting with PMP.

2. DESCRIPTION OF TYPES OF sUAS PLATFORMS AND SENSORS

2.1 LITERATURE REVIEW SUMMARY

The research team developed a literature review that focused on current standard pavement inspection methods and standards, the use of sUAS in transportation infrastructure inspection, details of representative sUAS platforms and sensors, and the scope of research in pavement inspection with sUAS technology. Appendix A provides a summary version of the literature review. The literature review provided published information that supported the concept that the deployment of sUAS could result in faster and more frequent inspection of airport pavements at a lower cost. Also, sUAS could enable the inspection of entire pavement sections rather than representative sample units, thus providing the potential for a comprehensive assessment of airfield pavement conditions. Moreover, sUAS-enabled inspections could ensure adequate data acquisition, as required for realistic pavement condition prediction and prudent resource allocation for maintenance work. Several transportation agencies are successfully implementing sUAS platforms with different sensor arrangements in various applications with a focus on infrastructure inspection, such as bridges, highways, light poles, and unpaved roads. In the past decade, technological advancements have allowed significant progress in sUAS capabilities and sensor accuracy. Powerful computers, computational efficacy, and robust software packages are available for an accurate and realistic interpretation of sUAS data. Therefore, a number of sUAS platforms and sensors can be practically implemented to complement the current airport pavement inspection method depending on the mission objectives, distress severity levels, and the required accuracy of measurements.

2.2 RECOMMENDATIONS AND USES FOR sUAS PLATFORMS AND SENSORS

Based on the literature review and the experience of the research team, multiple sUAS platforms and three categories of sensors were recommended for airfield pavement distress identification and rating for potential use in this study and beyond. All the recommended sUAS platforms are

rotorcraft (multirotor) of different sizes. In addition, the recommended sensor categories are photogrammetry and Light Detection and Ranging (LiDAR) sensors for three-dimensional (3D) sensing, thermal imaging cameras, and multispectral/hyperspectral imaging cameras. A description of these three sensor categories is provided in Section 2.2.2, along with the sUAS deployed by the research team.

2.2.1 Recommended and Used sUAS Platforms

Two types of sUAS platforms are used and recommended in this research (a) multirotor platform with user-installed sensors and (b) multirotor platform with integrated sensors. Table 1 provides details of these platforms and the sensors attached to them.

Table 1. sUAS Platforms Deployed at Different Airports

sUAS platform	Type	Sensor	Claimed Flight Time (minutes)
Bergen Hexacopter	Six rotors, larger	Nikon D850 45.7-mp RGB optical	16
		FLIR Vue Pro R 640x512 thermal	
		Tetracam Micro-MCA6	
Tarot X6	Six rotors, larger	Nikon D850 45.7-mp RGB optical	35
MicroDrones mdMapper1000+	Four rotors, larger	Sony RX1R-II 42.4-mp RGB optical	40
DJI Mavic 2 Pro	Four rotors, small	20-mp RGB optical	31
Mavic 2 Enterprise Advanced	Four rotors, small	48-mp RGB optical Quad Bayer and 640x512 thermal	31
DJI Mavic 2 Enterprise Dual	Four rotors, small	12-mp RGB optical and FLIR 160x120 thermal	31

FLIR = Forward-looking infrared mp = megapixel

2.2.1.1 Multirotor sUAS with User-installed Sensors

Multirotor platforms with user-installed sensors offer the most flexibility with data collection since a single platform can fly multiple sensors, including flying more than one sensor at a time for some applications. An example of this, well-tested by the research team, is the U.S.-made Bergen Hexacopter, which has a two-axis gimbal that can carry sensors up to 11 lb (5 kg) in weight. Other examples are the North American-made Tarot X6 by UAV Systems International (UAVSI) and the German-built mdMapper1000+ from Microdrones, which were used at several data collection sites for this study. While this type of larger sUAS is versatile with sensor payloads, it can also be more complex to operate, especially for older systems that do not have the most modern automated flight capabilities. Sensors must also be manually installed and removed by an expert as part of the data collection procedure. In addition, operator pilots must have expertise in sUAS platforms and data collection for the specific sensor being flown, including appropriate optical and thermal imaging system settings.

2.2.1.2 Multirotor sUAS with Integrated Sensors

sUAS with integrated sensors already have optical, thermal, or other sensors. These systems can be easier to operate and collect data than those with user-installed sensors, as they typically come with flight planning software tools that can automatically determine the optimal flight parameters. Examples of these smaller systems include (1) the Mavic 2 Pro with a 20-megapixel (mp) RGB optical camera on a three-axis gimbal, (2) the DJI Mavic 2 Enterprise (Dual) Universal Edition sUAS with integrated forward-looking infrared (FLIR) 160x120 thermal sensors and 12-mp RGB optical camera, and (3) the Mavic 2 Enterprise Advanced (M2EA) sUAS integrated 48-mp Quad Bayer RGB optical camera (actually 12 mp, with Quad Bayer interpolation to 48 mp) and a 640x512 pixel FLIR thermal sensor. The main disadvantages to these systems are that multiple sUAS could be required to collect different data types; for example, the Mavic 2 Pro only has an RGB camera. Newer sUAS could be deployed to take advantage of new integrated sensors as they become available.

2.2.2 Recommended and Used sUAS Sensors

Based on the literature review and the research team's experience, three categories of sensors were recommended that were available and likely to meet many, if not all, distress identification and rating needs. Details of the sensors are discussed below, and their properties are provided in Table 1.

2.2.2.1 Red, Green, and Blue Photogrammetric Sensing

sUAS-based sensing for pavement inspection typically has been accomplished through close-range photogrammetry using RGB images. This method has the capability to produce accurate high-resolution orthophotos with 3D outputs including DEMs and point clouds. Photogrammetry is generally less expensive to implement than alternatives such as LiDAR, and 3D point clouds can also be created with the same data set. To create a complete 3D output, at a minimum, there needs to be at least 60% forward overlap between successive imagery and 40% side lap between adjacent sUAS imageries. As the sUAS moves over the planned flight path and collects images of overlapping areas, 3D structural information is gained from a process known as Structure from Motion (SfM). During post-processing of the collected imagery, a 3D point cloud can be created at a resolution chosen by the user.

The ultimate quality and accuracy of this point cloud and RGB orthophoto depend on the sensor's resolution, the captured imagery's resolution (which influences the number of automatic tie points that SfM software can find between images), the sensor's flight altitude, and the amount of overlap between the captured imageries. The 3D point cloud can then be used to make high-resolution Digital Surface Models and DEMs. The output elevation values represent whatever is visible within the imagery; this could be a pavement surface but could also represent the height of a piece of vegetation or other features obscuring parts of the runway. High-resolution imagery obtained by the sUAS can be stitched together and accurately georeferenced with the help of ground control points (GCPs) surveyed with high-accuracy differential global navigation satellite system (GNSS) data, such as from the U.S.-controlled Global Positioning System (GPS). The exact definition of high-accuracy GPS varies by user need, but 1- to 10-cm horizontal and 1- to 20-cm vertical accuracy is adequate for airfield pavement distress detection based on this study and the research

team's previous experience in high-resolution geospatial data creation. In this research, several RGB optical sensors have been used with sUAS platforms: (a) Nikon D850 45.7-mp RGB optical camera with 50-mm prime lens, (b) Sony RX1R-II 42.4-mp RGB optical camera, (c) 20-mp integrated RGB optical camera, (d) 12-mp integrated RGB optical camera, and (e) 48-mp Quad Bayer RGB optical camera.

2.2.2.2 Thermal Sensors

Thermal data can be useful for surveying roadway and bridge conditions (Brooks et al., 2018, 2015). For instance, thermal radiometric imagery can highlight areas of a bridge experiencing subsurface concrete bridge deck delamination due to water intrusion into roadway cracks. The research team has extensive experience working with FLIR radiometric thermal sensors for the imaging of surfaces from sUAS (Escobar-Wolf, Oommen, Brooks, Dobson, & Ahlborn, 2018). Distresses that create a subsurface air gap (delamination or spalls), such as swelling of the rebar, can also have a thermal signal that makes them stand out in thermal imagery relative to surrounding healthy concrete and pavement. This is represented as a thermal hot spot (an area warmer than the surrounding pavement) if collected in the morning as ambient temperatures are rising. Concrete with an air gap warms more rapidly than the surrounding solid concrete. Similarly, this imagery can be collected as ambient temperatures cool during the evening. Delamination and some spalling would be expressed as cold spots as they cool down faster than the surrounding concrete. In this research, three thermal cameras have been used: (a) FLIR Vue Pro R 640x512 thermal sensor, (b) FLIR 640x512 integrated radiometric thermal sensor, and (c) FLIR 160x120 thermal sensor.

2.2.2.3 Multispectral and Hyperspectral

Multispectral (and hyperspectral) imaging has a wide variety of applications. Hyperspectral sensors work similarly to multispectral sensors but are able to capture much more information, albeit at a higher cost. Multispectral sensors collect surface reflectance images at many wavelengths (or bands) of light. There is not a single agreed-upon standard about what makes a multispectral vs hyperspectral sensor. In our experience, multispectral systems cover as many as 14 spectral bands, while hyperspectral systems have had 40 or more. Different wavelengths or groups of wavelengths can be used to observe different phenomena. Wavelengths of interest typically range from the visible to near-infrared wavelengths (450–1,000 nanometers [nm]) to shortwave-infrared wavelengths (850–1,800 nm, which are not thermal infrared wavelengths). A selection of wavelengths can be useful in identifying roadway cracks, cracks with sealant, and cracks with vegetation. A Tetracam multispectral sensor that can sense six narrow 10-nm-wide bands in the 400–1,000 nm range was used in this study for an initial evaluation of its performance. However, the sensor did not provide any additional benefits over the RGB optical, DEM, and thermal data at the one airport where it was deployed. Thus, it was not deployed in any other data collection sites. However, further in-depth analysis of multispectral and hyperspectral sensors is recommended to test their capabilities more fully.

3. AIRPORT SELECTION

Multiple airports in Michigan, Illinois, Iowa, and New Jersey were selected for field demonstration and validation. The criteria used for selecting the airport sites included location, pavement types (i.e., asphalt- and concrete-surfaced airfields and grooved and non-grooved), pavement distress

types and severity levels, airport operation (i.e., controlled or uncontrolled), class of the airspace, and interest in employing sUAS solutions. Airport sites with proximity to the research team members' locations were given priority to evaluate various experimental variables. Cape May County Airport (WWD) in New Jersey, which is close to the FAA William J. Hughes Technical Center, was also selected as an additional site to test and validate the final platform(s), sensor(s), sensor/system specifications/attributes, operational parameters, processes, and procedures recommended for use in this study as effective, representative systems. Among the airport selection criteria mentioned above, four major selection process criteria are described in the following section.

3.1 AIRPORT SELECTION CRITERIA

3.1.1 Airspace Class

According to FAA, there are two categories of airspace: regulatory and nonregulatory. Within these categories, there are four types of airspace: controlled, uncontrolled, special use, and other (FAA, 2016). The complexity or density of aircraft movements, the safety required, nature of the operations conducted within the airspace, and national and public interest dictate the airspace categories and types (FAA, 2016). An authorization from air traffic control (ATC) is required to fly an sUAS in controlled airspace (Class A, B, C, D, and E airspace); however, the uncontrolled airspace (Class G airspace) does not require such authorization. The airports inside Class G or uncontrolled airspace were given a higher priority to facilitate prompt and timely airport pavement inspections, whereas other airspaces require ATC clearance and could have led to a delay in the inspections. The data collection team always coordinated with the airport manager when flying at airports and used aviation radios to communicate during flight and to alert the crew of the status of nearby manned aircraft.

3.1.2 Presence of Both Asphalt Concrete and Portland Cement Concrete Pavements

For airfield pavements, ASTM identifies 17 AC pavement distresses and 16 PCC distresses as listed in Appendix E (ASTM International, 2020). In identifying airports to participate in this study, those that included both AC and PCC pavements were given priority to facilitate inspection of both pavement types in a single visit when possible and reduce the redundancy of field demonstration.

3.1.3 Higher Number of Distresses and Severity

Peshkin et al. (2019) provided an initial assessment of the capabilities of different sUAS sensing technologies, including sUAS imaging, to detect pavement distresses according to ASTM D5340 (ASTM International, 2020). The report noted that sUAS imaging is helpful in identifying many distresses with some differences based on severity levels. For AC pavements, these include alligator cracking, bleeding, block cracking, joint reflection cracking, longitudinal and transverse (L&T) cracking, patching, and utility cut patching. For PCC pavements, sUAS imaging was summarized as being likely to be able to identify blowup, corner break, longitudinal, transverse, and diagonal (LTD) cracks, joint seal damage, patching, pop-outs, pumping, high-severity scaling, high-severity settlement, shattered slab, spalling, and high-severity ASR. Airport pavements with

the highest number of distresses with different severity levels were prioritized to evaluate the usefulness of sUAS data and systems in identifying as many distresses as possible.

3.1.4 Lower PCI Values with a Range of Distresses

The PCI is a numerical rating of the pavement condition based on the available distress types and severity levels. The PCI value ranges between 0 and 100, where 100 is the best possible condition and 0 is the worst possible condition. Lower PCI values represent worse condition pavements, and pavements with low PCI values are more likely to have a wide variety of distresses with different and worse severity levels. Thus, airport pavements with lower PCI values were prioritized.

3.2 MICHIGAN AIRPORTS

Initially, five airports from Michigan were considered for airport pavement distress evaluation: Grosse Ile Municipal Airport (ONZ), Hillsdale Municipal Airport (JYM), Branch County Memorial (OEB), Custer Airport (TTF), and Ann Arbor Municipal Airport (ARB). The Michigan Department of Transportation (MDOT) and the FAA provided inputs on suitable airports that were close to the Michigan Tech Research Institute (MTRI). The five airports of Michigan were sorted based on the criteria mentioned in Section 3.1. ONZ and TTF were selected for preliminary field visits as they ranked the highest, as listed in Table 2. Both airports were close to the research team location and provided several types of distresses with different severity levels. In addition, due to their location in Class G airspace, no additional authorization was required to conduct the sUAS data collections beyond coordinating data collection with airport managers.

Table 2. Michigan Airport Ranking

Airport	Airport Type	Airspace	No. of Runways	Surface Type	Treatment	Overall PCI	Runway Condition	Rank
ONZ	UNCON	Class G	2	AC, PCC	UNGRVD	73	GOOD, POOR	1
TTF	UNCON	Class G	1	AAC	GRVD	82	GOOD	2
OEB	UNCON	Class G	3	AC, AC	UNGRVD	63	FAIR, FAIR	3
JYM	UNCON	Class G	1	AC	GRVD	87	GOOD	4
ARB	CON	Class D	1	PCC	GRVD	77	FAIR	N/A

UNCON = Uncontrolled Airport
CON = Controlled Airport
GRVD = Grooved
UNGRVD = Ungrooved
N/A = Not Applicable
AC = Asphalt concrete pavement

AAC = Asphalt overlay over asphalt concrete pavement
PCC = Portland cement concrete pavement
Class D = Airspace from the surface to 762 m (2,500 ft) above the airport elevation (charted in mean sea level [MSL]) surrounding those airports that have an operational control tower)
Class G = Uncontrolled airspace

3.3 ILLINOIS AIRPORTS

Four airports in Illinois were initially considered for sUAS operations: Coles County Memorial Airport (MTO), Vermilion Regional Airport (DNV), Effingham County Memorial Airport (1H2), and University of Illinois Willard Airport (CMI). Those four airports were sorted based on the criteria mentioned in Section 3.1. MTO was selected for the preliminary field visit as it ranked the highest, as listed in Table 3. MTO is in Class G airspace and had 11 AC pavement distresses and 10 PCC pavement distresses. The airport was also close to the research team, Applied Pavement Technology, Inc. (APTech), which is based in Urbana, Illinois. The lessons learned from the previous field visits in Michigan airports were incorporated for data collection at MTO and upcoming data collections.

Table 3. Illinois Airport Ranking

Airport	Airport Type	Airspace	No. of Runways	Surface Type	Treatment	Runway Condition	Rank
MTO	UNCON	Class G	2	AC	GRVD	GOOD	1
NV	UNCON	Class G	2	AC, AC	PFC, GRVD	GOOD, GOOD	2
1H2	UNCON	Class G	2	PCC, AC	UNGRVD, UNGRVD	GOOD, GOOD	3
CMI	CON	Class C	3	AC, PCC, AC-PCC	UNGRVD, GRVD, GRVD	GOOD, FAIR, FAIR	N/A

UNCON = Uncontrolled Airport
CON = Controlled Airport
GRVD = Grooved
UNGRVD = Ungrooved

PFC = Porous friction course
N/A = Not Applicable
AC = Asphalt concrete pavement

AAC = Asphalt overlay over asphalt concrete pavement
PCC = Portland cement concrete pavement
Class C = Airspace from the surface to 1,219.2 m (4,000 ft) above the airport elevation (charted in MSL) surrounding those airports that have an operational control tower
Class G = Uncontrolled airspace

3.4 IOWA AIRPORTS

The research team selected five Iowa airports to evaluate their potential as sites for the execution of the sUAS data collection plan: Boone Municipal Airport (BNW), Perry Municipal Airport (PRO), Ames Municipal Airport (AWM), Ankeny Regional Airport (IKV), and Marshalltown Municipal Airport (MIW). These five airports were sorted based on the criteria mentioned in Section 3.1. BNW and PRO were selected for preliminary sUAS field data collection as they ranked the highest, as listed in Table 4. Both airports are in Class G airspace, two runways each, and are close to the research team in Ames, Iowa.

Table 4. Iowa Airport Ranking

Airport	Airport Type	Airspace	No. of Runways	Surface Type	Overall PCI	Runway Condition	Rank
BNW	UNCON	Class G	2	TURF, PCC	87	GOOD, GOOD	1
PRO	UNCON	Class G	2	TURF, PCC	42	GOOD, FAIR	2
AWM	CON	Class E	2	AC, PCC	76	FAIR, GOOD	3
MIW	UNCON	Class G	2	AC	65	FAIR, GOOD	4
IKV	CON	Class E	2	PCC	79	GOOD, GOOD	5

AC = Asphalt concrete pavement
PCC = Portland cement concrete pavement
TURF = Unpaved turf surface
CON = Controlled airport
UNCON = Uncontrolled airport (No tower)
Class G = Uncontrolled airspace
Class E = Airspace from the surface to 700 ft above the airport elevation (charted in MSL) surrounding those airports that have an operational control tower

The field demonstration and validation of the lessons learned were performed at the selected airports in the order shown in Figure 1.

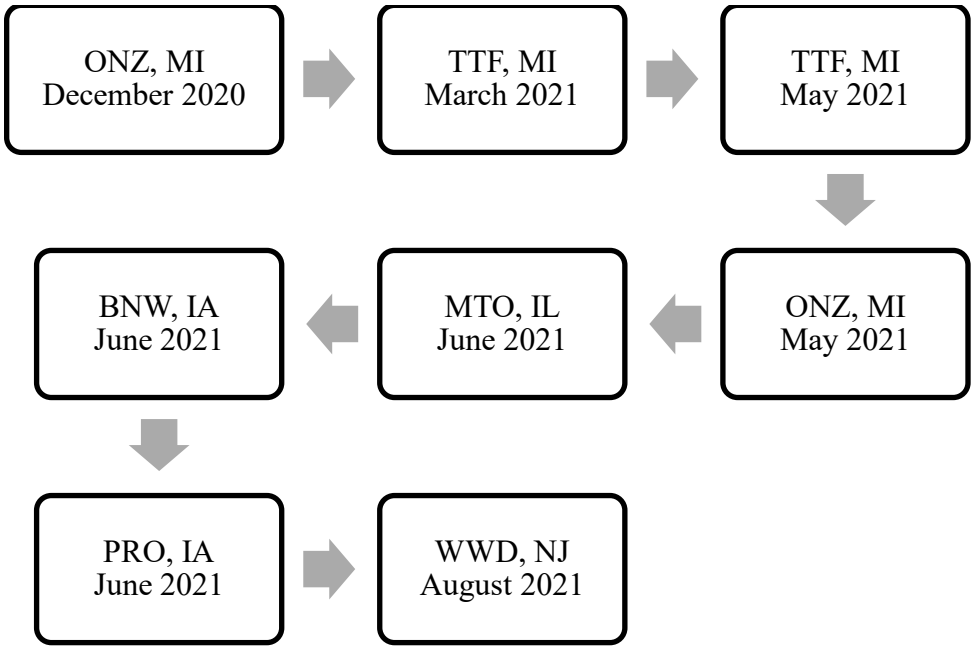

Figure 1. Field Demonstration and Result Validation Timeline

4. FIELD DEMONSTRATION IN MICHIGAN

4.1 GROSSE ILE MUNICIPAL AIRPORT IN DECEMBER 2020

4.1.1 Objectives

The research team executed the field demonstration plans developed for the sUAS data collection at Grosse Ile Municipal Airport (ONZ), Grosse Ile Township, Michigan, on December 10 and 11, 2020. The field demonstration plan developed for ONZ had the following objectives:

- Deploy and study the viability of the platforms and sensors that are available to the research team.
- Evaluate the performance of available sUAS platforms and sensors for various distress visualization.
- Study the effect of different flight altitudes and data resolution on distress identification.
- Downselect the sensors and platforms recommended in the literature review.

4.1.2 Field Demonstration in December 2020

The research team traveled from MTRI in Ann Arbor, Michigan, to the nearby ONZ airport, to collect sUAS data from the target areas shown in Figure 2. Total travel distance was 69 kilometers (km). The team closely monitored the wind speed and temperature before conducting each sUAS flight. The temperature varied between 6 degrees Celsius (°C) and 9 °C and the wind speed ranged from 3 kilometers per hour (km/h) to 19 km/h. The team followed the safety plan outlined for this data collection to ensure safe sUAS operation. The safety plan included monitoring the air traffic during the flight operation, yielding right of way to all other aircraft, operating at least 76.2 meters (m) away from the operational runways and taxiways, and minimizing the team's presence on the runway and taxiway.

As shown in Table 5, two sUAS platforms were used for the data collection: (a) a Mavic 2 Pro with its integrated 20-mp RGB optical sensor and (b) a Bergen Hexacopter that was used to deploy a thermal FLIR Vue Pro R camera (FLIR, 2020), and a 45.7-mp Nikon D850 full-frame RGB optical digital camera with 50-mm prime lens. A total of 31 GCPs were placed throughout different parts of the pavement to enable accurate, submeter positioning of geospatial output products, with the goal of having at least 0.5 m positional accuracy. The details of the sUAS platforms, sensors, flight altitudes, and expected resolutions are shown in Table 5.

A separate plan was developed for PCI survey data collection from airports in Michigan (Appendix D). A two-person crew from APTech traveled to ONZ and conducted an airfield pavement distress foot-on-ground (FOG) survey following the ASTM D5340-20 standard (ASTM International, 2020). On January 19 and 20, 2021, the FOG inspection team located, identified, and recorded pavement distresses for 20 sample units onto their handheld GPS-enabled field data collection tool. The data were processed, and the PCI values for all sample units and branches of the airfield pavement were calculated based on the ASTM D5340-20 standard. Because of overnight snowfall, the taxiway could not be inspected, and only data from the runway were collected. The PCI values for the different sections of PCC pavement ranged from 3 to 50. A survey report was generated, which included sample unit information, the types of distresses

present on the sample unit, and the PCI for each sample unit. The survey report was shared with other team members and the FAA.

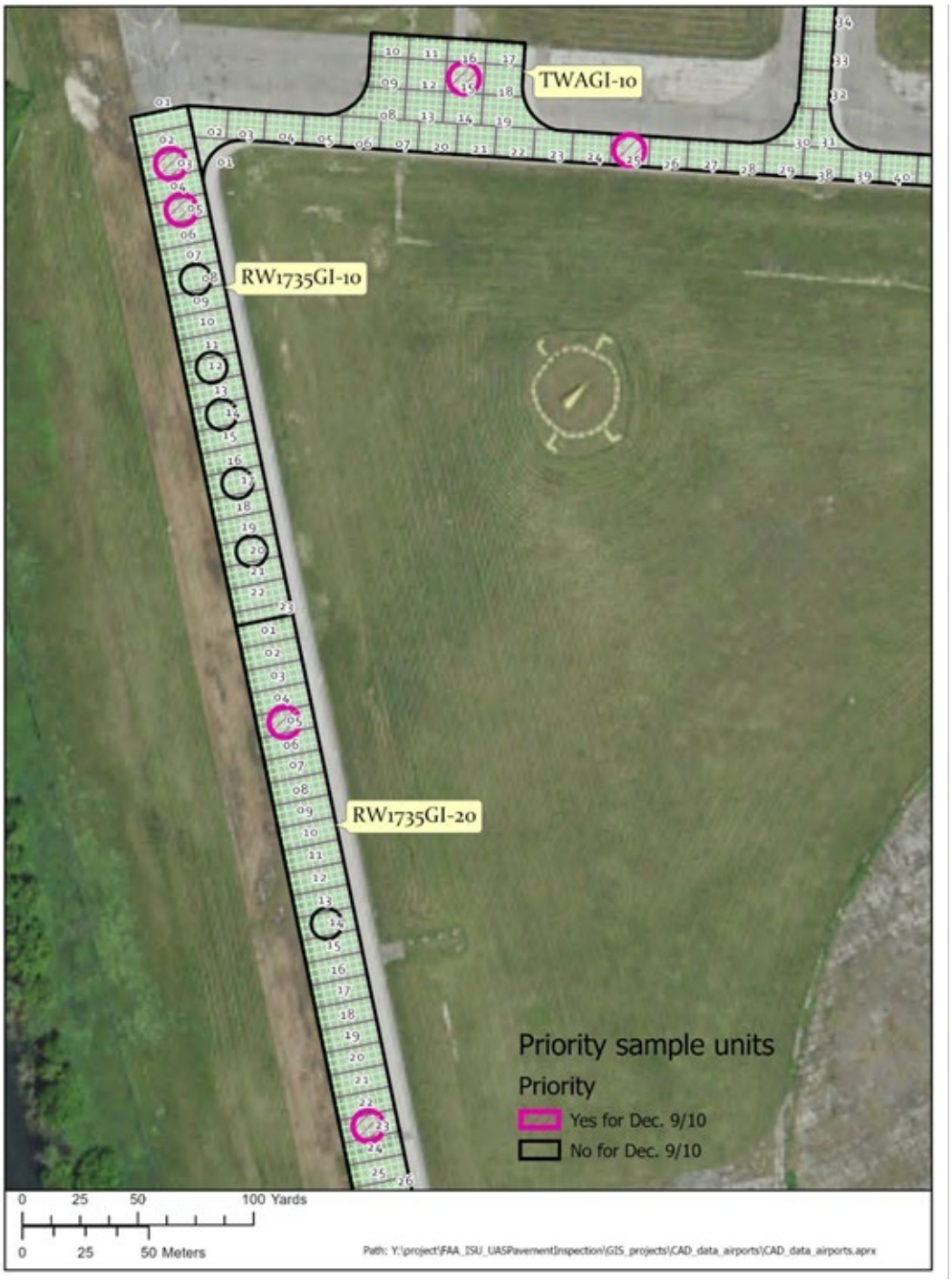

Figure 2. Focus Area for Data Collection with Six Selected Priority Sample Units Highlighted in Purple Circles

Table 5. Summary of sUAS Data Collection at ONZ in December 2020

Target Areas	sUAS Platforms	Sensor	Flight Altitude (m)	Resolution (mm/pix)	
				Orthophoto	DEM
RW1735 GI-10 SU 05, RW1735 GI-20 SU 05, RW1735 GI-20 SU 23, TWAHI-10 SU 15, TWAHI-10 SU 25	Bergen Hexacopter	45.7-mp optical RGB Nikon D850	9.1	0.8	3
	Bergen Hexacopter	FLIR Vue Pro R	9.1	8.0	N/A
Taxiway A	Mavic 2 Pro	20-mp optical RGB	91.5	21	84
Runway 17/35	Mavic 2 Pro	20-mp optical RGB	91.5	21	84
			30.5	7.3	29.1

RW1735 = Runway 17/35
GI-10 = Section 10
GI-20 = Section 20
DEM = Digital Elevation Model
TWAHI-10 = Taxiway A Section 10
SU = Sample Unit
N/A = Not applicable

4.2 GROSSE ILE MUNICIPAL AIRPORT IN MAY 2021

4.2.1 Objectives

The research team visited ONZ on May 14, 2021, to collect data from Runway 17/35 and Taxiway A. The field demonstration had the following objectives:

- Perform full data collection using M2EA.
- Evaluate the performance of the thermal data collected using M2EA.
- Compare the FOG inspection PCI value with PCI values calculated from the pavement distresses identified in RGB optical data of M2EA.
- Determine the minimum number of crews required for successful sUAS data collection from an airport.

4.2.2 Field Demonstration in May 2021

The second field demonstration plan developed for ONZ was executed on May 14, 2021. The research team, which consisted of three members, traveled from Ames, Iowa, and Ann Arbor, Michigan, to ONZ and collected sUAS data while following all the standard safety protocols, as recorded in the data-collection safety plan. The team also evaluated the possibility of complete sUAS data collection with a single sUAS system. Two M2EA sUAS were deployed for both optical RGB and stereo thermal data collection. The complete data of Runway 17/35 and Taxiway A were collected with M2EA's 48-mp Quad Bayer camera at 15.2-m flight altitude. A Quad Bayer camera enables a lower-resolution sensor (in this case, a 12-mp camera) to create images that are rated at higher resolution by placing more pixels behind a color filter. However, the underlying resolution is still the original (12-mp) resolution. This technology was first used in mobile phone cameras and was recently used in several Da-Jiang Innovations (DJI) drones (GSMArena, 2019).

Stereo thermal data were also collected from a selected sample unit using the same M2EA sUAS system at a flight altitude of 24.4 m. The M2EA has a dedicated thermally focused flight mode that enables the stereo overlapping thermal images to be collected with its thermal camera, which has a narrower field of view (FOV) than the RGB camera. The details of the collected data and their resolutions are provided in Table 6. In addition, 10 AeroPoints™ were used as the only GCPs in this data collection, as shown in Figure 3. The research team followed the standard safety protocols. The temperature and wind speeds were observed closely before deploying each flight, and they varied from 17 °C to 21 °C and 8 km/h to 24 km/h, respectively. Wind speeds and wind gusts of up to 24 km/h were considered to be safe for larger sUAS operations (in this case, the Bergen Hexacopter) and up to 40 km/h for the smaller sUAS (M2EA and Mavic 2 Pro).

The data collected in May 2021 was a full data collection with a single sUAS platform. The RGB optical data collected with M2EA at 15.2 m were processed with Agisoft Metashape using the location data of the 10 AeroPoints™, which are rated to have approximately 3-cm positional accuracy or better. Even though the RGB data were collected from Taxiway A, the data set was not further analyzed because the PCI survey team could not collect the data from the taxiway because of snowfall. RGB optical orthophoto and DEM were created for Runway 17/35 and exported to a local drive for further analysis. The resultant orthophoto and DEM had a resolution of 2.5 mm/pix and 10 mm/pix, respectively. A hillshade was generated using the DEM for further data analysis. The complete orthophoto of Runway 17/35 was imported into ArcGIS Pro and visually analyzed for each distress identification and rating of the severity level. The noted airfield pavement distresses were used to calculate the PCI value based on the methods outlined in the ASTM D5340-20 standard (ASTM International, 2020). The sUAS PCI values were then compared against the FOG survey PCI values.

Table 6. Summary of sUAS Data Collection at ONZ in May 2021

Target Areas	sUAS Platforms	Sensors	Flight Altitude (m)	Resolution (mm/pix)	
				Orthophoto	DEM
Runway 17/35 and Taxiway A Section 10	M2EA	48-mp optical RGB Quad Bayer	15.2	2.5*	10
Runway 17/35 Section 10 sample unit	M2EA	640-x512-pixel Stereo thermal	24.4	31.5	N/A

DEM = Digital Elevation Model N/A = Not applicable
*2.5 mm/pix is not true resolution due to being derived from the M2EA 48-mp Quad Bayer camera.

The data collected in May 2021 was a full data collection with a single sUAS platform. The RGB optical data collected with the M2EA at 15.2 m were processed with Agisoft Metashape using the location data of the 10 AeroPoints™, which are rated to have approximately 3-cm or better positional accuracy. Even though the RGB data were collected from Taxiway A, the data set was not further analyzed because the FOG inspection team could not collect the data from the taxiway because of snowfall. An RGB optical orthophoto and DEM were created for Runway 17/35 and exported to a local drive to study their usefulness in detecting pavement distresses. The resultant orthophoto and DEM had a resolution of 2.5 mm/pix and 10 mm/pix, respectively. A hillshade was generated using the DEM for further data analysis. The complete orthophoto of Runway 17/35

was imported into ArcGIS Pro and visually analyzed for each distress identification and rating of the severity level. The noted airfield pavement distresses were used to calculate the PCI value based on the methods outlined in the ASTM D5340-20 standard (ASTM International, 2020). The sUAS PCI values were then compared against the FOG survey PCI values.

Figure 3. Location of the Ground Control Points at ONZ

4.3 RESULTS AND DISCUSSION OF GROSSE ILE MUNICIPAL AIRPORT DATA ANALYSIS

4.3.1 Results and Discussion of December 2020 Data Analysis

During the first data collection of ONZ, the research team collected optical imagery at three different flight altitudes using two different optical sensors and thermal imagery. The flights at multiple altitudes were designed to assess the data quality collected at different flight altitudes with different amounts of time.

All collected photogrammetric, stereo, and overlapping-image data sets of the complete Runway 17/35 and the complete Taxiway A data set were imported separately into Agisoft Metashape for processing (Agisoft LLC, St. Petersburg, Russia). The locations of the sUAS imagery collected in December 2020 were corrected using the GCP locations, recorded with a Trimble® GeoExplorer® GeoXH 6000 GPS unit rated at approximately 10-cm or better positional accuracy. The images were processed on a high-end desktop workstation to create RGB optical orthophotos, DEMs, and a stereo thermal orthophoto. DEM is a raster image with each pixel representing the elevation. DEM was generated based on the dense cloud created in Agisoft Metashape. The resolution of the DEM depended on the resolution of the image captured by the optical RGB sensor. Each DEM was imported to ArcGIS Pro to produce a "hillshade DEM" for easier visualization and interpretation of elevation models (ESRI, West Redlands, CA, USA). As described by ESRI, a hillshade is derived from the DEM and "produces a grayscale 3D representation of the terrain surface, with the sun's relative position taken into account for shading the image" (ESRI, 2021a).

Mavic 2 Pro at 91.5-m flight altitude provided optical RGB orthophoto of 21 mm/pix and DEM of 84 mm/pix. The data collection was fast, but the DEM was too coarse to identify any distresses. In addition, the 21-mm/pix orthophotos were only useful to detect high-severity durability cracking, shattered slab, corner breaks, and large patching. By flying the Mavic 2 Pro at a lower flight altitude of 30.5 m, the resulting orthoimage resolution increased to 7.3 mm/pix, which allowed for the identification of smaller defects, such as cracks with lower severity, as shown in Section 2.3.1. The resulting DEM, having a resolution of 29 mm/pix, improved from flying at lower altitudes but still could only be used to identify larger defects. Examples of detectable distresses at a flight altitude of 30.5 m using the DJI Mavic 2 Pro include high-severity larger patches and durability cracks. Detailed comparisons are made with the May 2021 data collection, as shown in Figures 4 to 16.

The Bergen Hexacopter flights with the 45.7-mp Nikon D850 flown at 9.1-m altitude produced the highest resolution survey at ONZ. Orthomosaic resolution was improved to 0.8 mm/pix, which allows for the identification of minor cracks (Figures 4 and 7). To collect imagery over a single sample unit of approximately 210 m^2 required approximately 2.5 minutes of flight time. The primary disadvantage of the data collected by the Bergen Hexacopter with Nikon D850 at 9.1 m was that it would likely require too much time to complete an entire runway survey at this flight altitude, which might not be practical for airport pavement inspection, at least with this older sUAS system. Thermal imagery would take a similar amount of time with the separate sensor tested at ONZ (a FLIR Vue Pro R 640x512, 30-Hz system). This time estimate does not include the time required for landing, changing the batteries, and takeoff after every 16 minutes of flight time. Processing times for this anticipated high-resolution data set would also be significantly more than

the lower-resolution Mavic 2 Pro data. A single sample unit required approximately 150 images to be fully covered and took about an hour to process using 3D photogrammetry software, such as Agisoft Metashape and advanced computational capabilities of a multi-core processing workstation. The research team has estimated that it would require at least 9,000 images to cover Runway 17/35 at a 9.1-m flight altitude, and processing time for such a data set could be several days or even up to a week. Therefore, the same platform flown at 18.3-m altitude is recommended for a reasonable compromise between high-resolution outputs and data-collection time.

The initial findings after the first field demonstration at ONZ are summarized as follows:

1) Images with a resolution of 21 mm/pix collected using the 20-mp DJI Mavic 2 Pro sensor flown at 91.5 m were too coarse to detect or rate most airport pavement distresses (Figures 4 to 16).

2) Images with a resolution of 7.3 mm/pix collected using the 20-mp DJI Mavic 2 sensor flown at 30.5-m altitude appeared useful for detecting several airport pavement distresses. The detectable distresses (at least at one severity level) were LTD cracks, durability cracking, shattered slab, corner break, large patching, and small patching (Figures 5 to 10 and Figures 12 to 14). However, it was not always possible to accurately rate most of the identified distresses.

3) Flights at 9.1-m flight altitude with the Nikon D850 45.7-mp sensor produce functional and very high-resolution optical images and DEM data, yet it was likely to be challenging to deploy in a time-efficient manner at airports.

4) Thermal data appeared promising to detect at least some distresses, such as spalling, and to help emphasize crack locations.

4.3.2 Results and Discussion of May 2021 Data Analysis

The ONZ data collected in December 2020 were compared with May 2021 data for complete data analysis. The PCI values estimated using the pavement distresses identified in the 2.5-mm/pix data were also compared with manual FOG survey PCI values for evaluating the performance of sUAS in airfield pavement distress detection.

The following results are concluded from the field demonstration and analysis of data collected at ONZ in May.

- Images with a resolution of 2.5-mm/pix data are adequate to identify all crack-based distresses at all severity levels. The crack-based distresses found at ONZ were LTD cracks, durability cracking, shattered slabs, and corner breaks (Figures 4 to 10 and Figure 12).

- Identification of ASR was challenging with the 2.5-mm/pix data, especially for low-severity ASR (Figures 9 and 12).

- Faulting of 1 cm or less could not be detected with the 10-mm/pix DEM generated from processing the Mavic 2 Pro data. DEM of 3 mm/pix were useful for suspected faulting with medium-severity detection (Figure 17).

- A three-person sUAS crew can successfully collect sUAS data at an airport with a lower amount of air traffic without interrupting the general flow. The three-person team consists of a remote pilot in command, one visual observer, and one person responsible for managing the logistics and providing additional manual documentation of airfield distresses. These activities can include charging the sUAS batteries, taking location-tagged field photos, and placing and removing GCPs. It is also helpful for the crew to include an additional sUAS pilot with a dedicated observer to enable simultaneous data collection at two different airport locations. Each crew should have a dedicated aviation radio for efficient operations.

All the data collected from ONZ in December 2020 and May 2021 were compared to identify individual distresses with different severity. The results are summarized in Table 7.

Table 7. Summary of the Findings of ONZ

Distress Name (PAVER™ Distress Number)	Severity	Resolution Tested (mm/pix)		Distress Detected in Maximum Resolution (mm/pix)		Remarks
		Orthophoto	DEM	Orthophoto	DEM	
Corner breaks (62)	L	2.5, 7.3, 21	10, 29.1, 84	2.5*	ND	Figure 4
	M			21	ND	Figure 5
	H	0.8, 2.5, 7.3, 21	3, 10, 29.1, 84	21	ND	Figure 6
LTD cracks (63)	L	0.8, 2.5, 7.3, 21	3, 10, 29.1, 84	7.3	ND	Figure 7
	M			21	ND	Figure 8
Durability cracking (64)	L	2.5, 7.3, 21	10, 29.1, 84	7.3	ND	Figure 9
	M	0.8, 2.5, 7.3, 21	3, 10, 29.1, 84	21	10	Figure 8
	H				29.1	Figure 10
Joint seal damage (65)	H	0.8, 2.5, 7.3, 21	3, 10, 29.1, 84	7.3	ND	Figure 11
Large patching (66)	L	2.5, 7.3, 21	10, 29.1, 84	21	ND	Figure 14
	M	0.8, 2.5, 7.3, 21	3, 10, 29.1, 84	21	29.1	Figure 13
	H					Figure 12
Scaling (70)	M	2.5, 7.3, 21	10, 29.1, 84	21	10	Figure 15
Faulting (71)	L	0.8, 2.5, 7.3, 21	3, 10, 29.1, 84	ND	ND	Figure 16
	M				3	Figure 4
Shattered slab (72)	M	0.8, 2.5, 7.3, 21	3, 10, 29.1, 84	21	10	Figure 12
ASR (76)	**L, M	0.8, 2.5, 7.3, 21	3, 10, 29.1, 84	7.3	ND	Figure 12 Figure 9

L = Low, M = Medium, H = High
ND = Not detected
LTD cracks = Longitudinal, Transverse, and Diagonal cracks
* 2.5 mm/pix is not true resolution due to being derived from the Mavic 2 Enterprise Advanced 48-mp Quad Bayer camera.
** Low-severity ASR detection is not always possible.

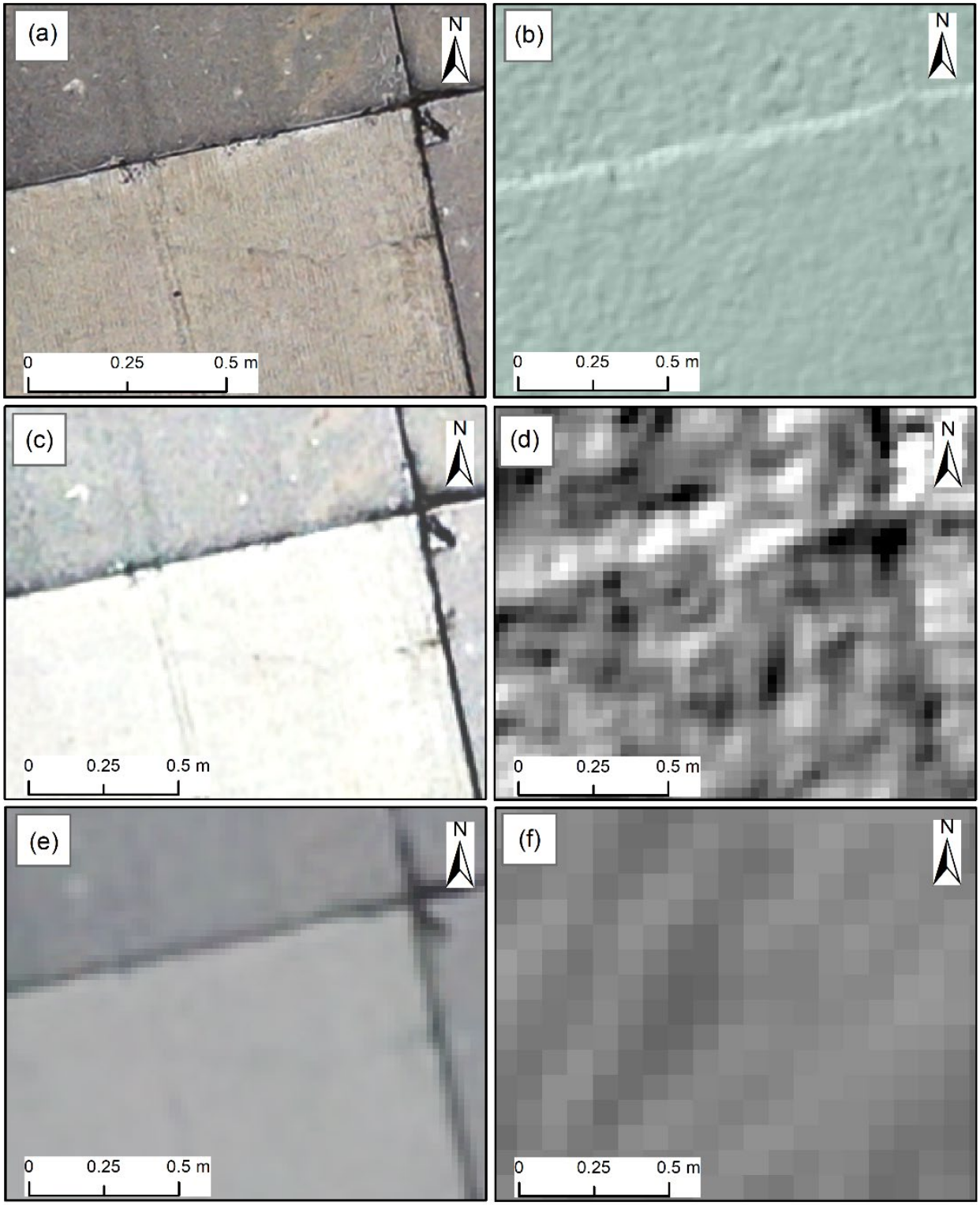

Figure 4. Corner Break (L) and Faulting (M) in (a) 2.5-mm/pix Orthophoto, (b) 10-mm/pix DEM, (c) 7.3-mm/pix Orthophoto, (d) 29.1-mm/pix DEM, (e) 21-mm/pix Orthophoto, and (f) 84-mm/pix DEM

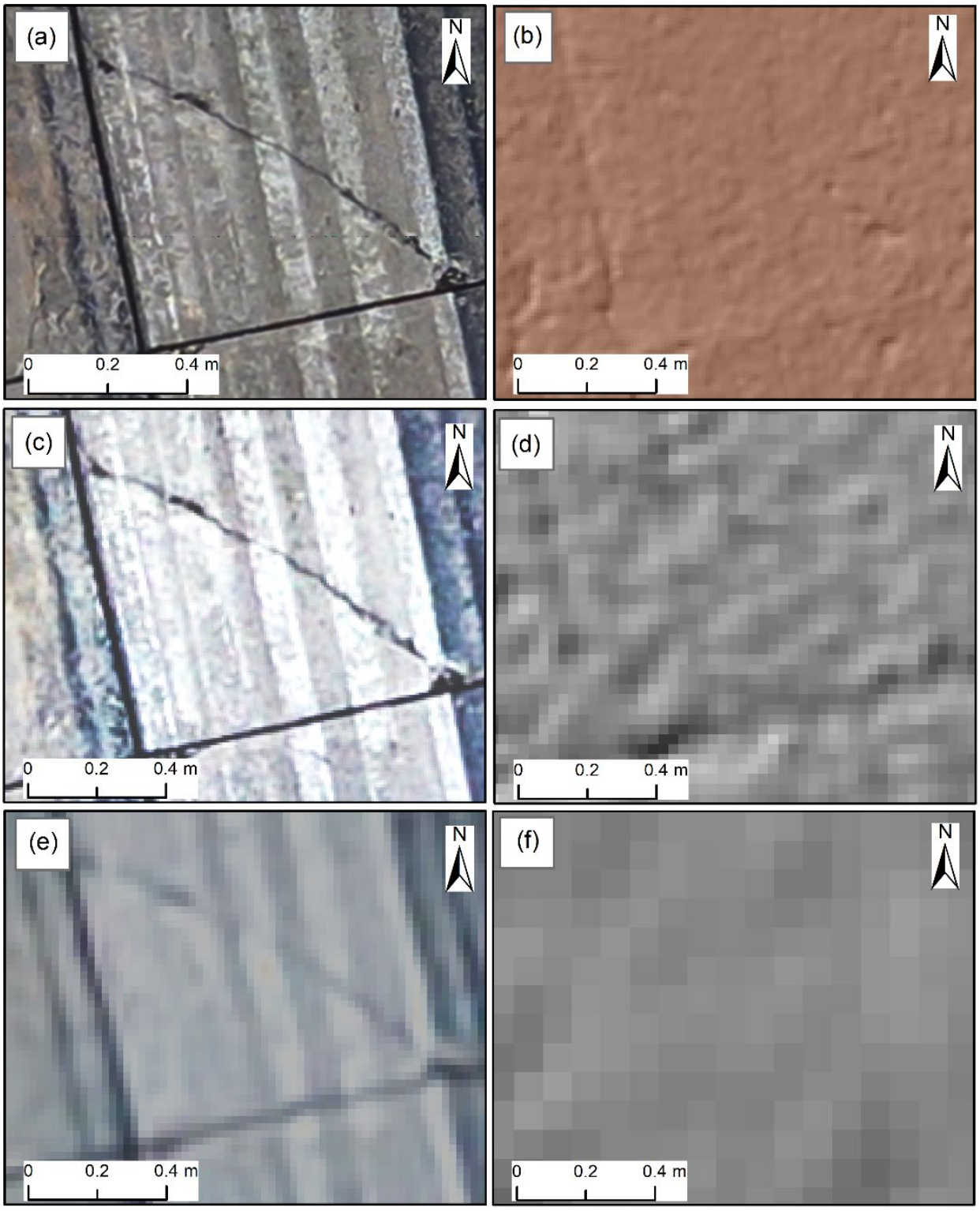

Figure 5. Corner Break (M) in (a) 2.5-mm/pix Orthophoto, (b) 10-mm/pix DEM, (c) 7.3-mm/pix Orthophoto, (d) 29.1-mm/pix DEM, (e) 21-mm/pix Orthophoto, and (f) 84-mm/pix DEM

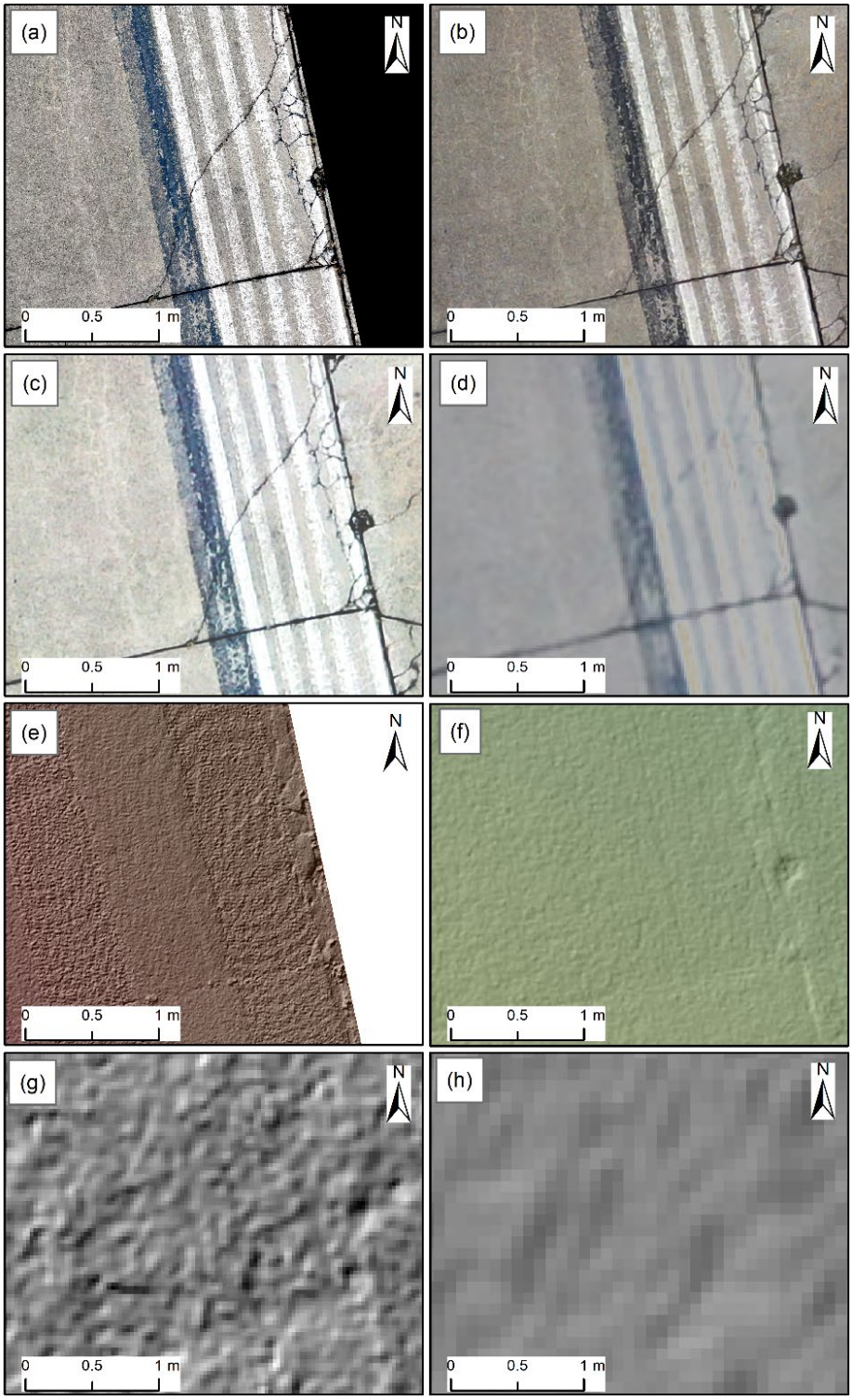

Figure 6. Corner Break (H) in (a) 0.8-mm/pix Orthophoto, (b) 2.5-mm/pix Orthophoto, (c) 7.3-mm/pix Orthophoto, (d) 21-mm/pix Orthophoto, (e) 3-mm/pix DEM, (f) 10-mm/pix DEM, (g) 29.1-mm/pix DEM, and (h) 84-mm/pix DEM

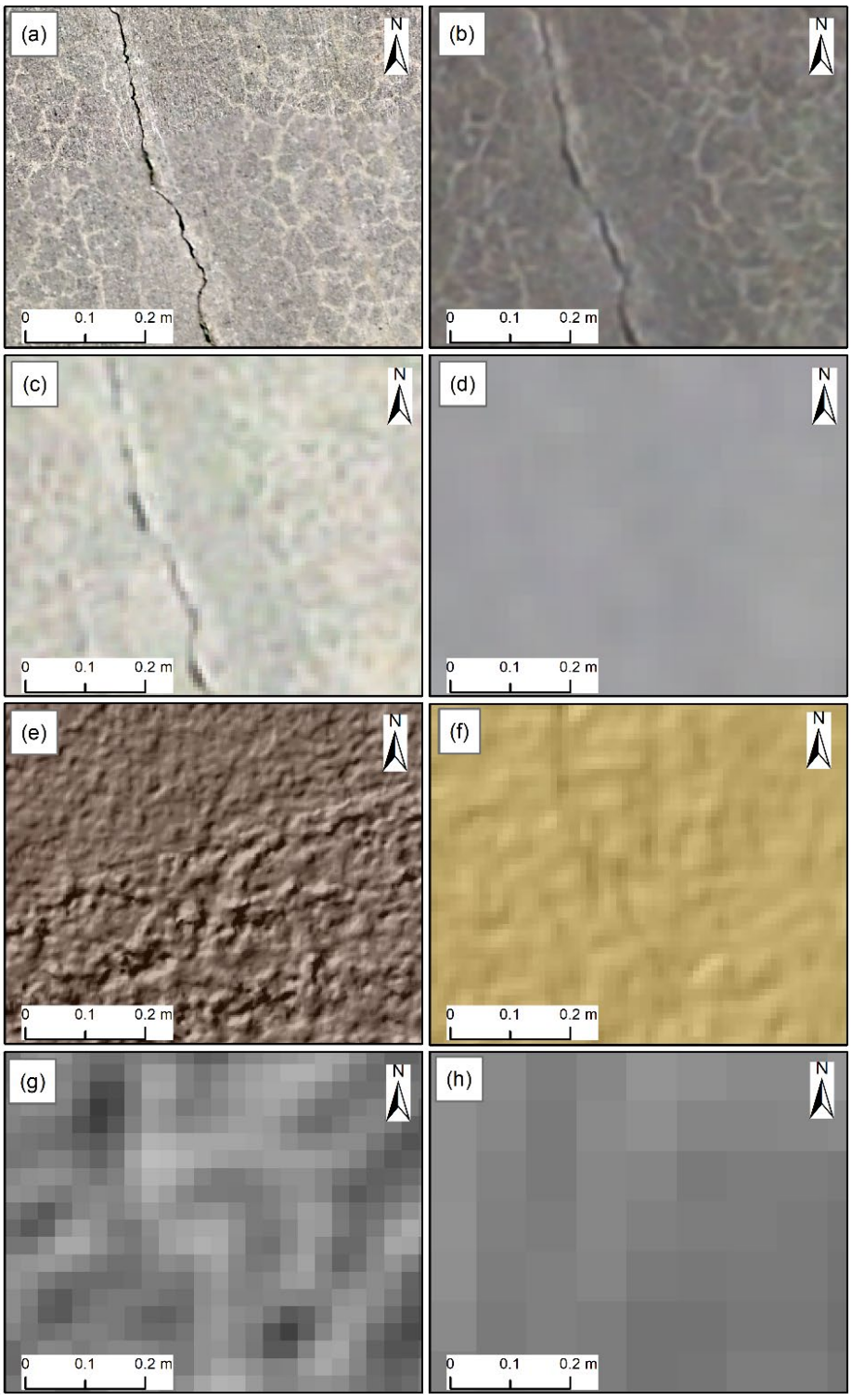

Figure 7. Longitudinal, Transverse, and Diagonal Cracking (L) in (a) 0.8-mm/pix Orthophoto, (b) 2.5-mm/pix Orthophoto, (c) 7.3-mm/pix Orthophoto, (d) 21-mm/pix Orthophoto, (e) 3-mm/pix DEM, (f) 10-mm/pix DEM, (g) 29.1-mm/pix DEM, and (h) 84-mm/pix DEM

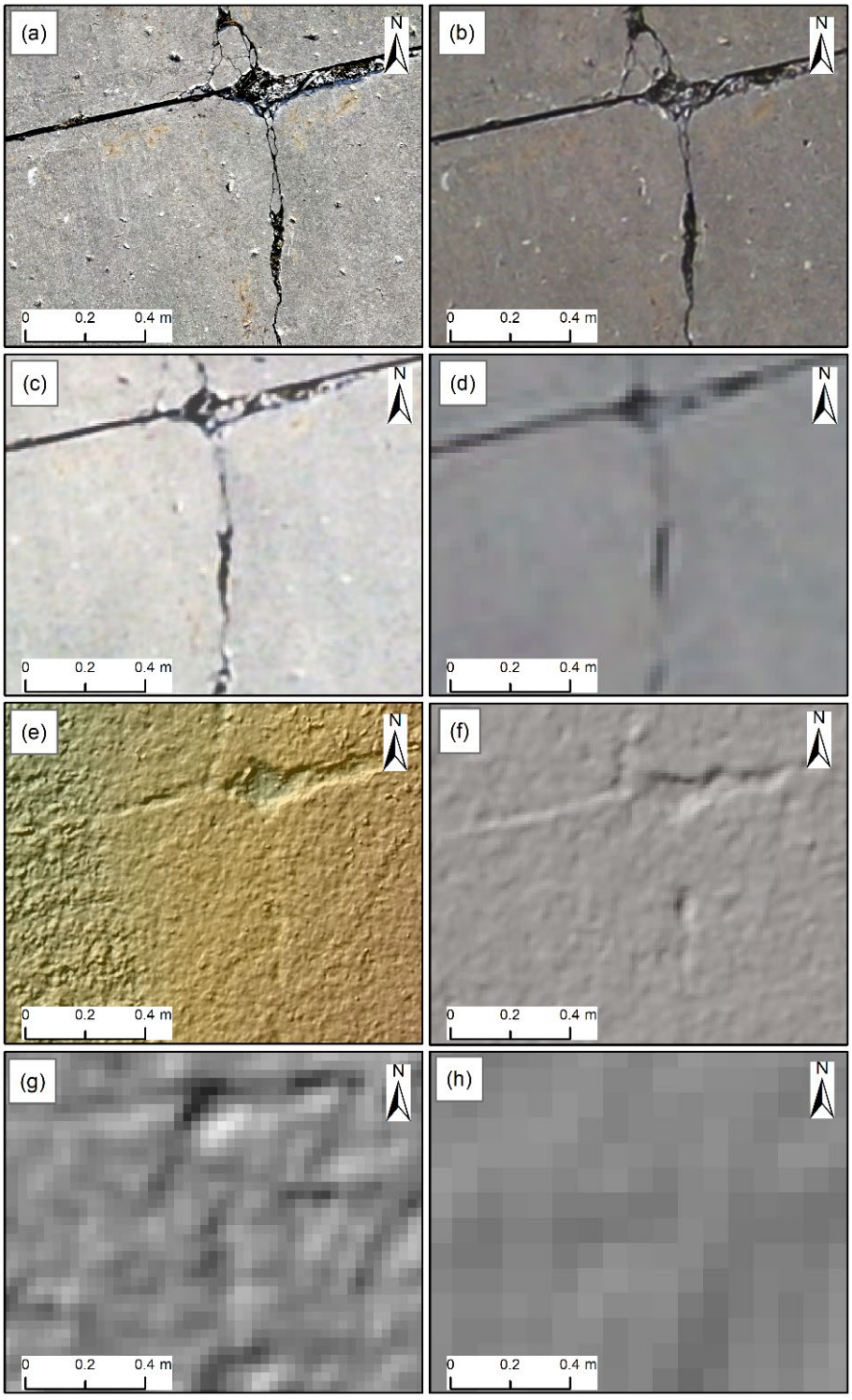

Figure 8. Longitudinal, Transverse, and Diagonal Cracks (M) and Durability Cracking (M) in (a) 0.8-mm/pix Orthophoto, (b) 2.5-mm/pix Orthophoto, (c) 7.3-mm/pix Orthophoto, (d) 21-mm/pix Orthophoto, (e) 3-mm/pix DEM, (f) 10-mm/pix DEM, (g) 29.1-mm/pix DEM, and (h) 84-mm/pix DEM

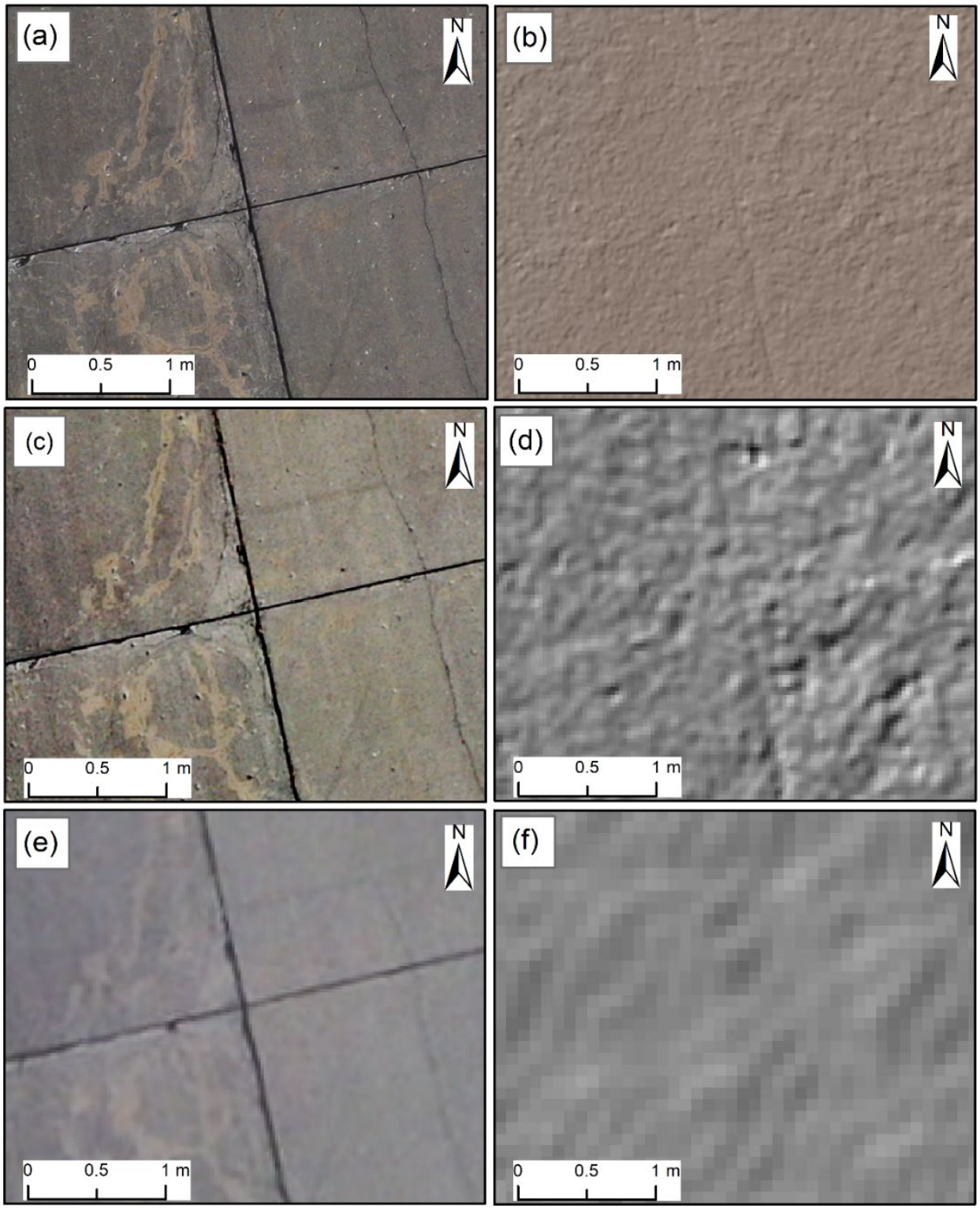

Figure 9. Durability Cracking (L), ASR (L), and ASR (M) in (a) 2.5-mm/pix Orthophoto, (b) 10-mm/pix DEM, (c) 7.3-mm/pix Orthophoto, (d) 29.1-mm/pix DEM, (e) 21-mm/pix Orthophoto, and (f) 84-mm/pix DEM

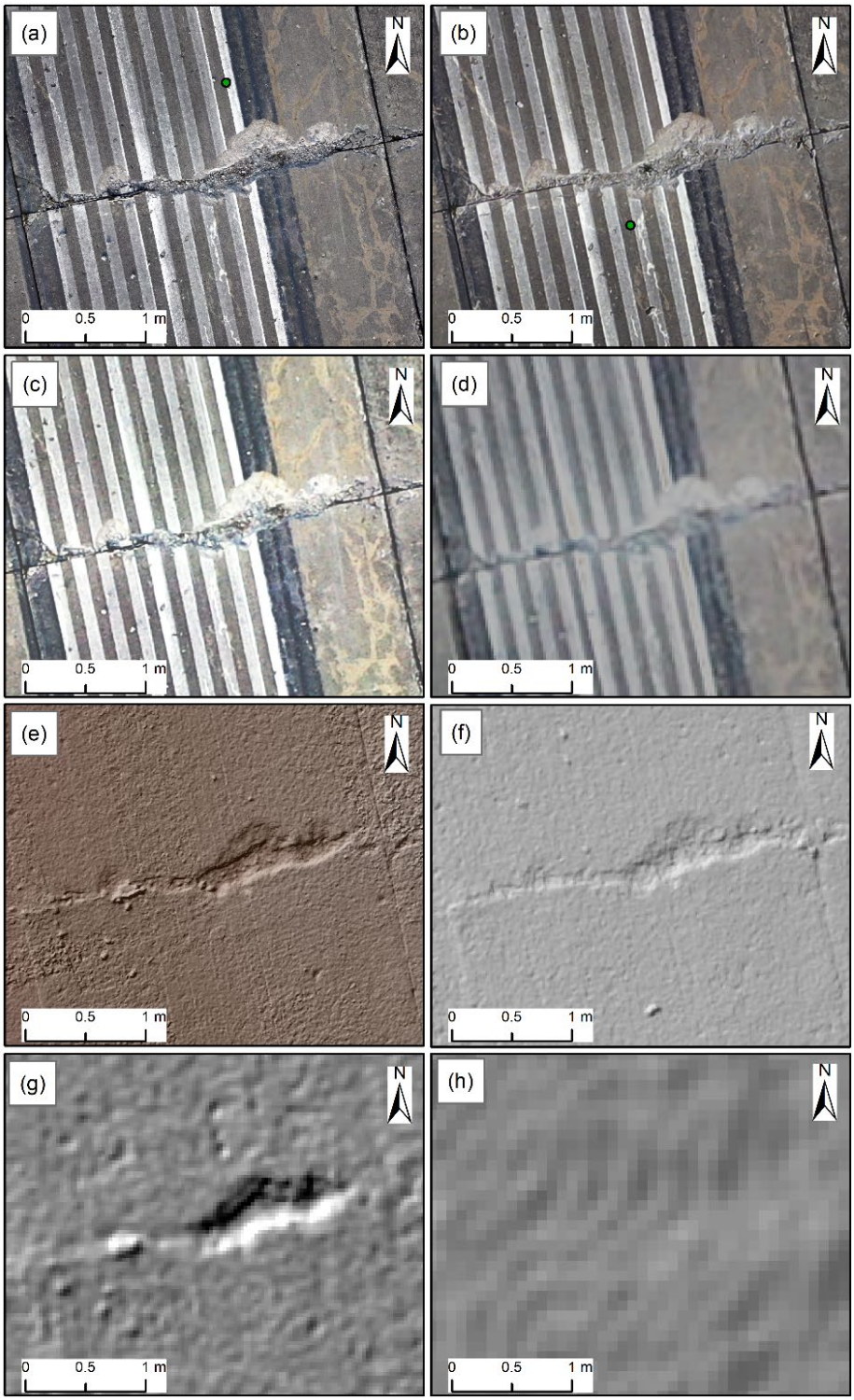

Figure 10. Durability Cracking (H) in (a) 0.8-mm/pix Orthophoto, (b) 2.5-mm/pix Orthophoto, (c) 7.3-mm/pix Orthophoto, (d) 21-mm/pix Orthophoto, (e) 3-mm/pix DEM, (f) 10-mm/pix DEM, (g) 29.1-mm/pix DEM, and (h) 84-mm/pix DEM

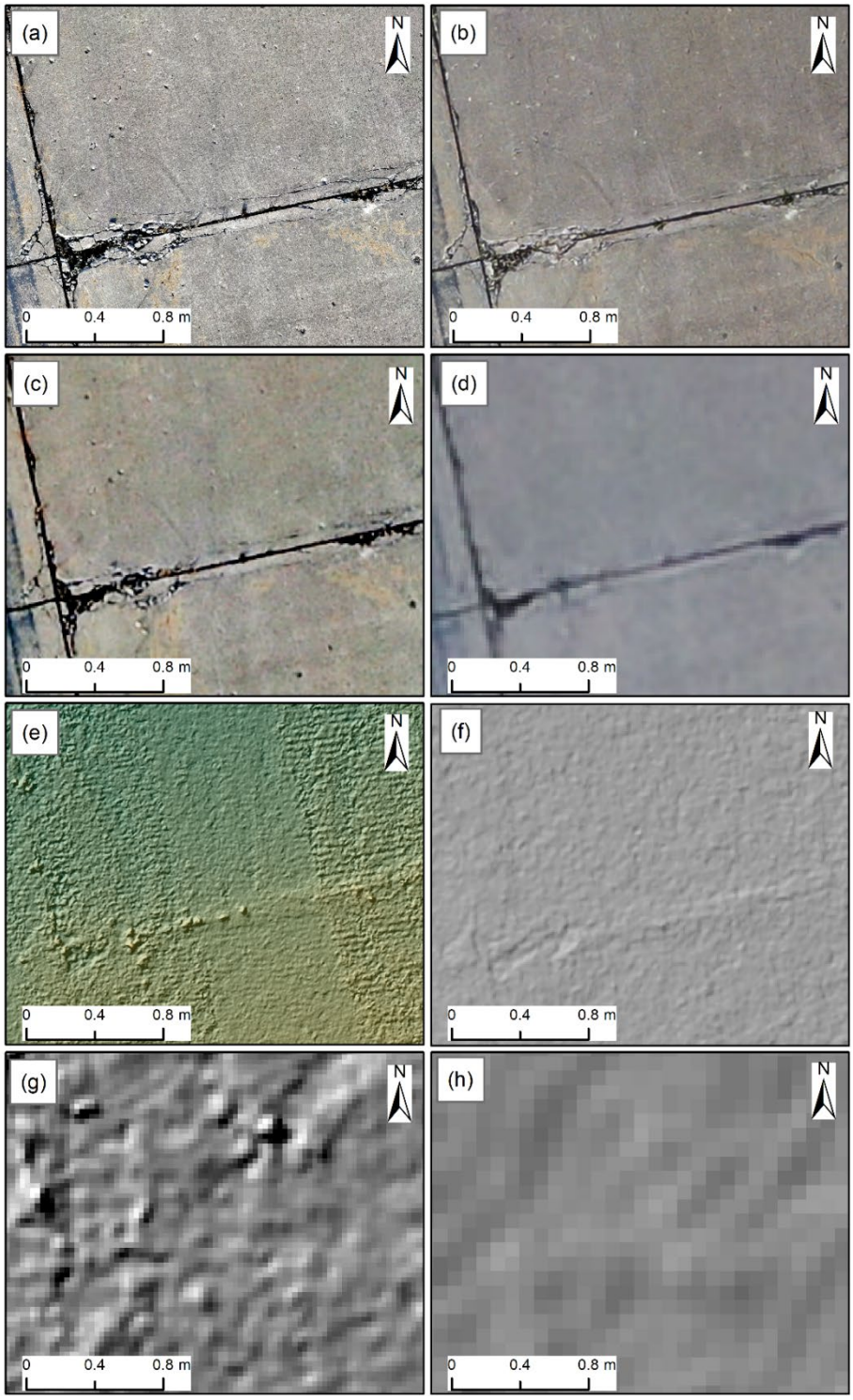

Figure 11. Joint Seal Damage (H) in (a) 0.8-mm/pix Orthophoto, (b) 2.5-mm/pix Orthophoto, (c) 7.3-mm/pix Orthophoto, (d) 21-mm/pix Orthophoto, (e) 3-mm/pix DEM, (f) 10-mm/pix DEM, (g) 29.1-mm/pix DEM, and (h) 84-mm/pix DEM

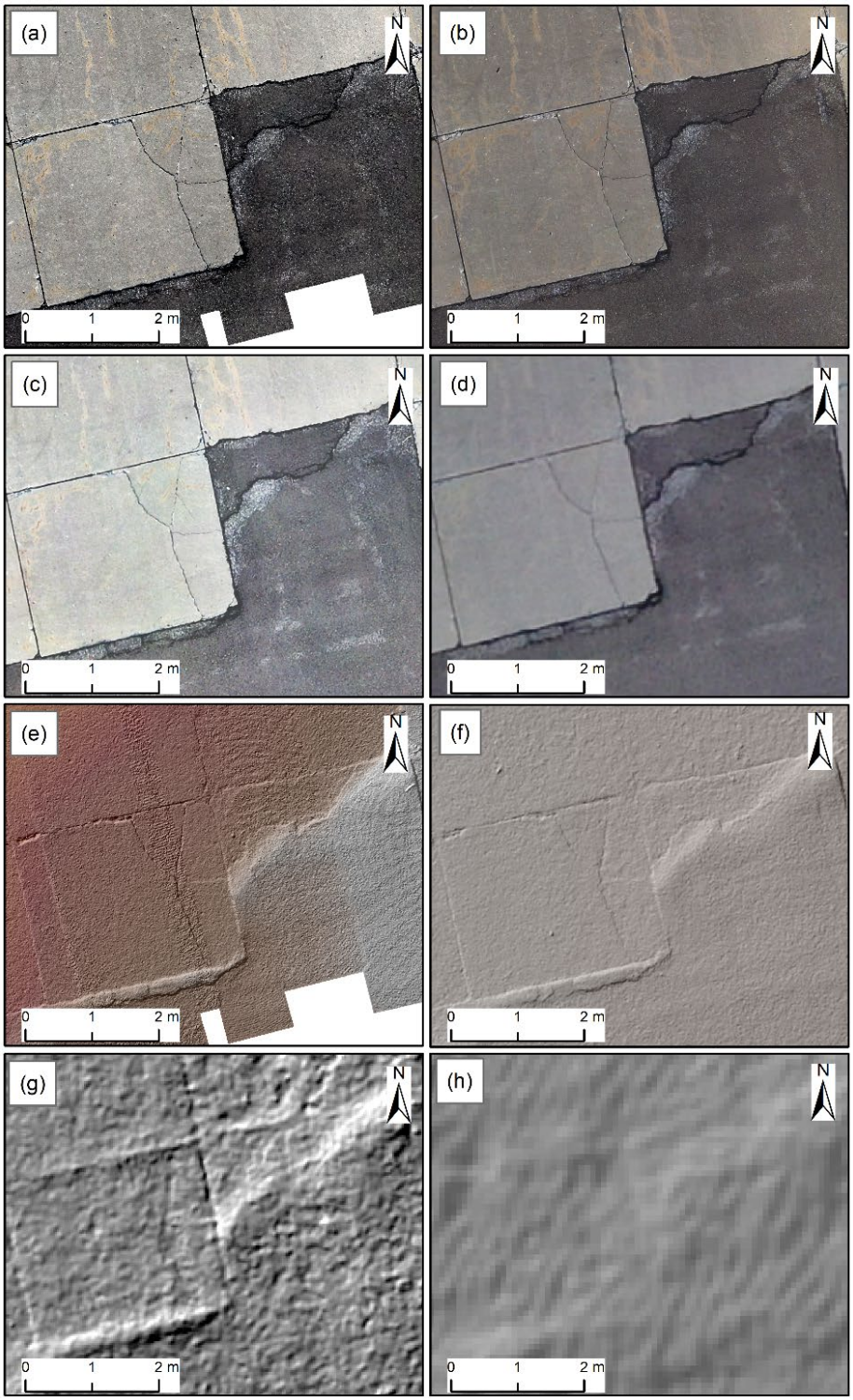

Figure 12. Shattered Slab (M), Large Patching (H), and ASR (L) in (a) 0.8-mm/pix Orthophoto, (b) 2.5-mm/pix Orthophoto, (c) 7.3-mm/pix Orthophoto, (d) 21-mm/pix Orthophoto, (e) 3-mm/pix DEM, (f) 10-mm/pix DEM, (g) 29.1-mm/pix DEM, and (h) 84-mm/pix DEM

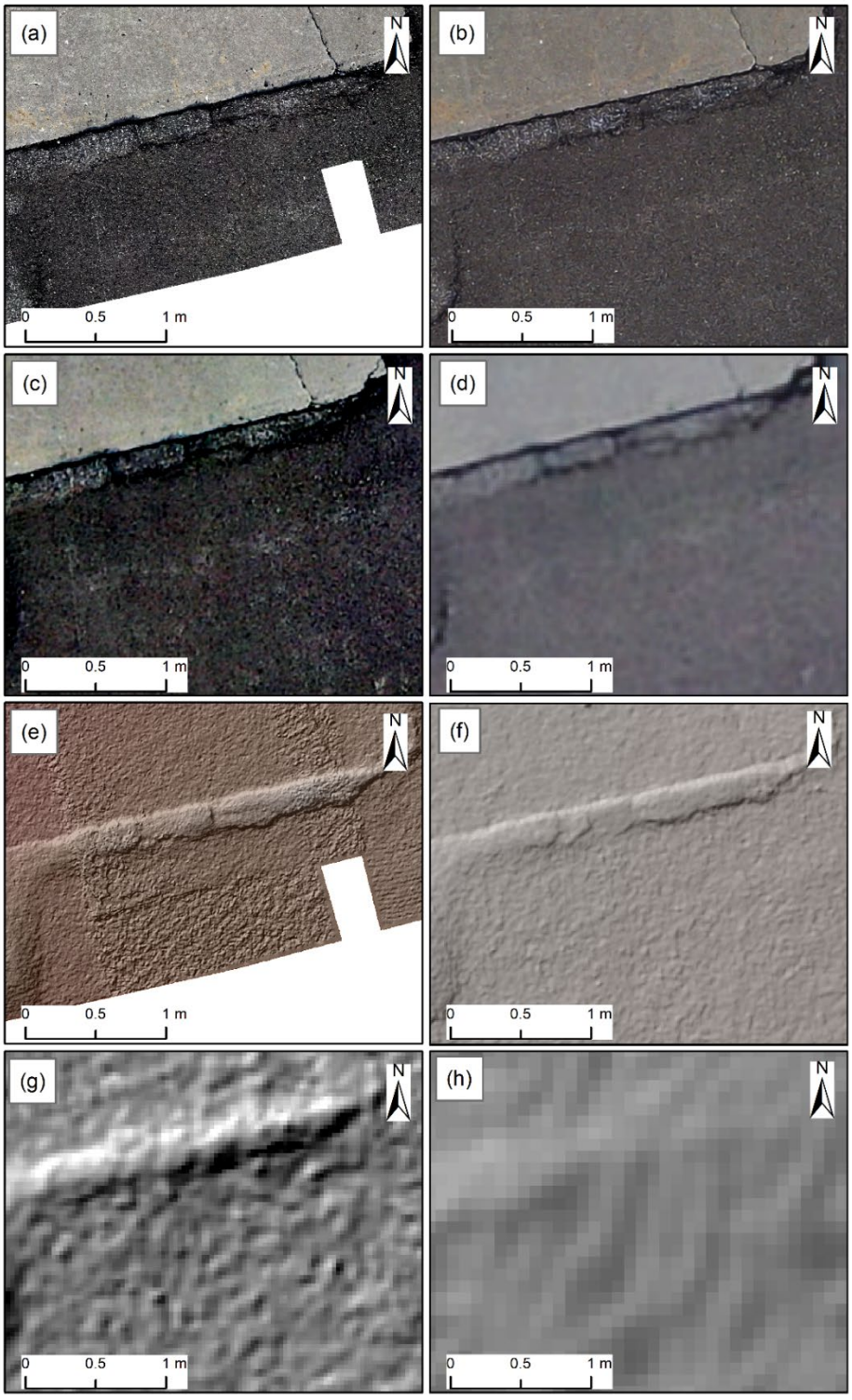

Figure 13. Large Patching (M) in (a) 0.8-mm/pix Orthophoto, (b) 2.5-mm/pix Orthophoto, (c) 7.3-mm/pix Orthophoto, (d) 21-mm/pix Orthophoto, (e) 3-mm/pix DEM, (f) 10-mm/pix DEM, (g) 29.1-mm/pix DEM, and (h) 84-mm/pix DEM

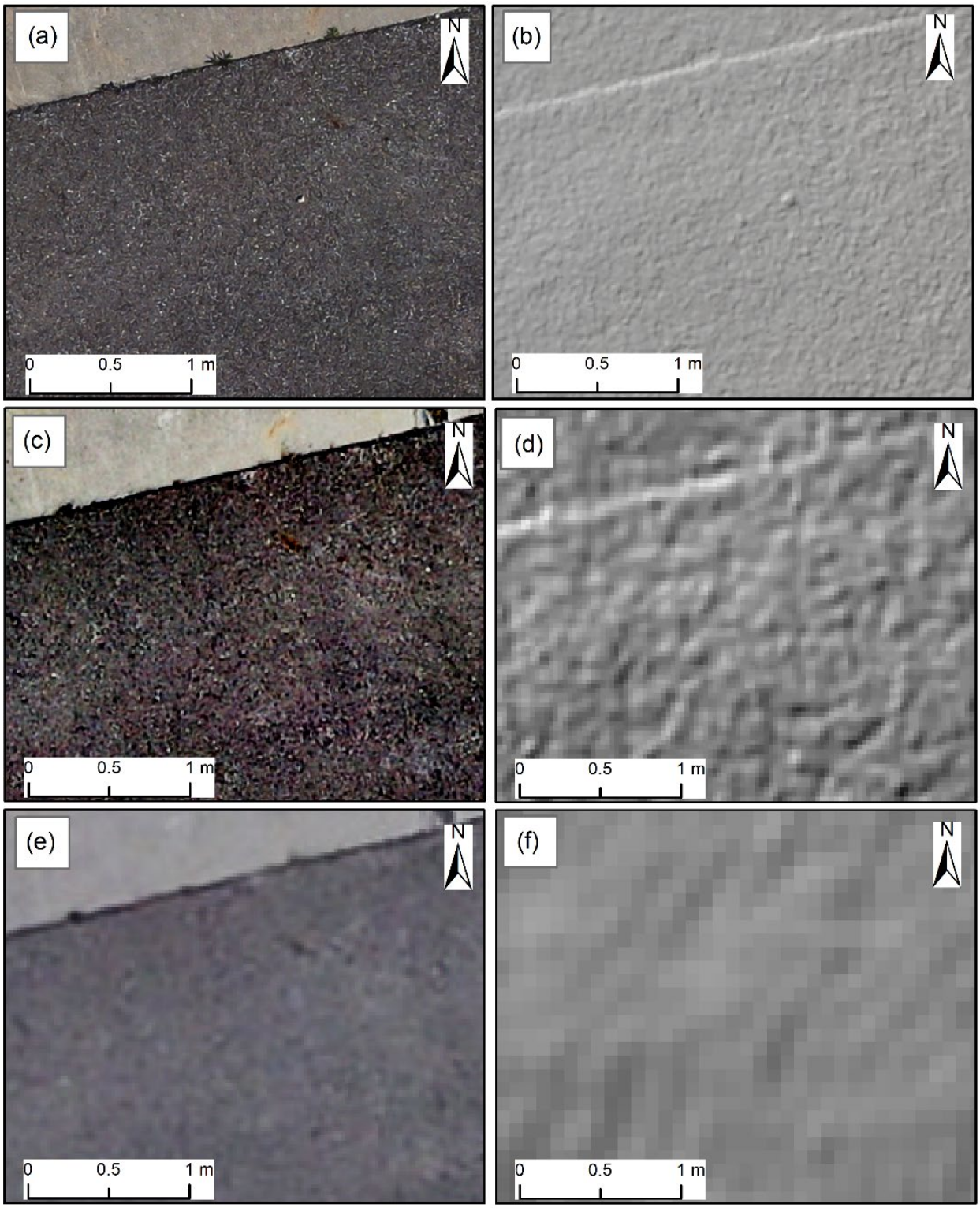

Figure 14. Large Patching (L) and Joint Seal Damage (H) in (a) 2.5-mm/pix Orthophoto, (b) 10-mm/pix DEM, (c) 7.3-mm/pix Orthophoto, (d) 29.1-mm/pix DEM, (e) 21-mm/pix Orthophoto, and (f) 84-mm/pix DEM

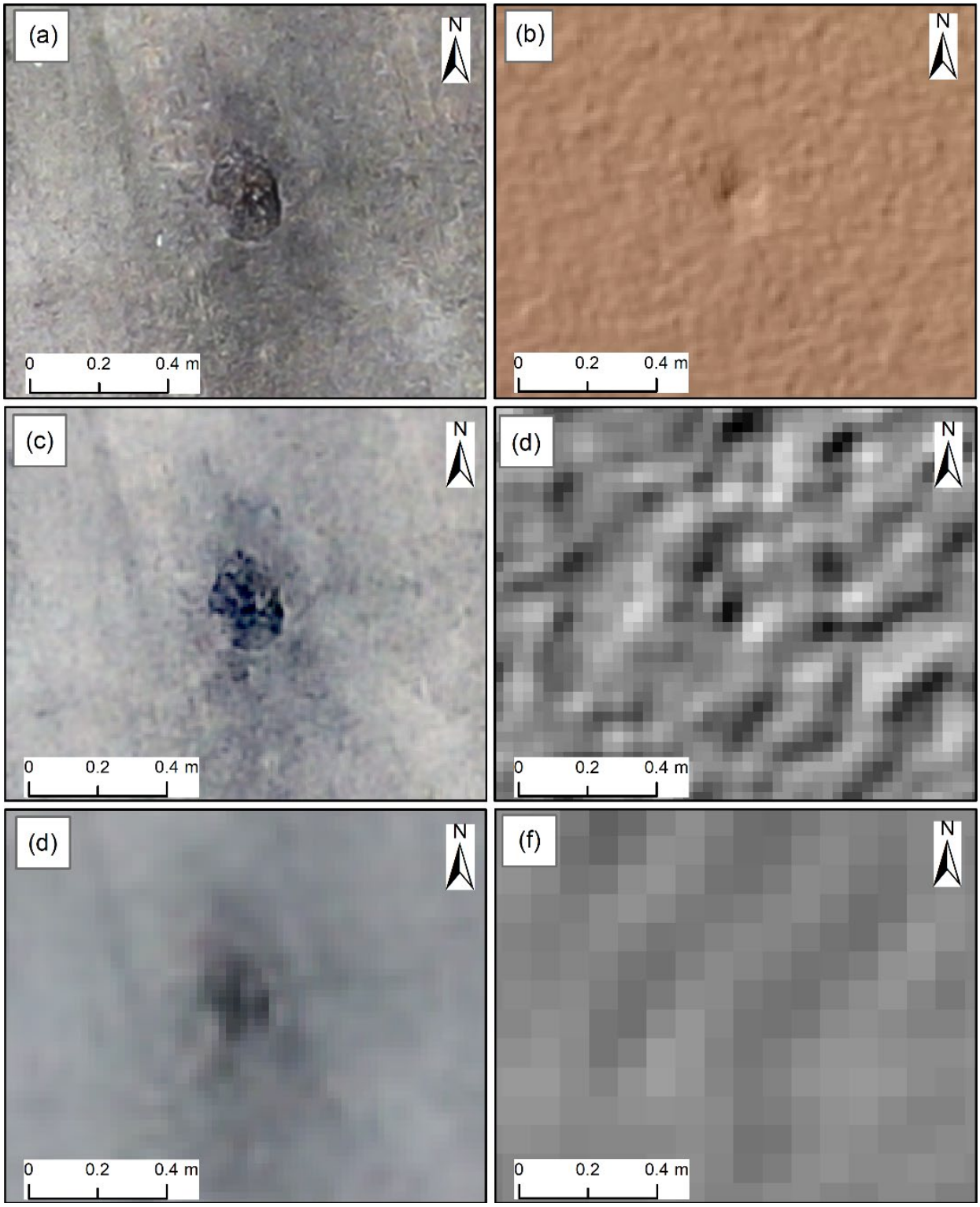

Figure 15. Scaling (M) in (a) 2.5-mm/pix Orthophoto, (b) 10-mm/pix DEM, (c) 7.3-mm/pix Orthophoto, (d) 29.1-mm/pix DEM, (e) 21-mm/pix Orthophoto, and (f) 84-mm/pix DEM

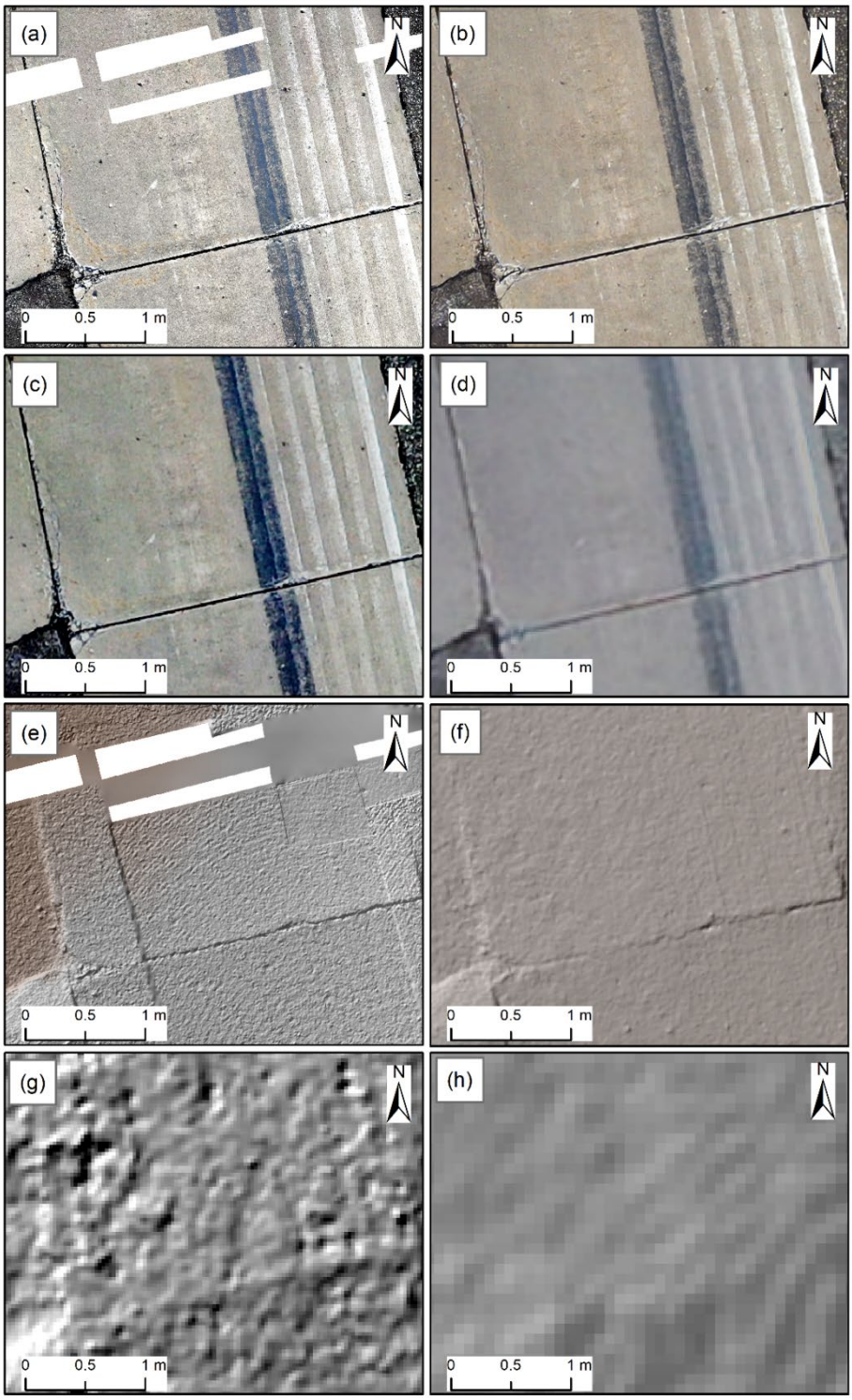

Figure 16. Faulting (M), Durability Cracking (M) in (a) 0.8-mm/pix Orthophoto, (b) 2.5-mm/pix Orthophoto, (c) 7.3-mm/pix Orthophoto, (d) 21-mm/pix Orthophoto, (e) 3-mm/pix DEM, (f) 10-mm/pix DEM, (g) 29.1-mm/pix DEM, and (h) 84-mm/pix DEM

The project team observed that the faulting was challenging to detect in optical RGB orthophoto, regardless of the resolution. Further analysis with 3-mm/pix DEM helped to confirm the location of the faulting through the slab joints. Several polylines were drawn in ArcGIS Pro perpendicular to the slab joint, in which faulting was suspected. Multiple polylines were also drawn perpendicular to the slab joints with no faulting. The Stack Profile (3D Analyst) tool of ArcGIS Pro was used to calculate the pixel value of DEM through the lines (ESRI, 2021b). The output was a table that contained the location of each pixel from the origin of the line and the pixel value, in this case elevation, in that particular point. Figure 17(a) and (b) represent two different lines drawn perpendicular to the slab joint with medium-severity faulting. The DEM showed a 1-cm elevation change where faulting was recorded. Figure 17(c) and (d) represent two additional lines drawn perpendicular to another slab joint without faulting. As shown, the lines on Figure 17(c) and (d) did not show a drastic change in the elevation. However, a similar analysis with a 10-mm/pix DEM created using a 2.5-mm/pix orthophoto collected with M2EA at 15.2 m did not clearly distinguish between slab joints with faulting and slab joints with no faulting.

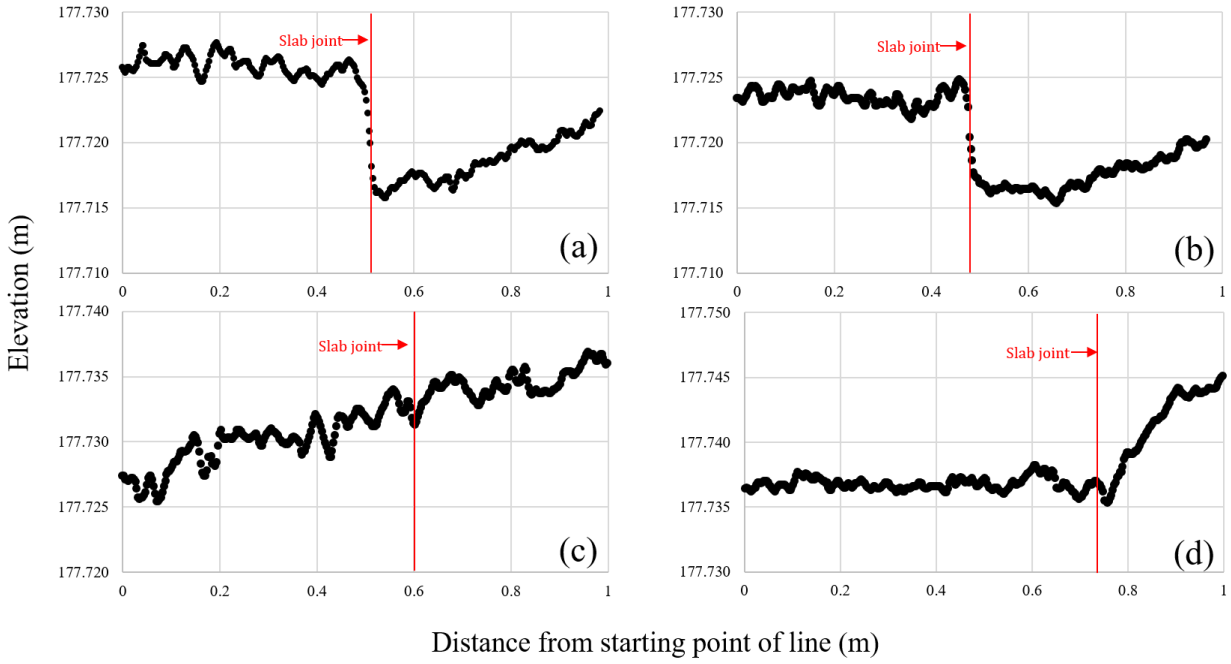

Figure 17. Faulting (M) Detection in 3-mm/pix DEM (a, b) Slab Joint with Faulting (M) Showing a 1-cm Sudden Drop in Elevation, (c, d) Slab Joint Without Faulting Showing No Elevation Drop

Runway 17/35 had a total of 20 sample units where FOG PCI data were collected. The same sample units were visually observed to identify and rate possible pavement distresses. The distresses, severity, and affected slabs or sample units were considered to calculate the PCI value according to the guidelines outlined in ASTM D5340-20. The sUAS PCI and FOG PCI values are plotted and shown in Figure 18. The sUAS PCI values were both higher and lower than the manual PCI. In some cases, low-severity ASR was not detected with the sUAS data, which is the main reason for higher sUAS PCI values compared to the FOG PCIs. Conversely, newly detected LTD cracks

and high-severity durability cracking resulted in lower sUAS PCIs than the FOG PCI. The mean FOG PCI was 34.6, whereas the mean sUAS PCI was 32.9 for all the sample units.

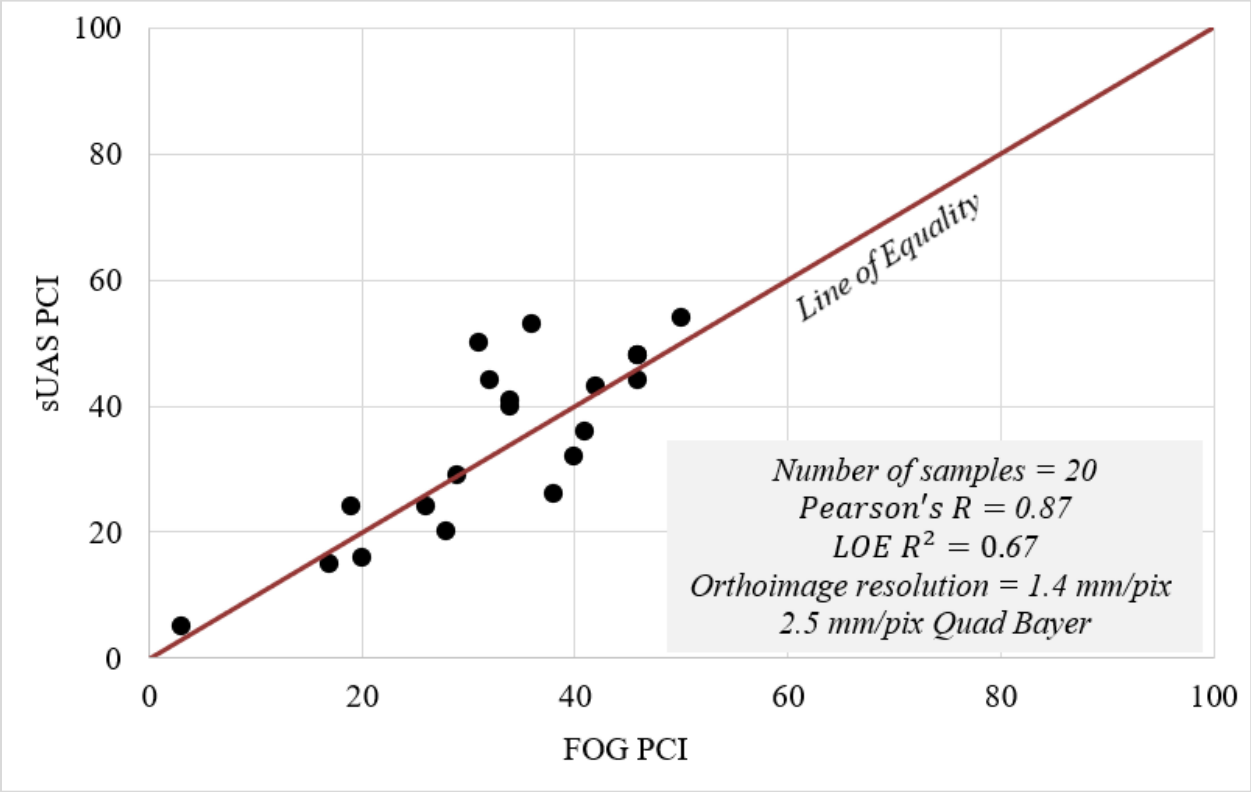

Figure 18. Comparison Between FOG PCI and sUAS PCI Calculated Using 1.4-mm/pix and 2.5-mm/pix Data from ONZ

4.4 CUSTER AIRPORT IN MARCH 2021

4.4.1 Objectives

The research team collected data from Custer Airport (TTF), Monroe, Michigan, at two different times. The first data collection was conducted on March 12, 2021, and the second occurred on March 22, 2021. Data collection efforts were limited on the first day because wind gusts exceeded 40 km/h, therefore a second day was added. The field demonstrations plan had the following objectives:

- Deploy and study the viability of the available platforms and sensors.
- Evaluate the performance of available sUAS platforms and sensors for various distress visualizations.
- Study the effect of different flight altitudes and data resolutions on distress identification.
- Narrow the list of sensors and platforms already recommended based on the first field demonstration at ONZ.

4.4.2 Field Demonstration on March 12, 2021

The research team traveled from MTRI in Ann Arbor, Michigan, to TTF on March 12, 2021, for sUAS data collection. The research team acquired the necessary site permission to fly sUAS at the airport by coordinating with the airport manager in the weeks leading up to the data collection, and the airport manager issued a Notice to Air Mission (NOTAM) for the date of the sUAS data collection. An example of a NOTAM issued at ONZ is "!ONZ 12/009 ONZ AD AP ALL SFC WIP INSPECTION FAA DRONE SURVEY 2012100504-2012102300." A stand-up safety briefing was led by the most senior remote pilot in command and attended by the collection team upon arriving at the airport (Figure 19). This briefing was conducted at the start of data collection. The research team closely monitored the weather in the week leading up to the scheduled data collection, focusing on the temperatures and wind gust speeds, which varied from 9 °C to 12 °C and 16 km/h to 40.2 km/h, respectively.

Figure 19. Safety Briefing at the TTF Airfield Before Beginning Fieldwork

Three sets of sUAS sensors were successfully deployed to collect data on March 12, 2021. These included (a) a Mavic 2 Pro with its integrated 20-mp optical RGB camera, (b) a Bergen Hexacopter with a Nikon D850 45.7-mp optical RGB camera with 50-mm prime lens mounted, and (c) a Mavic 2 Enterprise Dual with an integrated 12-mp optical RGB camera and FLIR 160x120 thermal sensor. Mavic 2 Enterprise Dual is an older model with lower resolutions than the new M2EA that became available later in this study.

The Bergen Hexacopter platform was used to carry the Nikon D850 optical RGB camera with a 50-mm prime lens to collect sUAS data of the sample units, shown in Figure 20, from 18.3 m flight altitude. The flights were conducted manually by an experienced sUAS pilot. The sample units were close to one another, and together they had all AC pavement distresses recorded at TTF. Table 8 presents the list of data collected at TTF in March 2021. As the table shows, high-resolution sample unit data were collected from Runway 3/21 sample unit 53 (RW321 SU 53) and

Taxiway A sample units 23 (TWA-10 SU 23) and 25 (TWA-10 SU 25). This high-resolution data collection aimed to narrow down the list of sensors for further deployment in future airports.

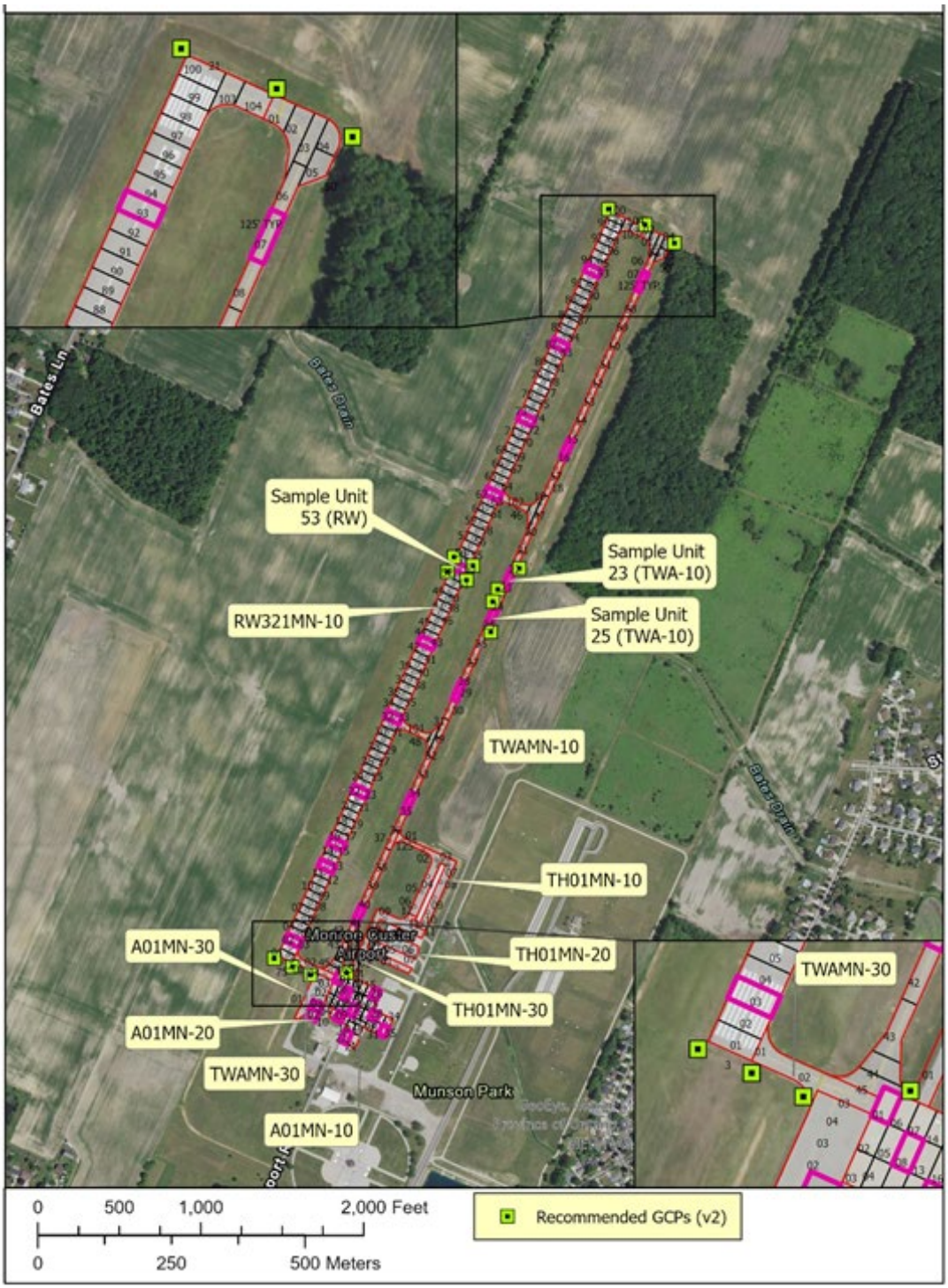

Figure 20. Sample Unit Focus Area at TTF with Recommended GCP Locations

Table 8. Summary of sUAS Data Collection at TTF in March 2021

Target Areas	sUAS Platforms	Sensors	Flight Altitude (m)	Resolution (mm/pix)	
				Orthophoto	DEM
TWA-10 SU 23 and SU 25	Bergen Hexacopter	45.7-mp optical RGB Nikon D850	18.3	1.5	6
		FLIR Vue Pro R	18.3	14.3	N/A
		Tetracam multispectral	18.3	10	N/A
RW321 SU 53	Bergen Hexacopter	45.7-mp optical RGB Nikon D850	9.1	0.8	3
			18.3	1.5	5.8
		FLIR Vue Pro R	18.3	14.3	N/A
		Tetracam multispectral	18.3	10	N/A
	Mavic 2 Enterprise Dual	12 mp optical RGB + FLIR 160x120 pixel thermal	15.2	4.9	19.6
	mdMapper1000 +	42.4-mp optical RGB Sony RX1R-II	18.3	2.3	9.2
Taxiway A	Mavic 2 Pro	20-mp optical RGB	24.4	5.6	22.5
			30.5	7.2	28.6
Runway 3/21	Mavic 2 Pro	20-mp optical RGB	24.4	5.8	23
			30.5	7.0	27.9

RW321 = Runway 3/21 TWA-10 = Taxiway A
SU = Sample unit N/A = Not applicable

4.4.3 Field Demonstration on March 22, 2021

The research team traveled from MTRI in Ann Arbor, Michigan to TTF on March 22, 2021, for a second sUAS data collection effort (Figure 21). The recorded temperature varied between 13 °C and 20 °C, whereas the recorded wind speed was from 4.8 km/h to 17.6 km/h with gusts up to 31.1 km/h in the afternoon, respectively. Five sUAS were successfully deployed to collect data on March 22, 2021: (a) a Mavic 2 Pro with its integrated 20-mp optical sensors, (b) a Bergen Hexacopter with Nikon D850 45.7-mp optical RGB Camera with 50-mm prime lens mounted, (c) a Bergen Hexacopter with a FLIR VUE Pro R 640x512 thermal sensor, (d) a Bergen Hexacopter with a Tetracam Micro-MCA6 multispectral camera, and (e) an mdMapper1000+ with a 42.4-mp optical RGB Sony RX1R-II. Table 8 provides the details of the focus area collected data type, sUAS platform, and sensors.

Figure 21. High-Resolution sUAS Data Collection with mdMapper1000+ and Bergen Hexacopter sUAS Platforms

The FOG pavement inspection team traveled to TTF and conducted an airfield pavement distress survey in accordance with the ASTM D5340-20 standard (ASTM International, 2020). The team located, identified, and recorded the pavement distresses system onto their handheld GPS-enabled field data collection tablet. The data were processed, and the PCI values for all sample units and branches of the airfield pavement were calculated based on the ASTM D5340-20 standard. Eleven sample units from Runway 3/21, and seven sample units from Taxiway A were surveyed. Both airfield pavement sections surveyed had AC surfaces, and the PCI values varied from 66 to 90 for Runway 3/21 and from 56 to 63 for Taxiway A. The predominant distresses were L&T cracks, swelling, weathering, raveling, and depressions. Eight apron sample units were also surveyed but sUAS data collection was not focused on this area.

4.5 CUSTER AIRPORT IN MAY 2021

4.5.1 Objectives

The research team collected full high-resolution data in May 2021 at TTF to enable use of a new sUAS and to test simultaneous flights. A particular set of sUASs and their flight altitudes were selected for this field demonstration based on the conclusions from earlier field demonstrations executed at ONZ and TTF. The objectives of this field demonstration are as follows:

- Perform full data collection using M2EA.
- Evaluate the performance of the thermal data collected using M2EA.
- Evaluate the applicability of simultaneous data collection using more than one sUAS.

4.5.2 Field Demonstration in May 2021

The research team traveled from MTRI in Ann Arbor, Michigan, to TTF to collect complete field data on May 21, 2021. The main focus of this data collection was to use a single sUAS to collect the complete data of Runway 3/21 and Taxiway A. The research team contacted the airport authority in advance and was permitted to collect data again. TTF is a general aviation airport with only a few daily aircraft operations, enabling the team to plan and complete data collection in 1 day. The wind speed was relatively low, fluctuating from 8 km/h to 16 km/h, and facilitated the flight of mdMapper1000+, which is susceptible to high wind speed. The highest recorded wind speed during data collection was 18 km/h.

The mdMapper1000+ with 42.4-mp optical RGB Sony RX1R-II camera was flown over Runway 3/21 sample unit 53, Taxiway A sample units 23 and 25 at 22 m and 30.5 m altitudes to collect 3 mm/pix and 5 mm/pix, as requested by the FAA representatives for this project. Three different flights were conducted and completed in 15 minutes total. An 80% forward overlap and 70% side overlap were used. Afterward, two M2EA were used for complete RGB optical data collection from Runway 3/21 and Taxiway A at 15.2 m. The same systems were used to collect sample unit thermal data from 24.4 m with the 640x512 pixel thermal sensor. The data were simultaneously collected with two pilots in command, each with a dedicated visual observer. Table 9 provides the flight details and data collection focus areas.

A total of 10 AeroPoints™ were used, as shown in Figure 22, which also shows the sample units. The AeroPoints™ locations were also used to adjust the location information of the images, which were recorded with the onboard GPS of the sUAS, and to generate orthophotos.

Table 9. Summary of sUAS Data Collection at TTF in May 2021

Target Areas	sUAS Platform	Sensors	Flight Altitude (m)	Resolution (mm/pix)	
				Orthophoto	DEM
TWA-10 SU 23 and SU 25, and RW321 SU 53	mdMapper1000+	42.4-mp optical RGB Sony RX1R-II	30.5	5.0	15
	M2EA	640x512 thermal	24.4	31.5	N/A
TWA-10 SU 23 and SU 25	mdMapper1000+	42.4-mp optical RGB Sony RX1R-II	22	3.1	6.2
Taxiway A	M2EA	48-mp optical RGB Quad Bayer	15.2	2.4*	9.7
RW321	M2EA	48-mp optical RGB Quad Bayer	15.2	2.4*	9.6

RW321 = Runway 3/21 TWA-10 = Taxiway A
SU = Sample unit DEM = Digital Elevation Model
N/A = Not applicable
*2.4 mm/pix is not the true effective resolution due to being derived from the M2EA 48-mp Quad Bayer camera.

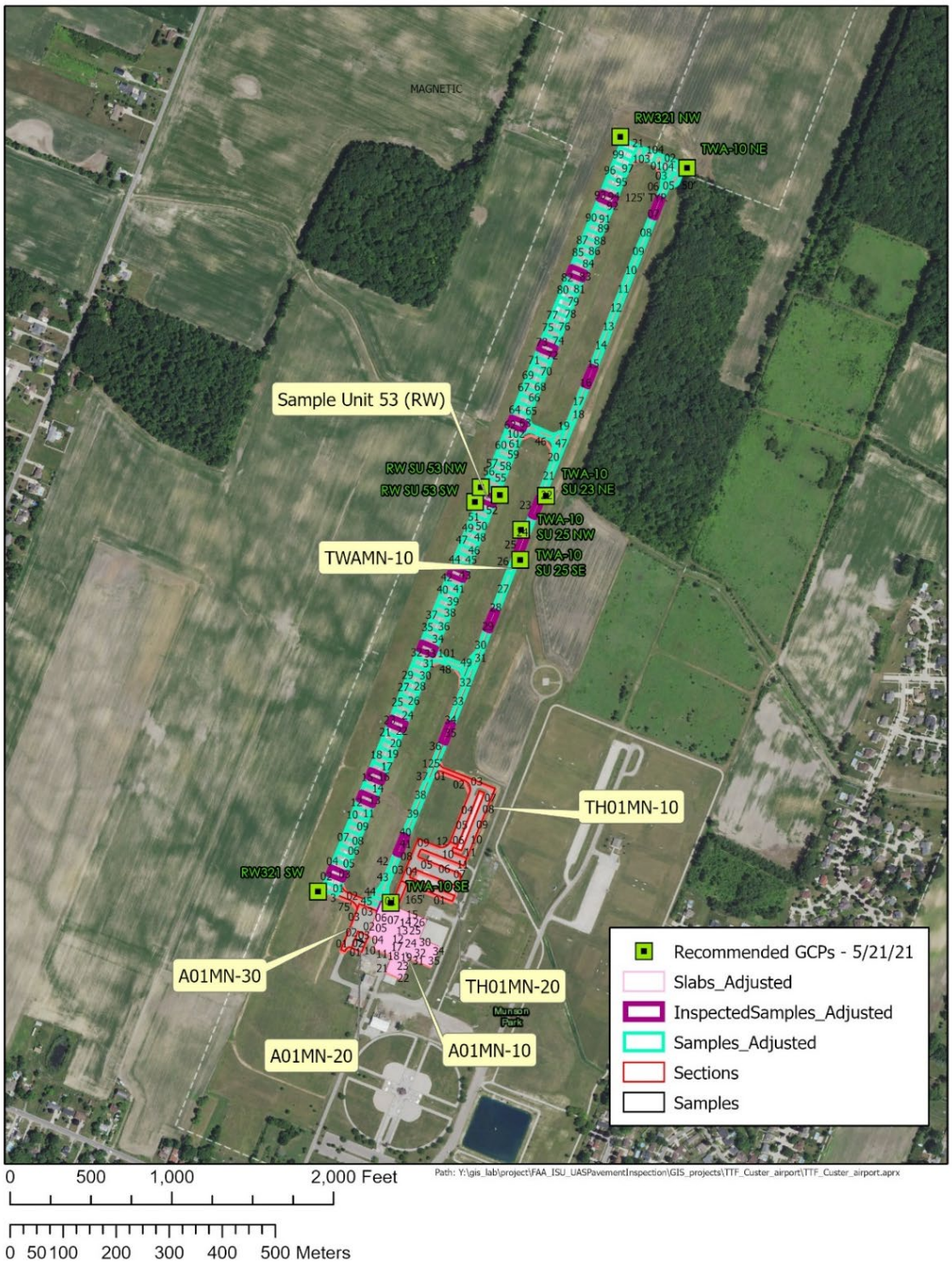

Figure 22. Location of the GCPs and Sample Units in May 2021

4.6 RESULTS AND DISCUSSION

4.6.1 Results and Discussion of March 2021 Data Analysis

All data collected from TTF were imported into Agisoft Metashape separately, and image locations were updated using the GCPs. The GCP data were collected with a combination of the Trimble® GeoExplorer® GeoXH 6000 GPS unit and AeroPoints™. The data were processed to export optical RGB orthophoto and DEM. The DEM images were further processed in ArcGIS Pro to create hillshades for better visualization of elevation changes. Different sets of RGB optical data were compared in ArcGIS Pro to check their capabilities for airfield pavement distress detection and severity rating. The results of the analysis of data collected in March 2021 are discussed below.

- Collecting 0.8-mm/pix data with the Nikon D850 mounted on the Bergen Hexacopter flying at 9.1 m altitude was very slow, requiring many closely spaced images to create the needed image overlap for orthophoto construction. Additionally, a complete orthophoto of the Runway 3/21 sample unit 53 was not constructed properly due to difficulties in achieving a consistent overlap when manually flying this older sUAS system that did not have pre-planned flight capabilities. The RGB orthophoto of this resolution was found to be useful for clearly viewing both sealed and unsealed L&T cracks and measuring their width for crack severity determination (Figures 23 to 25).

- The Bergen Hexacopter carrying the Nikon D850 and providing 1.5-mm/pix data performed slightly better than the 2.3 mm/pix of the mdMapper1000+ data collected at 18.3 m (Figures 23 to 25). However, the difference in the performance of their associated DEM (5.8 mm/pix and 6 mm/pix for Nikon D850 and 9.2 mm/pix for the mdMapper's Sony camera) was much more noticeable, especially for delineation of the width of sealed and unsealed L&T cracks (Figures 23 and 24). Both the resolutions are recommended for future airport pavement data collection.

- Both optical RGB orthophotos created using data collected by the Mavic 2 Pro and Mavic 2 Enterprise could be used to identify sealed and unsealed L&T cracks. However, the width of narrow sealed cracks could not be measured because of comparatively lower orthophoto resolution (4.9 mm/pix–7.2 mm/pix) (Figures 23 and 24).

- Mavic 2 Pro's 5.6-mm/pix to 7.2-mm/pix, and Mavic 2 Enterprise's 4.9-mm/pix RGB orthophoto can be used only to detect both sealed and unsealed L&T cracks, but not to detect associated severities (Figures 23 to 25).

- The 22.5-mm/pix to 28.6-mm/pix DEMs generated using Mavic 2 Pro data, collected at 24.4-m and 30.5-m heights, offered almost no value for any distress detection. In addition, DEM data of 19.6 mm/pix collected with the Mavic 2 Enterprise Dual provided minimum visual information. Nikon D850 data captured at 9.1-m and 18.3-m flight altitude with resolutions of 3 mm/pix and 5.8 mm/pix, respectively, were useful to detect delaminated areas and L&T cracks on the sample units. In addition, mdMapper1000+'s 9.2-mm/pix data also were very useful for L&T cracks detection (Figure 26). Thus, any DEM with a resolution finer than 20 mm/pix was recommended for future data collection.

- Regardless of the data format, swell, raveling, and weathering distresses were found to be difficult to identify using the collected data (Figure 27).

- The FLIR Vue Pro R thermal camera was mounted on the Bergen Hexacopter and flown at 18.3-m altitude over all three sample units. The resulting images had a resolution of 14.3 mm/pix, which proved to be sufficient for the identification of both sealed and unsealed L&T cracks (Figure 28). In addition, a sealed (and white-painted) L&T crack that ran through white-painted pavement markings was visible only in the thermal imagery (not in optical imagery) because this thermal sensor records temperature differences between cracks and their neighboring areas in both painted and unpainted areas.

The TTF data collection helped the research team to recommend the following platform, sensor, and flight altitudes for the full data collection:

- Bergen Hexacopter with Nikon D850 45.7 mp flown at 18.3 m altitude, or a system with equivalent optical RGB resolution capability.

- Bergen Hexacopter with FLIR Vue Pro R 640x512 flown at 18.3 m altitude, or a system with equivalent thermal resolution capability.

- M2EA with a 48-mp effective camera and 640x512 thermal system, flown at 15.2-m altitude, might be ideal for deployment. This could replace the need for the older, larger, and slower Bergen systems that exclusively require manual flight.

- DJI Mavic 2 Pro with 20-mp camera or DJI Mavic 2 Enterprise with 12-mp camera flown at 15.2 m altitude. However, these are likely to be redundant if the M2EA dual-imaging system meets expectations.

- mdMapper1000+ with Sony 42.4-mp Sony RX1R-II at 30.5 m altitude. This system has a longer duration (up to 30 minutes) flight time, is larger, and is a faster platform that could replace the need for the Bergen system. However, to operate properly, this system needs wind conditions consistently below 24 km/h, which limits its deployment practicality. Similar systems, such as the Tarot X6, were becoming available for the study, and the research team expected that system would replace the need for the mdMapper1000+ system, which it did.

The effect of using these platforms on the recommended resolutions for the rest of the data-collection efforts can be summarized as:

- Any system and elevation that produces RGB orthophoto outputs with smaller (better) than 5-mm/pix resolution or better, which provides the best results for distress detection and rating.

- Any system and elevation that produces DEM outputs with smaller (better) than 20-mm/pix resolution.

- Any system and elevation that produces thermal merged imagery outputs with smaller (better) than 20-mm/pix resolution.

Fixed-wing systems could meet the abovementioned recommendations if they can be safely operated in an airport environment. The survey team found that the rapid landing capabilities of multirotor systems are helpful for operating at airports. Some newer fixed-wing systems start as vertical takeoff and landing (VTOL) aircraft and then transition into fixed-wing flight. These could provide the rapid response to changing air traffic and weather conditions that is sometimes needed when collecting unmanned aircraft vehicle (UAV) data at operating airports.

4.6.2 Results and Discussion of May 2021 Data Analysis

The data collected from TTF in May 2021 were separately imported into Agisoft Metashape and processed to create RGB optical orthophotos and DEMs. These data were compared with the sUAS data collected in March 2021. The comparisons are shown in Figures 23 through 26.The following lessons were learned from the comparisons:

- The 2.4-mm/pix data collected using the M2EA provided less visual information than similar resolution data collected using mdMapper1000+ with a 42.4-mp optical RGB Sony RX1R-II camera. The M2EA's 48-mp sensor is a Quad Bayer sensor and has an actual resolution of 12 mp. Therefore, the Mavic 2 Pro with a 20-mp integrated RGB optical camera at 15.2 m was recommended for future data collection.

- The FLIR Vue Pro R and thermal sensor of the M2EA have identical resolution: 640x512. The FLIR Vue Pro R had to be mounted on the Bergen Hexacopter because of the combined weight of the sensor and its dedicated battery. This sUAS was manually operated over sample units with the older flight controller. In addition, the FLIR Vue Pro R does not collect and embed GPS information in its thermal images, making them challenging to process into a merged, georeferenced output geospatial layer. Conversely, the stereo-thermal camera data of M2EA can be collected using mission-planning software, and all captured images have embedded GPS data, making it easier to process into a merged, georeferenced output layer. In addition, the 31.5-mm/pix stereo-thermal data of the M2EA provides useful visual information regarding the location of the L&T cracks on the AC surface and the cracks under the pavement marking (Figure 28). Considering all these factors, the M2EA was recommended for stereo-thermal data.

Based on the data collected at TTF in March 2021 and May 2021, the airfield pavement distresses shown in Table 10 were found to be detectable.

Table 10. Summary of the Findings of TTF

Distress Name (PAVER™ Distress Number)	Severity	Resolution Tested (mm/pix)		Detected in Maximum Resolution (mm/pix)		Remarks
		Orthophoto	DEM	Orthophoto	DEM	
L&T cracking (48)	L	0.8, 1.5, 2.3, 2.4*, 4.9, 5.6, 5.8, 7, 7.2	3, 5.8, 6, 9.2, 9.6, 9.7, 19.6, 22.5, 23, 27.9, 28.6	7.3	9.2	Figure 23 to Figure 26
	M				19.6	
Raveling (52)	L	0.8, 1.5, 2.3, 2.4*, 4.9, 5.6, 5.8, 7, 7.2	3, 5.8, 6, 9.2, 9.6, 9.7, 19.6, 22.5, 23, 27.9, 28.6	ND	ND	
	M	2.4*, 5.6, 5.8, 7, 7.2	22.5, 23, 27.9, 28.6	ND	ND	
Swell (56)	L	2.4*, 5.6, 5.8, 7, 7.2	22.5, 23, 27.9, 28.6	ND	ND	Figure 27
Weathering (57)	L	0.8, 1.5, 2.3, 2.4*, 4.9, 5.6, 5.8, 7, 7.2	3, 5.8, 6, 9.2, 9.6, 9.7, 19.6, 22.5, 23, 27.9, 28.6	ND	ND	Figure 23 to Figure 27
	M	2.4*, 5.6, 5.8, 7, 7.2	22.5, 23, 27.9, 28.6	ND	ND	

L = Low, M = Medium, H = High
ND = Not detected
*2.4 mm/pix is not true resolution due to being derived from the Mavic 2 Enterprise Advanced 48-mp Quad Bayer camera.

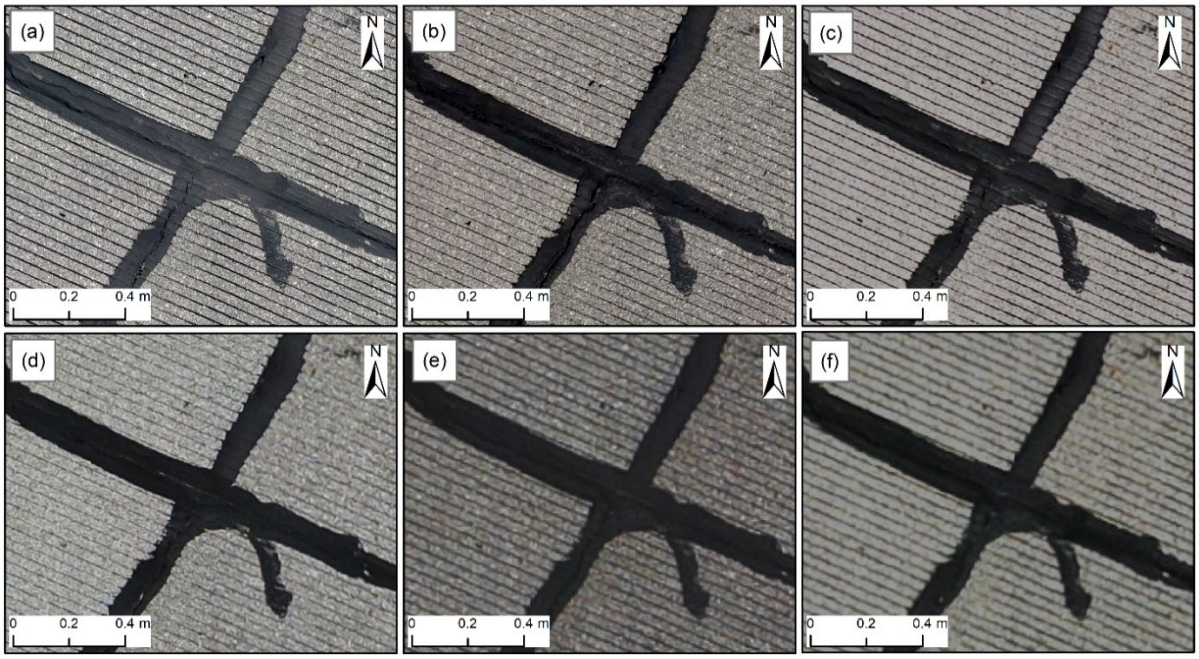

Figure 23. Sealed L&T Cracks (medium severity on top left side, low severity on top side) and Weathering (L) on Asphalt Overlay Over Asphalt Concrete Pavement at TTF: (a) 0.8-mm/pix Orthophoto, (b) 1.5-mm/pix Orthophoto, (c) 2.3-mm/pix Orthophoto, (d) 2.4-mm/pix Orthophoto, (e) 4.9-mm/pix Orthophoto, and (f) 5.8-mm/pix Orthophoto

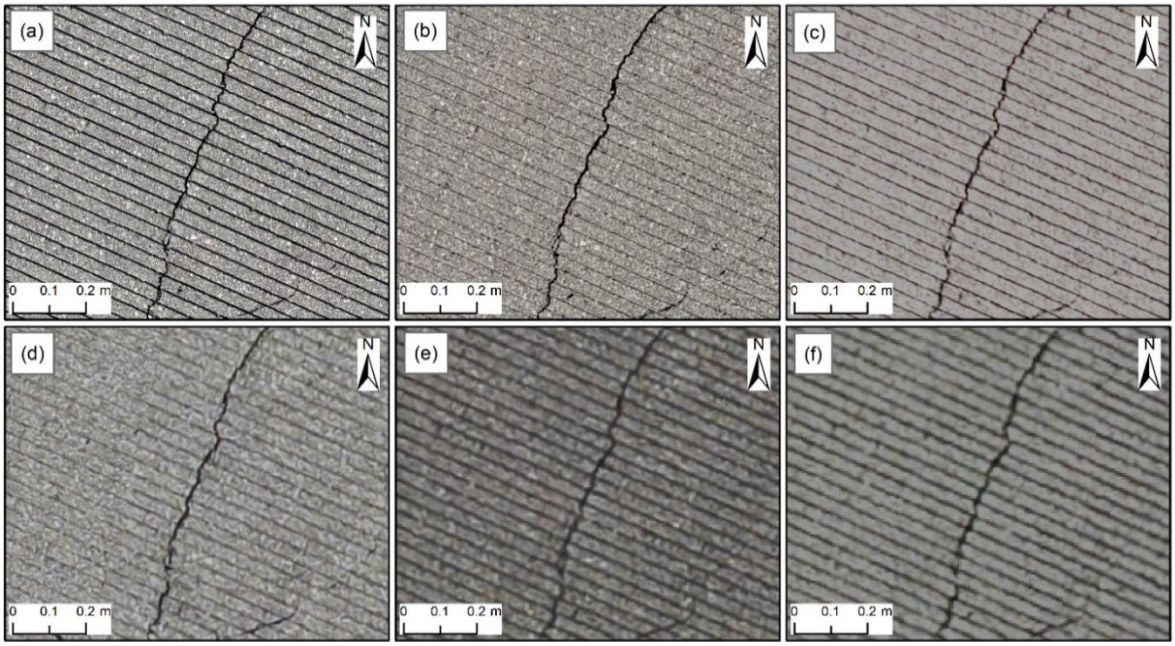

Figure 24. Unsealed L&T cracks (L) and Weathering (L) on Asphalt Overlay Over Asphalt Concrete Pavement at TTF: (a) 0.8-mm/pix Orthophoto, (b) 1.5-mm/pix Orthophoto, (c) 2.3-mm/pix Orthophoto, (d) 2.4-mm/pix Orthophoto, (e) 4.9-mm/pix Orthophoto, and (f) 5.8-mm/pix Orthophoto

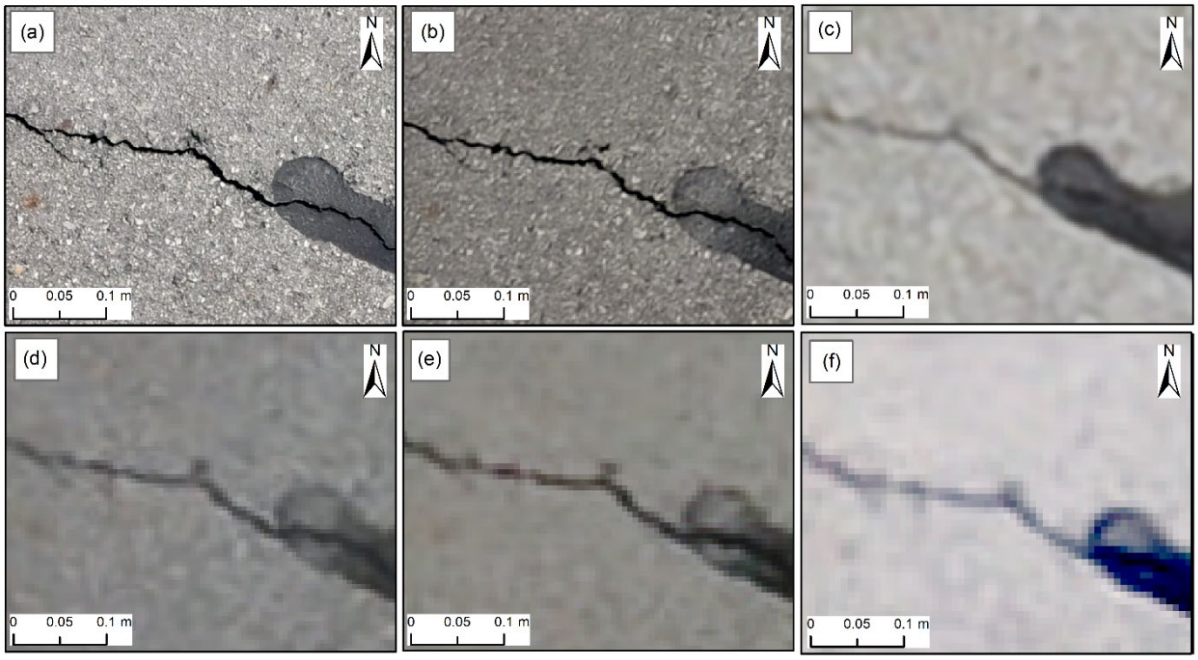

Figure 25. Unsealed L&T Cracks (M) and Weathering (L) on Asphalt Overlay Over Asphalt Concrete Pavement at TTF: (a) 0.8-mm/pix Orthophoto, (b) 1.5-mm/pix Orthophoto, (c) 2.4-mm/pix Orthophoto, (d) 4.9-mm/pix Orthophoto, (e) 5.6-mm/pix Orthophoto, and (f) 7.2-mm/pix Orthophoto

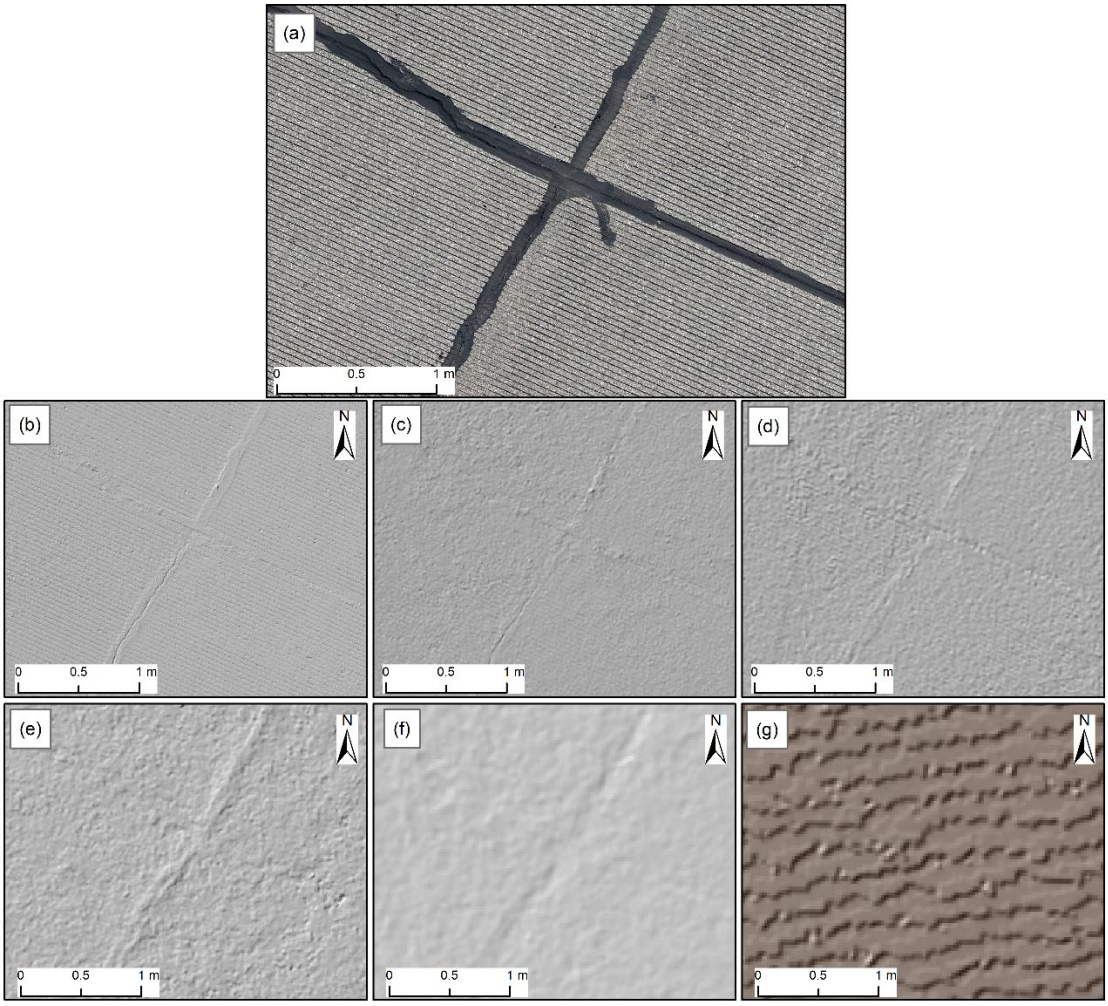

Figure 26. Sealed L&T Cracks and Weathering (L) on Asphalt Overlay Over Asphalt Concrete Pavement at TTF: (a) 0.8-mm/pix Orthophoto, (b) 3-mm/pix DEM, (c) 5.8-mm/pix DEM, (d) 9.2-mm/pix DEM, (e) 9.6-mm/pix DEM, (f) 19.6-mm/pix DEM, and (g) 23-mm/pix DEM

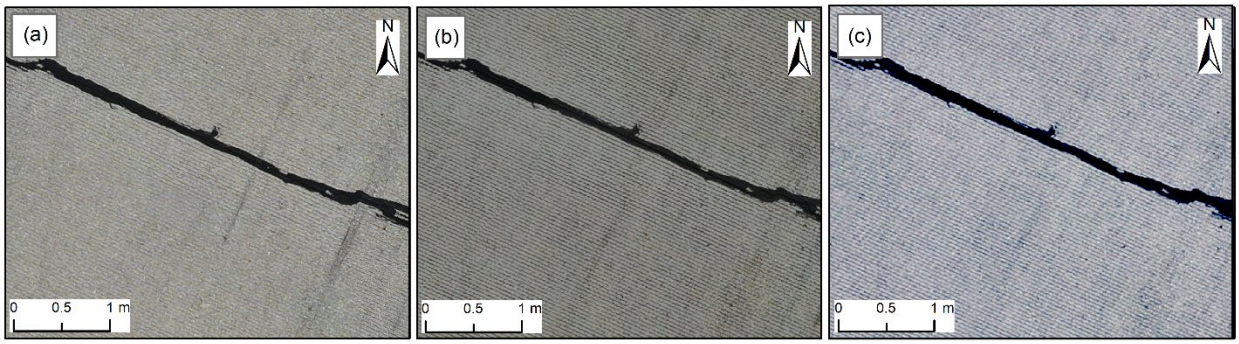

Figure 27. Swell (L) and Weathering (L) on Asphalt Overlay Over Asphalt Concrete Pavement at TTF: (a) 2.4-mm/pix Orthophoto, (b) 5.8-mm/pix Orthophoto, and (c) 7-mm/pix Orthophoto

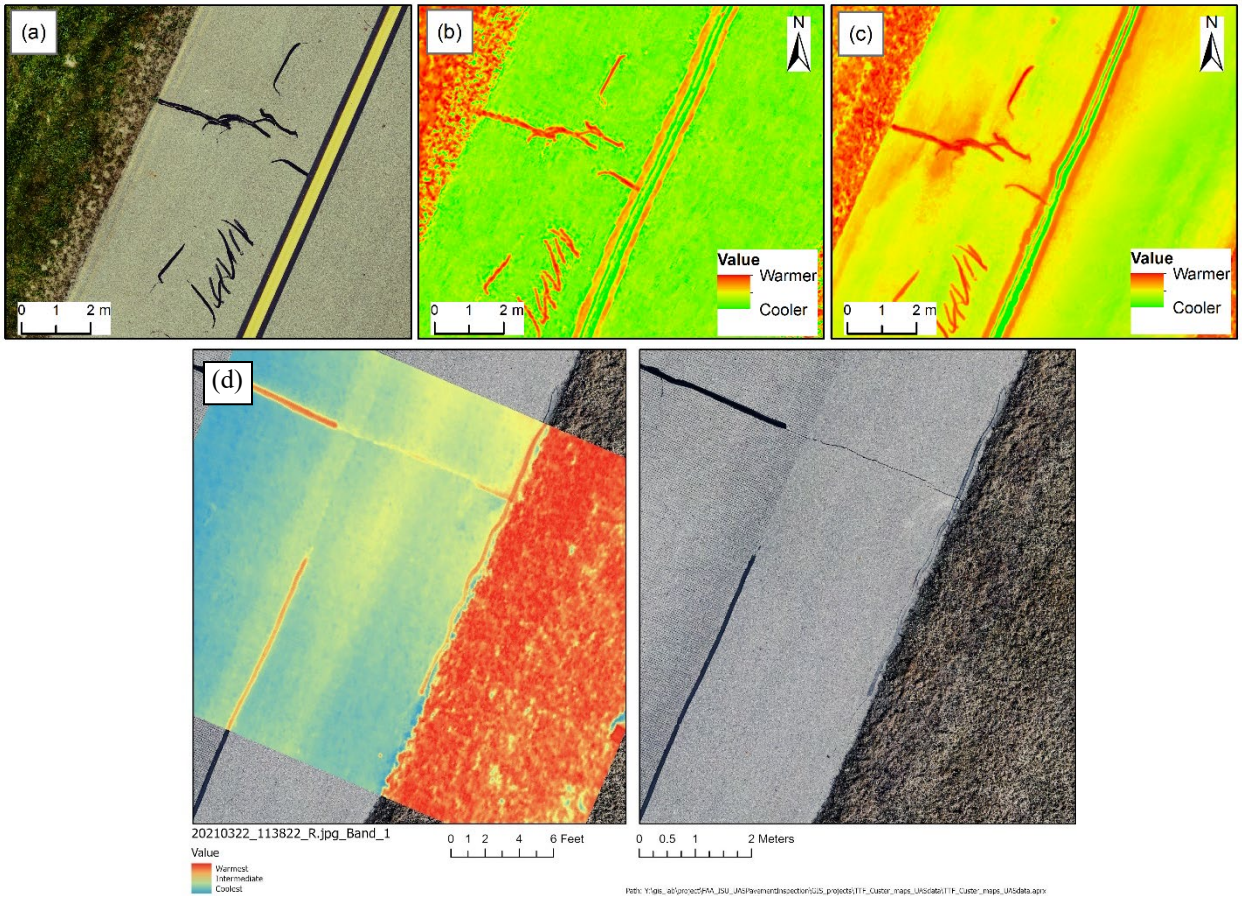

Figure 28. Sealed L&T Cracks on AC Pavement in Taxiway A Sample Unit 23 at TTF: (a) 1.5-mm/pix Orthophoto, (b) 31-mm/pix Stereo Thermal, (c) 14-mm/pix Stereo Thermal, and (d) Another View of Cracks in the 14-mm/pix Stereo-Thermal Results Compared to an Orthophoto of the Same Area

There were 18 priority sample units selected for high-resolution sensing on Runway 3/21 and Taxiway A, where FOG PCI data were also collected. The 2.4-mm/pix RGB optical data collected with the M2EA were visually observed in ArcGIS Pro. Each airfield pavement distress on the sample units was quantified, and associated severity levels were detected. The recorded data were used to estimate the PCI value by following the guidelines outlined in ASTM D5340-20 (ASTM International, 2020). Apart from one sample unit, all sample units had higher PCI values in sUAS-based inspections compared to the FOG inspection PCI values, as shown in Figure 29. The higher PCI values were mostly due to weathering, swell, and raveling that could not be detected from the sUAS data with 2.4-mm/pix resolution.

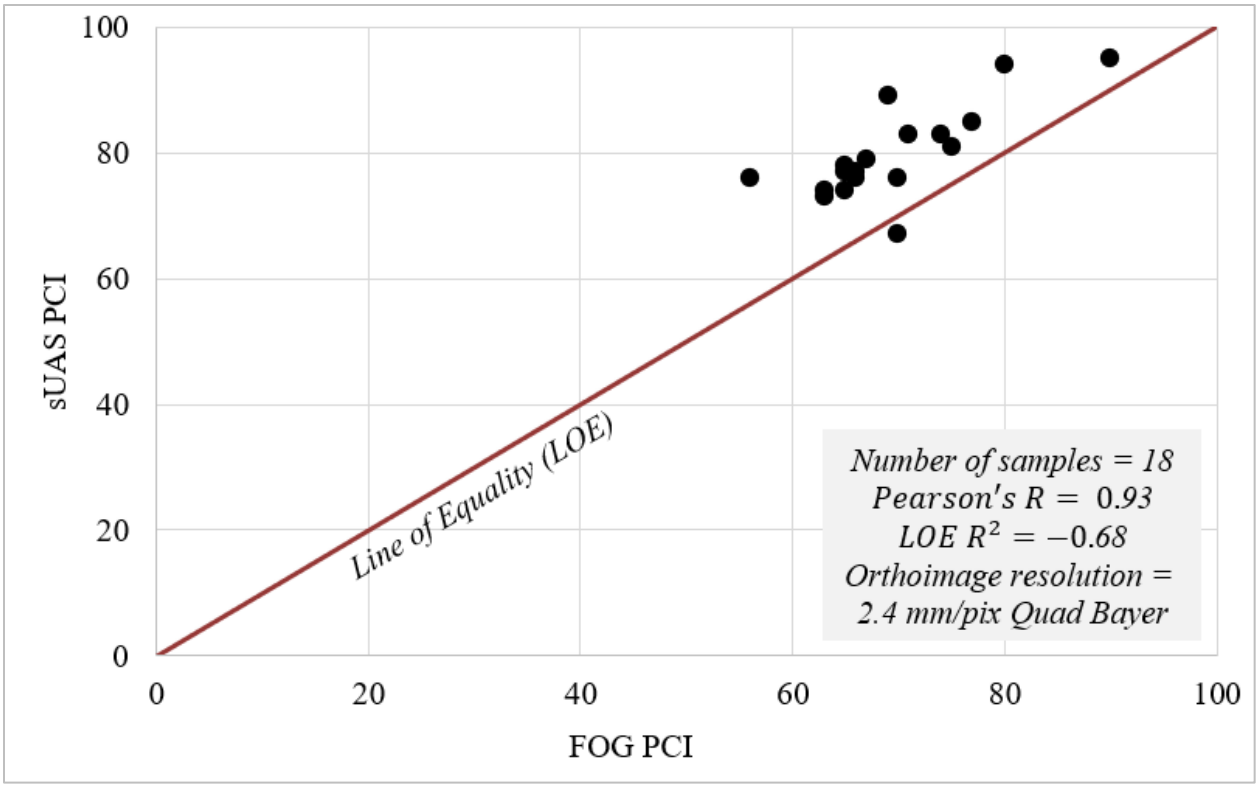

Figure 29. Comparison Between FOG PCI and sUAS PCI Calculated Using 2.4-mm/pix Data from TTF

5. FIELD DEMONSTRATION IN ILLINOIS

5.1 COLES COUNTY MEMORIAL AIRPORT IN JUNE 2021

5.1.1 Objectives

The research team collected sUAS data from Coles County Memorial Airport (MTO), Mattoon, Illinois, on June 16 and 17, 2021. MTO was the largest airport surveyed during this research. Based on the lessons learned from ONZ and TTF, the following objectives were identified for this data collection:

- Collect sUAS data of the complete airfield pavements with a single sUAS
- Evaluate the performance of the Mavic 2 Pro for complete optical data collection
- Evaluate the feasibility of simultaneous data collection with three sUAS
- Evaluate the performance of available sUAS platforms and sensors for various types of distress visualization.

5.1.2 Field Demonstration in June 2021

Airfield pavement data were collected from MTO using multiple sUAS on June 16 and 17, 2021, to complete the above objectives. The airport manager was contacted, and a NOTAM was issued for this data collection. MTO had specific safety guidelines and protocols that every member of

the research team on airport property had to follow. All members of the data collection team completed the safety training conducted by the airport manager on June 16, 2021, before entering the airfield. Standard sUAS and airport safety plans were also followed. Because of the size and frequency of air traffic at MTO, the data collection focused on Runway 6/24, Taxiway D, and the apron, along with high-resolution priority sample units mainly on taxiways. The data were also collected over a 2-day period: Runway 6/24, Taxiway D, and apron data on the first day and high-resolution sample unit data collection on the second day. The original data collection plan included high-resolution sample unit data collection over Runway 6/24 sample units 01, 02, and 03. However, the pavement areas were recently reconstructed, and the research team collected Taxiway D sample units 01 and 02 instead.

A Mavic 2 Pro with 20-mp integrated optical RGB sensor was chosen as the main sUAS for full data collection on Runway 6/24 and Taxiway D. Thermal data were collected using M2EA from the Apron at 15.2 m and 24.4 m to further evaluate this system (the M2EA also collected optical data, but based on previous testing, using this for distress detection was not anticipated). The high-resolution priority sample unit data were also collected using the same system from the same flight altitude, as shown in Table 11. A Nikon D850 45.7-mp camera mounted on the Bergen Hexacopter was flown at 18.3 m altitude to collect optical RGB data with 1.5-mm/pix resolution. In addition, an mdMapper1000+ with Sony RX1R-II 42.4-mp optical RGB camera was also flown at 30.5 m altitude for 5 mm/pix data collection. Table 11 shows the details of the sUAS platforms, sensors, and flight altitudes used in the data collection at MTO.

Table 11. Summary of sUAS Data Collection at MTO

Target Areas	sUAS Platforms	Sensors	Flight Altitude (m)	Resolution (mm/pix)	
				Orthophoto	DEM
TWD3MTO-01 SU 01 and 02, TWD4MTO SU 01, RW 6MTO-04 SU 01, 02, and 03	Bergen Hexacopter	45.7-mp optical RGB Nikon D850	18.3	1.5	6
	M2EA	48-mp optical RGB	15.2	2.5*	5
	M2EA	512x640 thermal	24.4	31	N/A
	mdMapper1000+	42.4-mp optical RGB Sony RX1R-II	30.5	5	15
Runway 6/24	Mavic 2 Pro	20-mp optical RGB	15.2	3.6	14.3
Taxiway D	Mavic 2 Pro	20-mp optical RGB	15.2	3.6	14.3
Apron	Mavic 2 Pro	20-mp optical RGB	15.2	2.5*	5

RW 6MTO-04 = Runway 6/24
SU = Sample Unit
TWD3MTO = Taxiway D3
TWD4MTO = Taxiway D4
DEM = Digital Elevation Model
N/A = Not Applicable
*2.5 mm/pix is not the true effective resolution due to being derived from the M2EA 48-mp Quad Bayer camera.

The collected photogrammetric stereo overlapping image data sets of the focus areas were imported separately into Agisoft Metashape for processing. The locations of the sUAS images were corrected using location information from 10 AeroPoints™ (with built-in GPS) and 16 cloth GCPs placed at different sections of the airfield and locations were measured with a Trimble®

GeoExplorer® GeoXH 6000 GPS unit (Figure 30). The images were parallelly processed on multiple high-end desktop Windows workstations to create optical RGB orthophotos and DEMs.

The research team conducted an FOG distress survey at MTO. A two-person ground crew traveled from Urbana, Illinois, to MTO on July 5 and 6, 2021, and recorded the airfield distresses onto a handheld GPS-enabled tablet. The data were processed, and the PCI values for all sample units and branches of the airfield pavement were calculated based on the ASTM D5340-20 standard. The PCI values for the different sections of AC pavement ranged from 16 to 91, and the PCC pavement PCI values ranged from 40 to 84. A survey report was generated, including the types of distresses present on each sample unit and their estimated PCI values.

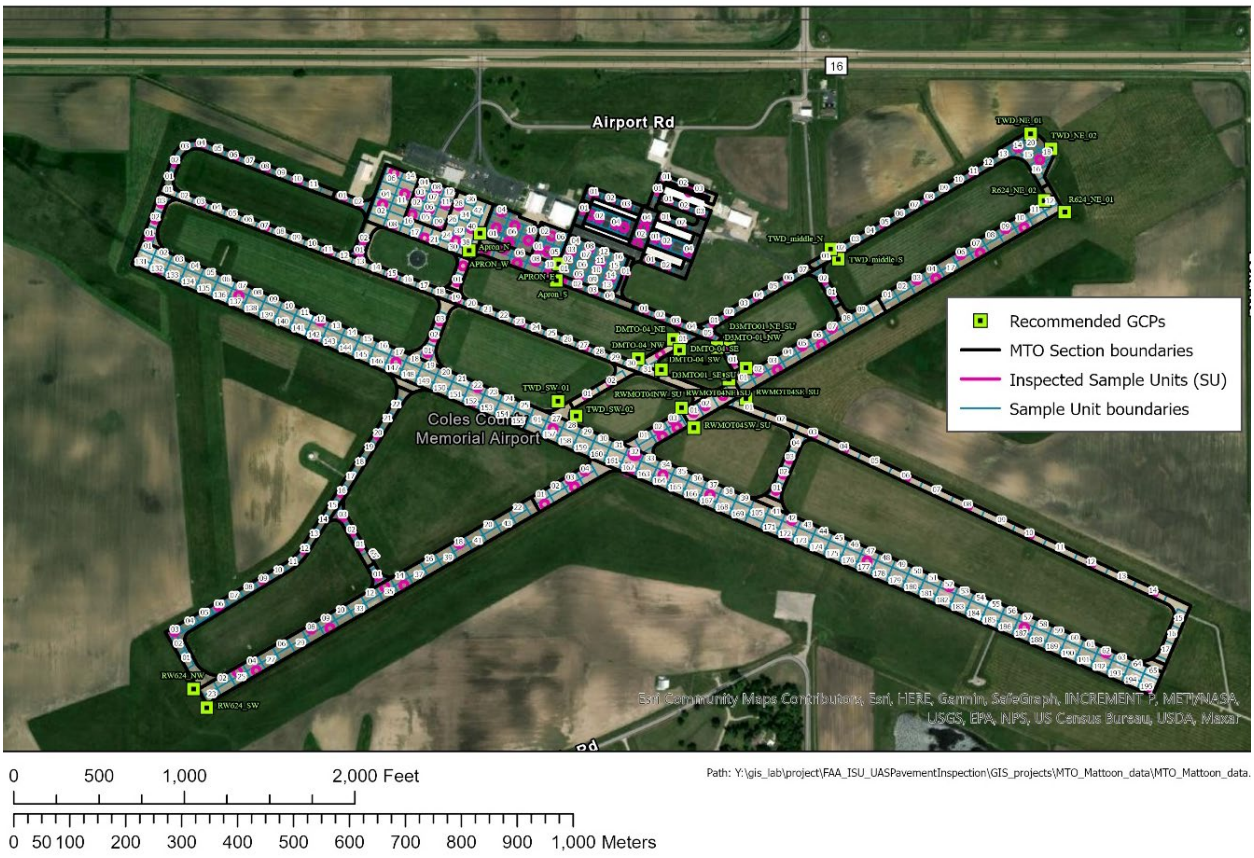

Figure 30. Recommended Locations for GCPs

5.1.3 Results and Discussion

The FOG PCI data were collected from 28 sample units. The FOG inspection team inspected several sample units on the PCC pavement of the apron. However, no sUAS data were collected from those PCC sample units of the apron due to time limitations. The PCI FOG and sUAS data had 15 common sample units, and from them, 10 sample units were selected for further analysis. The distresses at MTO, which were not found at ONZ and TTF, included depression, shoving, shrinkage cracking, and joint spalling. The orthophotos, DEMs, and hillshade DEMs of the 10 sample unit images were imported to ArcGIS Pro. Each pavement distress was quantified, and its

severity was determined using the data collected with Mavic 2 Pro over the runway and taxiway and with M2EA over the apron at 15.2-m flight altitude. The AC pavement system at MTO was in poor condition and extensive block cracking was reported. The FOG PCI team recorded L&T cracks in place of the block cracking to facilitate the performance comparison of different sensors. In sUAS-based PCI calculation, the sample units were noted to have block cracking with associated severity. Some of the sUAS-based inspection results were uploaded to FAA PAVEAIR, which provided estimated PCI values as outputs (FAA, 2021). Figure 31 shows a plot diagram of the sUAS-based PCI values and FOG PCI values (and they are also provided in Appendix G). The results showed that the sUAS-based PCI values were higher than FOG PCI values due to missing weathering and raveling. A sample unit on Taxiway D3 had a PCI value of 16, but the sUAS calculated PCI value was 57 due to missing medium-severity raveling on the whole sample unit. Table 12 provides the distresses that were correctly detected and rated on the sUAS-based data.

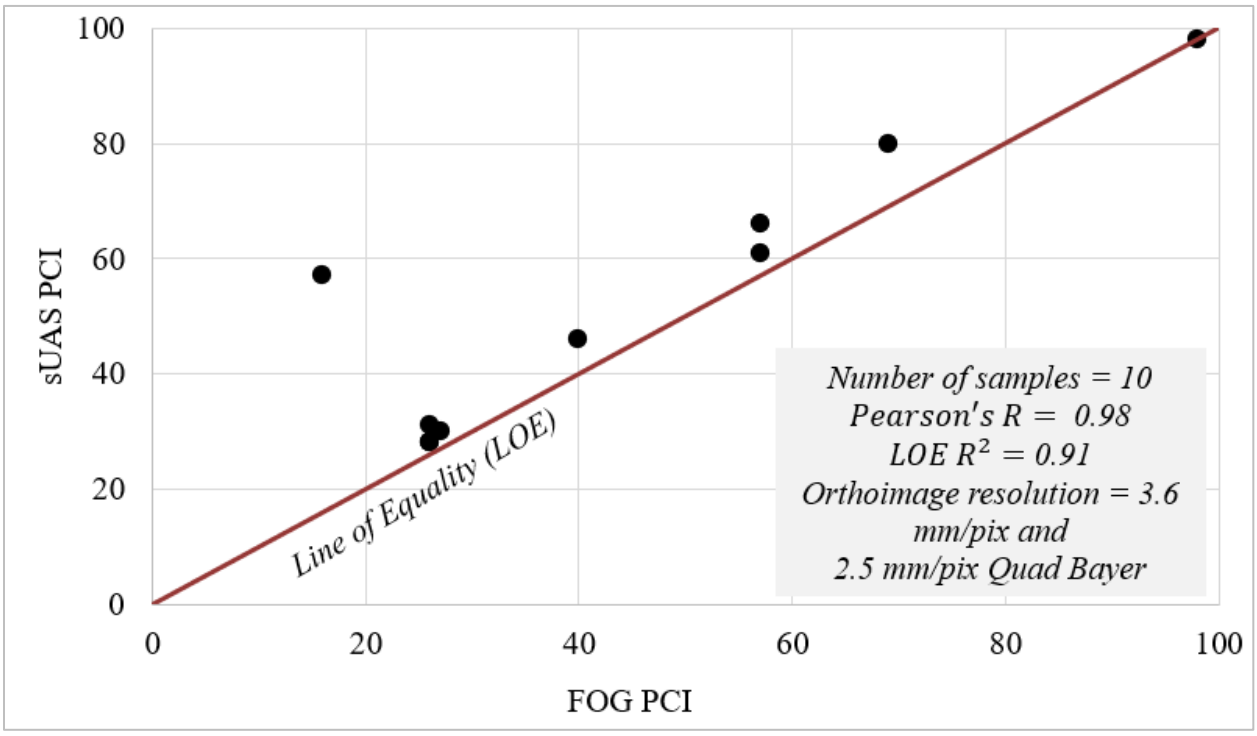

Figure 31. Comparison Between FOG PCI and sUAS PCI Calculated Using 2.5-mm/pix and 3.6-mm/pix Data from MTO

Table 12. Summary of the Findings of MTO

Distress Name (PAVER™ Distress Number)	Severity	Resolution Tested (mm/pix)		Distress Detected in Highest Resolution (mm/pix)		Remarks
		RGB	DEM	RGB	DEM	
Alligator cracking (41)	L	2.5*, 3.6	5, 14.3**	3.6	ND	
Block cracking (42) and L&T cracking (48)	L	2.5*, 3.6	5, 14.3**	3.6	ND	Figure 32 Figure 33
	M	2.5*, 3.6	5, 14.3**	3.6	ND	
	H	2.5*, 3.6	5, 14.3**	3.6	5	
Raveling (52)	M	2.5*, 3.6	5, 14.3**	ND	ND	
Weathering (57)	M	2.5*, 3.6	5, 14.3**	ND	ND	
LTD cracks (63)	L	2.5*, 3.6	5, 14.3**	3.6	ND	Figure 34
	M	2.5*, 3.6	5, 14.3**	3.6	5	
Joint seal damage (65)	L	2.5*, 3.6	5, 14.3**	ND	ND	
Shattered slab (72)	M	2.5*, 3.6	5, 14.3**	3.6	5	Figure 35
Shrinkage crack (73)	N/A	2.5*, 3.6	5, 14.3**	3.6	ND	Figure 35
Joint spalling (74)	L, M	2.5*, 3.6	5, 14.3**	3.6	ND	Figure 37
Corner spalling (75)	L	2.5*, 3.6	5, 14.3**	3.6	ND	

L = Low, M = Medium, H = High ND = Not detected
DEM = Digital Elevation Model N/A = Not applicable
*2.5 mm/pix is not the true effective resolution due to being derived from the M2EA 48-mp Quad Bayer camera.
**14.3 mm/pix DEM contained some reconstruction issues.

Based on the abovementioned analysis, the following lessons were learned:

- L&T and block cracking of all severity levels were detected and rated in both 2.5-mm/pix and 3.6-mm/pix data as shown in Figures 32 and 33.
- Shoving was detected in 5-mm/pix hillshade DEM data generated using an optical orthophoto of 2.5-mm/pix data collected with M2EA.

LTD cracks, shattered slabs, shrinkage cracking, and joint spalling were identifiable in both 2.5- and 3.6-mm/pix data (Figures 34 to 37). However, there is a possibility of missing shrinkage cracks in a similar resolution data set (Figure 35).

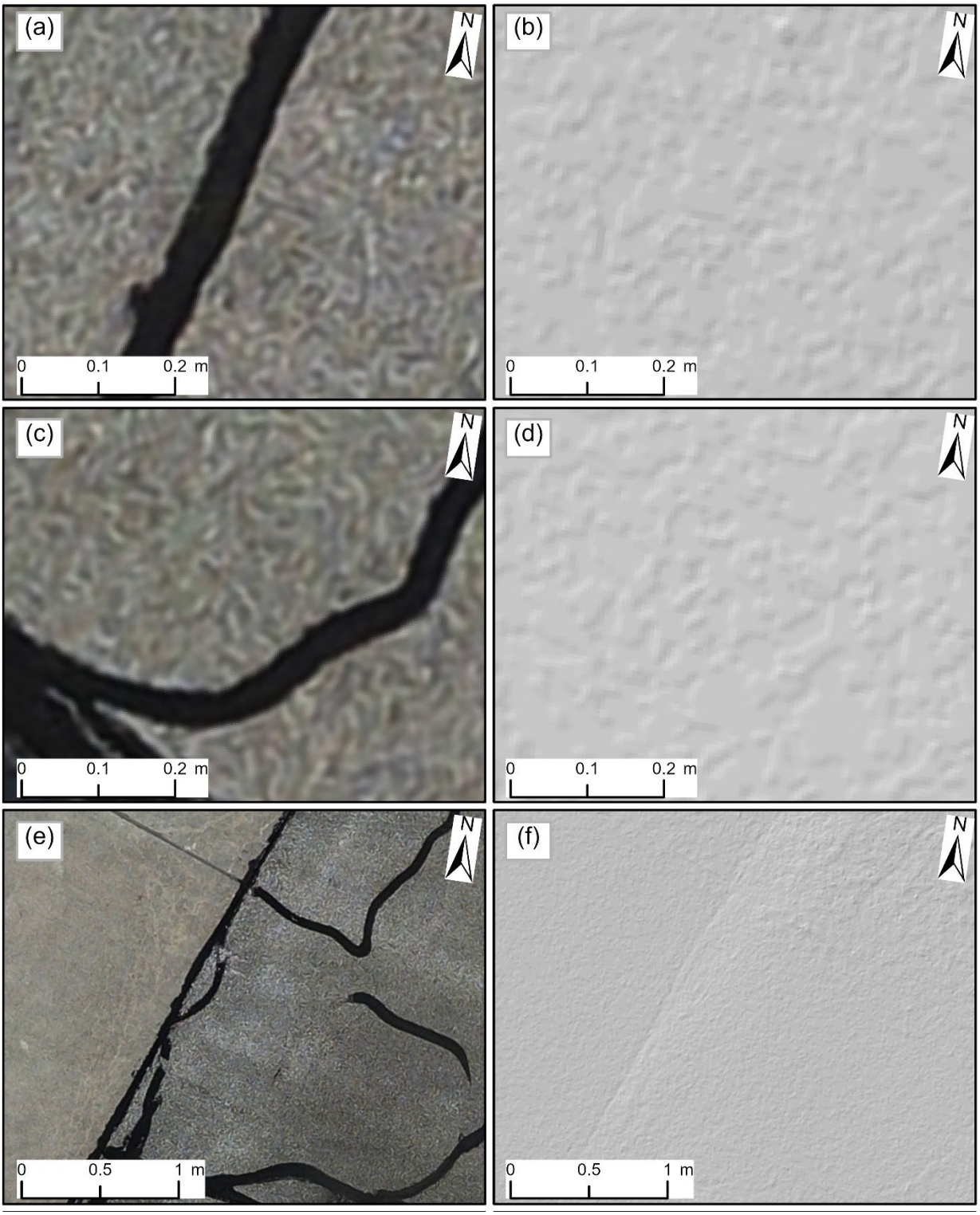

Figure 32. Longitudinal and Transverse Cracks (L) in (a) 2.5-mm/pix Orthophoto and (b) 5-mm/pix DEM; L&T Cracks (M) in (c) 2.5-mm/pix Orthophoto and (d) 5-mm/pix DEM; and Shoving (L) in (e) 2.5-mm/pix Orthophoto and (f) 5-mm/pix DEM

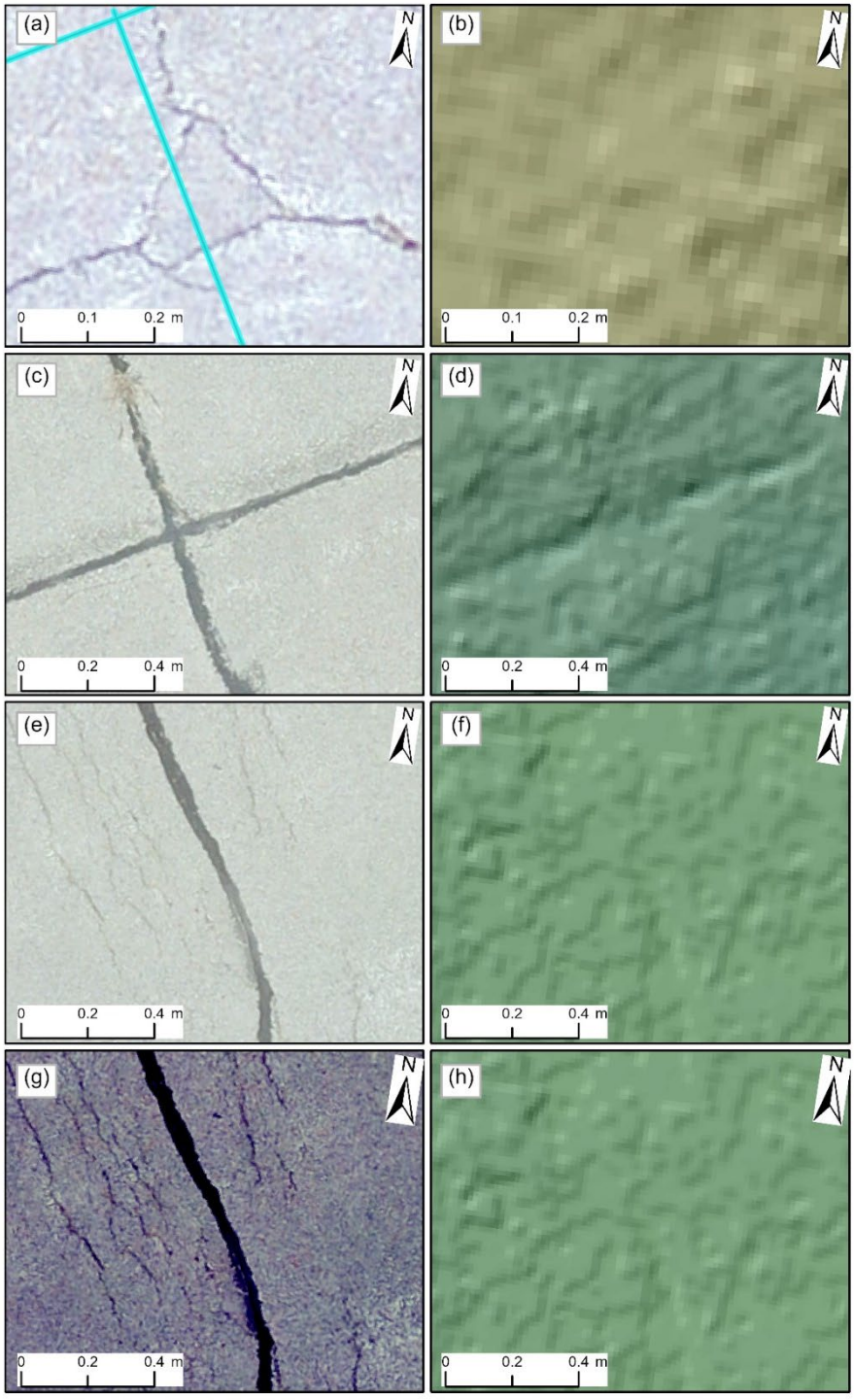

Figure 33. Longitudinal and Transverse Cracks (L) in (a) 3.6-mm/pix Orthophoto and (b) 14.3-mm/pix DEM; L&T Cracks (M) in (c) 3.6-mm/pix Orthophoto and (d) 14.3-mm/pix DEM; Shoving (L) in (e) 3.6-mm/pix Orthophoto and (f) 14.3-mm/pix DEM; and L&T Cracks (H) in (g) 2.5-mm/pix Orthophoto and (h) 5-mm/pix DEM

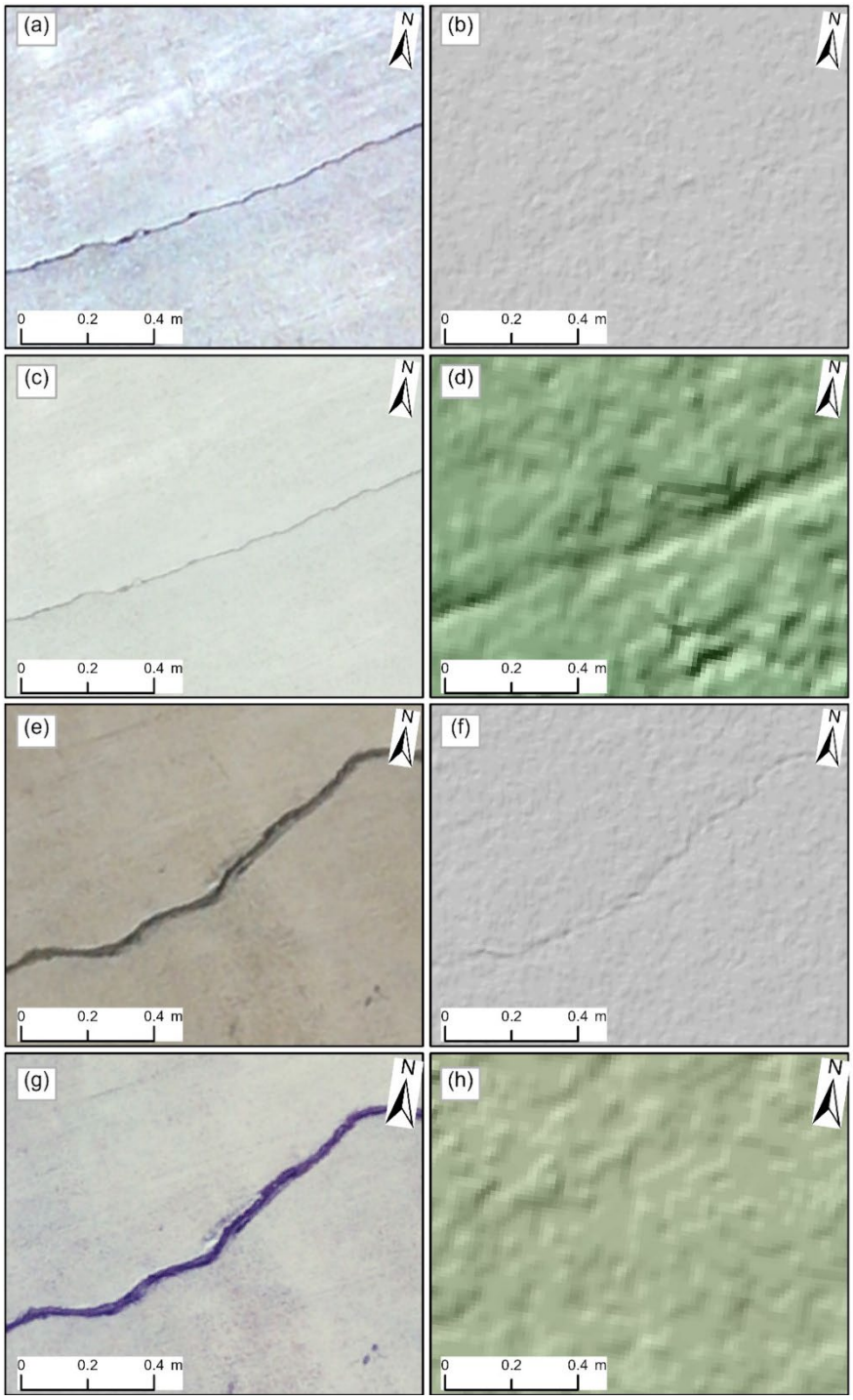

Figure 34. Longitudinal, Transverse, and Diagonal Cracks (L) in (a) 2.5-mm/pix Orthophoto, (b) 5-mm/pix DEM, (c) 3.6-mm/pix Orthophoto, and (d) 14.3-mm/pix DEM; and LTD Cracks (M) in (e) 2.5-mm/pix Orthophoto, (f) 5-mm/pix DEM, (g) 2.5-mm/pix Orthophoto, and (h) 5-mm/pix DEM

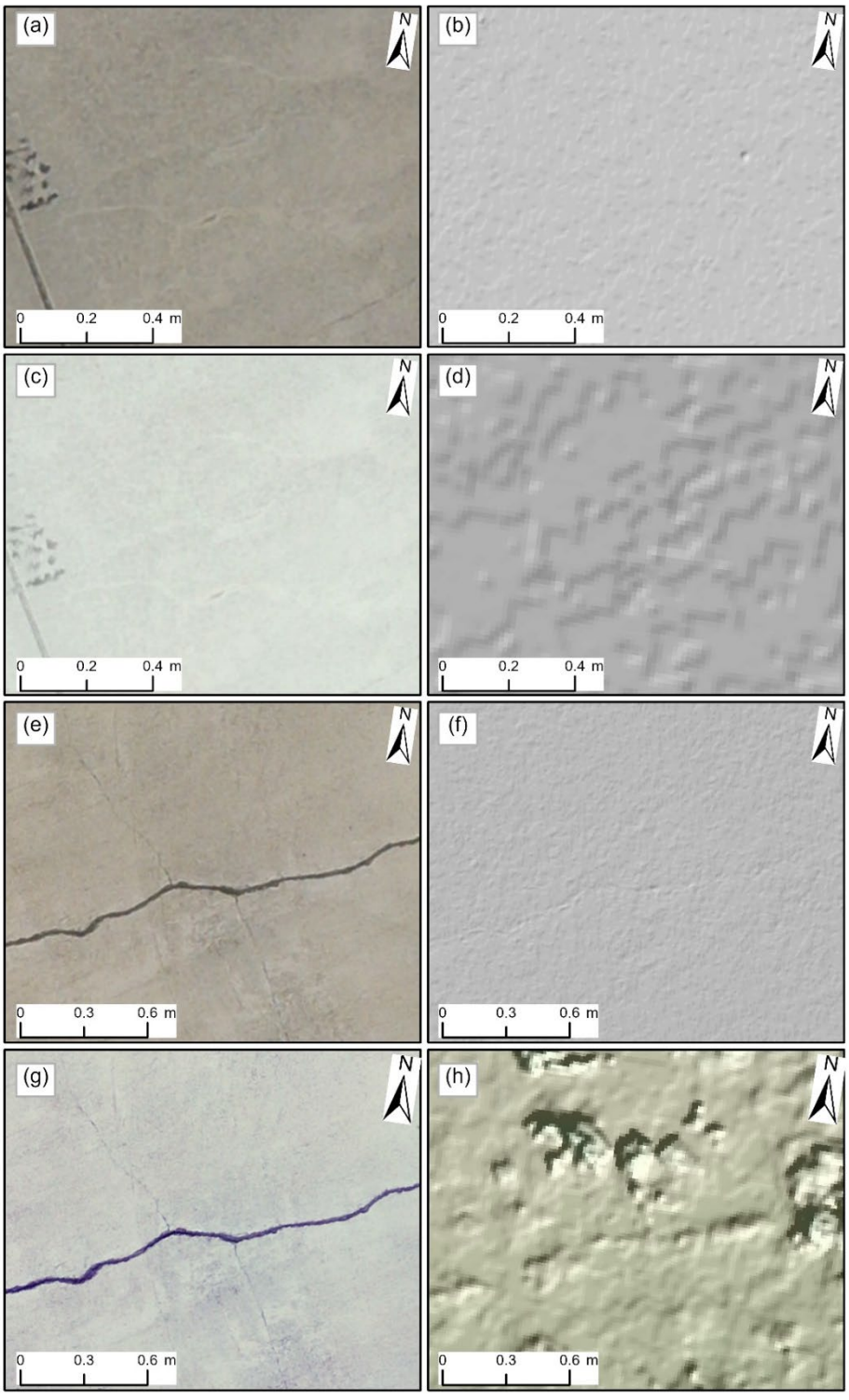

Figure 35. Shrinkage Cracks (L) in (a) 2.5-mm/pix Orthophoto, (b) 5-mm/pix DEM, (c) 3.6-mm/pix Orthophoto, and (d) 14.3-mm/pix DEM; and Shattered Slab (M) in (e) 2.5-mm/pix Orthophoto, (f) 5-mm/pix DEM, (g) 2.5-mm/pix Orthophoto, and (h) 5-mm/pix DEM

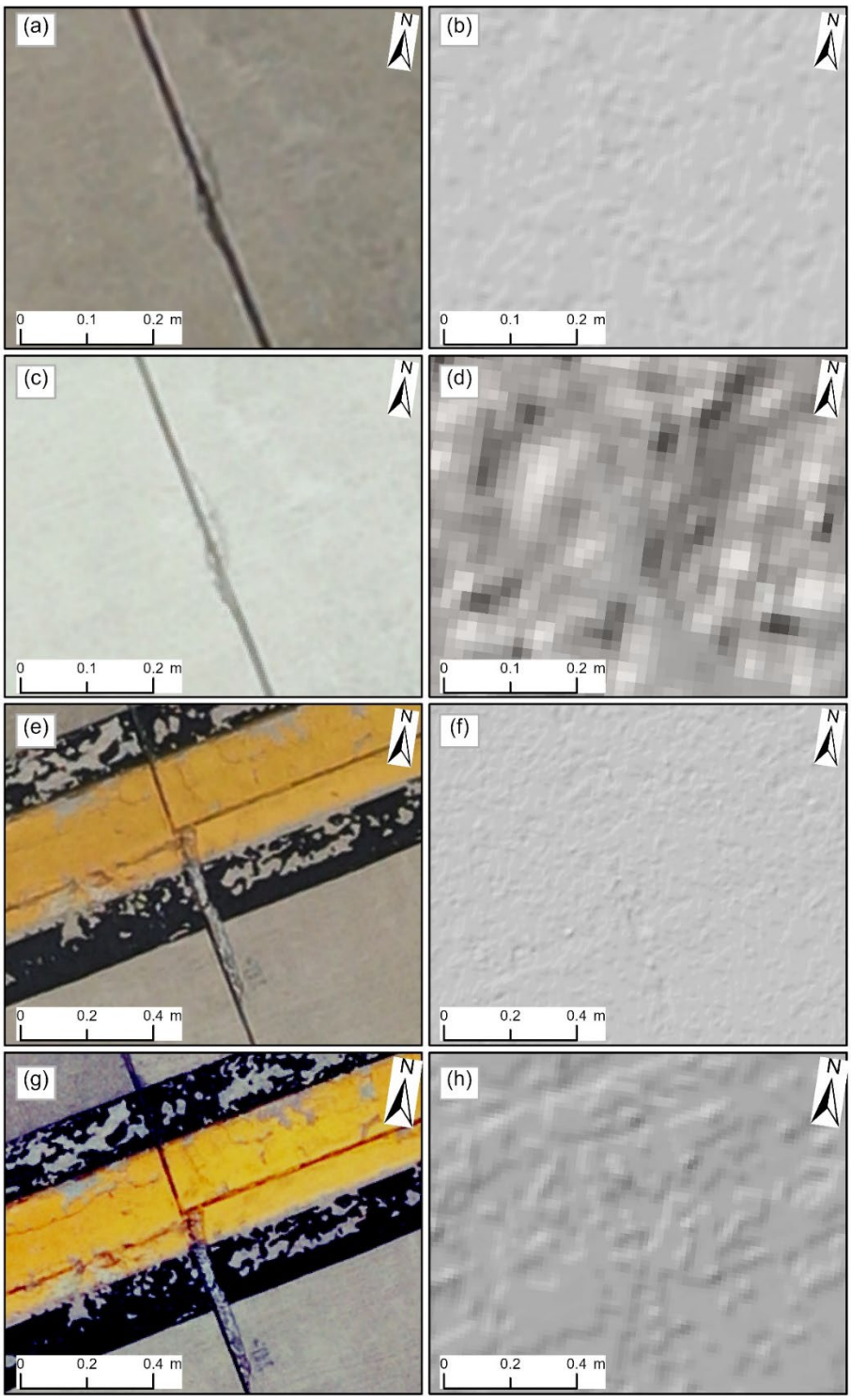

Figure 36. Joint Spalling (L) in (a) 2.5-mm/pix Orthophoto, (b) 5-mm/pix DEM, (c) 3.6-mm/pix Orthophoto, and (d) 14.3-mm/pix DEM; and Joint Spalling (M) in (e) 2.5-mm/pix Orthophoto, (f) 5-mm/pix DEM, (g) 2.5-mm/pix Orthophoto, and (h) 5-mm/pix DEM Derived

6. FIELD DEMONSTRATION IN IOWA

6.1 BOONE MUNICIPAL AIRPORT IN JUNE 2021

6.1.1 Objectives

The research team collected sUAS data from Boone Municipal Airport (BNW), Boone, Iowa, on June 29, 2021. The condition of the runway and taxiway pavements at this airport was rated good, but the T-hangar pavement condition was rated poor in earlier PCI inspections. The field demonstration plans for BNW were similar to the field demonstration plans for WWD in Lower Township, New Jersey, as described in Appendices B and C. sUAS data collection at BNW had the following objectives:

- Collect sUAS data from the taxiway and runway pavements with a single sUAS.
- Evaluate the performance of the Mavic 2 Pro for complete data collection.
- Evaluate the performance of available sUAS platforms and sensors for various distress visualization.

6.1.2 Field Demonstration in June 2021

The field demonstration plan for sUAS data collection developed for BNW was executed on June 29, 2021. The research team collection team travelled from Ames, Iowa, to Boone, Iowa, for this data collection. Eight team members, including four Part 107-certified sUAS pilots, participated in data collection. The Mavic 2 Pro with 20-mp RGB optical camera was used for the complete data collection over Taxiway A and Runway 15/33. Optical RGB and thermal images of the T-hangars were collected using the M2EA. As shown in Table 13, data were collected using three different sUAS: a Bergen Hexacopter with a 45.7-mp optical RGB Nikon D850 camera, a Mavic 2 Pro with a 20-mp optical camera, and a M2EA with its 48-mp Quad Bayer optical RGB and 640x512 pixel thermal sensor.

Table 13. Summary of sUAS Data Collection at BNW

Target Area	sUAS Platforms	Sensors	Flight Altitude (m)	Resolution (mm/pix)	
				Orthophoto	DEM
Runway 15/33 sample units 01, 03, and 07	Bergen Hexacopter	45.7-mp optical RGB Nikon D850	18.3	1.5	6
	M2EA	48-mp optical RGB	15.2	2.1*	8.6
	M2EA	512x640 thermal	24.4	31	N/A
Runway 15/33	Mavic 2 Pro	20-mp optical RGB	15.2	3.3	13.5
Taxiway A	Mavic 2 Pro	20-mp optical RGB	15.2	3.3	13.5
	M2EA	48-mp optical RGB	15.2	2.4*	9.5
T-hangar 1 and T-hangar 2	M2EA	48-mp optical RGB	15.2	2.4*	9.5
	M2EA	512x640 thermal	24.4	31	N/A

N/A = Not applicable.
*2.4 and *2.1 mm/pix is not true resolution due to being derived from the M2EA 48-mp Quad Bayer camera.

The focus of the data collection was on Runway 15/33, Taxiway A, T-hangar 1, T-hangar 2, and high-resolution sample units. Table 13 provides the details of the sUAS data collected at BNW. The research team planned to collect sUAS data using a mdMapper1000+ with a Sony RX1R-II 42.4-mp optical RGB camera, but the system did not take off because of technical difficulties related to a recent software update.

Each photogrammetric stereo overlapping image data set of the complete Runway 15/33, T-hangar 1, and T-hangar 2 of BNW collected with Mavic 2 Pro and M2EA was imported separately into Agisoft Metashape for processing. The locations of the sUAS images were corrected using the location information of 19 AeroPoints™ (with built-in GPS), along with 16 cloth GCPs placed at different sections of the airfield whose location was recorded with a decimeter-accuracy Trimble® GeoExplorer® GeoXH 6000 GPS unit (Figure 37). The images were processed on a desktop Windows workstation to create optical RGB orthophotos and DEMs. However, because of the long, narrow shape of the taxiway, which can cause quality issues with photogrammetry software, the orthophoto output contained unexpected spatial deviation resulting in poor-quality spatial positioning of some parts of Taxiway A. Therefore, another set of optical RGB optical data was collected from Taxiway A using M2EA on August 2, 2021. In this data collection, 10 AeroPoints™ were reused three times to increase the number of GCPs, which proved to be a practical method of obtaining a larger number of GCPs while using only 10 AeroPoints™ at a time. The GCPs were placed at one section of the taxiway followed by sUAS data collection, then moved to the next section. It was observed that 10 minutes of AeroPoints™ placement could provide centimeter-level GPS accuracy, although at least 30 minutes is the standard method in this research to ensure the high centimeter-level accuracy.

An airfield pavement distress FOG survey was conducted at BNW in accordance with the ASTM D5340-20 standard. The two-person team traveled to Boone, Iowa, on August 4 and observed, rated, and recorded the airfield distresses onto a handheld GPS-enabled tablet. The data were processed and the PCI values for all sample units and branches of the airfield pavement were calculated based on the ASTM D5340-20 standard. Selected sample units of apron, Taxiway A, and Runway 15/33 were inspected. The PCI values for the apron sample units were 86 and 87, and for Runway 15/33 they ranged from 43 to 82. The condition of the Taxiway A sample units was relatively better, and the PCI values were between 57 and 95. A total of 33 PCC sample units were inspected. The predominant airfield pavement distresses were corner breaks, LTD cracks, small patching, large patching, pop-outs, joint spalling, corner spalling, and ASR of different severities.

6.1.3 Results and Discussion

The sUAS data collection focused on the complete data collection from Taxiway A, Runway 15/33, T-hangar 1, and T-hangar 2 at BNW. However, the PCI data were collected from Taxiway A, Runway 15/33, and a part of the apron. Both the sUAS data and PCI data were collected from 27 common sample units. The 2.4-mm/pix orthophoto was generated using collected data from the M2EA over Taxiway A at 15.2-m flight altitude. In addition, Mavic 2 Pro was flown over Runway 15/33 at 15.2-m altitude used to generate the 3.3-mm/pix orthophoto. In both cases, the sample units were visually observed, and distresses were quantified. The recorded data were used to calculate the PCI values for each sample unit and plotted against the FOG PCI results, as shown in Figure 38.

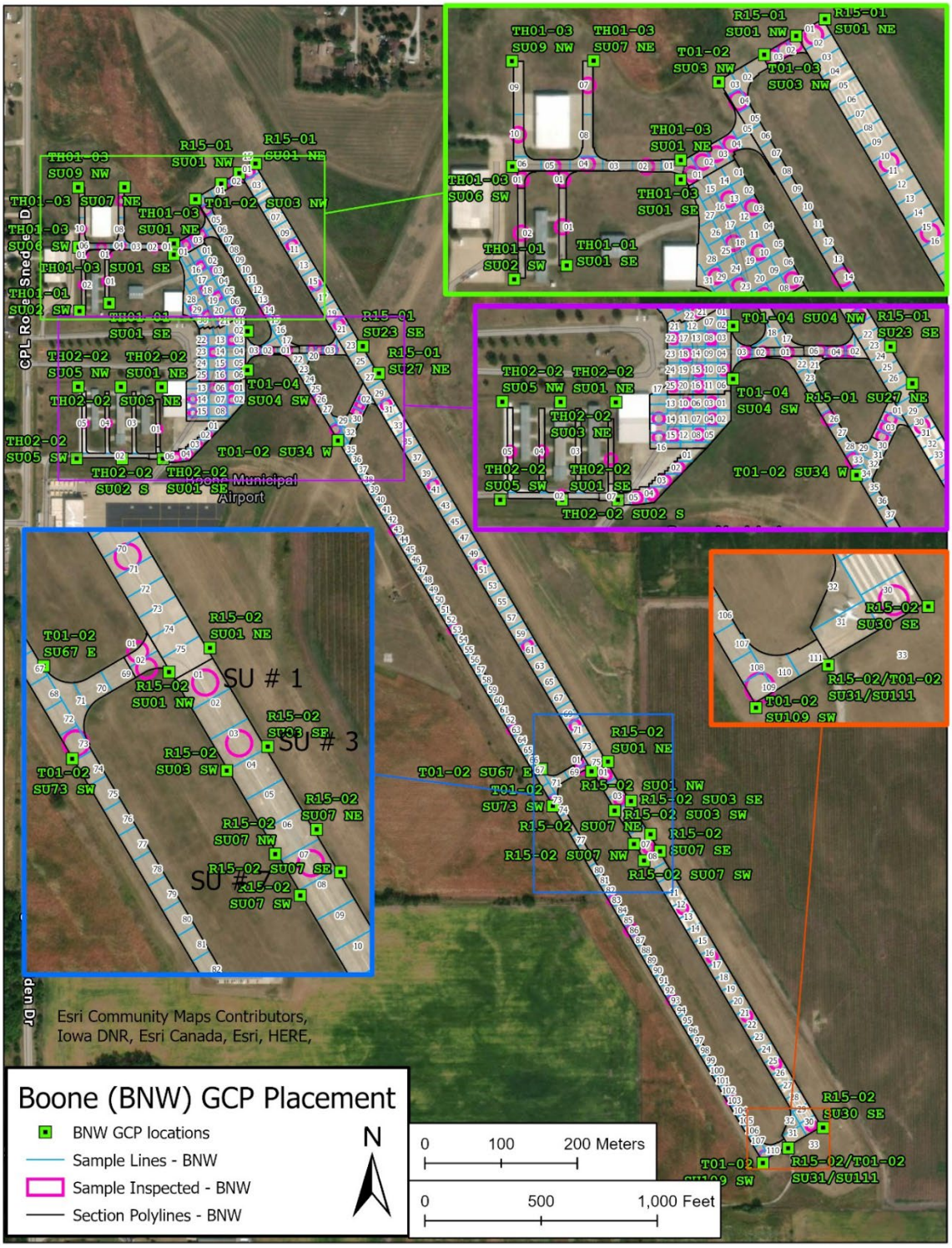

Figure 37. Recommended Locations for GCPs

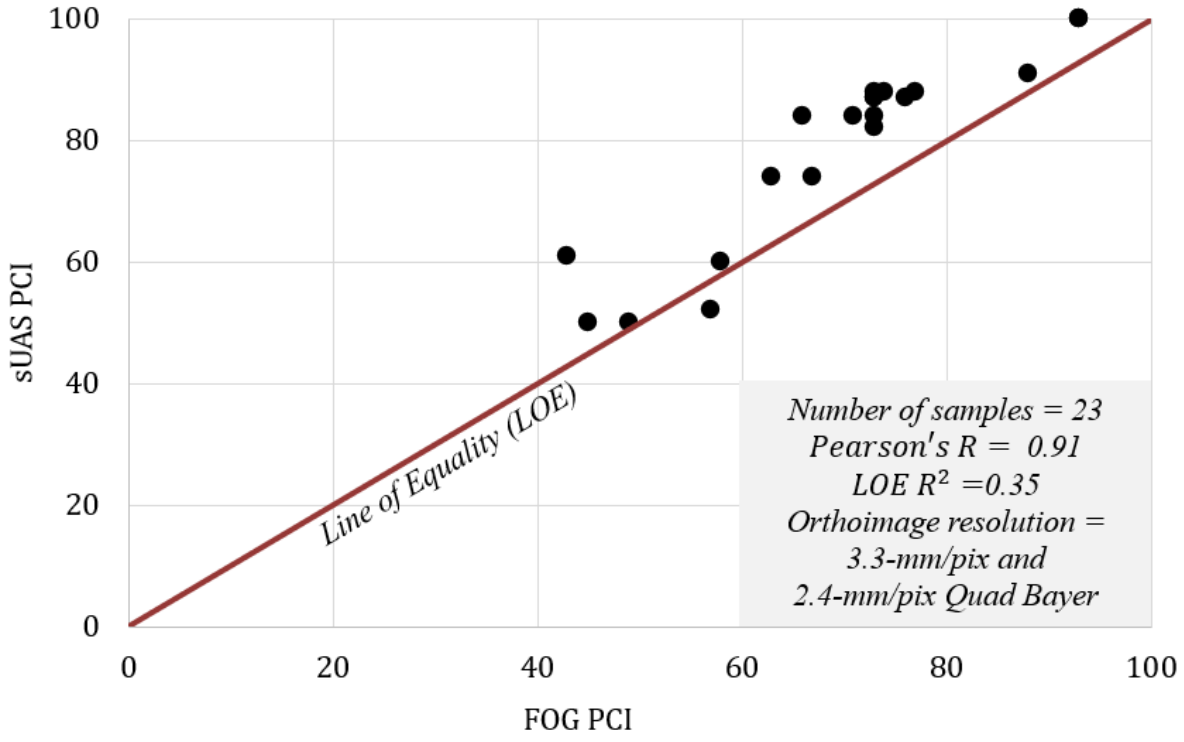

Figure 38. Comparison Between FOG PCI and sUAS PCI Calculated Using 2.4-mm/pix and 3.3-mm/pix Data from BNW

A summary of the results from the analysis are listed below:

- The sUAS PCI values are higher than the FOG PCI. This can be explained, in part, by the difficulty in identifying low- and medium-severity ASR on sUAS image-based interpretation.
- The crack-based distresses (LTD cracks, corner breaks, corner spalling, and joint spalling) were detectable, and their associated severity was accurately measured in both 2.4-mm/pix and 3.3-mm/pix optical RGB data.
- Small and large patching of medium- and low-severity and pop-outs were clearly visible. Severity levels were accurately detected in all data regardless of their resolutions.
- Joint seal damage with high severity was detectable at 2.4 mm/pix but medium severity was challenging to identify. The low-severity joint seal damage was completely unidentifiable.

The orthophoto, DEM, and hillshade of different resolutions were imported into ArcGIS Pro to study their capabilities in detecting and rating airfield pavement distresses. The PCI data set collected from a manual survey was designated the ground truth data in this visual analysis. Table 14 presents the comparison summary, and Figures 39 through 50 show the results.

Table 14. Summary of the Findings of BNW

Distress Name (PAVER™ Distress Number)	Severity	Resolution Tested (mm/pix)		Distress Detected in Maximum Resolution (mm/pix)		Remarks
		RGB	DEM	RGB	DEM	
Corner breaks (62)	L	1.5, 2.1*, 2.4*, 3.3	6, 8.6, 9.5, 13.5	3.3**	ND	Figure 39
	M	2.4*	9.5	3	ND	Figure 41
LTD cracks (63)	L	1.5, 2.1*, 2.4*, 3.3	6, 8.6, 9.5, 13.5	3.3	ND	Figure 40
	M			3.3	ND	Figure 41
Joint seal damage (65)	L	3.3, 2.4*	9.5, 13.5	ND	ND	
	M	2.4*	9.5	ND	ND	Figure 49
	H	2.4*	9.5	2.4	9.5	Figure 42
Small patching (66)	L	1.5, 2.1*, 2.4*, 3.3	6, 8.6, 9.5, 13.5	3.3	ND	Figure 43 Figure 48
	M			3.3	6	Figure 44
Large patching (67)	L	1.5, 2.1*, 2.4*, 3.3	6, 8.6, 9.5, 13.5	3.3	6	Figure 45
Pop-outs (68)		1.5, 2.1*, 2.4*, 3.3	6, 8.6, 9.5, 13.5	3.3	6	Figure 46
Faulting (71)	L	2.4*	9.5	ND	ND	
Shrinkage crack (73)	N/A	2.4*	9.5	ND	ND	Figure 42
Joint spalling (74)	L	3.3	13.5	3.3	ND	Figure 49
	M	3.3	13.5	3.3	ND	
Corner spalling (75)	L	1.5, 2.1*, 2.4*, 3.3	6, 8.6, 9.5, 13.5	ND	ND	Figure 47
	M			3.3	ND	Figure 48
ASR (76)	L	1.5, 2.1*, 2.4*, 3.3	6, 8.6, 9.5, 13.5	ND	ND	
	M			3.3	ND	Figure 50

L = Low, M = Medium, H = High ND = Not Detected
N/A = Not Applicable (no severity level for shrinkage crack)
*2.1 mm/pix and 2.4 mm/pix are not true resolutions due to being derived from the M2EA 48-mp Quad Bayer camera.
** Distress detected in 1.5 and 3.3 mm/pix, not 2.4-mm/pix.

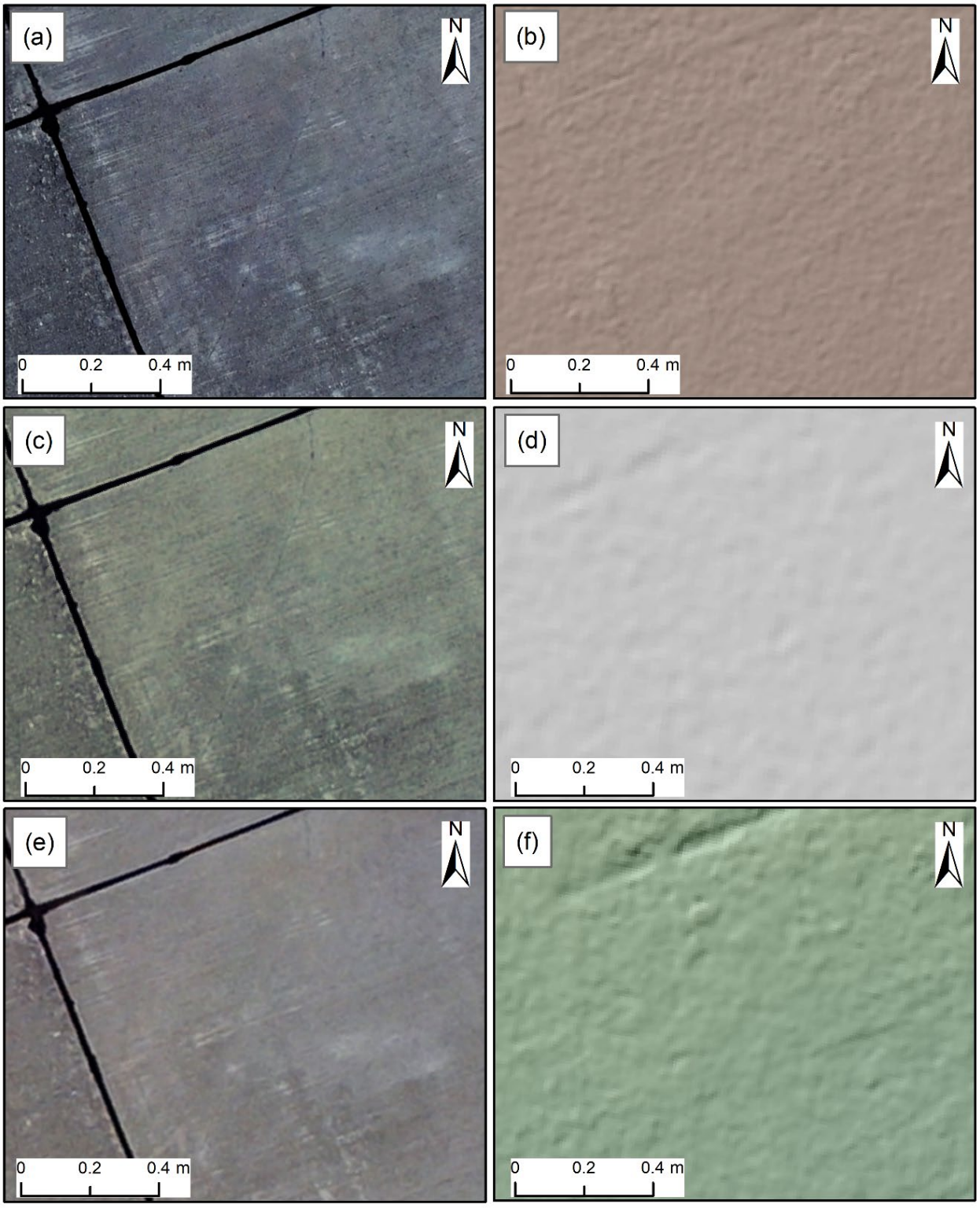

Figure 39. Corner Break (L) in (a) 1.5-mm/pix Orthophoto, (b) 6-mm/pix DEM, (c) 3.3-mm/pix Orthophoto, (d) 13.5-mm/pix DEM, (e) 2.1-mm/pix Orthophoto, and (f) 8.6-mm/pix DEM

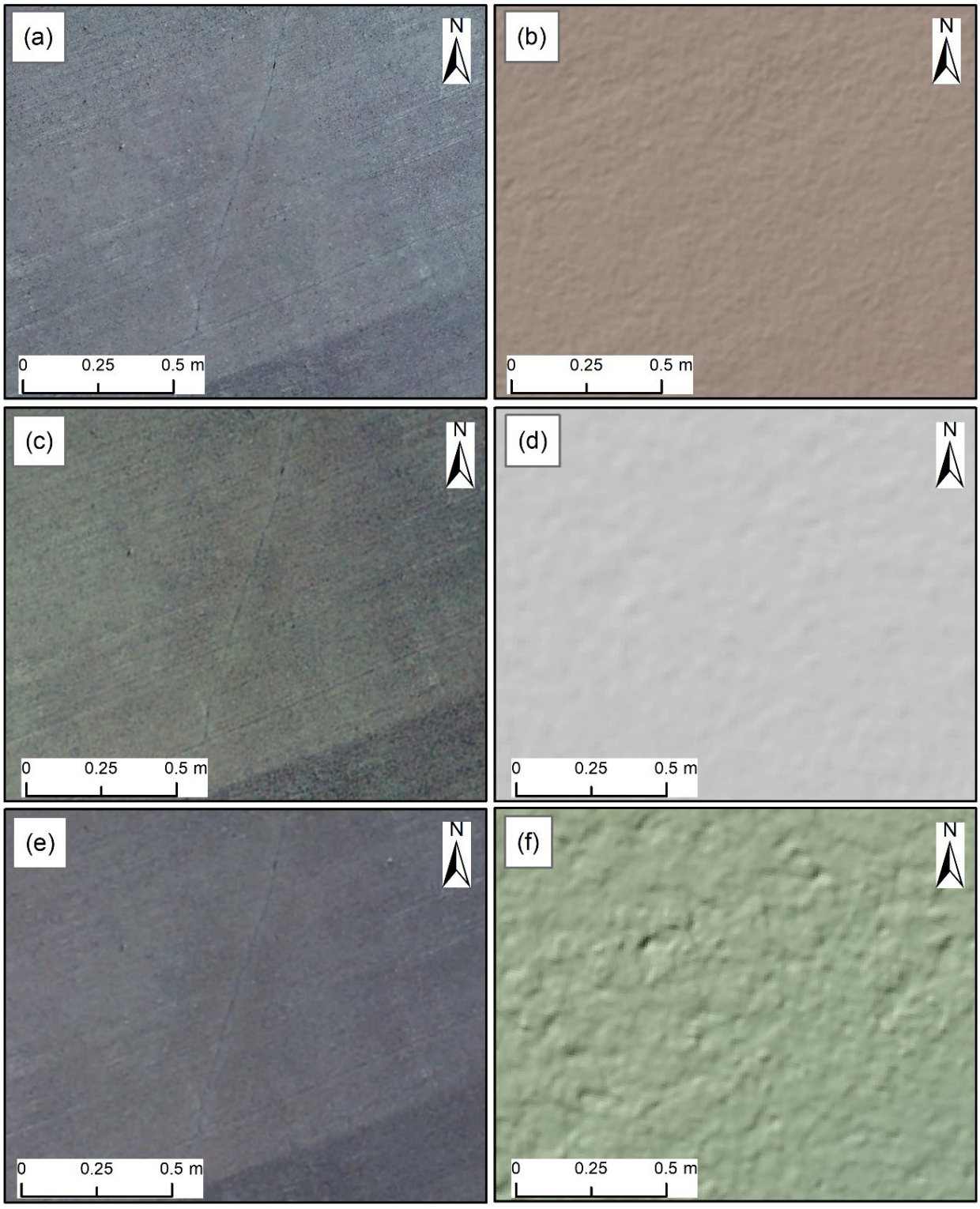

Figure 40. Longitudinal, Transverse, and Diagonal Cracks (L) in (a) 1.5-mm/pix Orthophoto, (b) 6-mm/pix DEM, (c) 3.3-mm/pix Orthophoto, (d) 13.5-mm/pix DEM, (e) 2.1-mm/pix Orthophoto, and (f) 8.6-mm/pix DEM

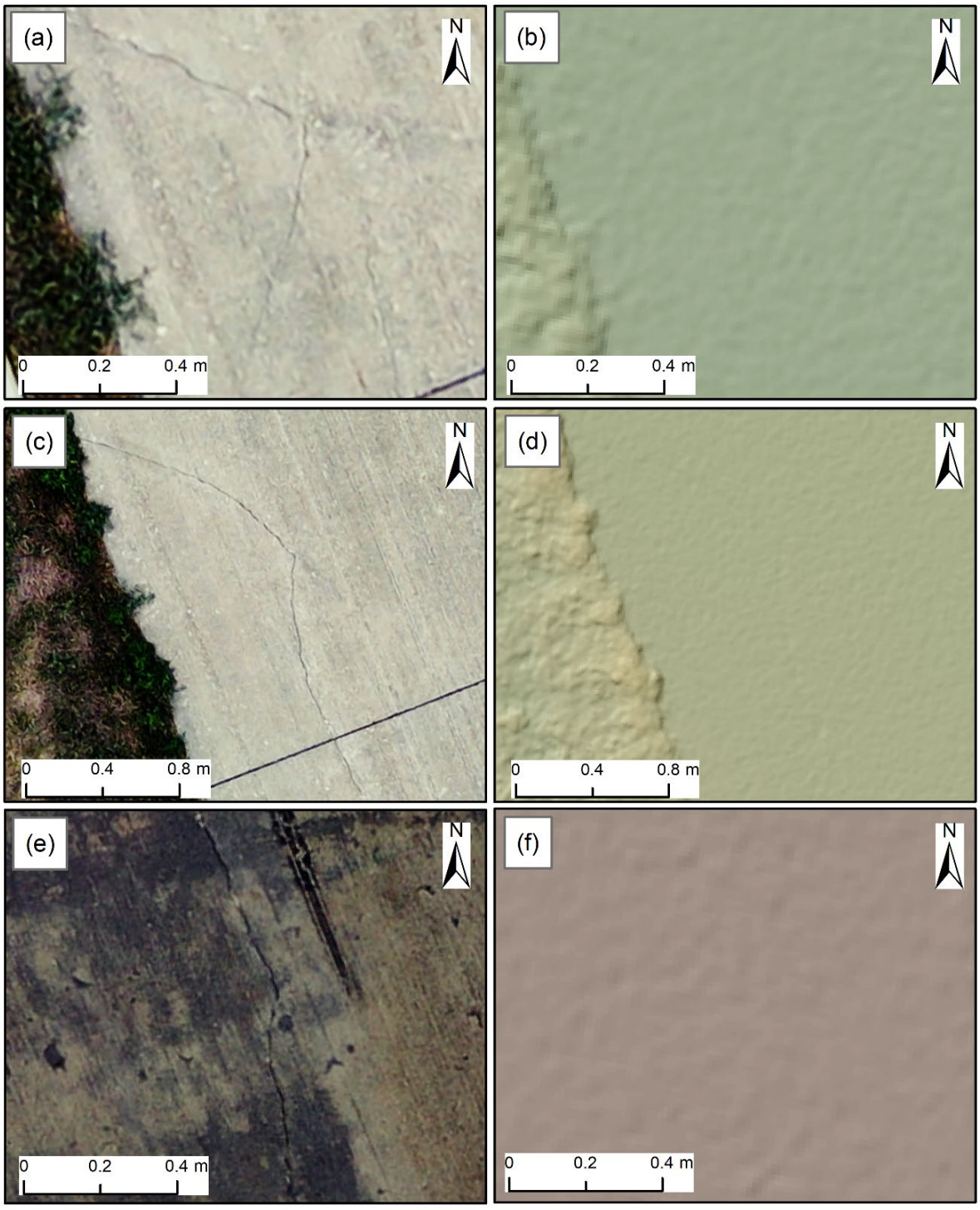

Figure 41. Corner Break (M) in (a) 2.4-mm/pix Orthophoto and (b) 9.5-mm/pix DEM; LTD Cracks (M) in (c) 2.4-mm/pix Orthophoto, (d) 9.5-mm/pix DEM, (e) 3.3-mm/pix Orthophoto, and (f) 13.5-mm/pix DEM

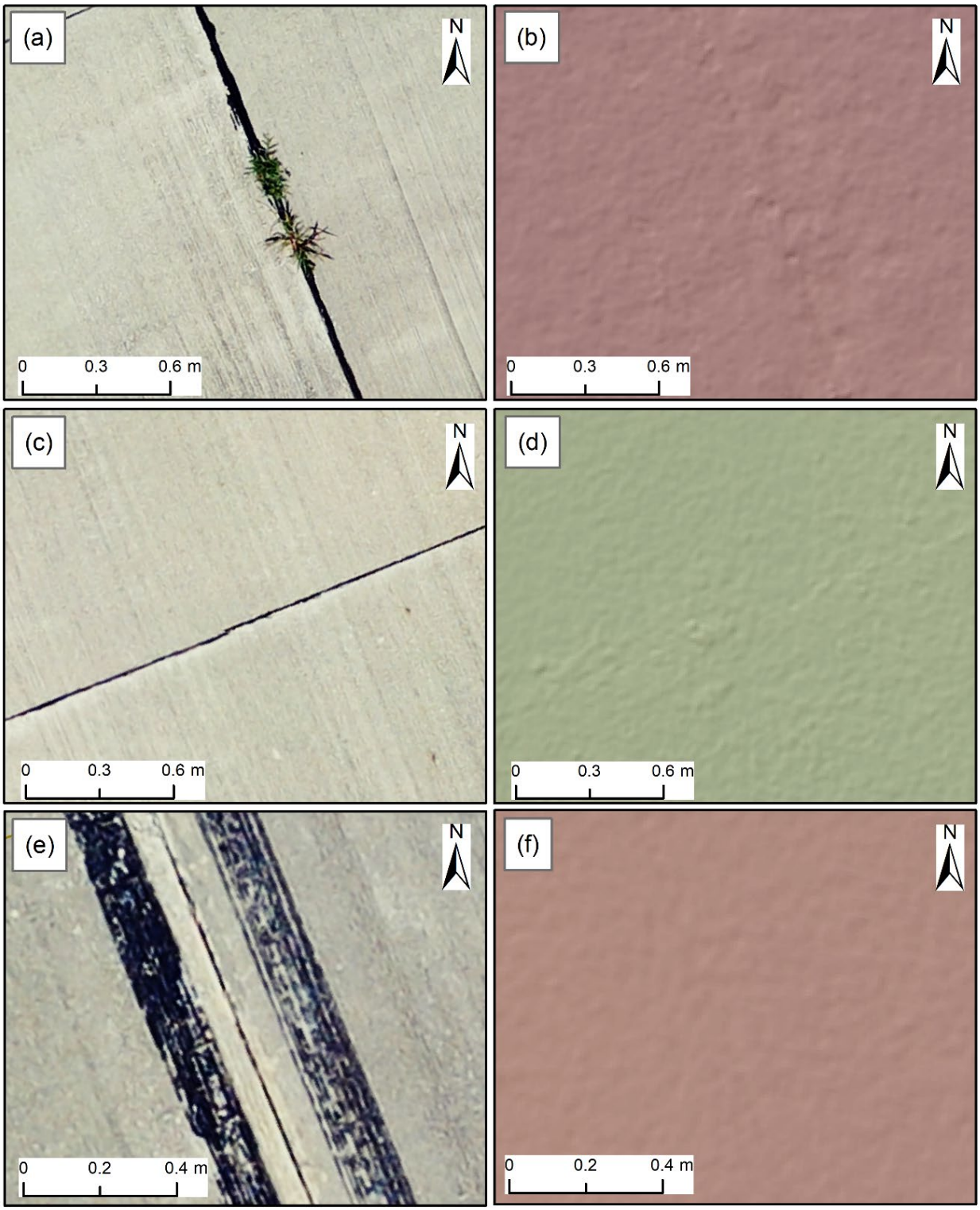

Figure 42. Joint Seal Damage (H) in (a) 2.4-mm/pix Orthophoto and (b) 9.5-mm/pix DEM; Faulting (L) in (c) 2.4-mm/pix Orthophoto and (d) 9.5-mm/pix DEM; and Shrinkage Crack in (e) 2.4-mm/pix Orthophoto and (f) 9.5-mm/pix DEM

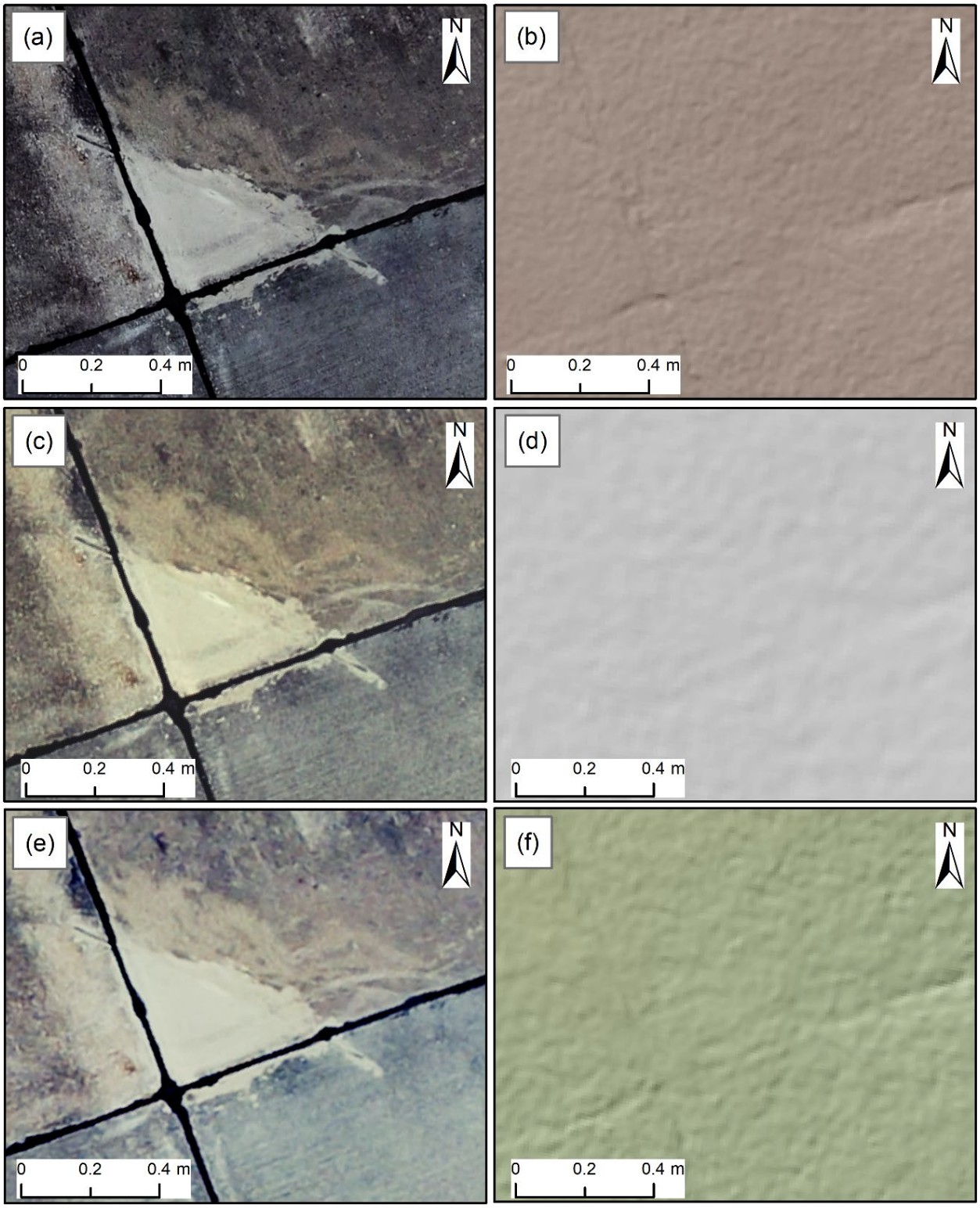

Figure 43. Small Patching (L) in (a) 1.5-mm/pix Orthophoto, (b) 6-mm/pix DEM, (c) 3.3-mm/pix Orthophoto, (d) 13.5-mm/pix DEM, (e) 2.1-mm/pix Orthophoto, and (f) 8.6-mm/pix DEM

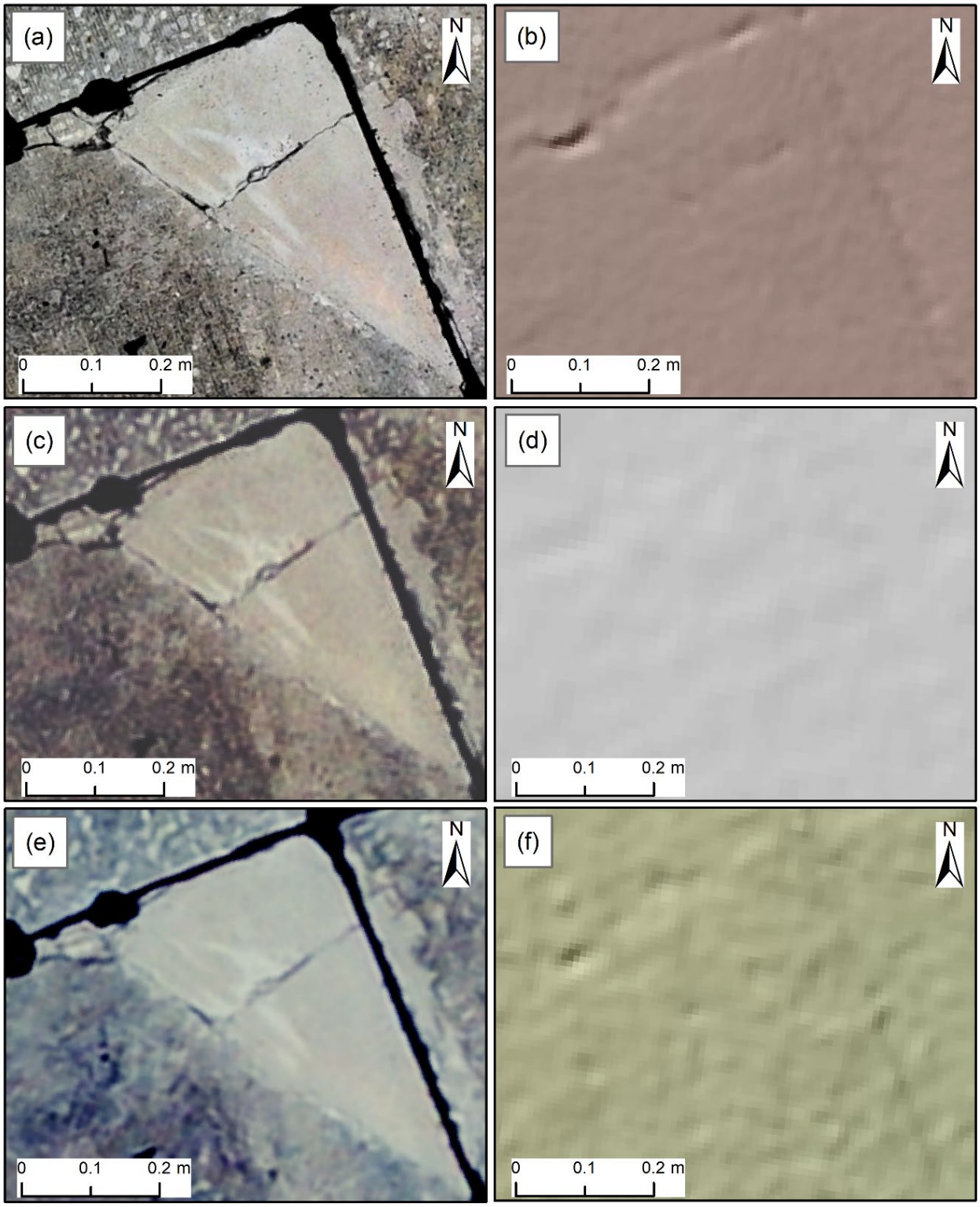

Figure 44. Small Patching (M) in (a) 1.5-mm/pix Orthophoto, (b) 6-mm/pix DEM, (c) 3.3-mm/pix Orthophoto, (d) 13.5-mm/pix DEM, (e) 2.1-mm/pix Orthophoto, and (f) 8.6-mm/pix DEM

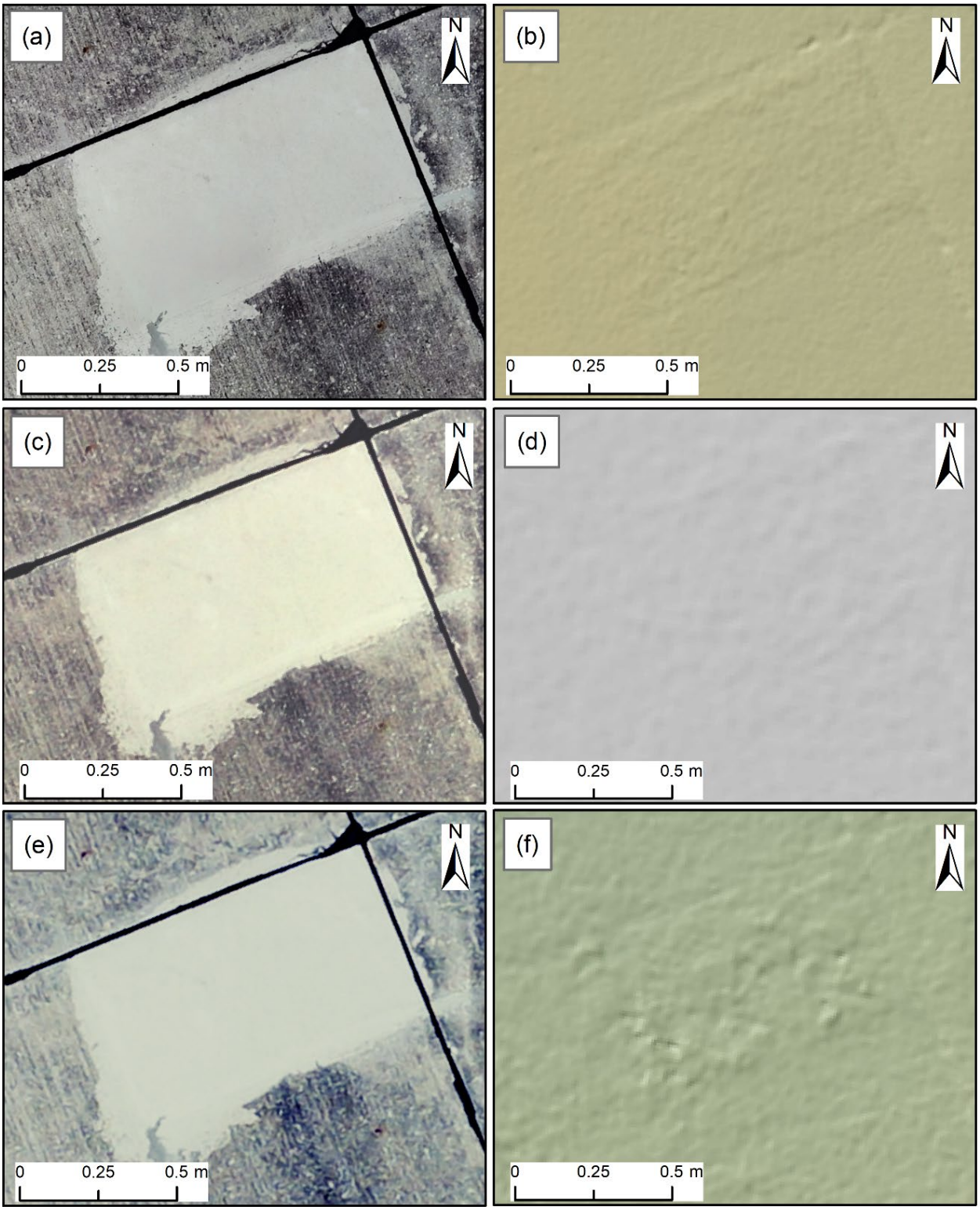

Figure 45. Large Patching (L) in (a) 1.5-mm/pix Orthophoto, (b) 6-mm/pix DEM, (c) 3.3-mm/pix Orthophoto, (d) 13.5-mm/pix DEM, (e) 2.1-mm/pix Orthophoto, and (f) 8.6-mm/pix DEM

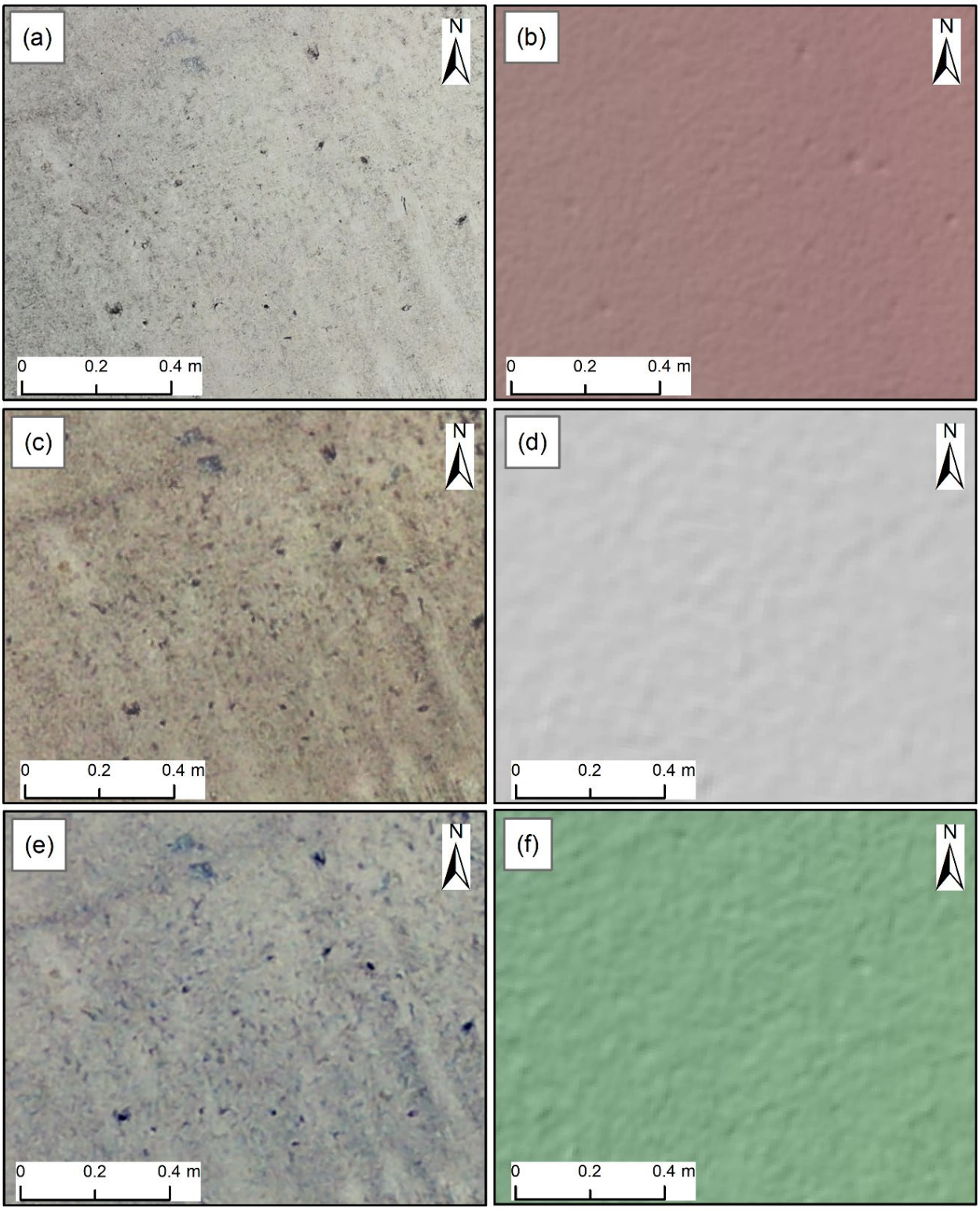

Figure 46. Pop-outs in (a) 1.5-mm/pix Orthophoto, (b) 6-mm/pix DEM, (c) 3.3-mm/pix Orthophoto, (d) 13.5-mm/pix DEM, (e) 2.1-mm/pix Orthophoto, and (f) 8.6-mm/pix DEM

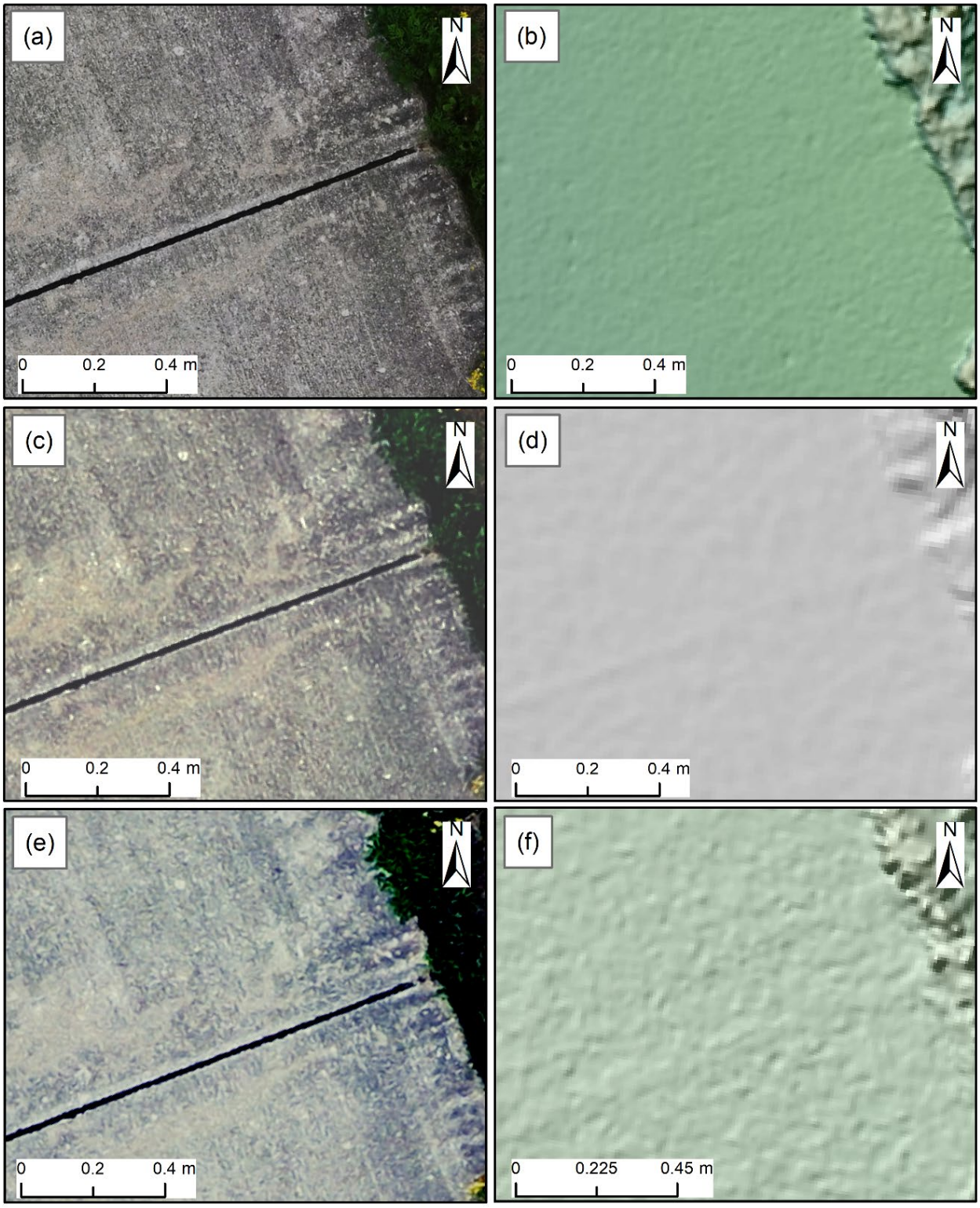

Figure 47. Corner Spalling (L) in (a) 1.5-mm/pix Orthophoto, (b) 6-mm/pix DEM, (c) 3.3-mm/pix Orthophoto, (d) 13.5-mm/pix DEM, (e) 2.1-mm/pix Orthophoto, and (f) 8.6-mm/pix DEM

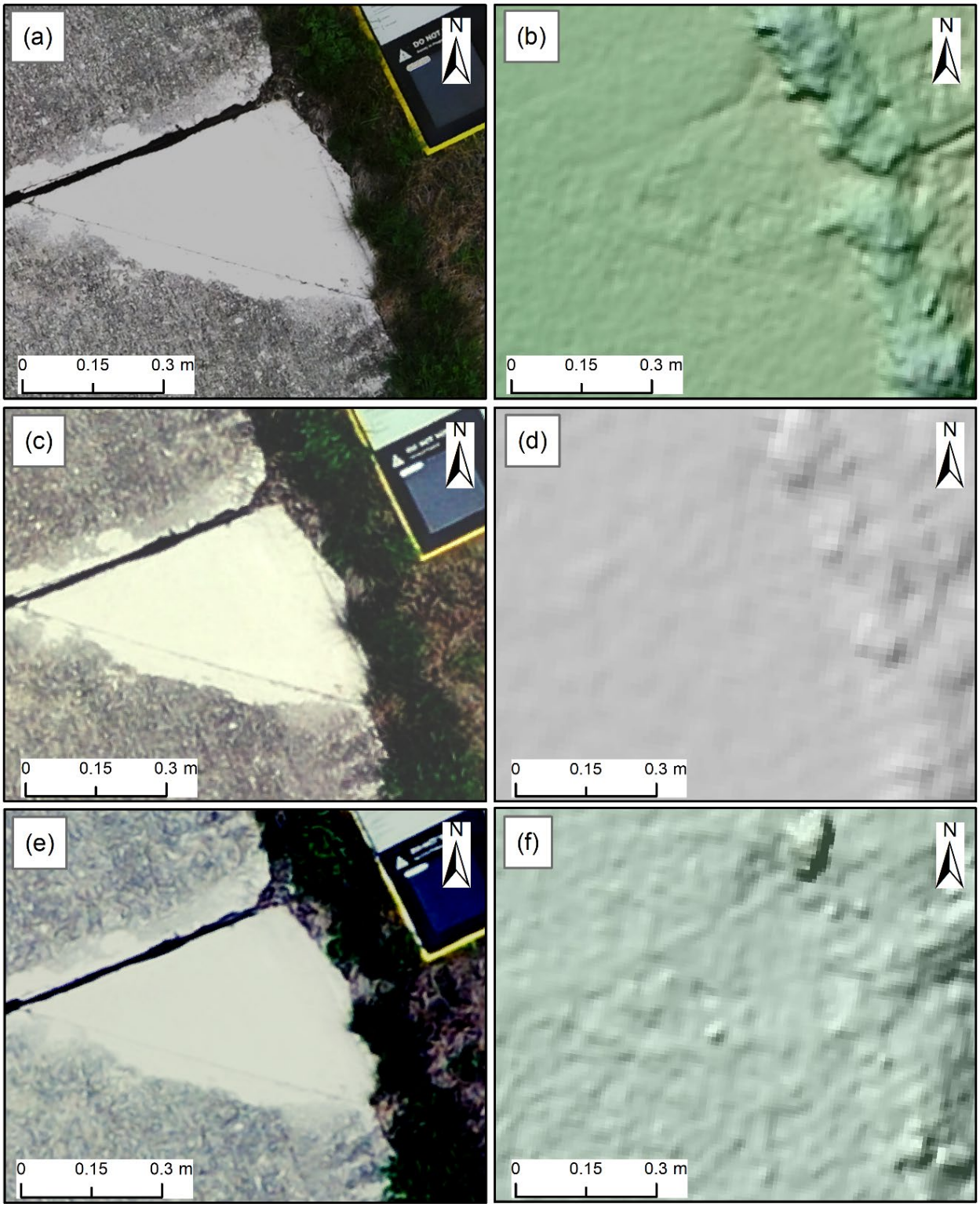

Figure 48. Small Patching (L) and Corner Spalling (M) in (a) 1.5-mm/pix Orthophoto, (b) 6-mm/pix DEM, (c) 3.3-mm/pix Orthophoto, (d) 13.5-mm/pix DEM, (e) 2.1-mm/pix Orthophoto, and (f) 8.6-mm/pix DEM

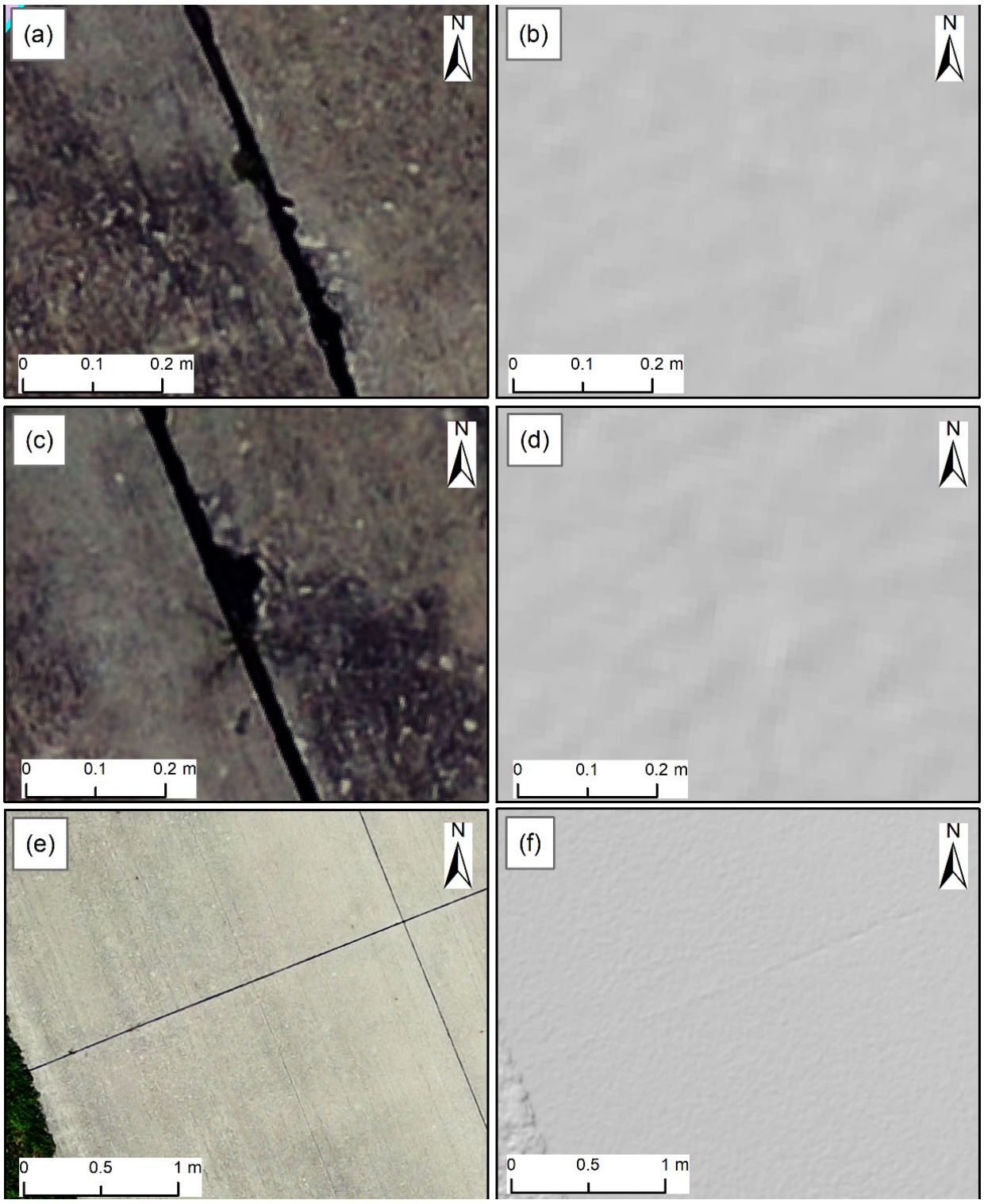

Figure 49. Joint Spalling (L) in (a) 3.3-mm/pix Orthophoto and (b) 13.5-mm/pix DEM; Joint Spalling (M) in (c) 3.3-mm/pix Orthophoto and (d) 13.5-mm/pix DEM; and Joint Seal Damage (M) in (e) 2.4-mm/pix Orthophoto and (f) 9.5-mm/pix DEM

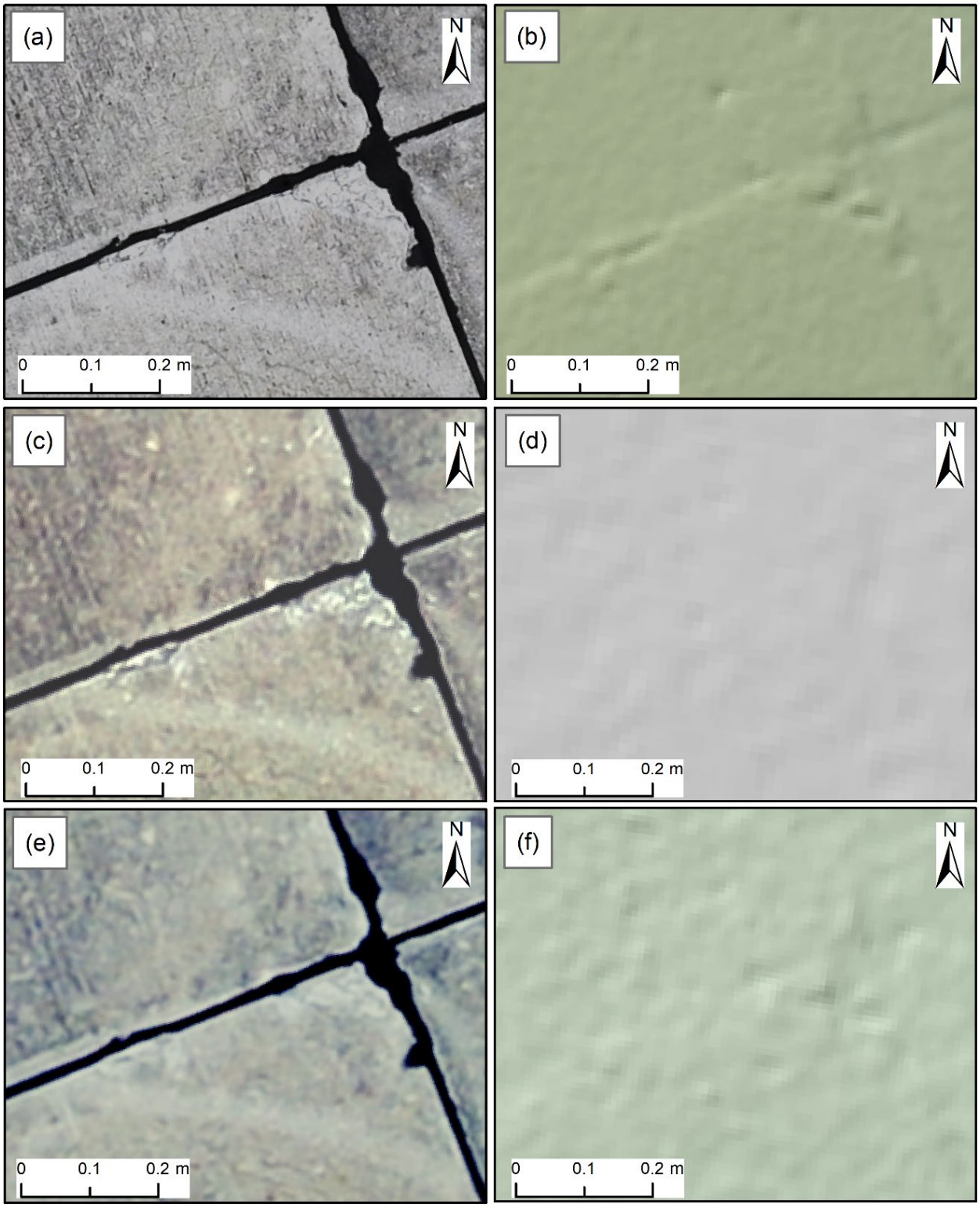

Figure 50. Alkali-Silica Reaction (M) in (a) 1.5-mm/pix Orthophoto, (b) 6-mm/pix DEM, (c) 3.3-mm/pix Orthophoto, (d) 13.5-mm/pix DEM, (e) 2.1-mm/pix Orthophoto, and (f) 8.6-mm/pix DEM

6.2 PERRY MUNICIPAL AIRPORT IN JUNE 2021

6.2.1 Objectives

The research team collected sUAS data from Perry Municipal Airport (PRO), in Perry, Iowa, on June 30, 2021. The runway of PRO was in relatively poor condition compared to the pavements of other airports included in this study, with numerous pavement distresses. Based on the lessons learned from ONZ, TTF, and MTO, the following objectives were determined for data collection at PRO:

- Collect sUAS data from focus areas of the airfield pavements with a single sUAS.
- Evaluate the performance of the Mavic 2 Pro for complete data collection (also part of the BNW effort completed the same week).
- Evaluate the performance of available sUAS platforms and sensors for visualization of various distresses.

6.2.2 Field Demonstration in June 2021

On June 30, 2021, the research team travelled to Perry, Iowa, from Ames, Iowa, to collect sUAS data from PRO by following the sUAS data-collection plan developed beforehand. Eight team members with four Part 107-certified sUAS pilots took part in this data collection. The same set of sUAS used at BNW were also used at PRO. Runway 14/32, Taxiway A, the apron, and high-resolution sample units were the focus of the data collection. Table 15 shows the details of the sUAS platform, sensors, and types of data.

Table 15. Summary of sUAS Data Collection at BNW

Target Areas	sUAS Platforms	Sensors	Flight Altitude (m)	Resolution (mm/pix)	
				Orthophoto	DEM
R14PR-02 SU 01, 04, and 08	Bergen Hexacopter	45.7-mp optical RGB Nikon D850	18.3	1.5	6
	M2EA	48-mp optical RGB	15.2	2.5*	10
	M2EA	512x640 thermal	24.4	31	N/A
Runway 14/32	Mavic 2 Pro	20-mp optical RGB	15.2	3.2	12.9
Taxiway A	Mavic 2 Pro	20-mp optical RGB	15.2	3.2	12.9
Apron 01	M2EA	48-mp optical RGB	15.2	2.5*	10
	M2EA	512x640 thermal	24.4	31	N/A

R14PR-02 = Runway 14/32 SU = Sample unit
N/A = Not applicable
*2.5-mm/pix is not the true effective resolution due to being derived from the M2EA 48-mp Quad Bayer camera.

The data collected from Runway 14/32 and Taxiway A and the apron of PRO were separately imported and processed in Agisoft Metashape. The locations of the sUAS images were corrected using the location information of 19 AeroPoints™ (with built-in GPS) and 6 cloth GCPs (recorded

with the decimeter-resolution Trimble® GeoExplorer® GeoXH 6000 GPS unit) placed throughout the airfield at strategic points likely to result in well-positioned orthophoto output, as shown in Figure 51. The images were processed on a desktop workstation to create optical RGB orthophotos and DEMs. Because Taxiway A is very short, it was processed with Runway 14/32. The down-sampled orthophotos of Runway 14/32, Taxiway A, and the apron were exported and shared with the PCI data collection team.

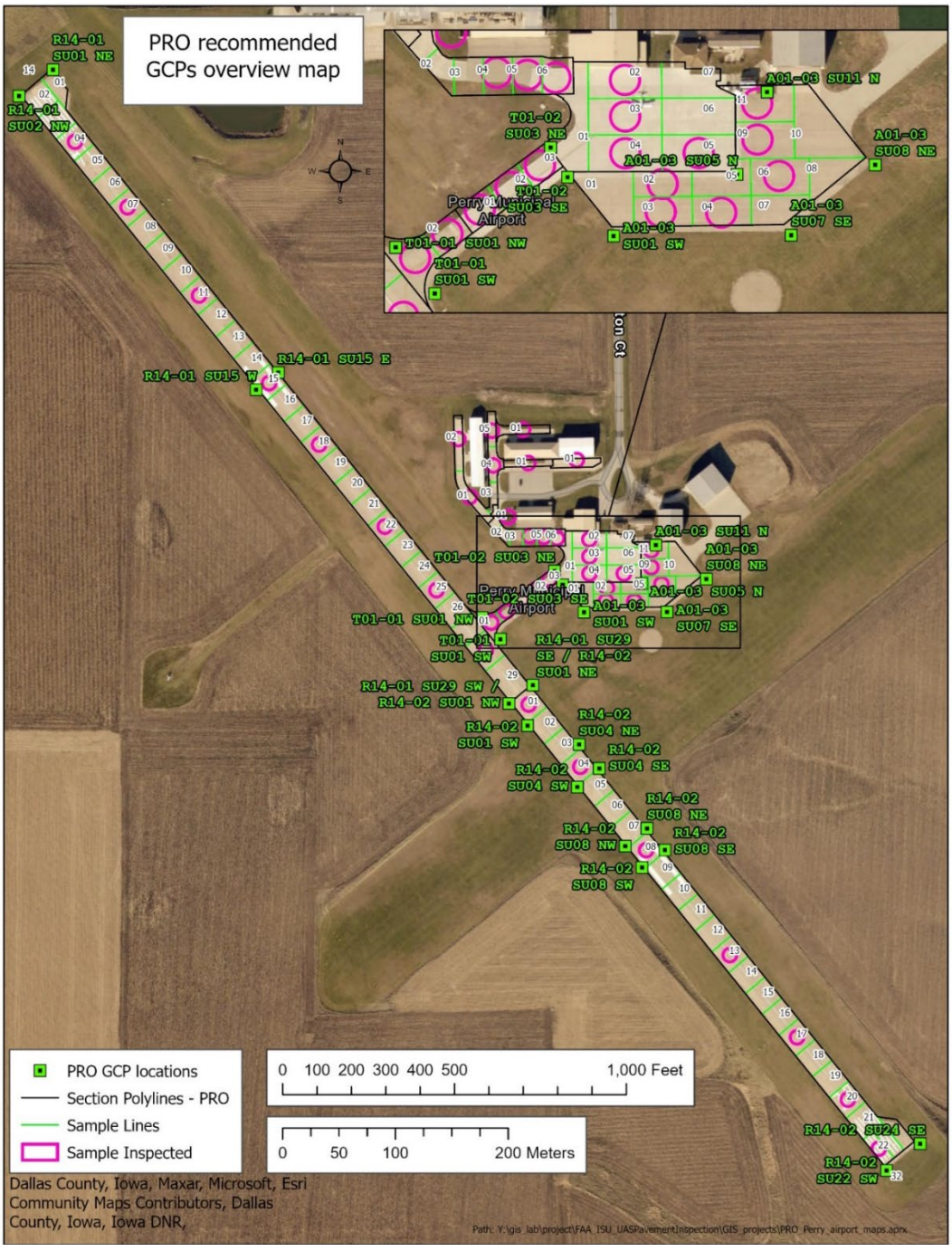

Figure 51. Recommended Locations for GCPs at PRO

On August 3, 2021, an airfield pavement distress FOG survey was conducted at PRO in accordance with the ASTM D5340-20 standard, and the airfield distresses were recorded on a GPS-enabled tablet. The data were processed, and the PCI values for all sample units and branches of the airfield pavement were calculated based on the ASTM D5340-20 standard. Six sample units on the apron, two sample units on Taxiway A, and eight sample units on Runway 14/32 were inspected. The PCI values for the apron sample units varied from 3 to 20, whereas the PCI values for the Runway 14/32 sample units ranged from 14 to 51. The condition of the Taxiway A sample units was relatively better, and the PCI was 57 for both inspected sample units. The predominant distresses were corner breaks, LTD cracks, joint seal damage, small patching, large patching, faulting, shattered slabs, shrinkage cracking, joint spalling, corner spalling, and ASR.

6.2.3 Results and Discussion

The data collected from PRO on June 2021 were separately imported in Agisoft Metashape and processed to create an RGB optical orthophoto and DEM. Different resolutions of sUAS data collected using M2EA and Mavic 2 Pro data were compared to study their usefulness in airfield pavement distress detection. In addition, PCI values calculated using sUAS data were also compared with FOG inspection PCI values (Figure 52). The comparisons of the different data resolution are discussed and shown in Figures 53 through 66 and summarized in Table 16. No PCI data were collected from Runway 14/32, where sample units were located. Therefore, the 1.5-mm/pix RGB orthophoto and 6-mm/pix DEM results are also excluded from this data analysis. The analysis of the available data is summarized as follows:

- 2.5-mm/pix and 3.2-mm/pix RGB orthophoto data were adequate to detect corner breaks, LTD cracks, joint seal damage, small patching, large patching, faulting, shattered slab shrinkage crack, joint spalling, corner spalling, and ASR with different severities.
- 10-mm/pix DEM could be used to detect high-severity shattered slab and corner spalling. However, higher-resolution DEMs generated using data collected with Nikon D850 have already proven very useful for distress detection at other airports.

The RGB orthophoto and DEM data of Runway 14/32 and Taxiway A of PRO were imported to the ArcGIS Pro for visual identification of the pavement distresses. Each PCC pavement distress was identified with its associated severity levels and documented on a shapefile. PCI values for the sample units were calculated based on the documented distresses and their severity level by following the standard procedure outlined in ASTM D5340-20. The sUAS-based PCI value and FOG PCI value for each sample are plotted and shown in Figure 52.

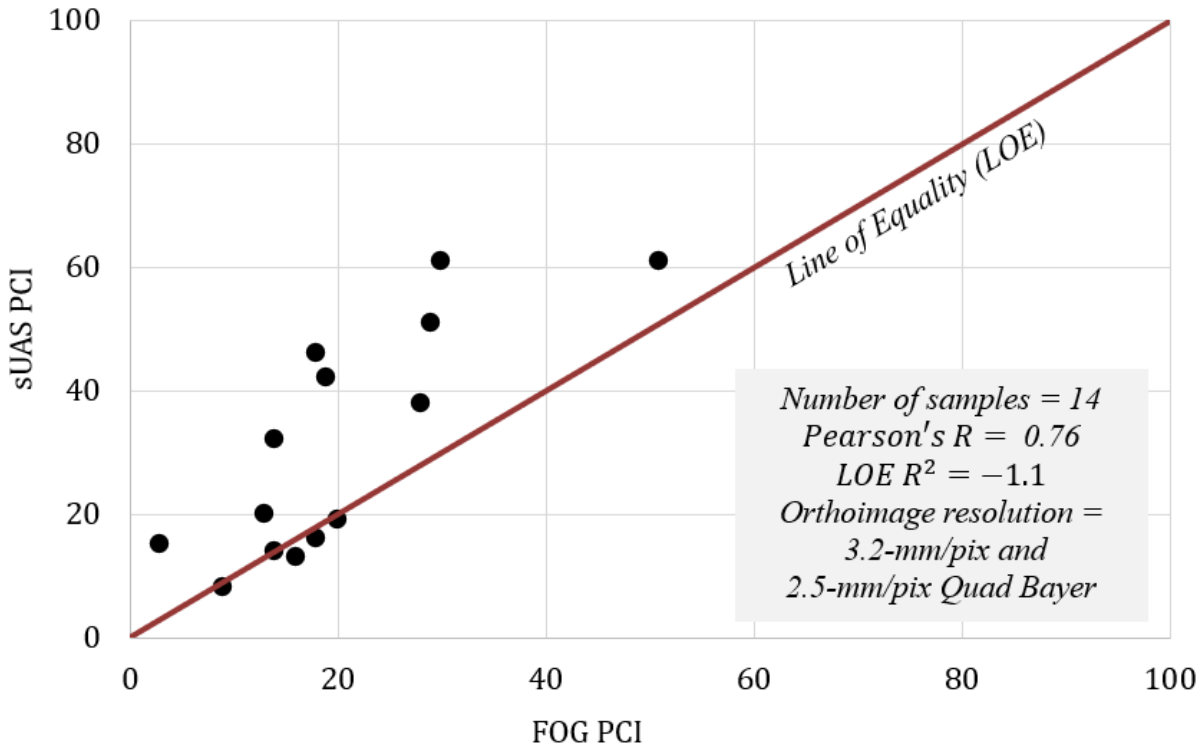

Figure 52. Comparison Between FOG PCI and sUAS PCI Calculated Using 2.5-mm/pix and 3.2-mm/pix Data from PRO

The sUAS PCI values were relatively higher than the FOG PCI value because faulting of different severity was challenging to identify in DEM with resolution of more than 10 mm/pix. DEM of 3 mm/pix was useful in confirming the suspected location faulting at ONZ. The PRO data also showed that the low-severity ASR was often not identified adequately, similar to BNW and ONZ.

Table 16. Summary of the Findings of PRO

Distress Name (PAVER™ Distress Number)	Severity	Resolution Tested (mm/pix)		Distress Detected and Severity Rating (mm/pix)		Remarks
		RGB	DEM	RGB	DEM	
Corner breaks (62)	L	2.5*, 3.2	10, 12.9	3.2	ND	Figure 53
	M	3.2	12.9	3.2	ND	Figure 54
	H	3.2	12.9	3.2	ND	
LTD cracks (63)	L	2.5*, 3.2	10, 12.9	3.2	ND	Figure 54
	M	2.5*, 3.2	10, 12.9	3.2	ND	Figure 55
Joint seal damage (65)	L	2.5*	10	ND	ND	Figure 56
	M	2.5*	10	2.5	ND	
	H	3.2	12.9	3.2	ND	Figure 55
Small patching (66)	L	2.5*	10	2.5	ND	Figure 57
	M	3.2	12.9	3.2	ND	Figure 56
	H	3.2	12.9	3.2	12.9	
Large patching (67)	L	3.2	12.9	3.2	ND	Figure 58
Faulting (71)	L	2.5*, 3.2	10, 12.9	ND	ND	Figure 58
	M	3.2	12.9	ND	ND	Figure 59
	H	3.2	12.9	ND	ND	
Shattered slab (72)	M	2.5*, 3.2	10, 12.9	ND	ND	Figure 61
	H	2.5*	10	2.5	10	Figure 60
Shrinkage crack (73)	N/A	2.5*, 3.2	10, 12.9	3.2	ND	Figure 60
Joint spalling (74)	L	2.5*, 3.2	10, 12.9	3.2	ND	Figure 63
	M	2.5*, 3.2	10, 12.9	3.2	12.9**	Figure 62
	H	2.5*, 3.2	10, 12.9	3.2	12.9**	
Corner spalling (75)	L	2.5*, 3.2	10, 12.9	3.2	ND	Figure 65
	M	2.5*, 3.2	10, 12.9	3.2	12.9**	Figure 63
	H	2.5*, 3.2	10, 12.9	3.2	12.9	Figure 64
ASR (76)	L	2.5*, 3.2	10, 12.9	3.2	ND	Figure 65
	M	2.5*, 3.2	10, 12.9	3.2	ND	Figure 61
	H	2.5*, 3.2	10, 12.9	3.2	12.9**	Figure 66

L = Low, M = Medium, H = High ND = Not Detected
N/A = Not Applicable (no severity level for shrinkage crack)
*2.5 mm/pix is not the true resolution due to being derived from the M2EA 48-mp Quad Bayer camera.
** Only 12.9 mm/pix DEM were found to be useful, and 10 mm/pix was excluded.

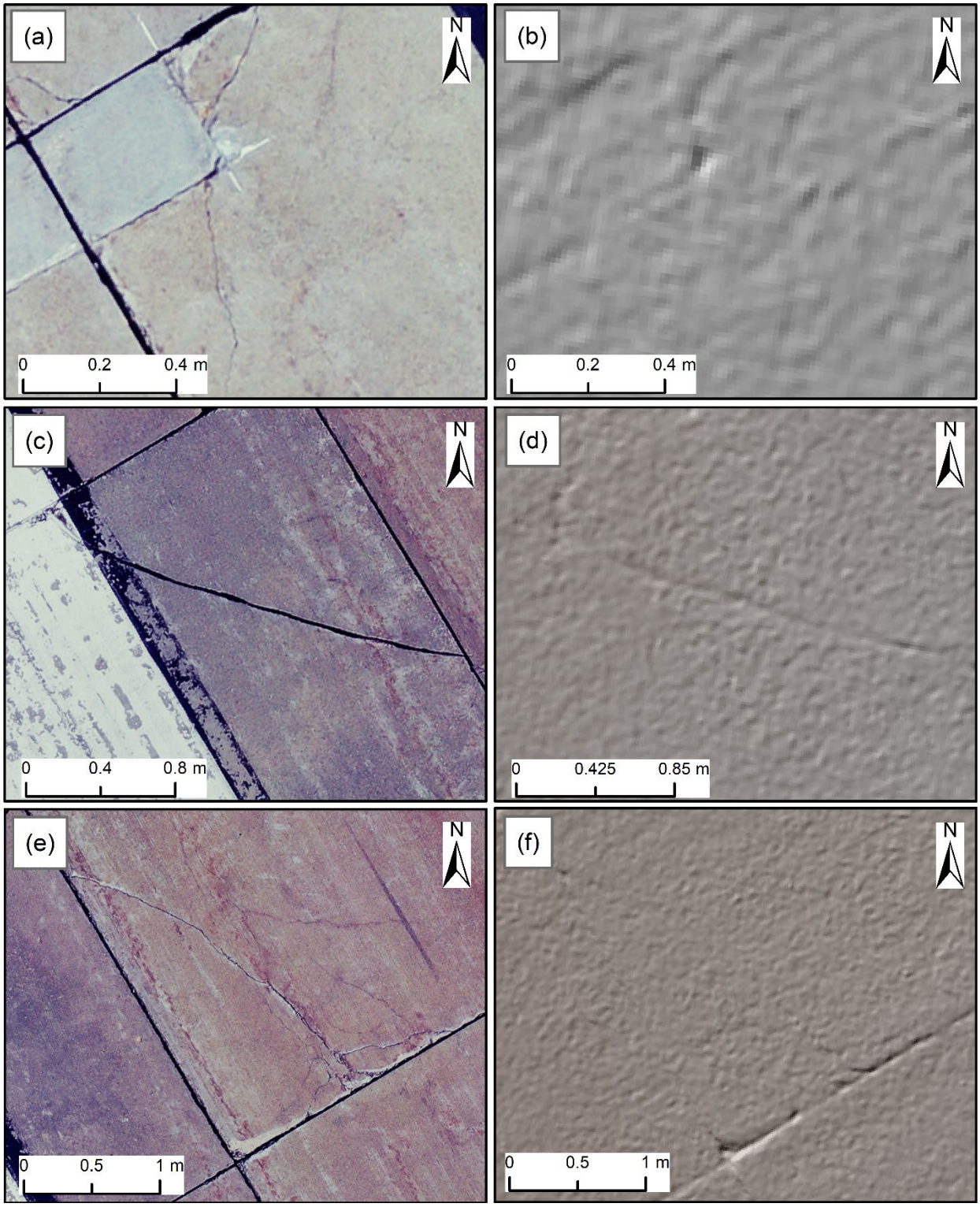

Figure 53. Corner Breaks (L) in (a) 3.2-mm/pix Orthophoto and (b) 12.9-mm/pix DEM; Corner Breaks (M) in (c) 3.2-mm/pix Orthophoto and (d) 12.9-mm/pix DEM; and Corner Break (H) in (e) 3.2-mm/pix Orthophoto and (f) 12.9-mm/pix DEM

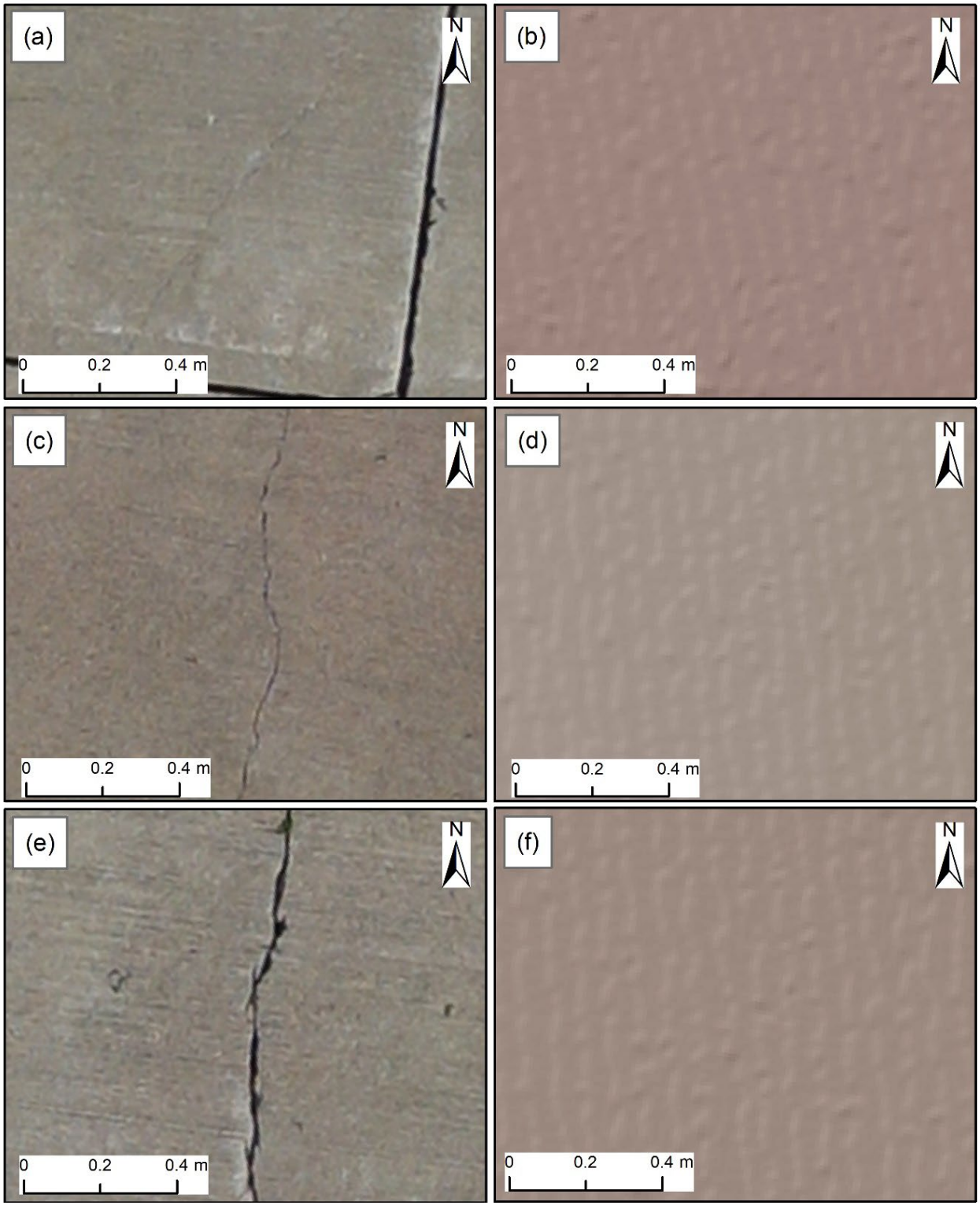

Figure 54. Corner Break (L) in (a) 2.5-mm/pix Orthophoto and (b) 10-mm/pix DEM; LTD Cracks (L) in (c) 2.5-mm/pix Orthophoto and (d) 10-mm/pix DEM; and LTD Cracks (M) in (e) 2.5-mm/pix Orthophoto and (f) 10-mm/pix DEM

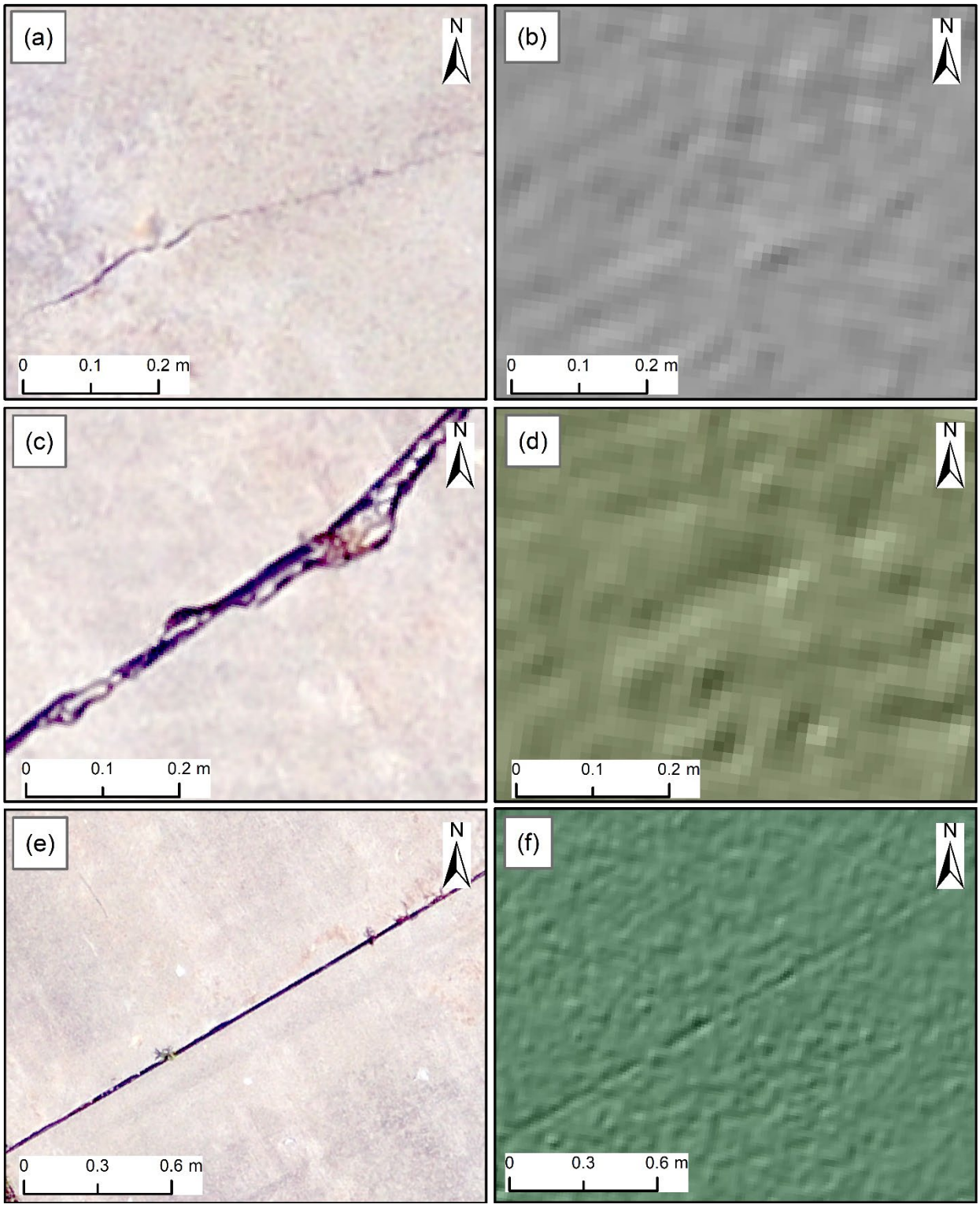

Figure 55. Longitudinal, Transverse, and Diagonal Cracks (L) in (a) 3.2-mm/pix Orthophoto and (b) 12.9-mm/pix DEM; LTD Cracks (M) in (c) 3.2-mm/pix Orthophoto and (d) 12.9-mm/pix DEM; and Joint Seal Damage (H) in (e) 3.2-mm/pix Orthophoto and (f) 12.9-mm/pix DEM

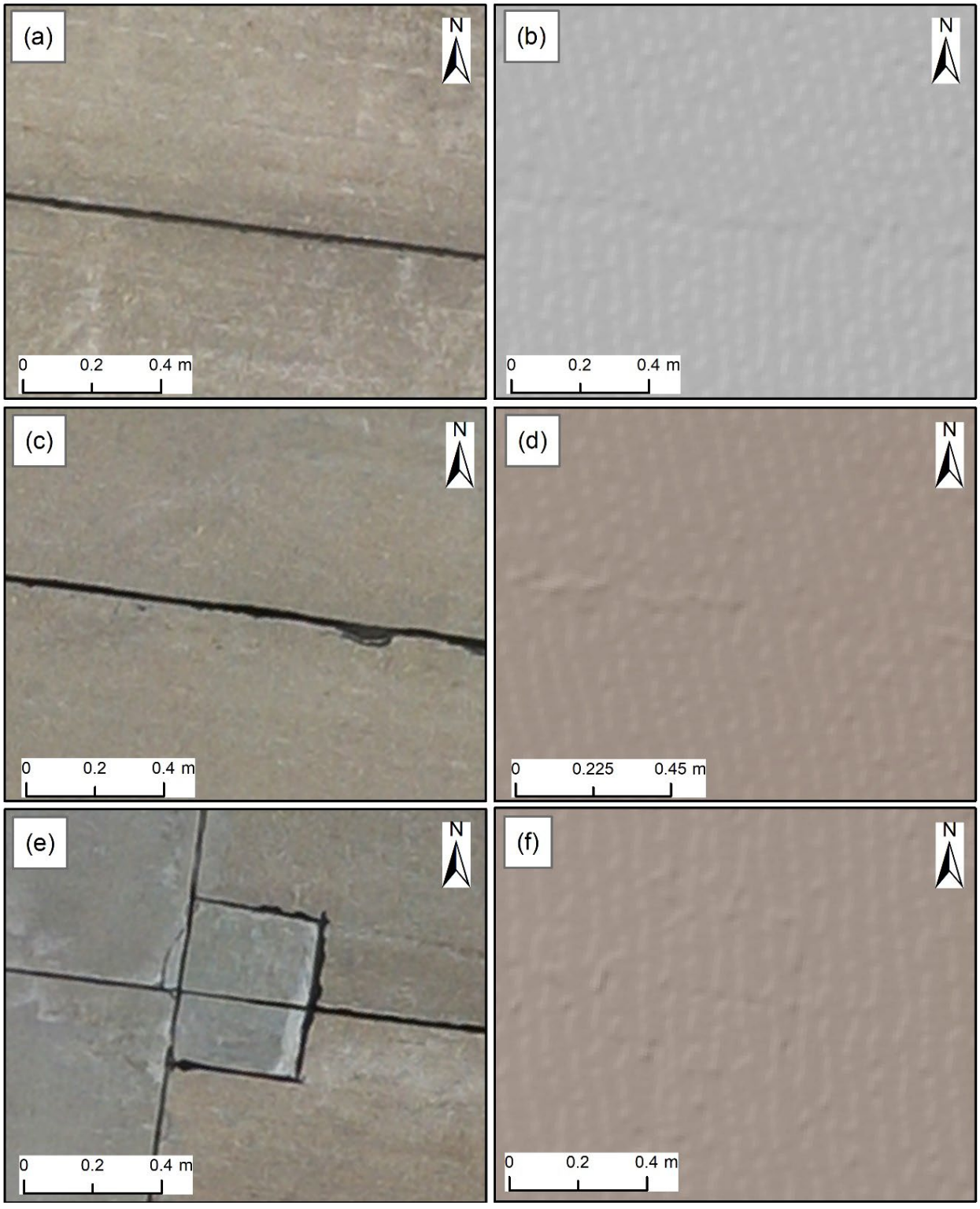

Figure 56. Joint Seal Damage (L) in (a) 2.5-mm/pix Orthophoto and (b) 10-mm/pix DEM; Joint Seal Damage (M) in (c) 2.5-mm/pix Orthophoto and (d) 10-mm/pix DEM; and Small Patching (L) in (e) 2.5-mm/pix Orthophoto and (f) 10-mm/pix DEM

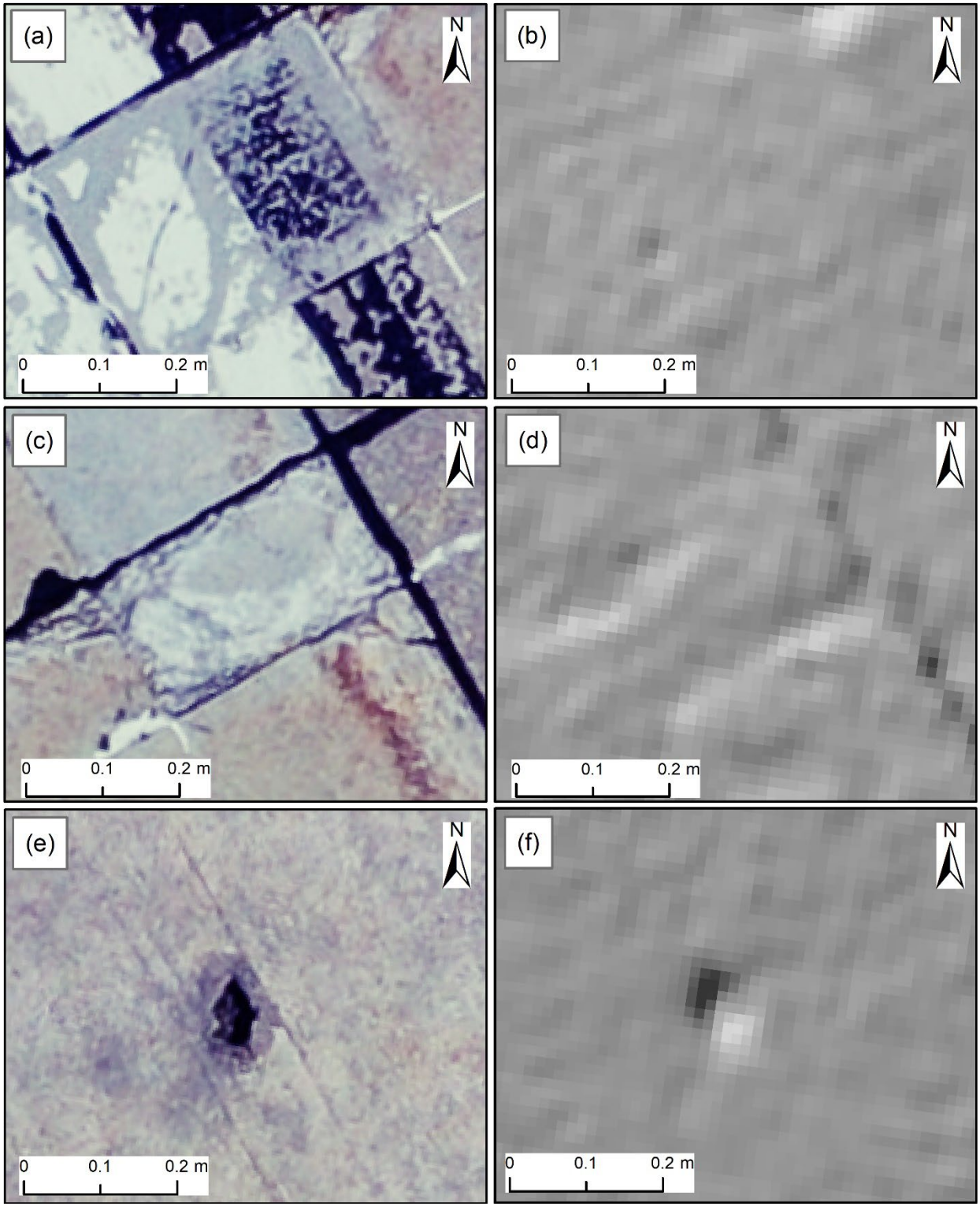

Figure 57. Small Patching (L) in (a) 3.2-mm/pix Orthophoto and (b) 12.9-mm/pix DEM; Small Patching (M) in (c) 3.2-mm/pix Orthophoto and (d) 12.9-mm/pix DEM; and Small Patching (H) in (e) 3.2-mm/pix Orthophoto and (f) 12.9-mm/pix DEM

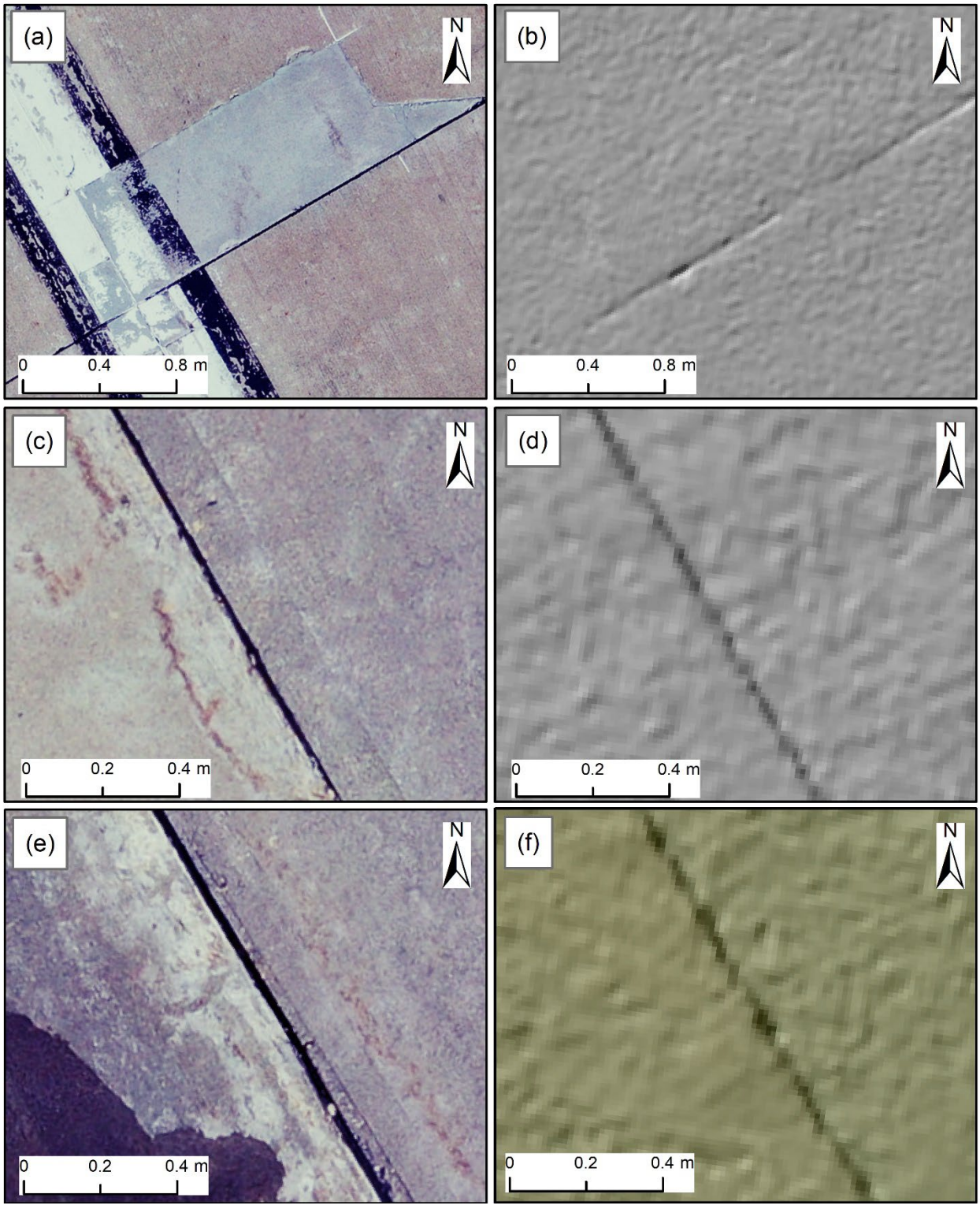

Figure 58. Large Patching (L) in (a) 3.2-mm/pix Orthophoto and (b) 12.9-mm/pix DEM; Faulting (M) in (c) 3.2-mm/pix Orthophoto and (d) 12.9-mm/pix DEM; and Faulting (H) in (e) 3.2-mm/pix Orthophoto and (f) 12.9-mm/pix DEM

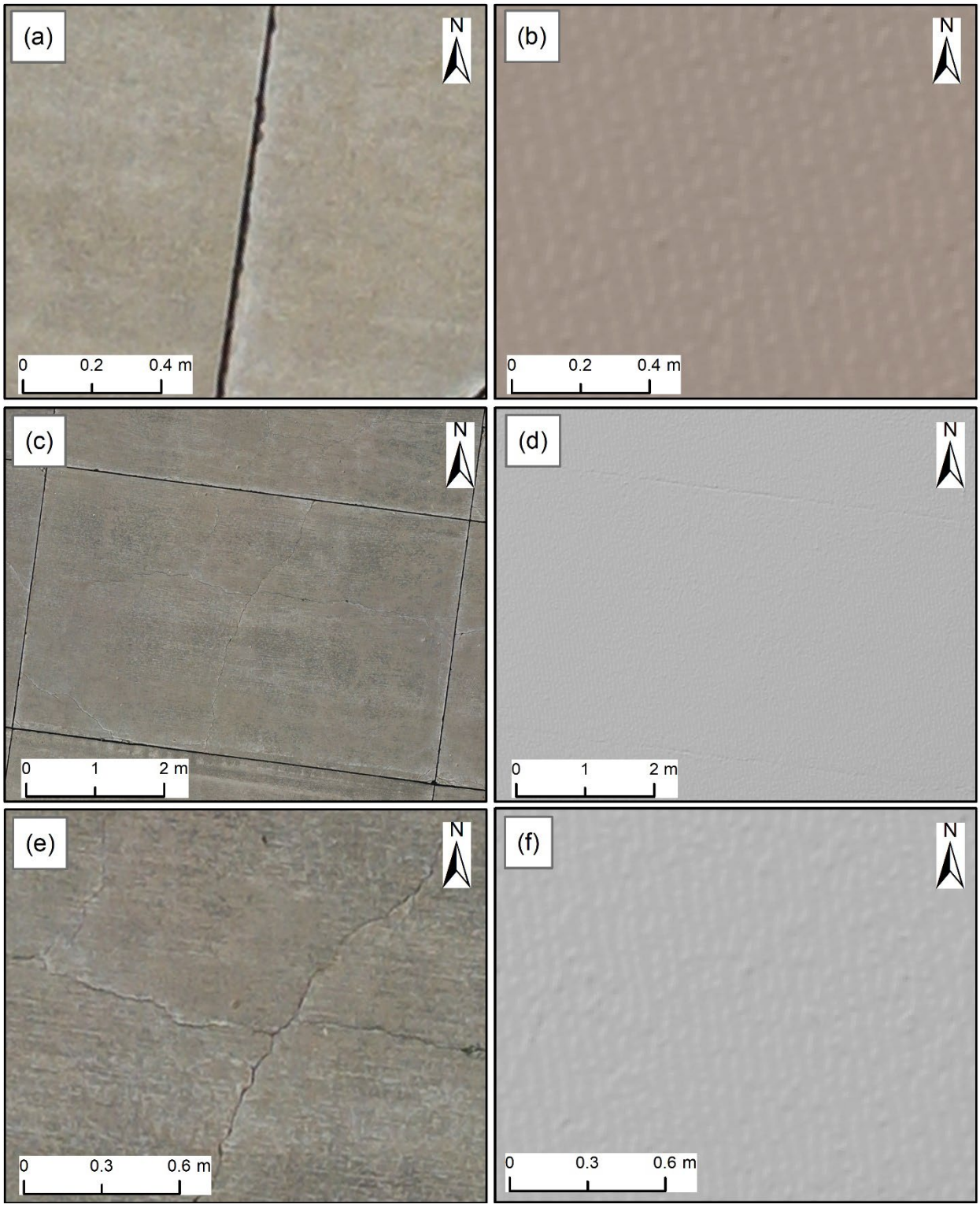

Figure 59. Faulting (L) in (a) 2.5-mm/pix Orthophoto and (b) 10-mm/pix DEM; and Shattered Slabs (M) in (c, e) 2.5-mm/pix Orthophoto and (d, f) 10-mm/pix DEM

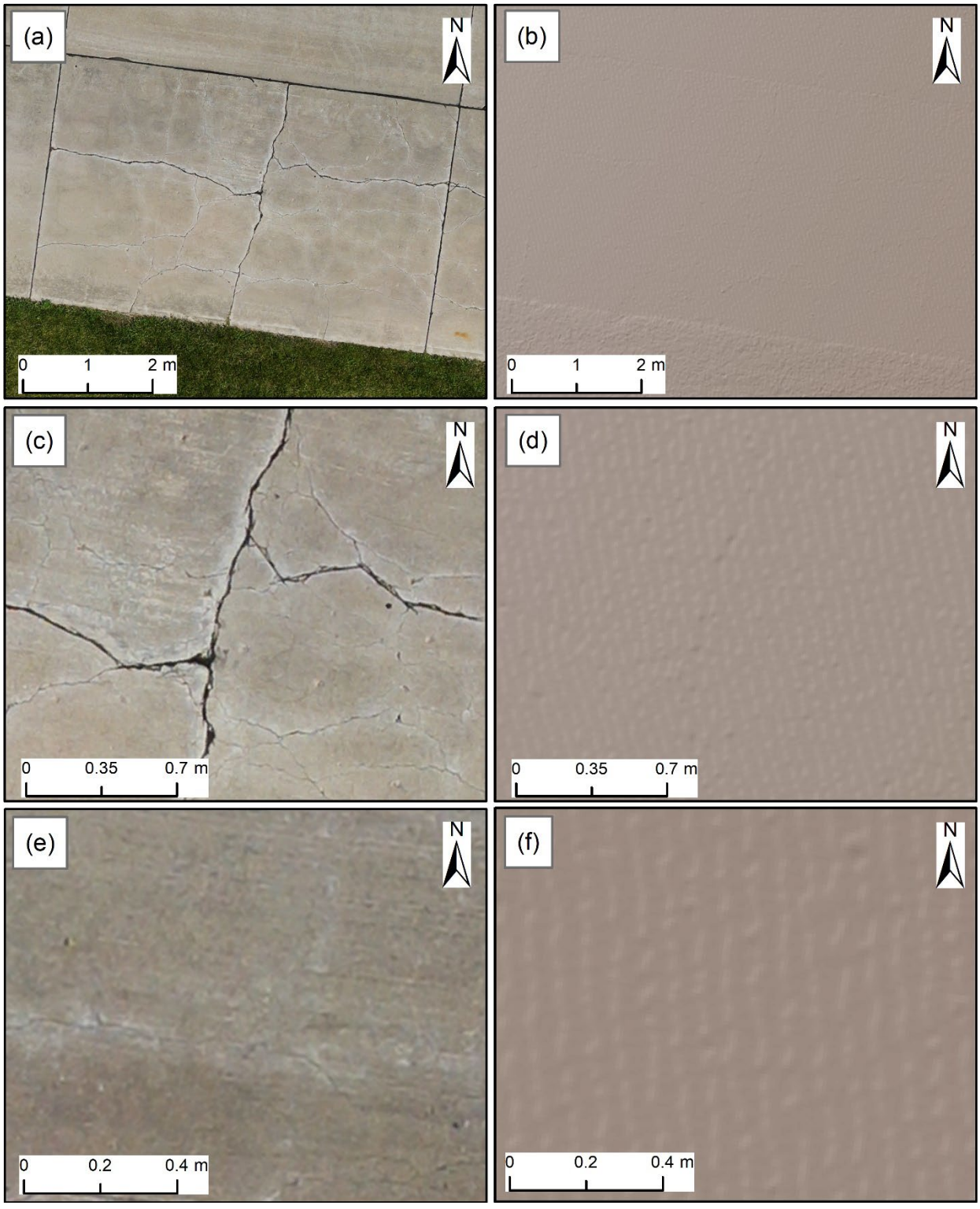

Figure 60. Shattered Slab (H) in (a, c) 2.5-mm/pix Orthophoto and (b, d) 10-mm/pix DEM; and Shrinkage Crack in (e) 2.5-mm/pix Orthophoto and (f) 10-mm/pix DEM

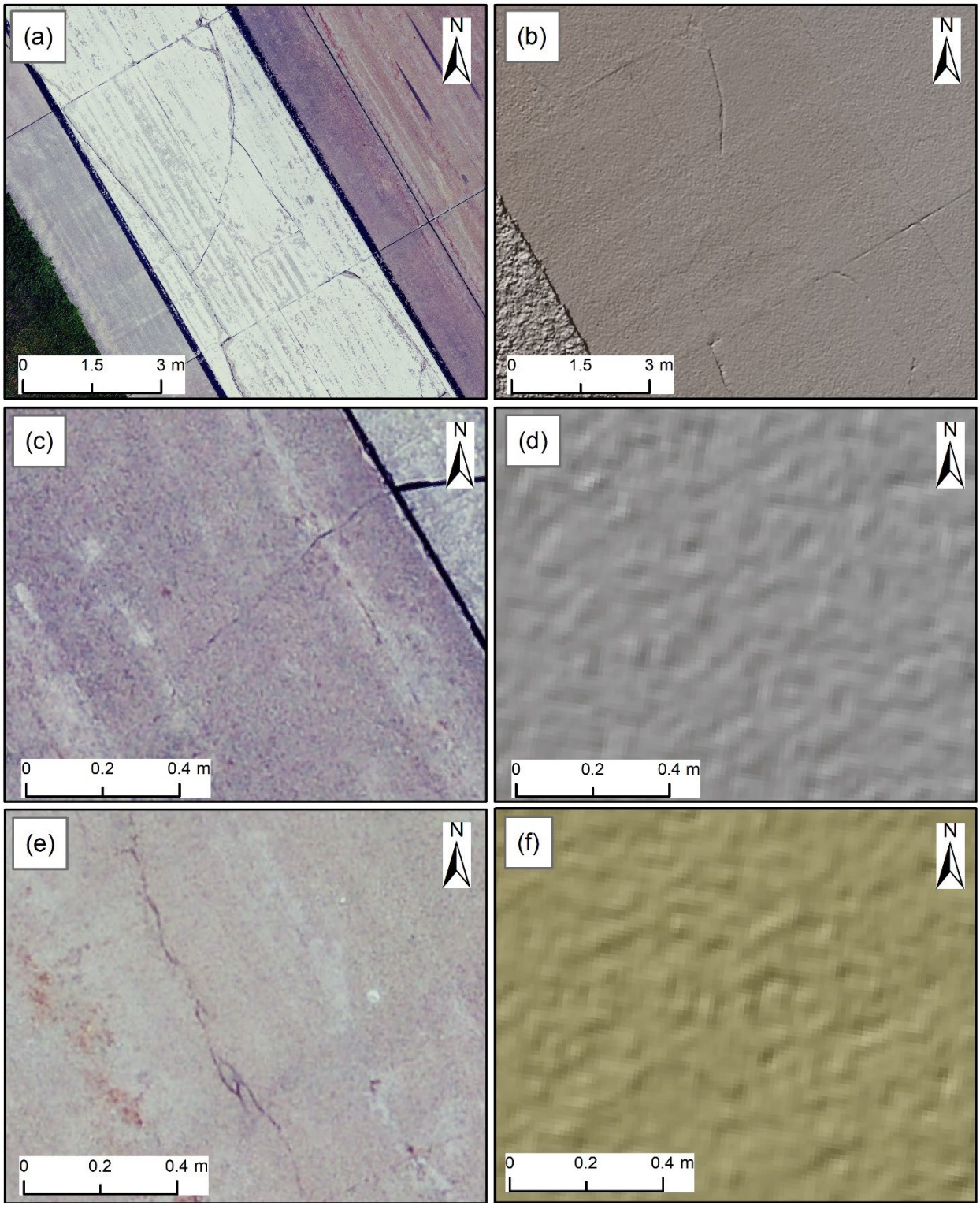

Figure 61. Shattered Slab (M) in (a) 3.2-mm/pix Orthophoto and (b) 12.9-mm/pix DEM; Shrinkage Crack in (c) 3.2-mm/pix Orthophoto and (d) 12.9-mm/pix DEM; and ASR (L) in (e) 3.2-mm/pix Orthophoto and (f) 12.9-mm/pix DEM

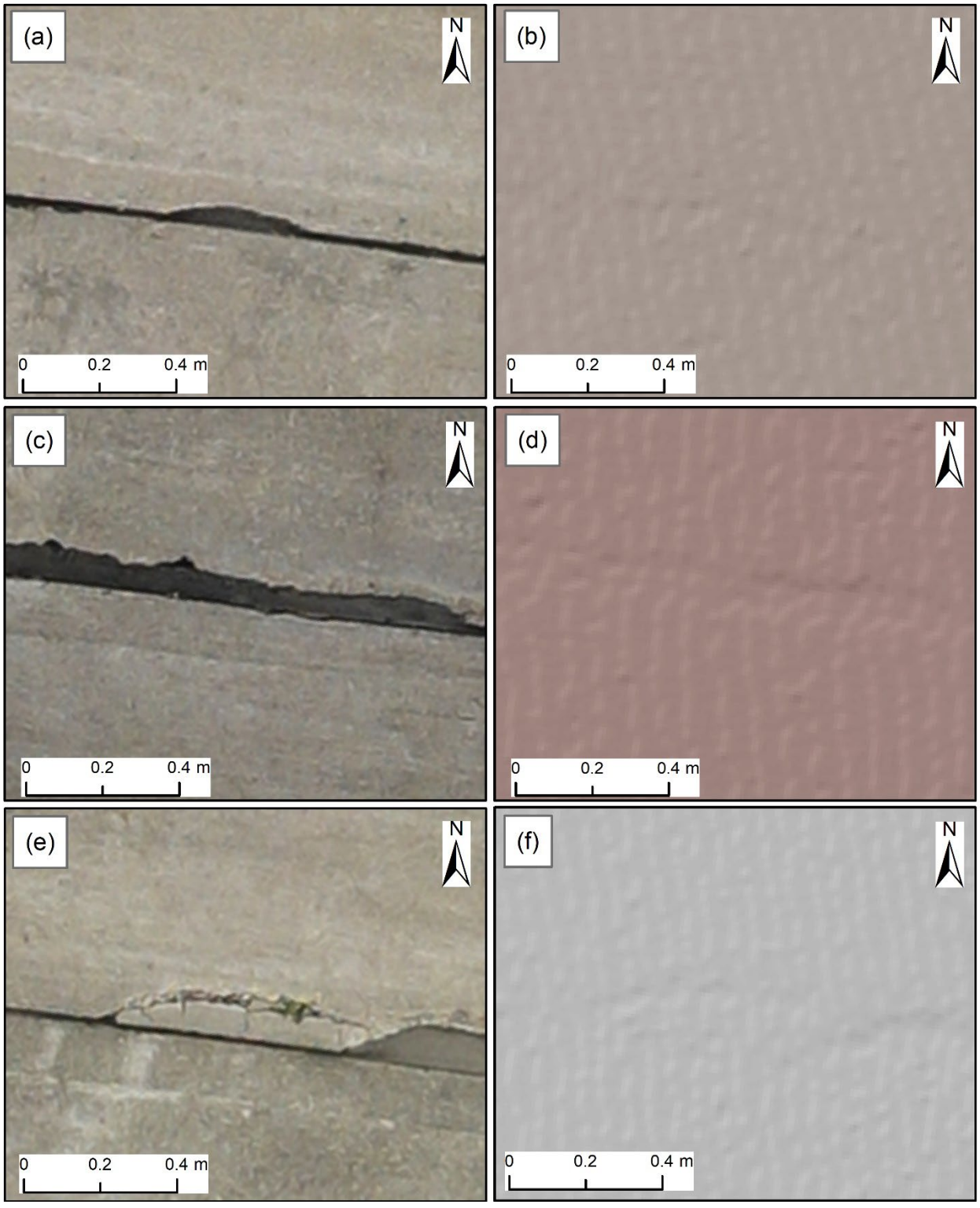

Figure 62. Joint Spalling (L) in (a) 2.5-mm/pix Orthophoto and (b) 10-mm/pix DEM; Joint Spalling (M) in (c) 2.5-mm/pix Orthophoto and (d) 10-mm/pix DEM; and Joint Spalling (H) in (e) 2.5-mm/pix Orthophoto and (f) 10-mm/pix DEM

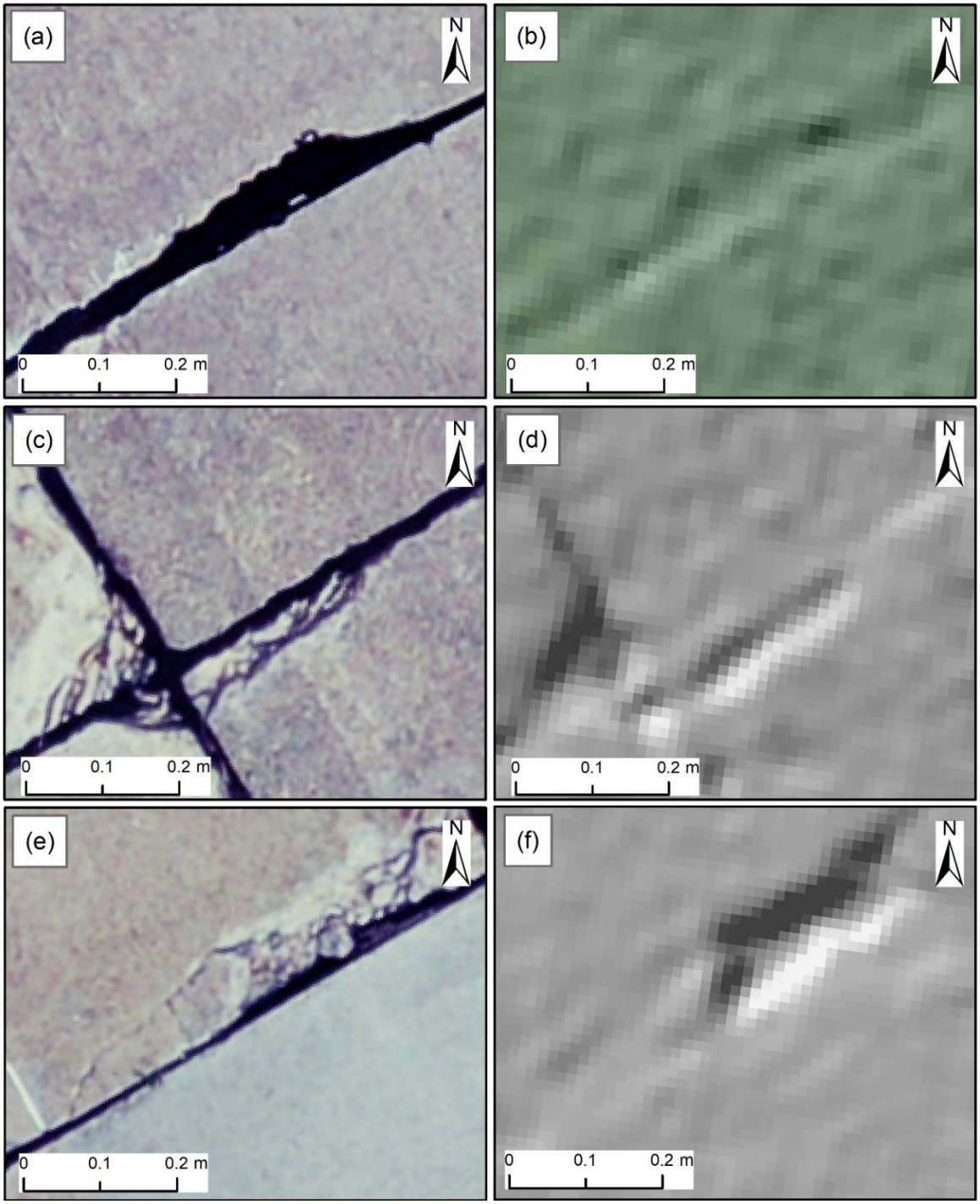

Figure 63. Joint Spalling (L) in (a) 3.2-mm/pix Orthophoto and (b) 12.9-mm/pix DEM; Joint Spalling (M) on Right and Corner Spalling (M) on Left in (c) 3.2-mm/pix Orthophoto and (d) 12.9-mm/pix DEM; and Joint Spalling (H) in (e) 3.2-mm/pix Orthophoto and (f) 12.9-mm/pix DEM

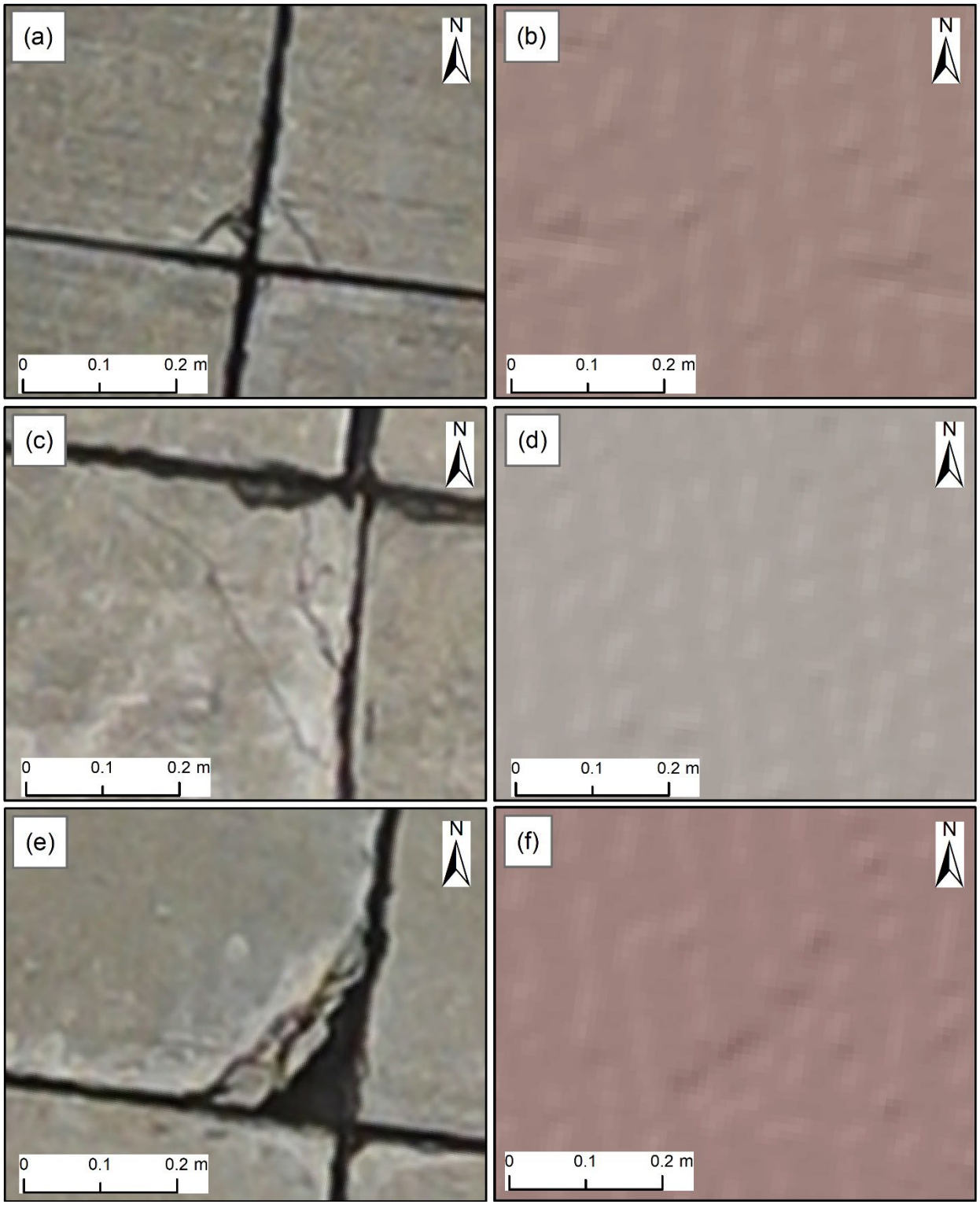

Figure 64. Corner Spalling (L) in (a) 2.5-mm/pix Orthophoto and (b) 10-mm/pix DEM; Corner Spalling (M) in (c) 2.5-mm/pix Orthophoto and (d) 10-mm/pix DEM; and Corner Spalling (H) in (e) 2.5-mm/pix Orthophoto and (f) 10-mm/pix DEM

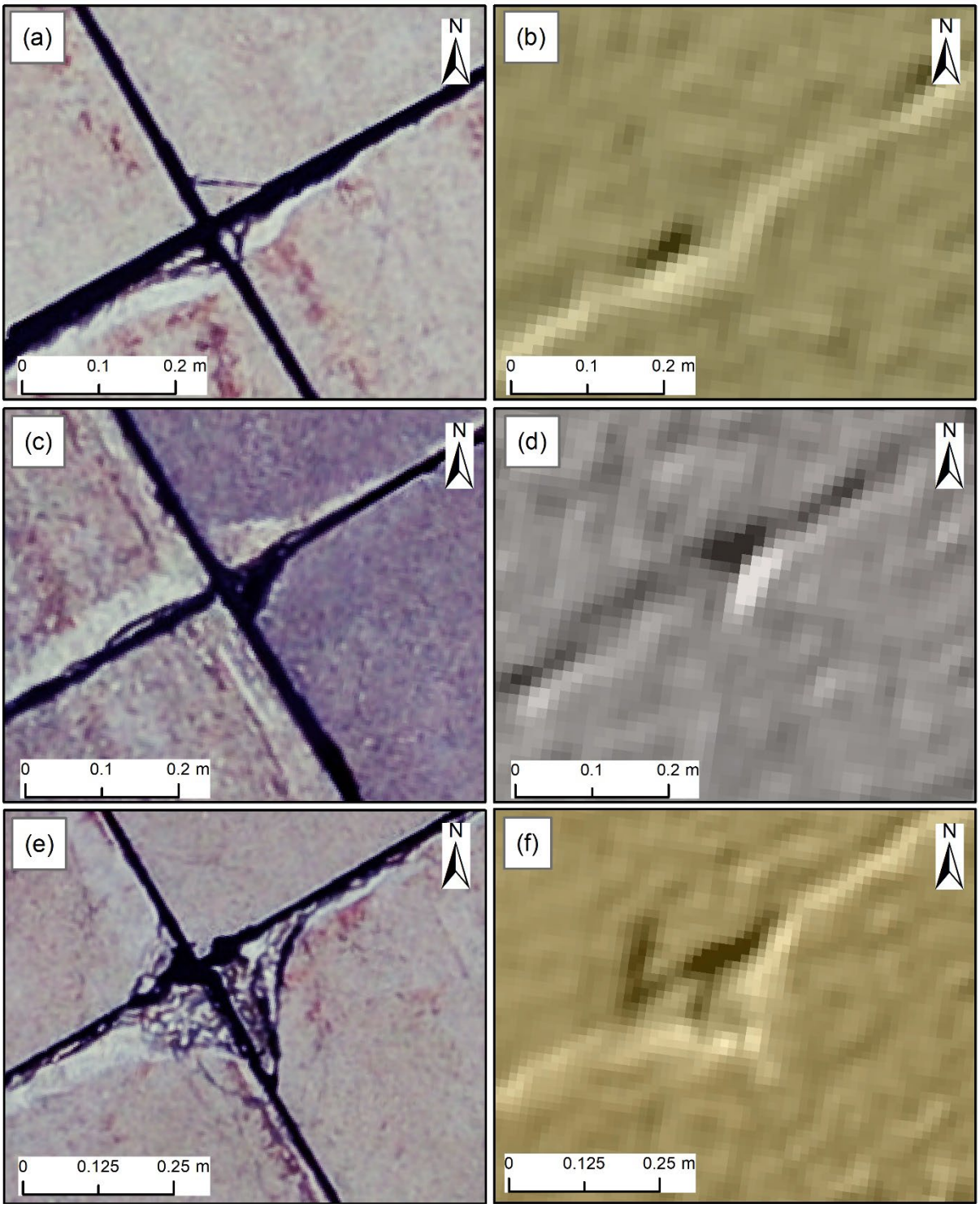

Figure 65. Corner Spalling (L) on Top and ASR (L) on Bottom-left and Bottom-right of Joint Intersection in (a) 3.2-mm/pix Orthophoto and (b) 12.9-mm/pix DEM; Corner Spalling (M) on Left in (c) 3.2-mm/pix Orthophoto and (d) 12.9-mm/pix DEM; and ASR (H) in (e) 3.2-mm/pix Orthophoto and (f) 12.9-mm/pix DEM

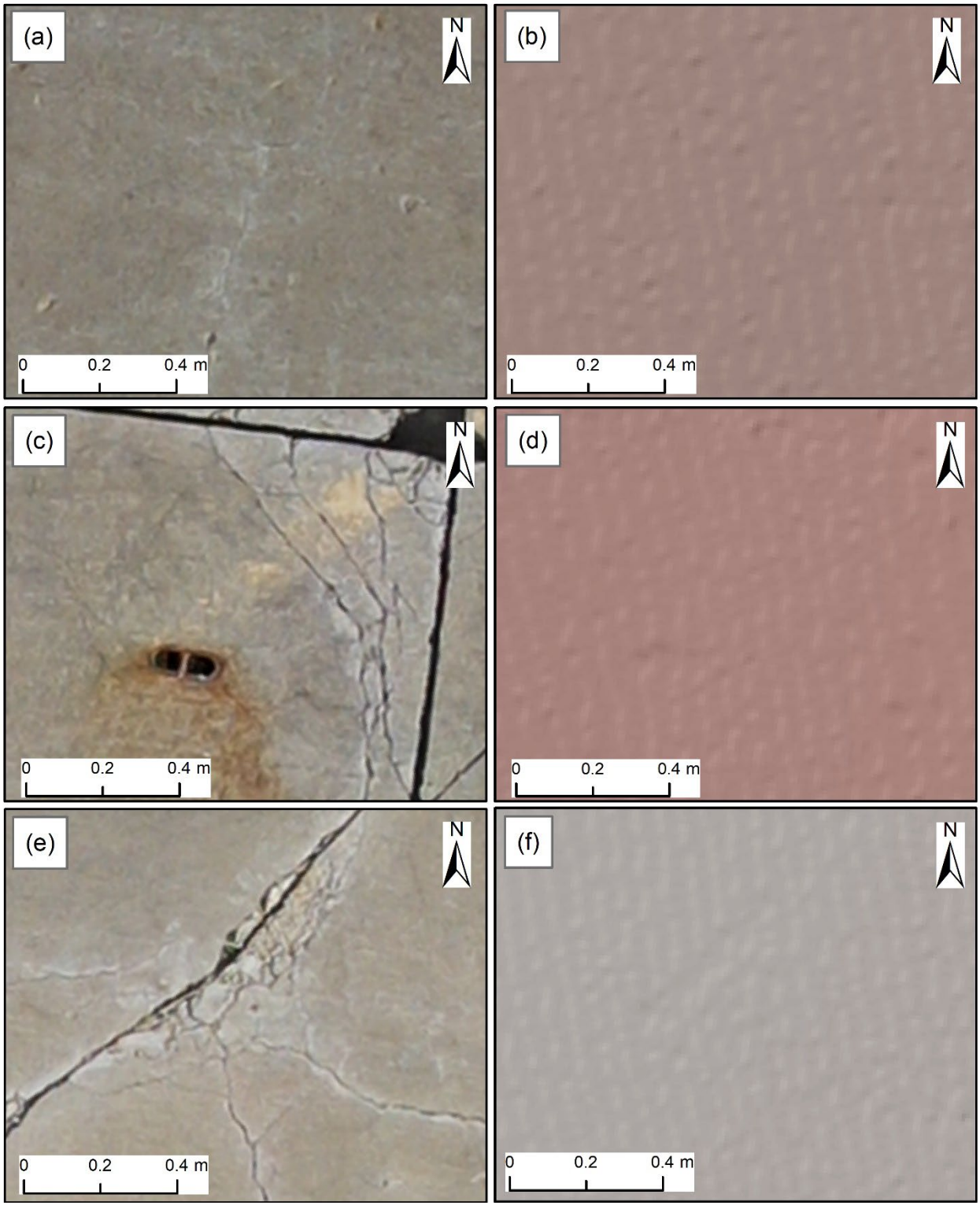

Figure 66. Alkali-Silica Reaction (L) in (a) 2.5-mm/pix Orthophoto and (b) 10-mm/pix DEM; ASR (M) in (c) 2.5-mm/pix Orthophoto and (d) 10-mm/pix DEM; and ASR (H) in (e) 2.5-mm/pix Orthophoto and (f) 10-mm/pix DEM

7. FIELD DEMONSTRATION IN NEW JERSEY

7.1 CAPE MAY AIRPORT IN AUGUST 2021

7.1.1 Objectives

Cape May Airport (WWD) in Lower Township, New Jersey, was selected by the FAA to demonstrate the capability of sUAS to identify and rate different airfield pavement distresses using results and findings from airports in Michigan, Illinois, and Iowa earlier in this study. The research team collected PCI and sUAS data at WWD from August 23 to 26, 2021. The lessons learned from the airports in Michigan, Illinois, and Iowa were used to select sUAS platforms, sensors, and flight parameters for deployment at this airport. The objectives of this field demonstration are summarized as follows:

- Showcase the capabilities of the recommended sUAS platform and sensors for airfield pavement distress identification.
- Collect sUAS data from identical sample units where PCI surveys were also conducted.

7.1.2 Field Demonstration in August 2021

A complete field demonstration plan developed for WWD was executed from August 23 to 26, 2021. The data collection team collected sUAS and PCI survey data following all the standard safety protocols. The PCI data collection team arrived at Lower Township, New Jersey, on August 22, 2021, and collected PCI inspection data at WWD from August 23 to 25, 2021. The sUAS data collection team arrived at Atlantic City, New Jersey, on August 23, 2021, and collected the sUAS data at WWD from August 24 to 26, 2021. At the request of the FAA, the research team focused on collecting complete sUAS data at 2.0 mm/pix or higher from the Runway 10/28 and the fixed-base operator (FBO) Apron. The Nikon D850 45.7-mp camera with 50-mm prime lens was mounted on the newly available Tarot X6 (manufactured by UAVSI of Las Vegas, Nevada, with the U.S.-made Pixhawk flight controller) and flown at 18.3-m altitude to collect the 1.5-mm/pix resolution data. In addition, backup data were collected using Mavic 2 Pro with 20-mp optical RGB camera at 15.2-m flight altitude and M2EA with 48-mp Quad Bayer RGB camera at 24.4 m, which resulted in orthophoto resolutions of 3.5 mm/pix and 4.1 mm/pix, respectively. The M2EA UAV also collected thermal data to potentially help with distress detection using its onboard 640x512 radiometric 30-Hz thermal camera. In addition to the complete data collection, the highest resolution (<1 mm/pix) sample unit data were also collected for nine focus sample units, as shown in Table 17. The mdMapper1000+ with its Sony RX1R-II 42.4-mp camera was flown to collect data from 18.3 m and 9.1 m altitude to demonstrate its potential in sufficiently low wind conditions, but an unexpected software bug in the flight control application prevented successful data collection over most areas. For the limited areas collected, the 18.3-m height data collected with mdMapper with Sony RGB camera yielded orthophotos with 2.2-mm/pix resolution and DEMs with 8.9-mm/pix resolution. The 9.1-m height mdMapper/Sony data collections yielded resolutions of 1.2 mm/pix for orthophotos and 4.8 mm/pix for DEMs.

As shown in Table 17, the sUAS data collection spanned 3 days. Collecting high-resolution 45.7-mp data with the Nikon D850 at a low flight altitude (18.3 m) required significant time with the Tarot X6 platform. In addition, there was longer downtime for battery charging and swapping

because practical flight times with the batteries available were limited to approximately 8 to 9 minutes. Therefore, the highest priority was given to this sUAS. GCP placement was planned as shown in Figure 67 to facilitate reusing the AeroPoints™ for multiple data collections. Seventy-six GCPs were placed around the WWD data collection areas over 3 days of data collection, with most of them collected using the 20 AeroPoints™ owned by the research team.

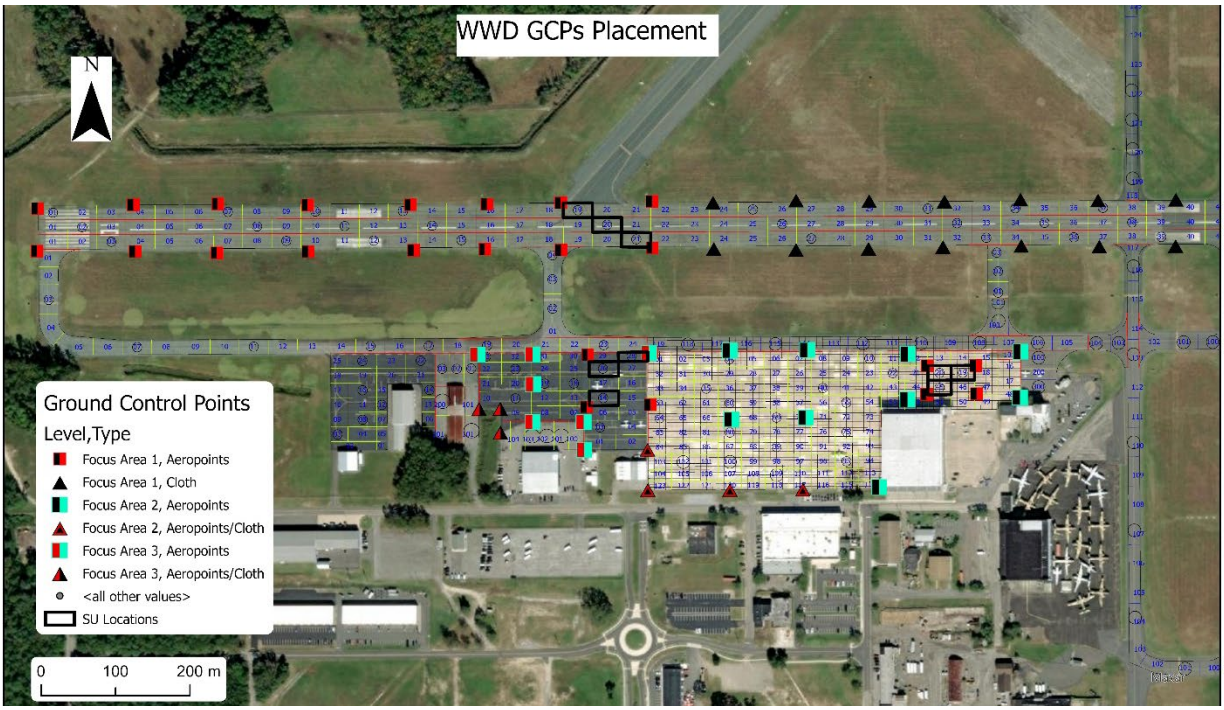

Figure 67. Overview of WWD and Sampling Focus Areas, Including Recommended Locations for 60 Planned GCPs

The data collection team followed the standard sUAS and airport safety guidelines as outlined in Appendices B and C. Support was provided by two FAA employees to assist with the data collection. An FAA field vehicle was used to recharge the sUAS batteries and take shade. The inverter on the vehicle facilitated fast-charging multiple Tarot X6 batteries that would have taken longer using the research team's charging station (usually a generator).

At WWD, a FOG condition survey was conducted in accordance with ASTM D5340-20. A two-person ground crew recorded the airfield distresses with a GPS-enabled tablet system between August 23 and August 25, 2021. The PCI data collection team collected PCI data from 55 selected sample units of the different parts of Runway 10/28 and FBO Apron. The sample units were selected based on the suggestions of the FAA representative for this project and previous PCI inspection reports.

Table 17. Summary of sUAS Data Collection at WWD

Date	Target Area	sUAS Platform	Sensors	Flight Altitude (m)	Resolution (mm/pix)	
					Orthophoto	DEM
August 24, 25, and 26	Runway 10/28 and FBO Aprons	Tarot X6	45.7-mp optical RGB Nikon D850	18.3	1.5	5.9
		Mavic 2 Pro	20-mp optical RGB	15.2	3.5	14
		M2EA	512x640 thermal	24.4	31.5	N/A
			48-mp Quad Bayer optical RGB	24.4	4.1	16.2
August 26	SUs (9 focus sample units)	mdMapper1000+	42.4-mp optical RGB Sony RX1R-II	18.3*	2.2	8.5
				9.1*	1.3	5.4
		Tarot X6	45.7-mp optical RGB Nikon D850	9.1	0.8	3

SU = Sample unit N/A = Not applicable
* Collected over limited areas due to unexpected bug in mdMapper1000+ flight control software.

7.1.3 Results and Discussion

All sUAS optical RGB data collected with different sensors were imported to Agisoft Metashape for processing. The locations of the images were corrected with GCP location information. Agisoft Metashape exported high-resolution RGB orthophoto and DEM as output, as listed in Table 17. The primary sUAS sensor data, i.e., the Nikon D850 45.7 mp, had considerable processing time because of the data volume. DEMs were also used to generate hillshades for better visualization. DEMs and orthophotos of different resolutions were compared to evaluate their capabilities in individual airfield pavement distress detection as shown in Figures 68 through 92. A summary of the comparisons is also provided in Table 18. The data comparisons showed:

- An RGB orthophoto with a 4-mm/pix resolution was adequate to detect most of the crack-based distresses and patching with different severity levels. However, they were not very useful in spalling detection and rating.
- A 3.5-mm/pix orthophoto detected all the distresses detected by 4-mm/pix data. Additionally, spalling and ASR with different severities in PCC pavement and alligator cracking in AC pavement were also identified. However, misidentification between spalling and ASR in PCC pavement was also observed. In some cases, spalling and ASR detection were also found to be challenging.
- 1.5 mm/pix performed the best in the detection of different PCC and AC pavement distresses. PCC pavement shrinkage cracking was identified only in this resolution.
- 2.7- and 5.9-mm/pix DEMs were useful in some distress detection.

- The presence of shoving and faulting was successfully confirmed by plotting elevation change perpendicular to the shoving and faulting using the 3D stack tool of ArcGIS Pro, as shown in Figures 68 and 69.

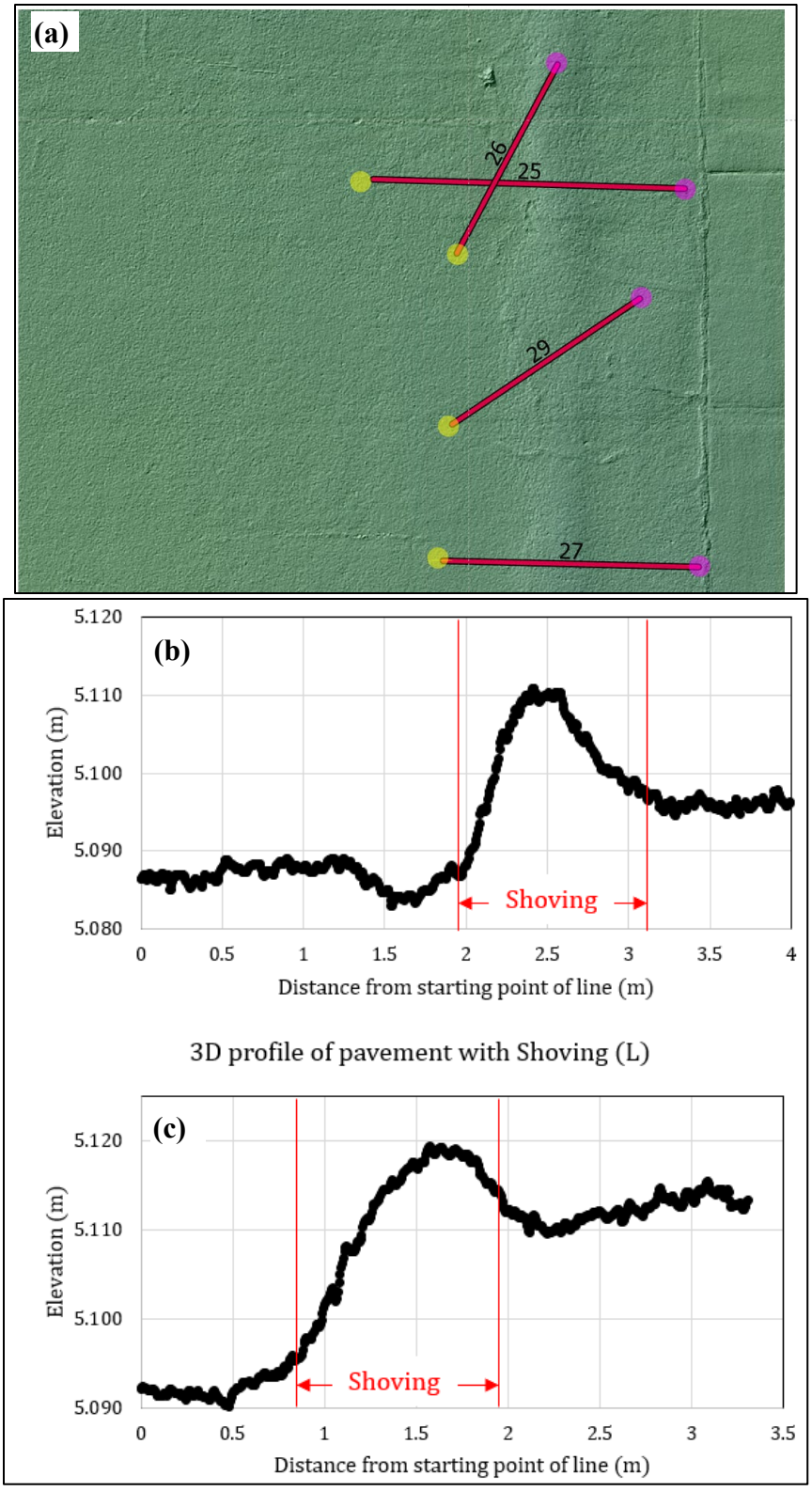

Figure 68. Shoving (L) in 5.9-mm/pix Data in (a) a 3D Profile of Pavement Sample and (b) Graph Showing the Elevation Difference of the DEM on Line 25, and (c) Graph Showing the Elevation Difference of the DEM on Line 25 on Line 27

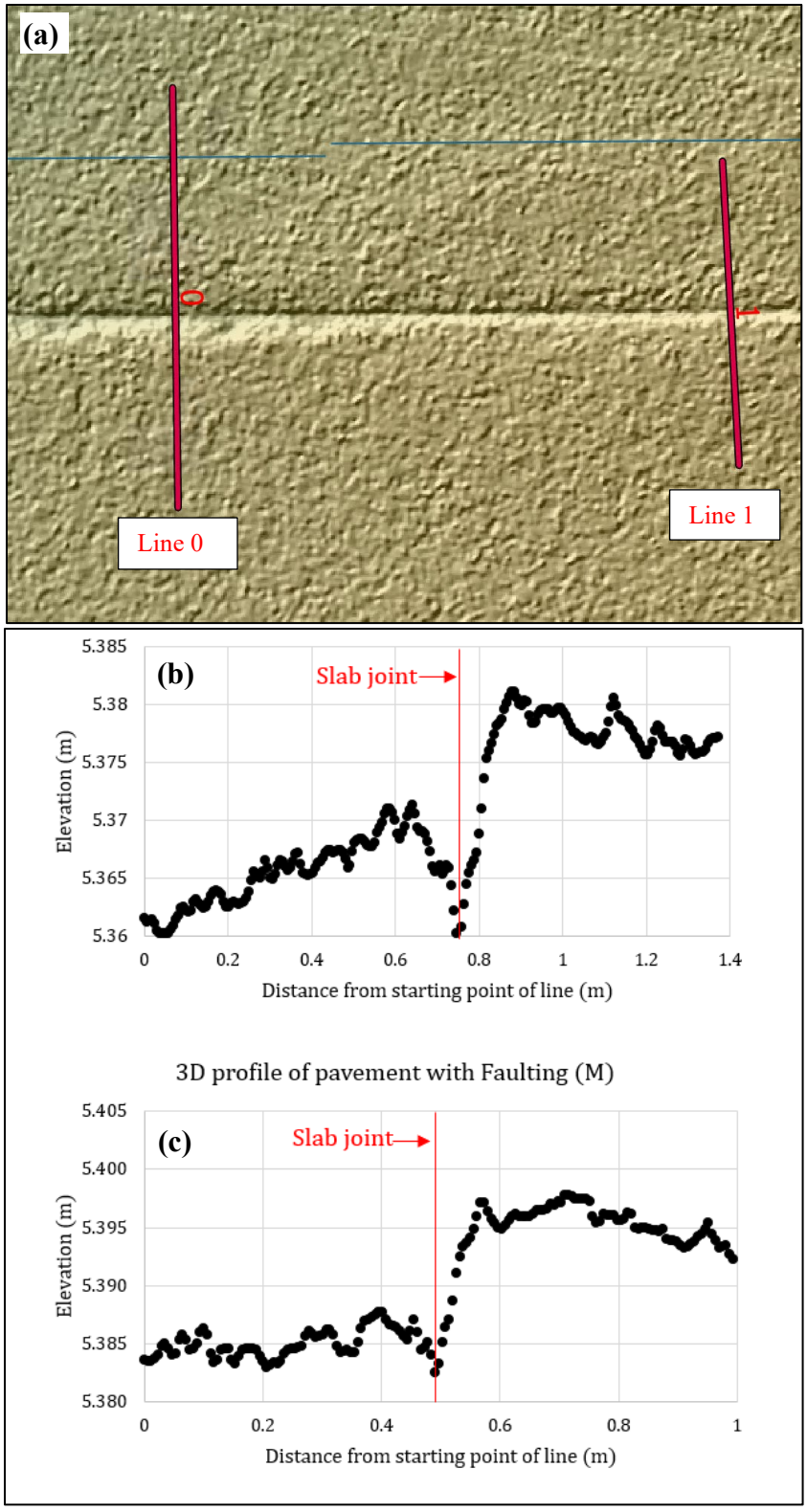

Figure 69. Faulting (M) in 5.9-mm/pix Data in (a) a 3D Profile of Pavement Sample and (b) Graph Showing the Elevation Difference of the DEM on Line 0 and (c) Graph Showing the Elevation Difference of the DEM on Line 1

The 1.5-mm/pix RBP optical orthophoto, 6-mm/pix DEM, and 6-mm/pix DEM hillshade were imported to ArcGIS Pro for visual identification and rating of distresses present on the FBO PCC pavement section. The RGB orthophoto was mainly used for distress detection, and DEMs were used for the severity rating. Fifteen of 19 sample units on the FBO Apron Section 40, 8 of 9 sample units on FBO Apron Section 30, and 27 sample units on Runway 10/28 were visually analyzed. The remaining four sample units in the FBO Apron either had aircraft over a large area or were missing some data. The recorded distresses were summarized and added to the FAA PAVEAIR portal to calculate the PCI value (FAA, 2021). The FOG PCI values and sUAS PCI values were plotted, as shown in Figure 70. In most cases, the sUAS-based PCI values were higher than the FOG PCI values because of missing low-severity spalling, ASR, faulting, and shrinkage cracks. Misidentification of the severity level of spalling and ASR was also observed in multiple sample units, which included rating low-severity distress as medium-severity and vice-versa. The same phenomena were observed for AC pavement, as identification of weathering, swell, and raveling was challenging. However, raveling was identified accurately in the FBO Apron Section 30. Some block cracking was recorded as L&T cracks on the PCI survey and they were noted as block cracking in sUAS-based PCI survey. Block cracking has been excluded from Table 18 but was considered for the sUAS-based PCI calculation.

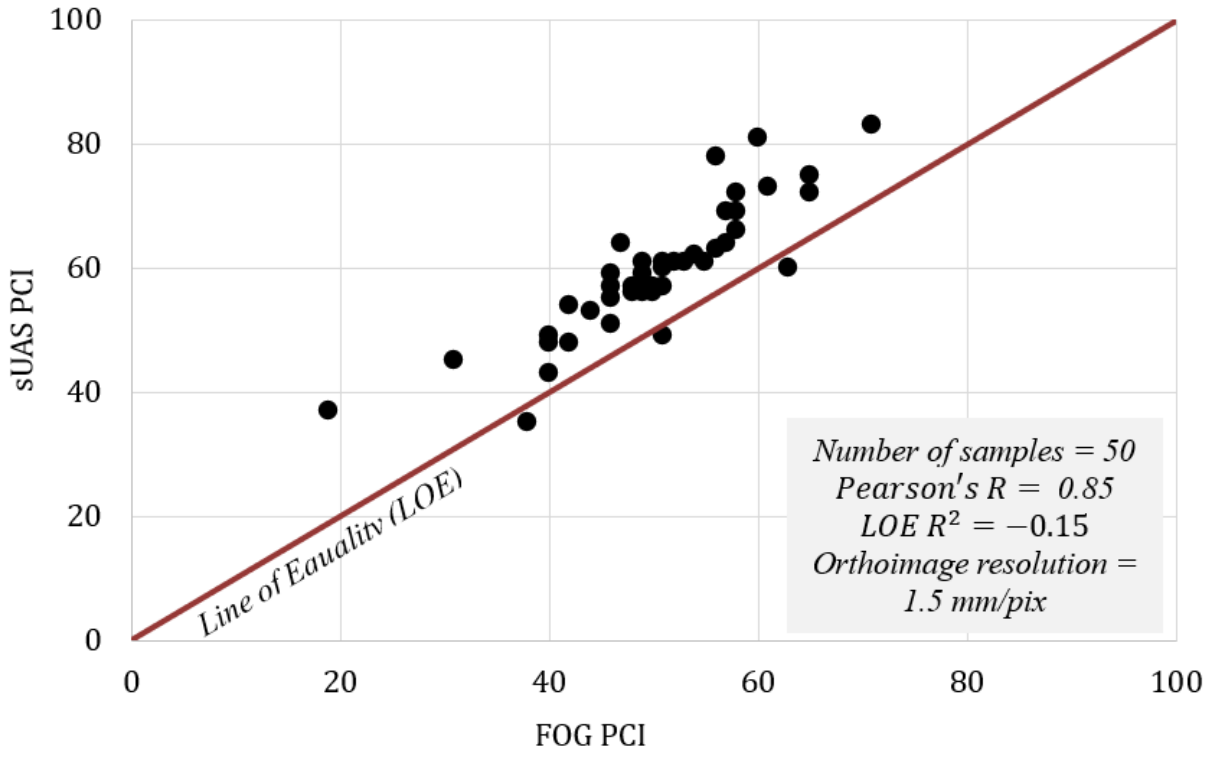

Figure 70. Comparison Between FOG PCI and sUAS PCI Calculated Using 1.5-mm/pix Data from WWD

Table 18. Summary of the Findings from WWD

Distress Name (PAVER™ Distress Number)	Severity	Resolution Tested (mm/pix)		Distress Detected in Highest Resolution (mm/pix)		Remarks
		RGB	DEM	RGB	DEM	
Alligator Cracking (41)	L	1.5, 3.5, 4.1	5.9, 14, 16.2	3.5	5.9	Figure 71
Depression (45)	H	1.5, 2.2, 3.5, 4.1	5.9, 8.9, 14, 16.2	4.1	16.2	Figure 72
L&T Cracking (48)	L, M	0.7, 1.5, 3.5, 4.1	2.7, 5.9, 14, 16.2	4.1	5.9	Figure 73 Figure 74
	H	1.5, 3.5, 4.1	5.9, 14, 16.2	4.1	16.2	Figure 75
Patching (50)	L,H,M	1.5, 2.2, 3.5, 4.1	5.9, 8.9, 14, 16.2	4.1	16.2	
Raveling (52)	L,M,H	1.5, 2.2, 3.5, 4.1	5.9, 8.9, 14, 16.2	1.5	ND	
Shoving (54)	L	1.5, 3.5, 4.1	5.9, 14, 16.2	ND	5.9	
Weathering (57)	L,M,H	1.5, 2.2, 3.5, 4.1	5.9, 8.9, 14, 16.2	ND	ND	Figure 76
LTD Cracks (63)	L	0.7, 1.5, 3.5, 4.1	2.7, 5.9, 14, 16.2	4.1	5.9	Figure 77
	M			4.1	5.9	Figure 78
	H	1.5, 3.5, 4.1	5.9, 14, 16.2	4.1	5.9	Figure 79
Joint Seal Damage (65)	L	1.5, 3.5, 4.1	5.9, 14, 16.2	ND	ND	
Small Patching (66)	L, M	0.7, 1.5, 3.5, 4.1	2.7, 5.9, 14, 16.2	4.1	2.7	Figure 80
	H	1.5, 3.5, 4.1	5.9, 14, 16.2	4.1	5.9	Figure 81
Large Patching (67)	L	0.7, 1.5, 3.5, 4.1	2.7, 5.9, 14, 16.2	4.1	5.9	Figure 82
	M	1.5, 3.5, 4.1	5.9, 14, 16.2	4.1	5.9	Figure 83
Faulting (71)	L	1.5, 3.5, 4.1	5.9, 14, 16.2	ND	ND	
	M	1.5, 3.5, 4.1	5.9, 14, 16.2	ND	5.9	
Shrinkage Crack (73)	N/A	1.5, 3.5, 4.1	5.9, 14, 16.2	1.5	ND	Figure 84
Joint Spalling (74)	L	0.7, 1.5, 3.5, 4.1	2.7, 5.9, 14, 16.2	3.5	5.9	Figure 85
	M	1.5, 3.5, 4.1	5.9, 14, 16.2	3.5	14	Figure 86
Corner Spalling (75)	L	0.7, 1.5, 3.5, 4.1	2.7, 5.9, 14, 16.2	3.5	5.9	Figure 87
	M			3.5	5.9	Figure 88
	H			4.1	5.9	Figure 89
ASR (76)	L	0.7, 1.5, 3.5, 4.1	2.7, 5.9, 14, 16.2	3.5	5.9	Figure 80 Figure 90
	M			3.5	5.9	Figure 91
	H	1.5, 3.5, 4.1	5.9, 14, 16.2	3.5	5.9	Figure 92

L = Low, M = Medium, H = High
ND = Not detected
N/A = Not Applicable (no severity level for shrinkage crack)
All 4.1 mm/pix is not true resolution due to being derived from the Mavic 2 Enterprise Advanced 48-mp Quad Bayer camera.

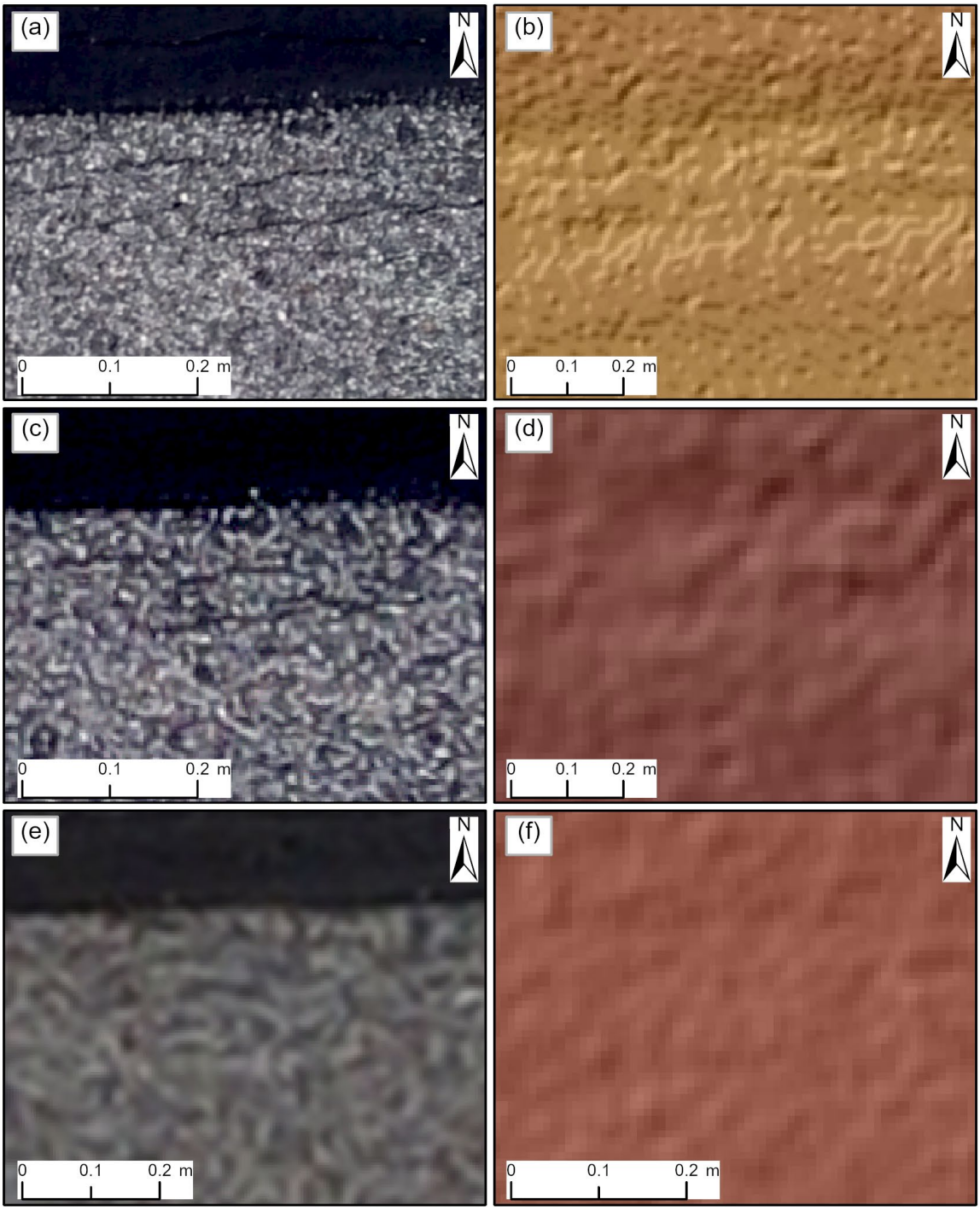

Figure 71. Alligator Cracking (L) in (a) 1.5-mm/pix Orthophoto, (b) 5.9-mm/pix DEM, (c) 3.5-mm/pix Orthophoto, (d) 14-mm/pix DEM, (e) 4.1-mm/pix Orthophoto, and (f) 16.2-mm/pix DEM

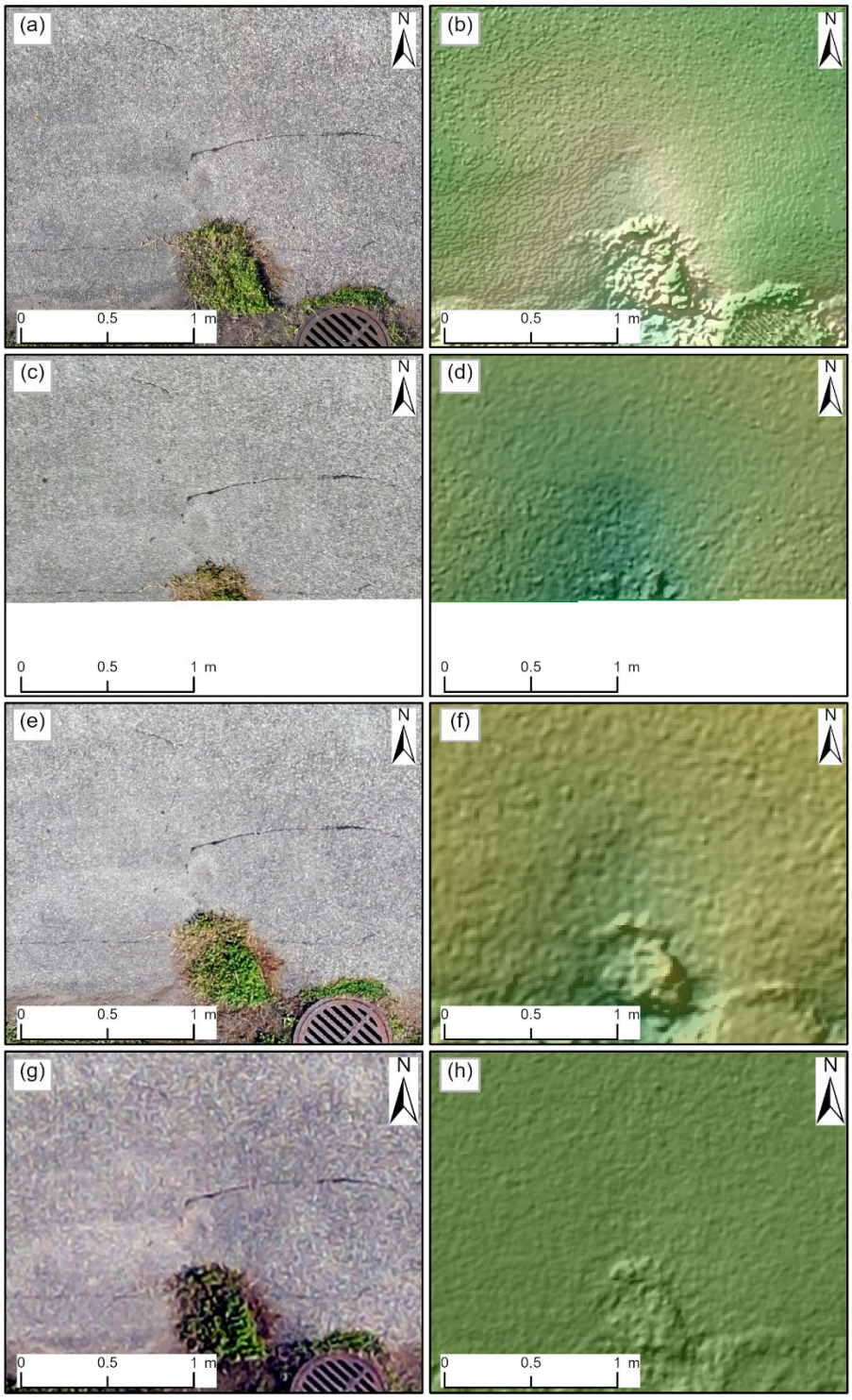

Figure 72. Depression in (a) 1.5-mm/pix Orthophoto, (b) 5.9-mm/pix DEM, (c) 2.2-mm/pix Orthophoto, (d) 8.9-mm/pix DEM, (e) 3.5-mm/pix Orthophoto, (f) 14-mm/pix DEM, (g) 4.1-mm/pix Orthophoto, and (h) 16.2-mm/pix DEM

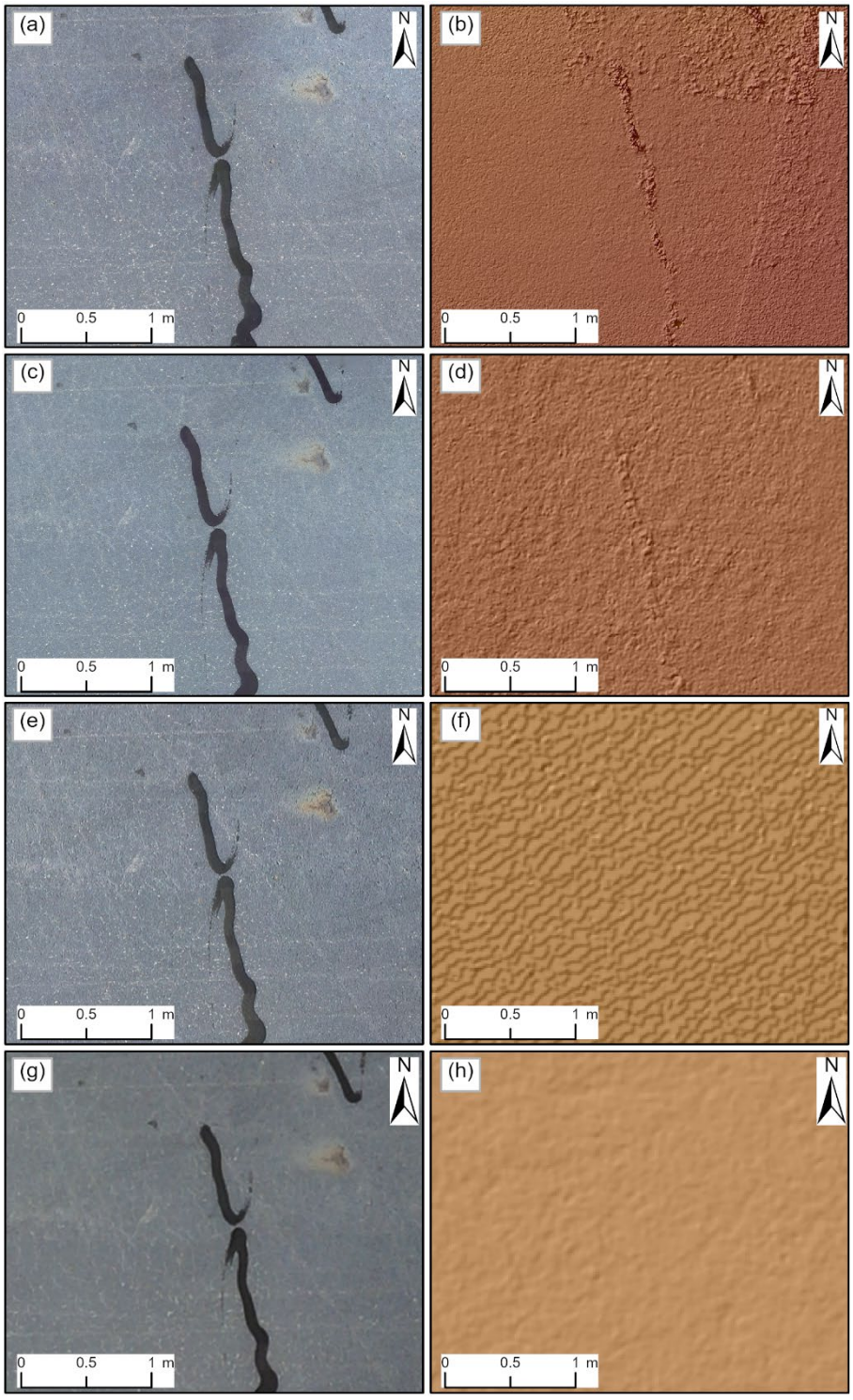

Figure 73. Longitudinal and Transverse Cracks (L) in (a) 0.7-mm/pix Orthophoto, (b) 2.7-mm/pix DEM, (c) 1.5-mm/pix Orthophoto, (d) 5.9-mm/pix DEM, (e) 3.5-mm/pix Orthophoto, (f) 14-mm/pix DEM, (g) 4.1-mm/pix Orthophoto, and (h) 16.2-mm/pix DEM

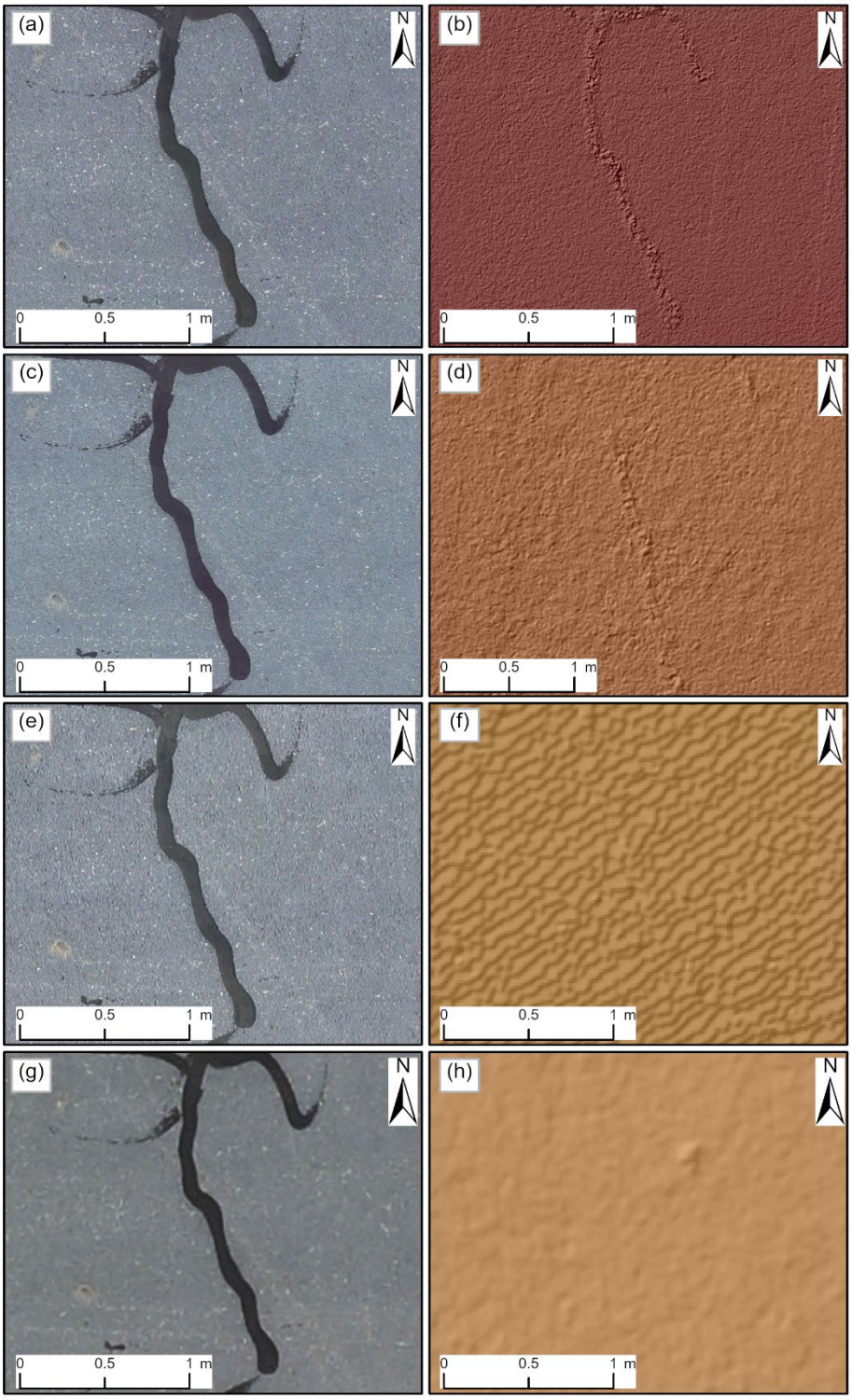

Figure 74. Longitudinal and Transverse Cracks (M) in (a) 0.7-mm/pix Orthophoto, (b) 2.7-mm/pix DEM, (c) 1.5-mm/pix Orthophoto, (d) 5.9-mm/pix DEM, (e) 3.5-mm/pix Orthophoto, (f) 14-mm/pix DEM, (g) 4.1-mm/pix Orthophoto, and (h) 16.2-mm/pix DEM

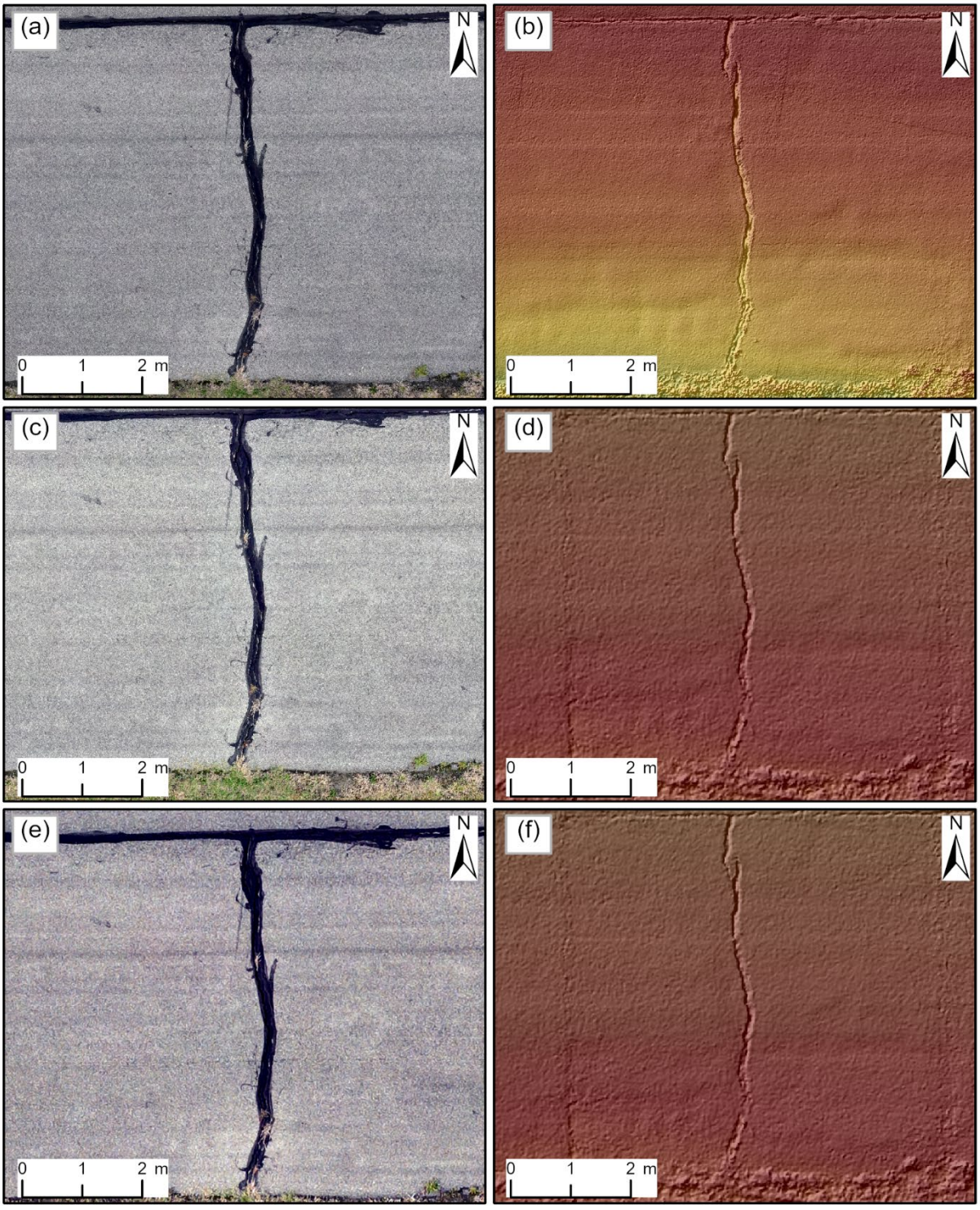

Figure 75. Longitudinal and Transverse Cracks (H) in (a) 1.5-mm/pix Orthophoto, (b) 5.9-mm/pix DEM, (c) 3.5-mm/pix Orthophoto, (d) 14-mm/pix DEM, (e) 4.1-mm/pix Orthophoto, and (f) 16.2-mm/pix DEM

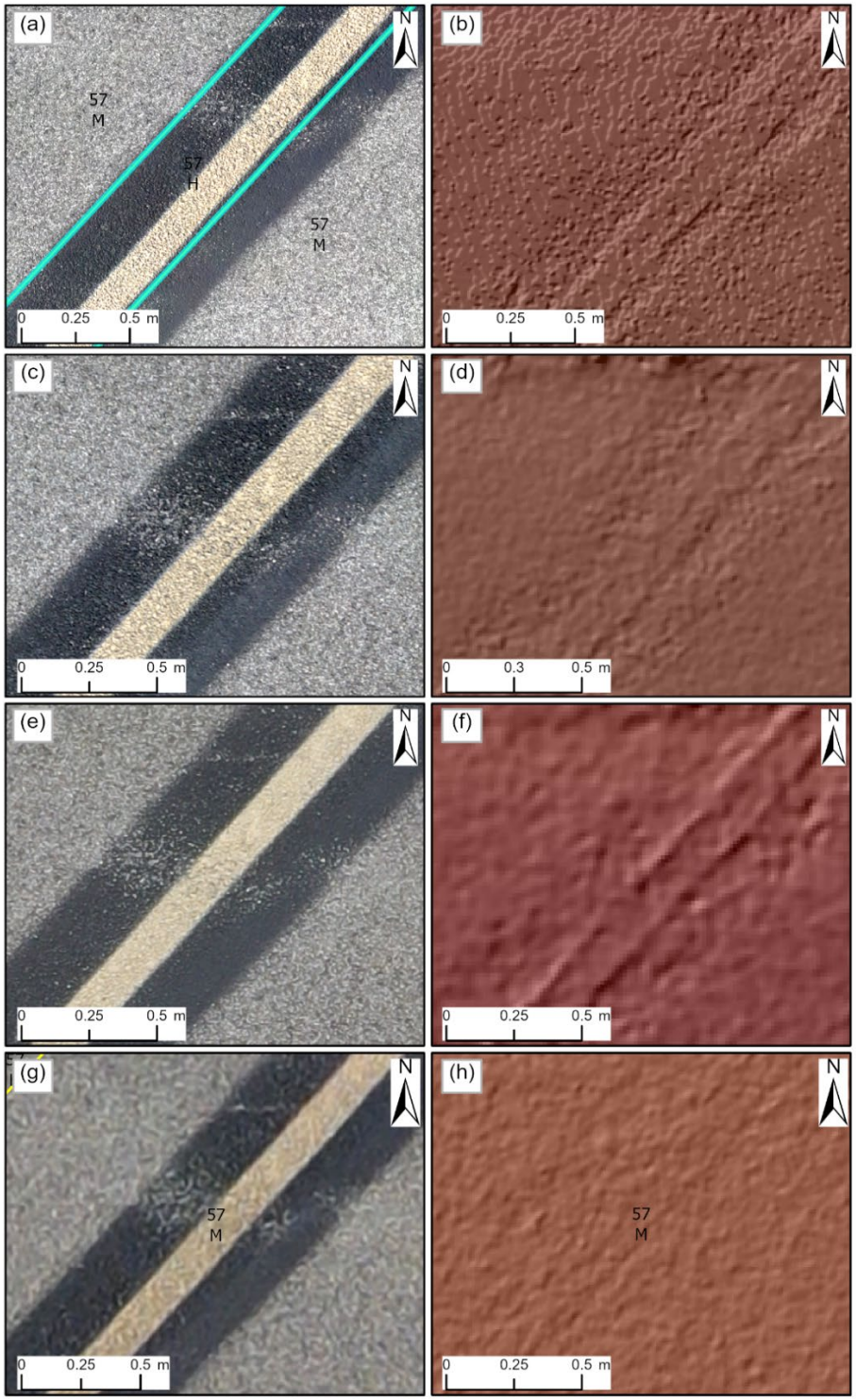

Figure 76. Weathering (H) in (a) 1.5-mm/pix Orthophoto, (b) 5.9-mm/pix DEM, (c) 2.2-mm/pix Orthophoto, (d) 8.9-mm/pix DEM, (e) 3.5-mm/pix Orthophoto, (f) 14-mm/pix DEM, (g) 4.1-mm/pix Orthophoto, and (h) 16.2-mm/pix DEM

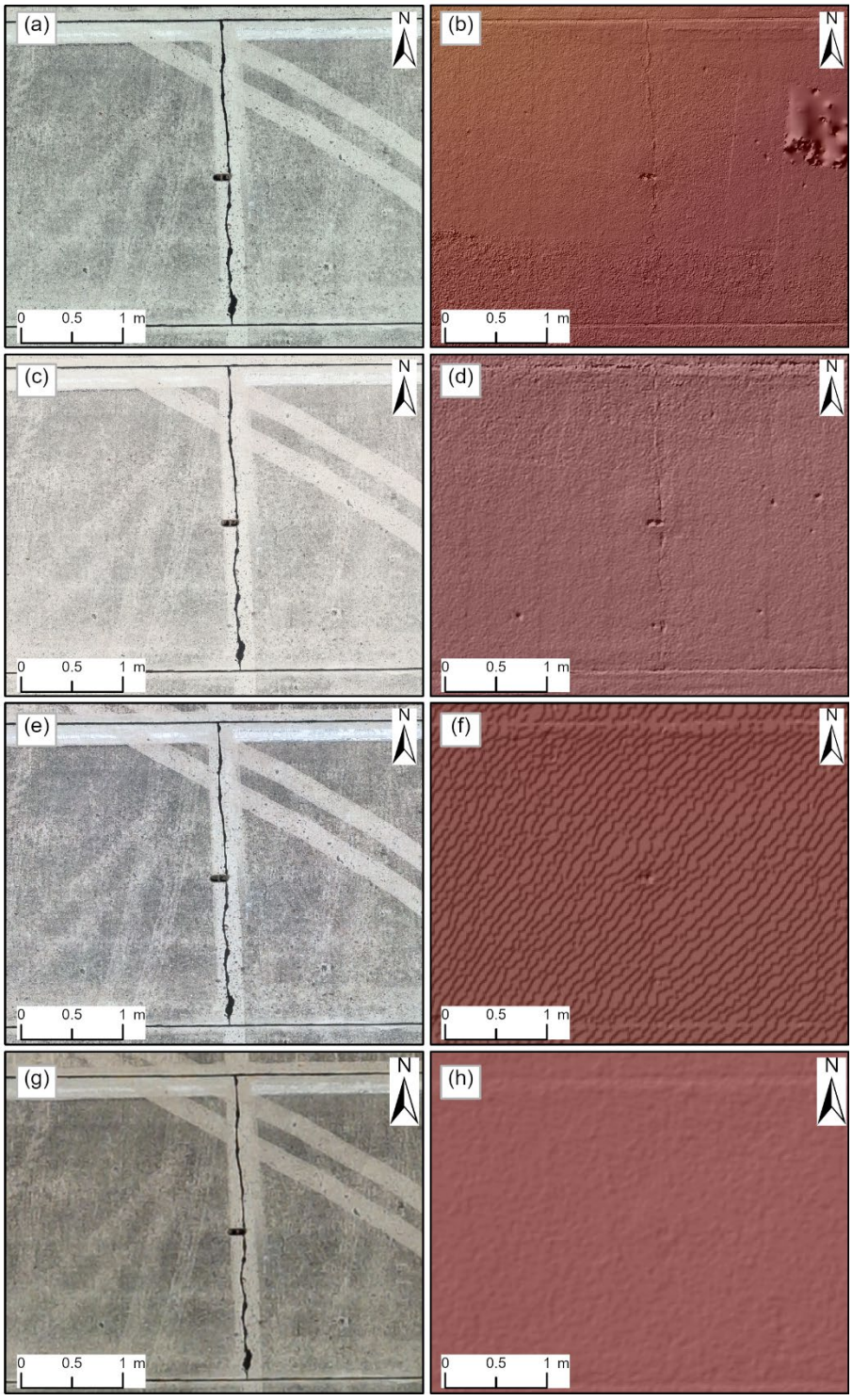

Figure 77. Longitudinal, Transverse, and Diagonal Cracks (L) in (a) 0.7-mm/pix Orthophoto, (b) 2.7-mm/pix DEM, (c) 1.5-mm/pix Orthophoto, (d) 5.9-mm/pix DEM, (e) 3.5-mm/pix Orthophoto, (f) 14-mm/pix DEM, (g) 4.1-mm/pix Orthophoto, and (h) 16.2-mm/pix DEM

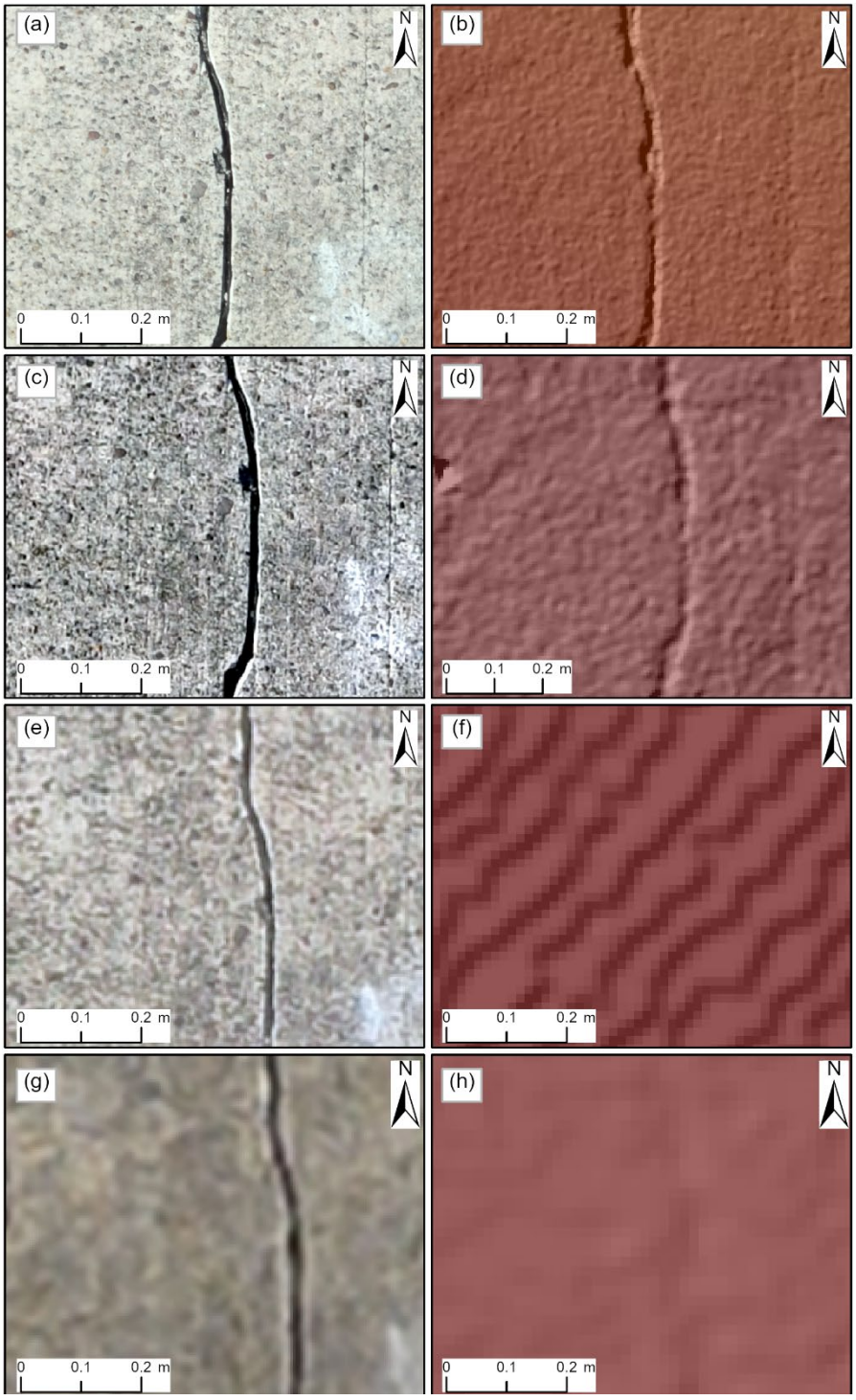

Figure 78. Longitudinal, Transverse, and Diagonal Cracks (M) in (a) 0.7-mm/pix Orthophoto, (b) 2.7-mm/pix DEM, (c) 1.5-mm/pix Orthophoto, (d) 5.9-mm/pix DEM, (e) 3.5-mm/pix Orthophoto, (f) 14-mm/pix DEM, (g) 4.1-mm/pix Orthophoto, and (h) 16.2-mm/pix DEM

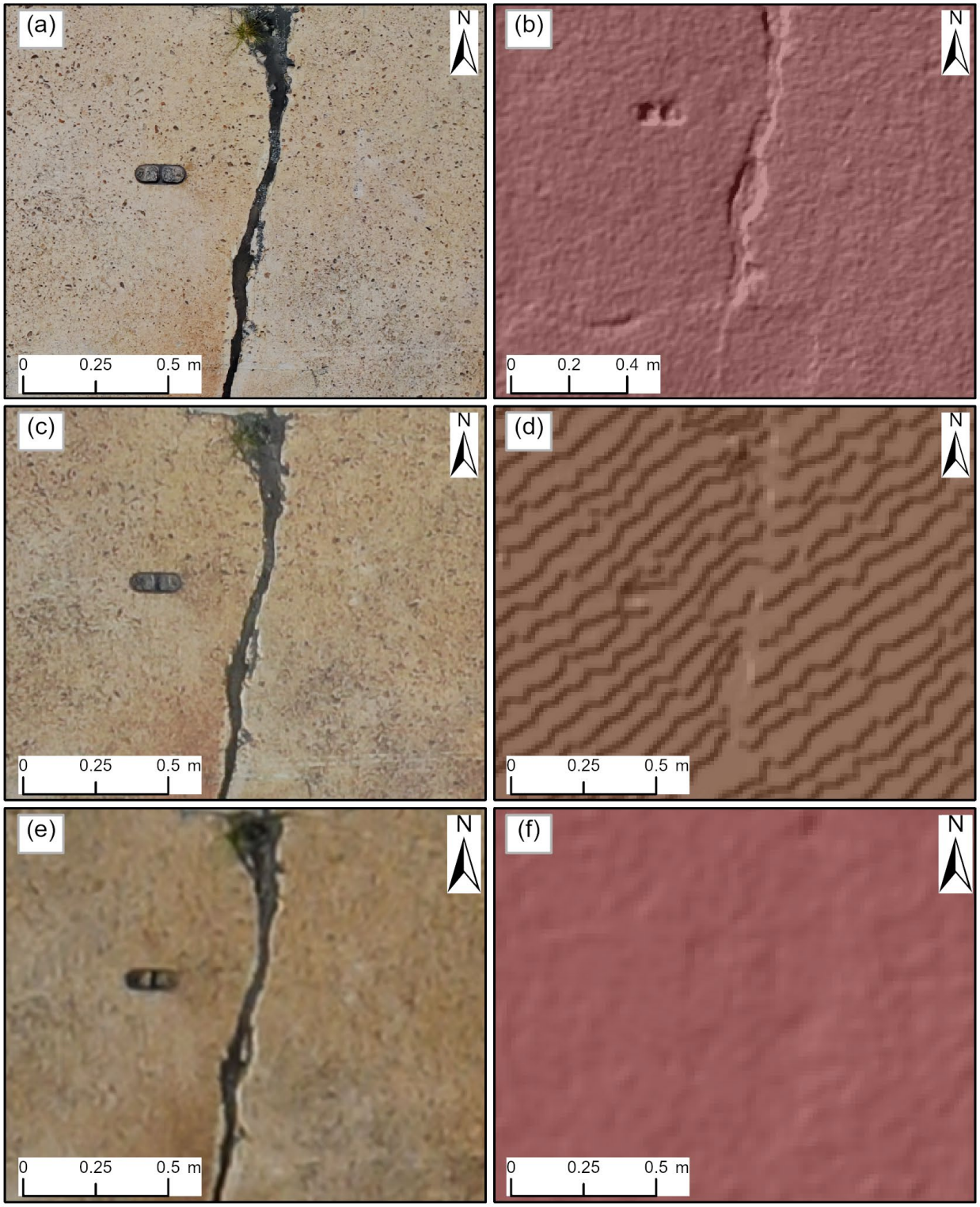

Figure 79. Longitudinal, Transverse, and Diagonal Cracks (H) in (a) 1.5-mm/pix Orthophoto, (b) 5.9-mm/pix DEM, (c) 3.5-mm/pix Orthophoto, (d) 14-mm/pix DEM, (e) 4.1-mm/pix Orthophoto, and (f) 16.2-mm/pix DEM

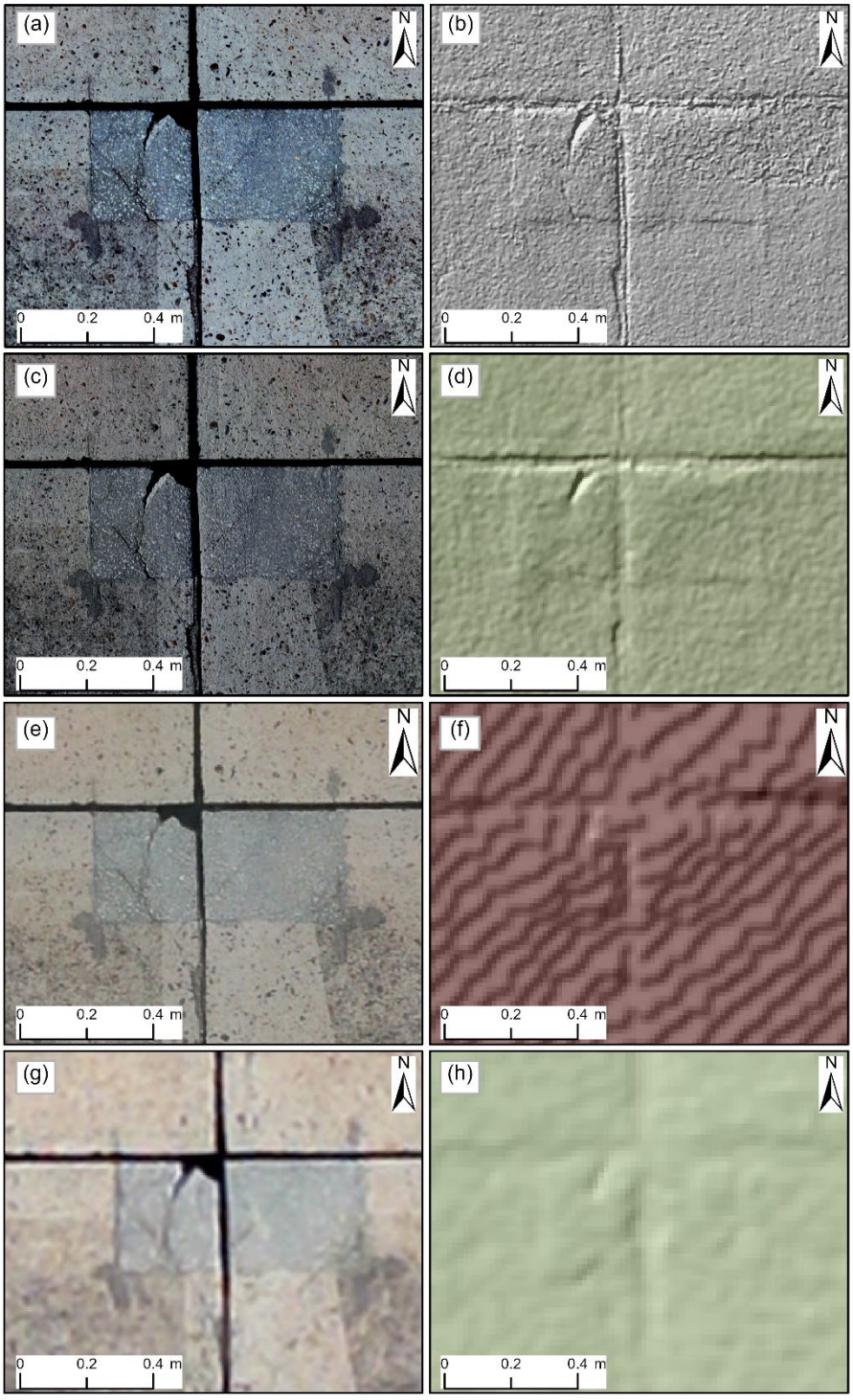

Figure 80. Low-Severity Small Patching (L) on Right Quadrant, Medium-Severity Small Patching on Left Quadrant, and Low-Severity ASR in bottom of the Low-Severity Small Patching in (a) 0.7-mm/pix Orthophoto, (b) 2.7-mm/pix DEM, (c) 1.5-mm/pix Orthophoto, (d) 5.9-mm/pix DEM, (e) 3.5-mm/pix Orthophoto, (f) 14-mm/pix DEM, (g) 4.1-mm/pix Orthophoto, and (h) 16.2-mm/pix DEM

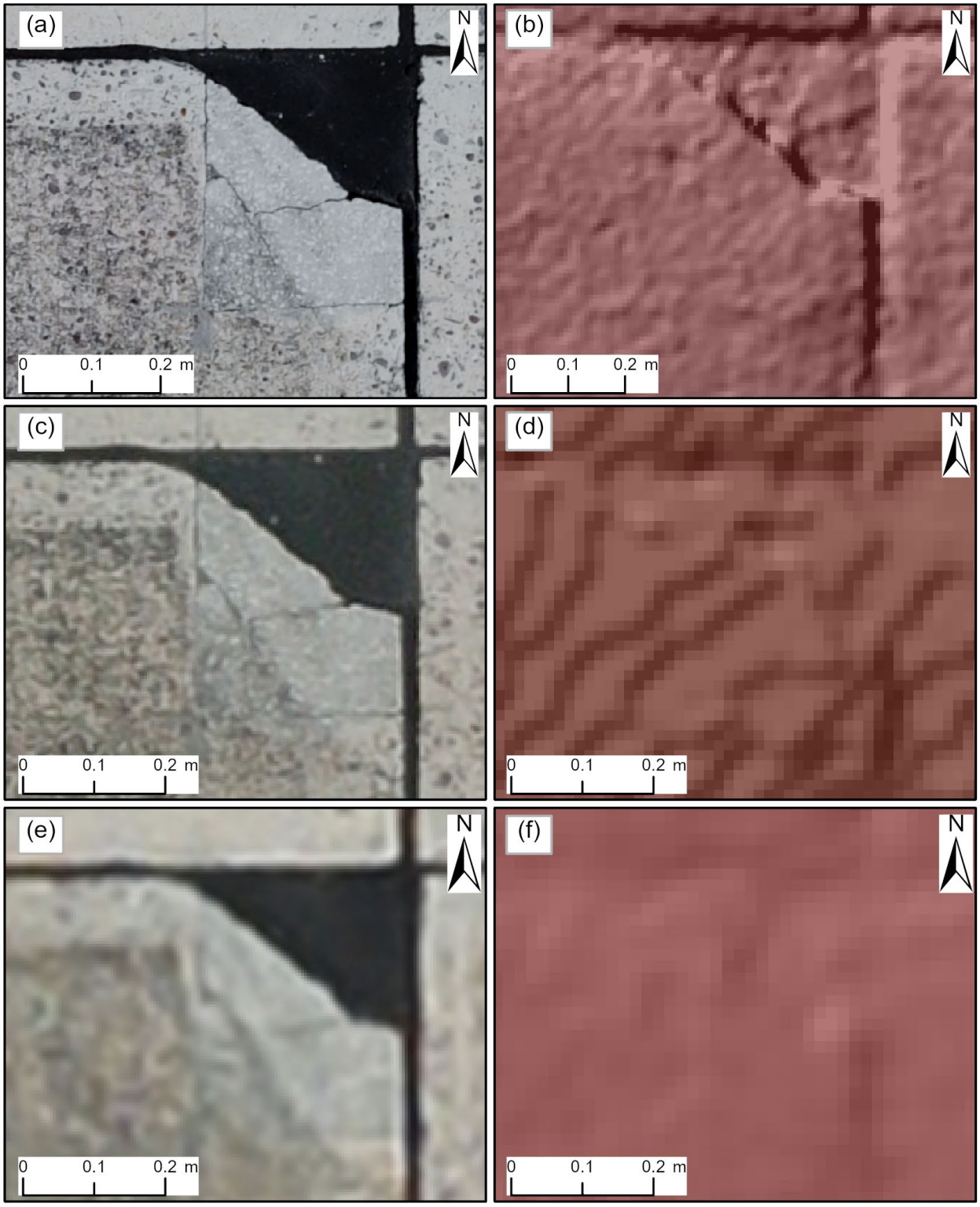

Figure 81. Small Patching (H) in (a) 1.5-mm/pix Orthophoto, (b) 5.9-mm/pix DEM, (c) 3.5-mm/pix Orthophoto, (d) 14-mm/pix DEM, (e) 4.1-mm/pix Orthophoto, and (f) 16.2-mm/pix DEM

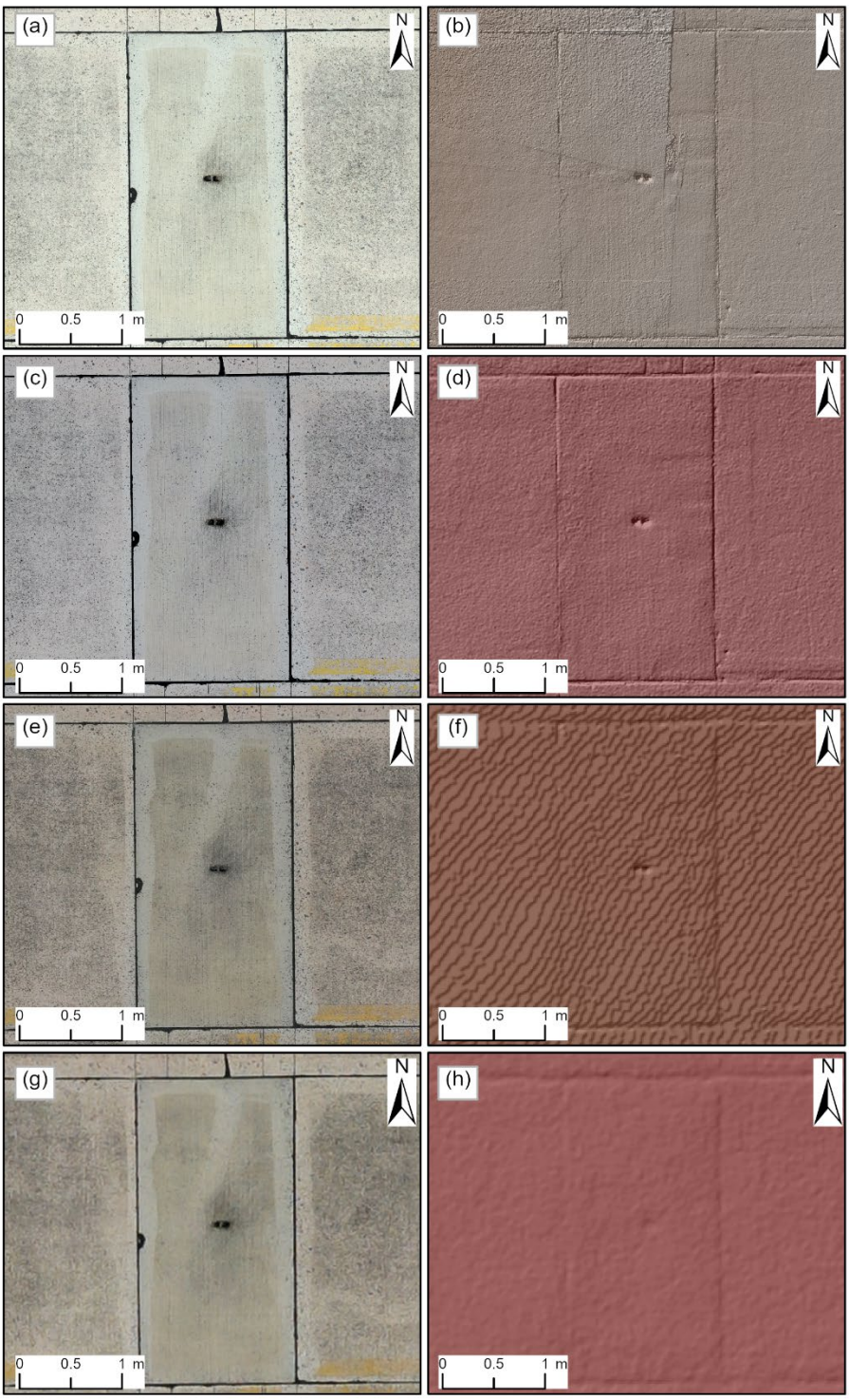

Figure 82. Large Patching (L) in (a) 0.7-mm/pix Orthophoto, (b) 2.7-mm/pix DEM, (c) 1.5-mm/pix Orthophoto, (d) 5.9-mm/pix DEM, (e) 3.5-mm/pix Orthophoto, (f) 14-mm/pix DEM, (g) 4.1-mm/pix Orthophoto, and (h) 16.2-mm/pix DEM

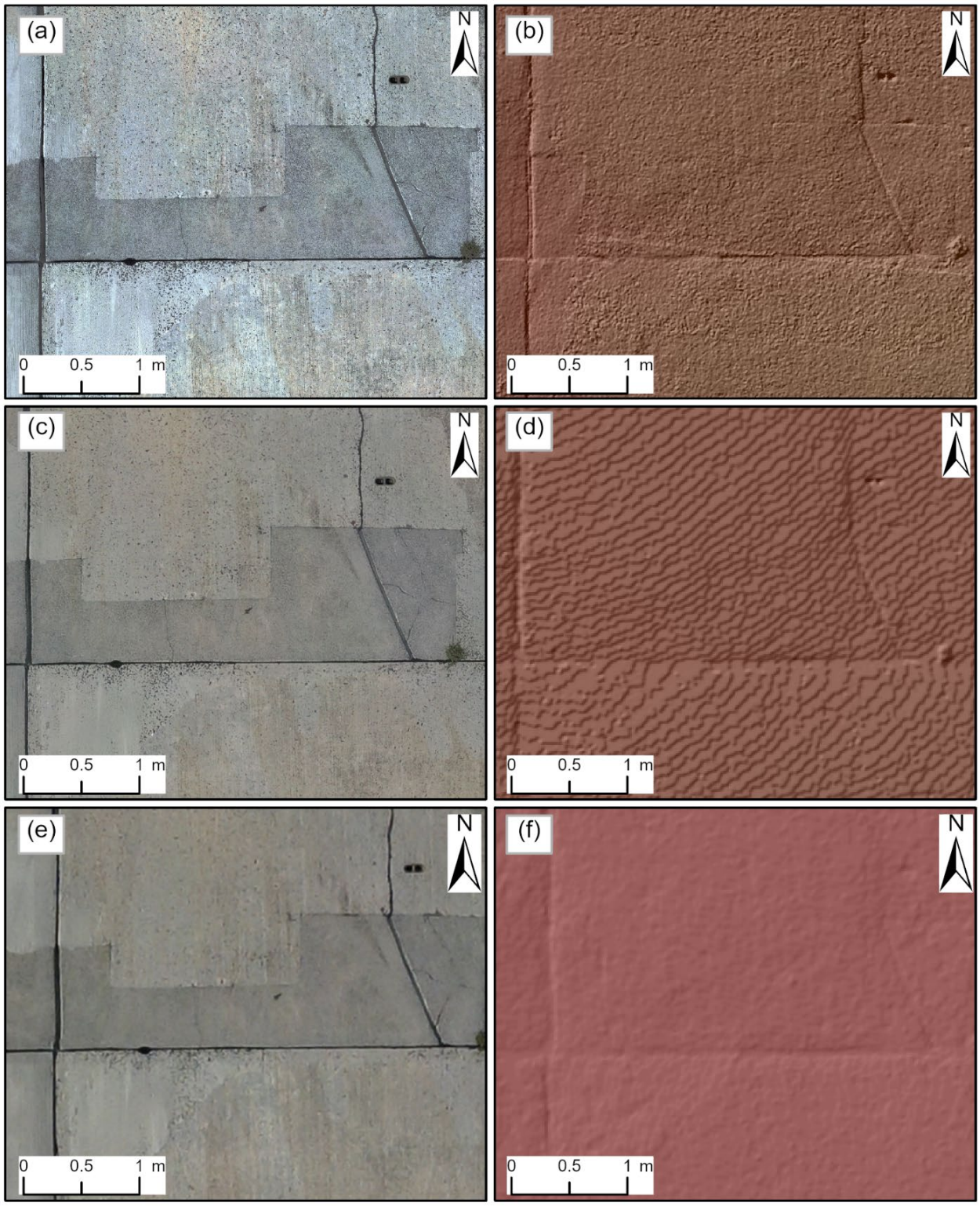

Figure 83. Large Patching (M) in (a) 1.5-mm/pix Orthophoto, (b) 5.9-mm/pix DEM, (c) 3.5-mm/pix Orthophoto, (d) 14-mm/pix DEM, (e) 4.1-mm/pix Orthophoto, and (f) 16.2-mm/pix DEM

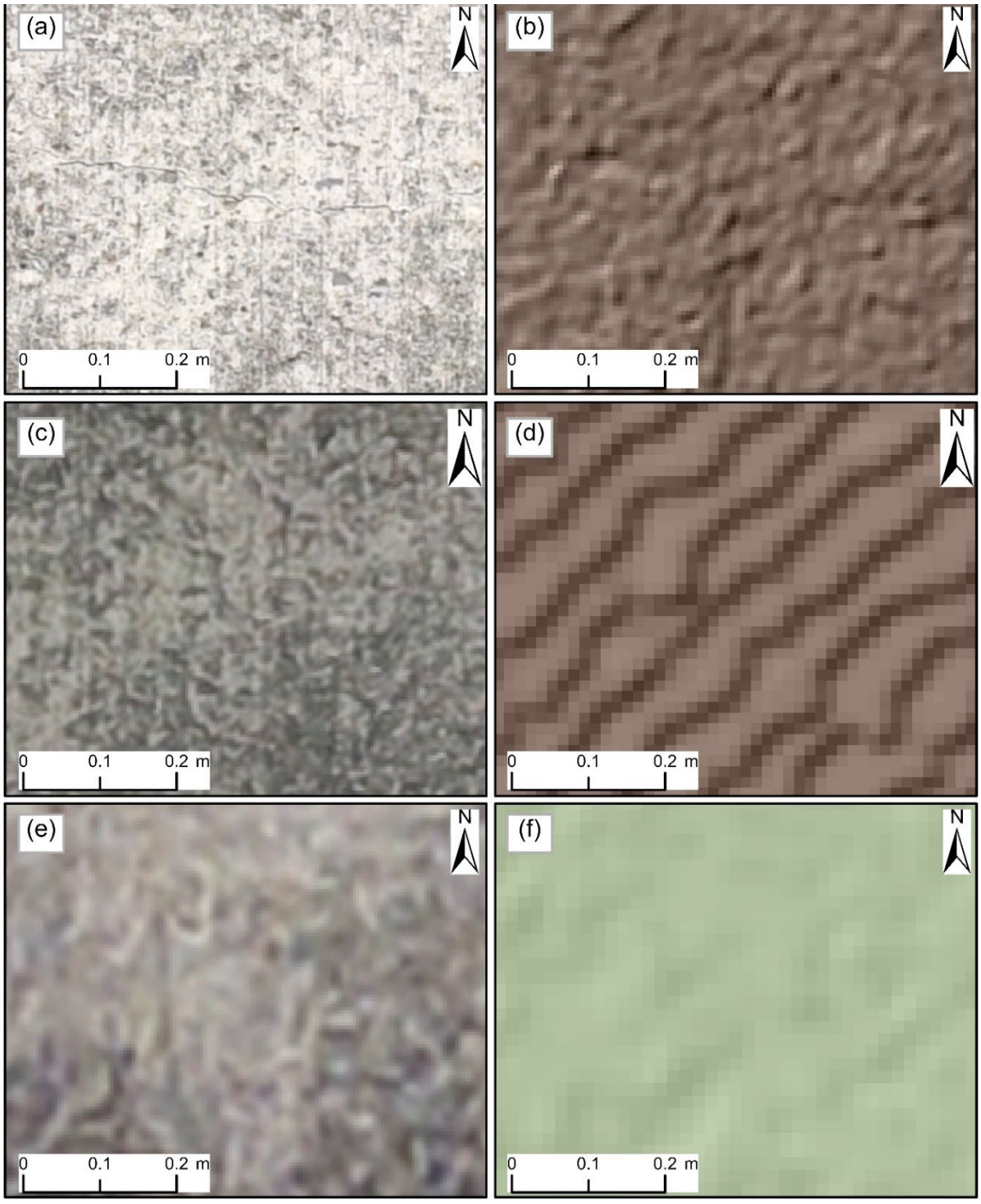

Figure 84. Shrinkage Cracks in (a) 1.5-mm/pix Orthophoto, (b) 5.9-mm/pix DEM, (c) 3.5-mm/pix Orthophoto, (d) 14-mm/pix DEM, (e) 4.1-mm/pix Orthophoto, and (f) 16.2-mm/pix DEM

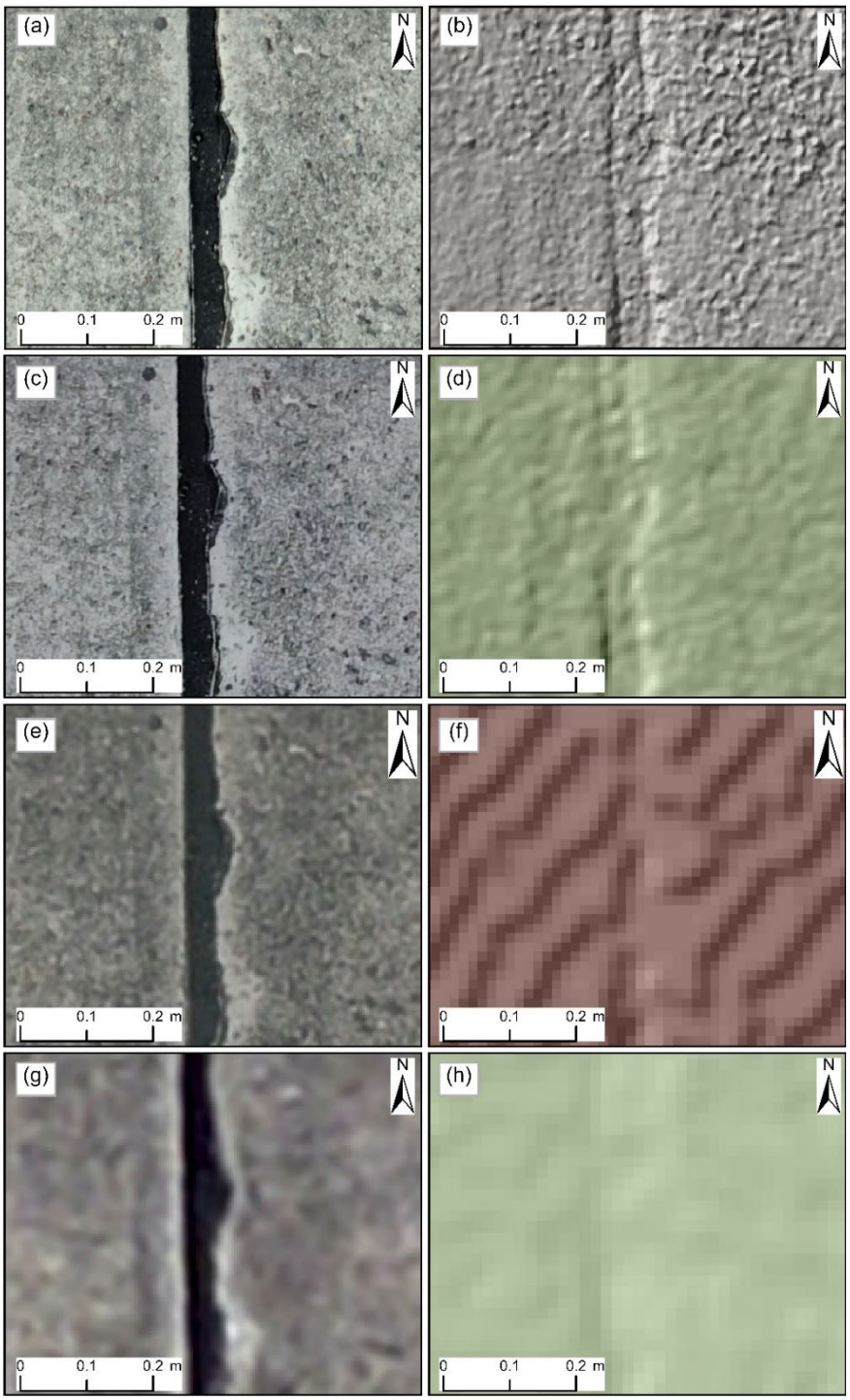

Figure 85. Joint Spalling (L) in (a) 0.7-mm/pix Orthophoto, (b) 2.7-mm/pix DEM, (c) 1.5-mm/pix Orthophoto, (d) 5.9-mm/pix DEM, (e) 3.5-mm/pix Orthophoto, (f) 14-mm/pix DEM, (g) 4.1-mm/pix Orthophoto, and (h) 16.2-mm/pix DEM

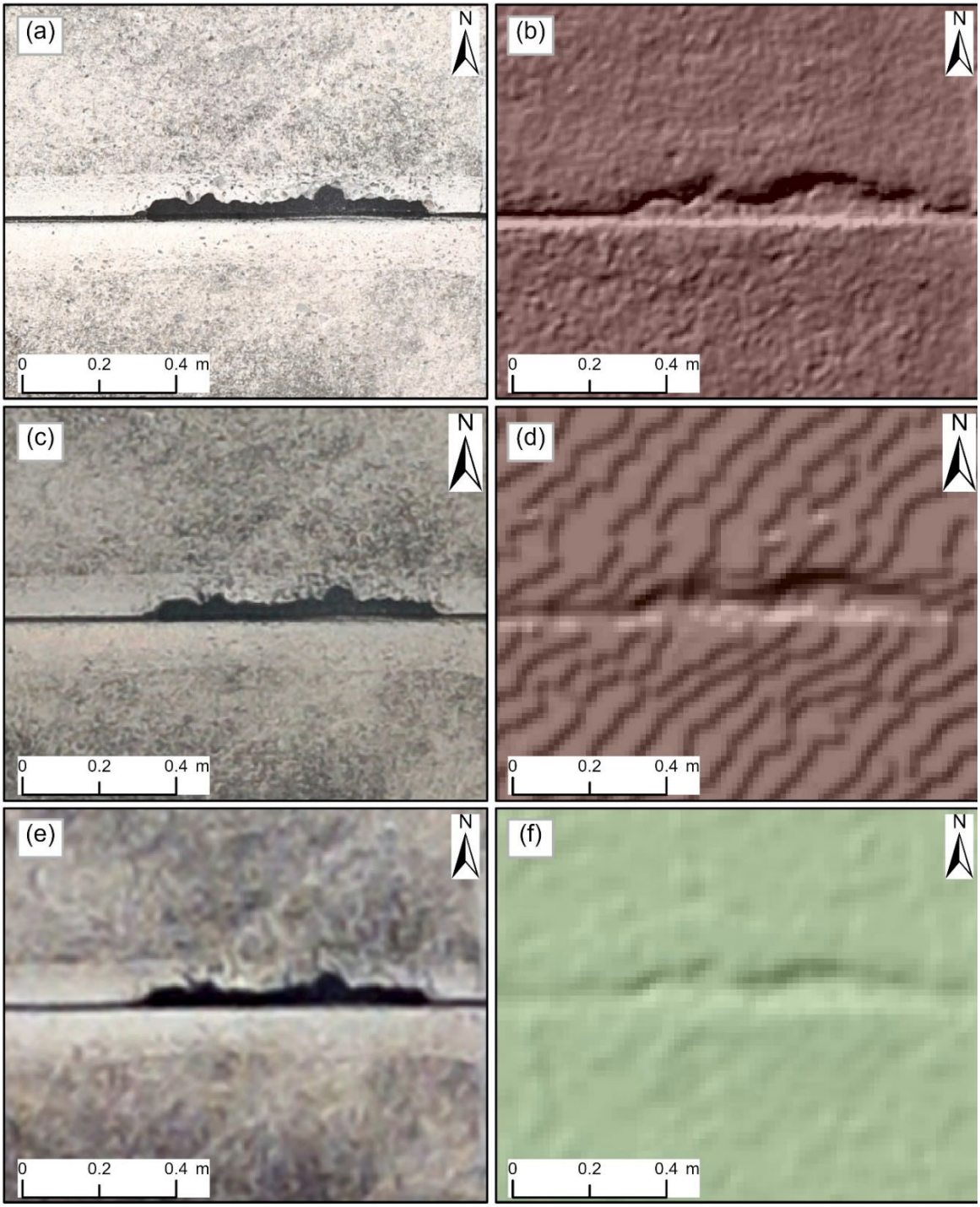

Figure 86. Joint Spalling (M) in (a) 1.5-mm/pix Orthophoto, (b) 5.9-mm/pix DEM, (c) 3.5-mm/pix Orthophoto, (d) 14-mm/pix DEM, (e) 4.1-mm/pix Orthophoto, and (f) 16.2-mm/pix DEM

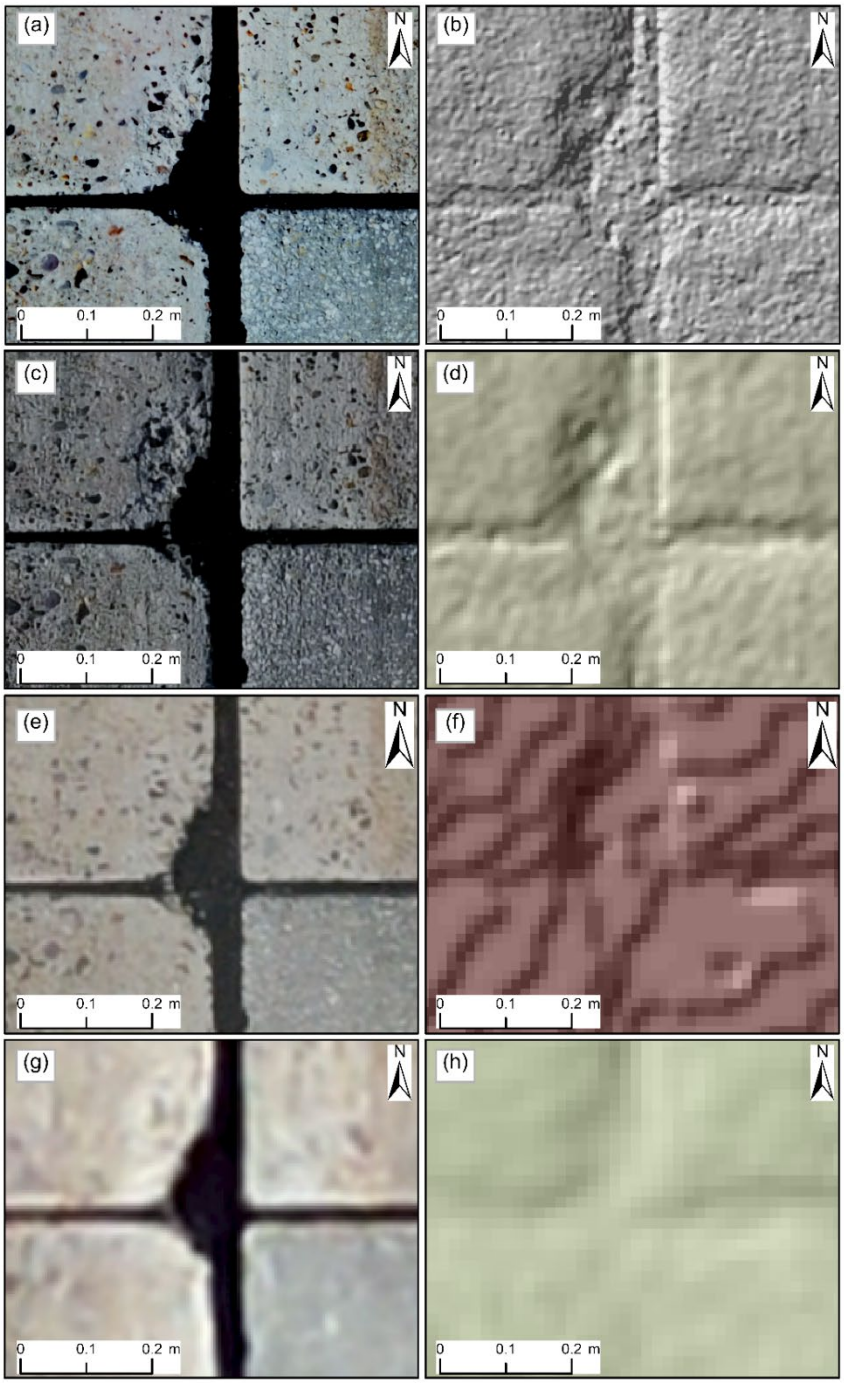

Figure 87. Corner Spalling (L) in (a) 0.7-mm/pix Orthophoto, (b) 2.7-mm/pix DEM, (c) 1.5-mm/pix Orthophoto, (d) 5.9-mm/pix DEM, (e) 3.5-mm/pix Orthophoto, (f) 14-mm/pix DEM, (g) 4.1-mm/pix Orthophoto, and (h) 16.2-mm/pix DEM

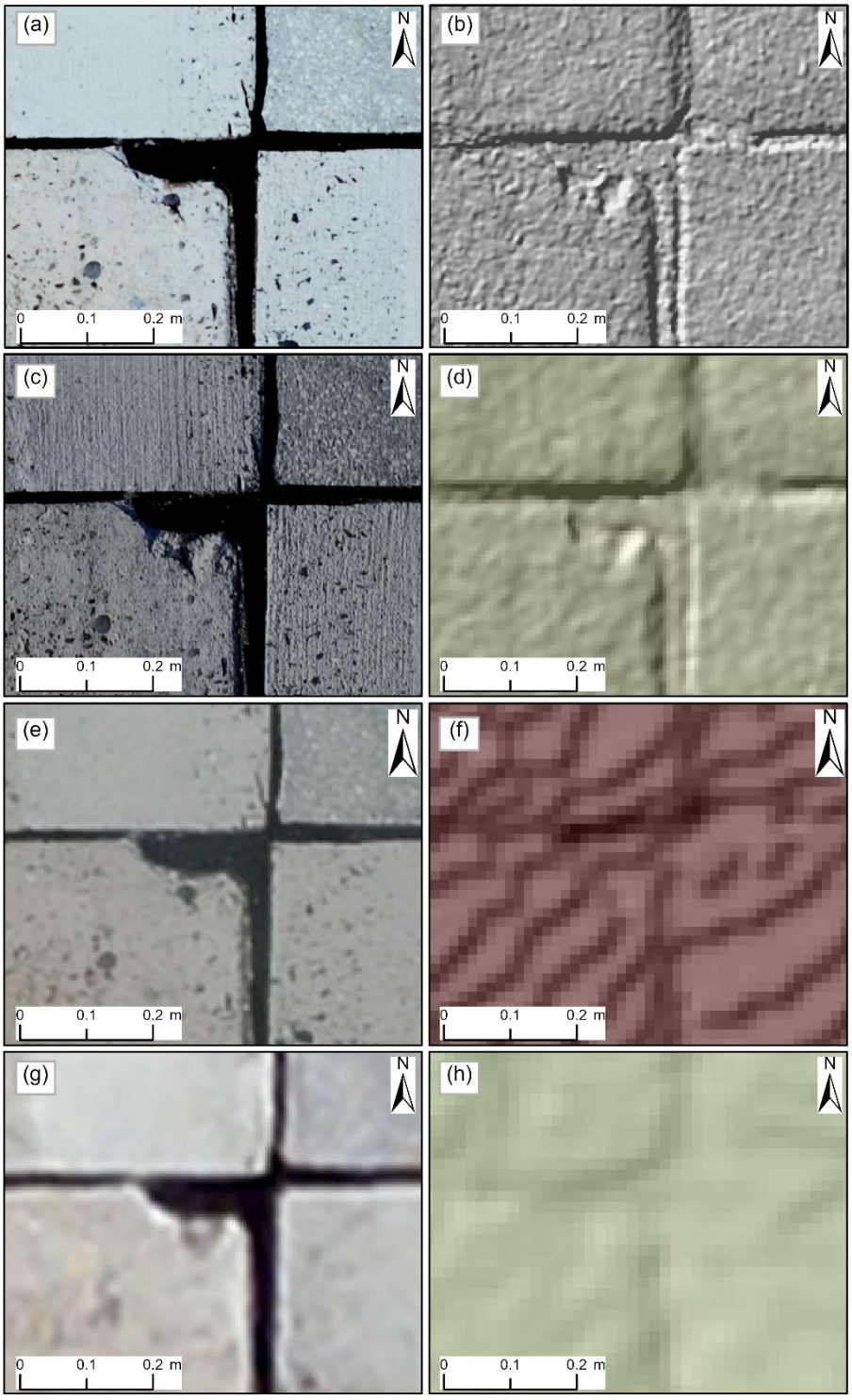

Figure 88. Corner Spalling (M) in (a) 0.7-mm/pix Orthophoto, (b) 2.7-mm/pix DEM, (c) 1.5-mm/pix Orthophoto, (d) 5.9-mm/pix DEM, (e) 3.5-mm/pix Orthophoto, (f) 14-mm/pix DEM, (g) 4.1-mm/pix Orthophoto, and (h) 16.2-mm/pix DEM

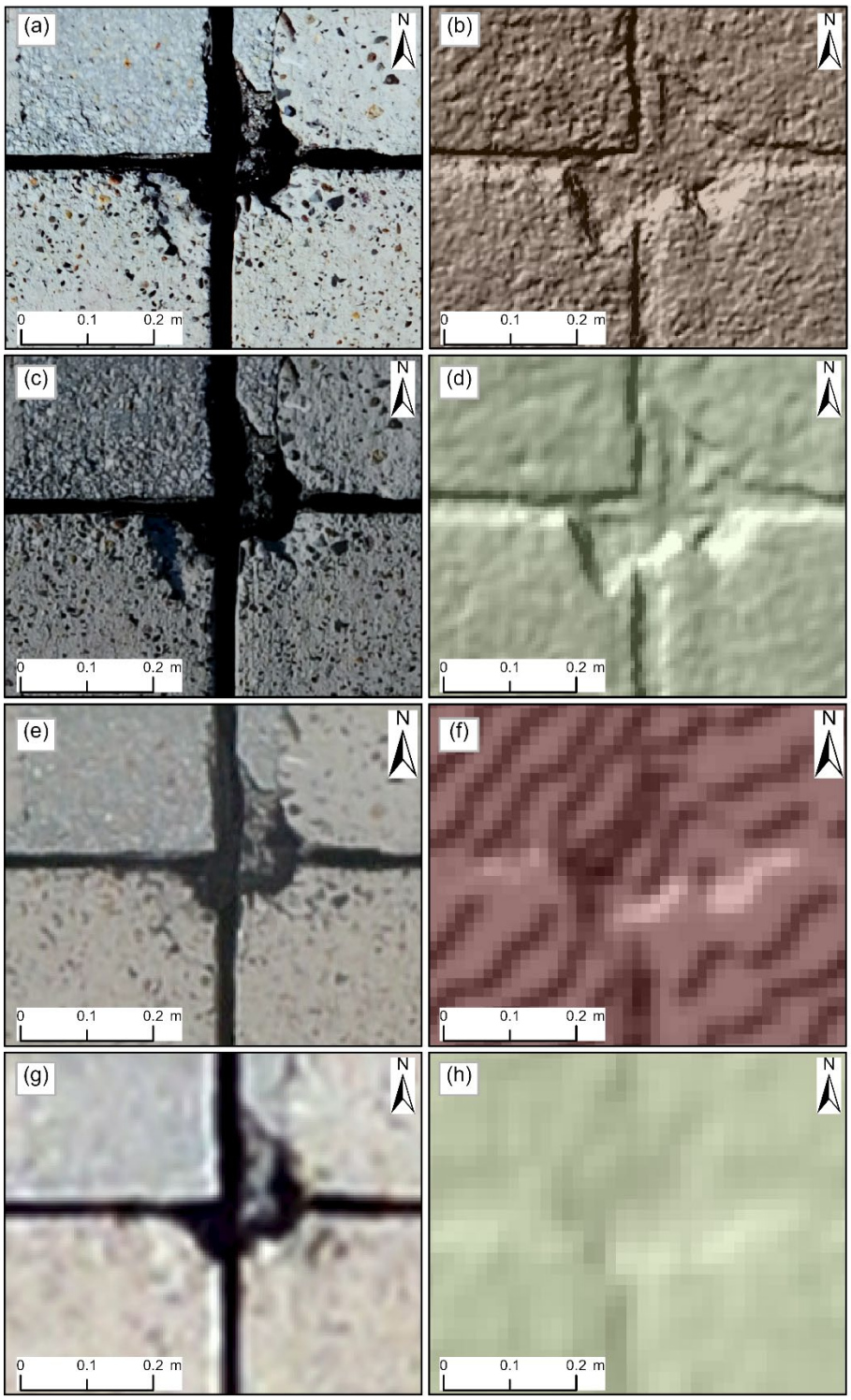

Figure 89. Corner Spalling (H) in (a) 0.7-mm/pix Orthophoto, (b) 2.7-mm/pix DEM, (c) 1.5-mm/pix Orthophoto, (d) 5.9-mm/pix DEM, (e) 3.5-mm/pix Orthophoto, (f) 14-mm/pix DEM, (g) 4.1-mm/pix Orthophoto, and (h) 16.2-mm/pix DEM

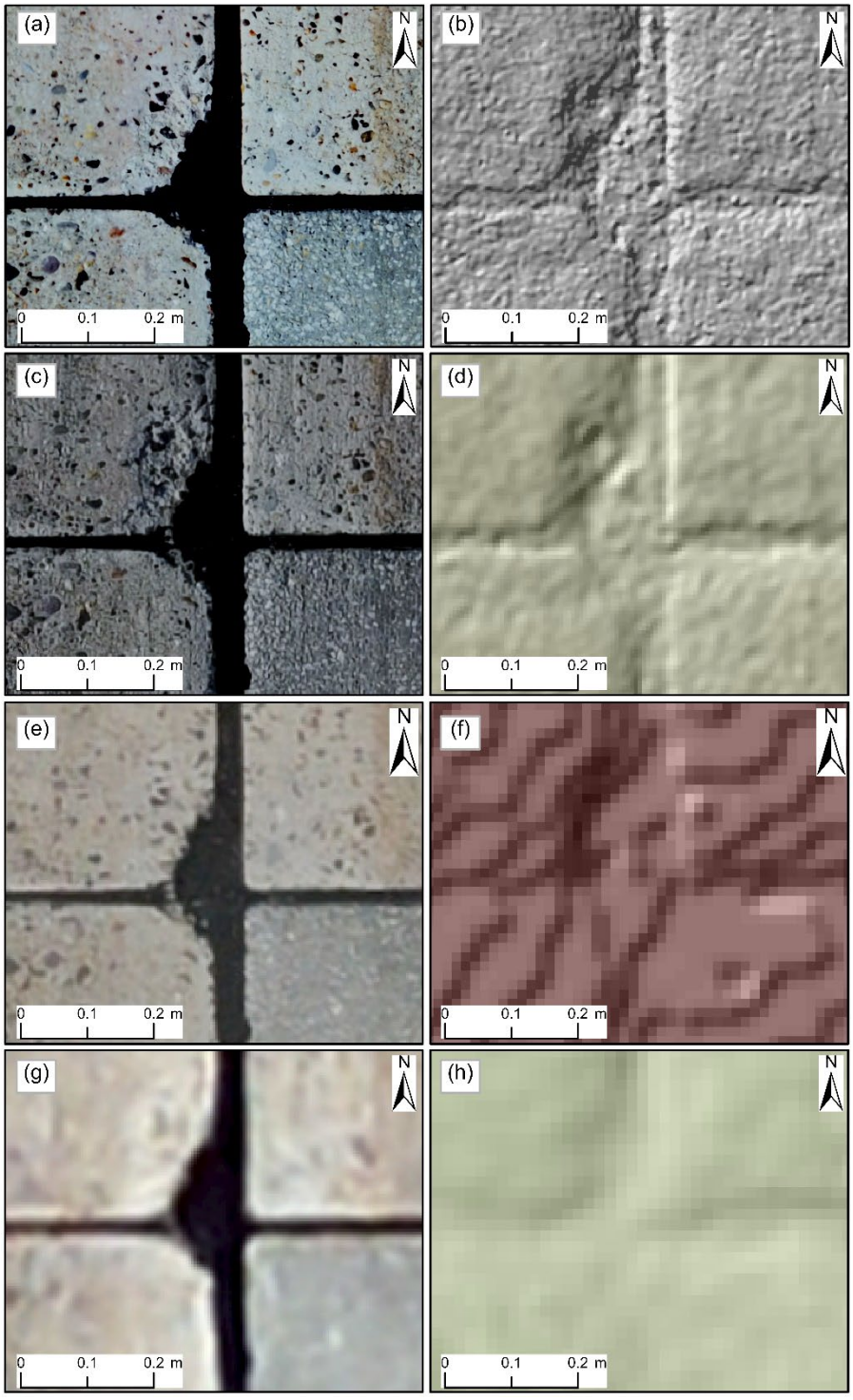

Figure 90. Alkali-Silica Reaction (L) in (a) 0.7-mm/pix Orthophoto, (b) 2.7-mm/pix DEM, (c) 1.5-mm/pix Orthophoto, (d) 5.9-mm/pix DEM, (e) 3.5-mm/pix Orthophoto, (f) 14-mm/pix DEM, (g) 4.1-mm/pix Orthophoto, and (h) 16.2-mm/pix DEM

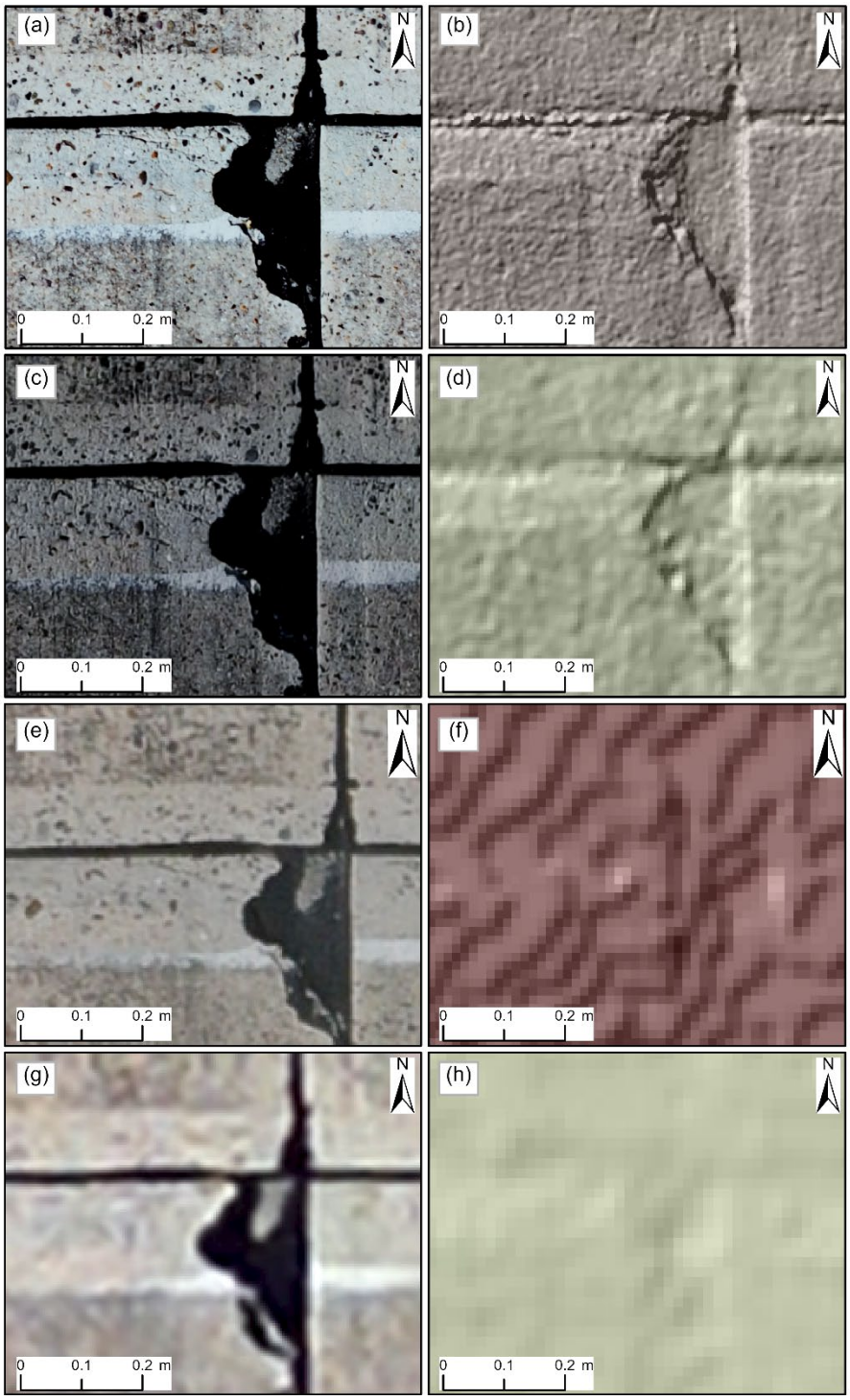

Figure 91. Alkali-Silica Reaction (M) in (a) 0.7-mm/pix Orthophoto, (b) 2.7-mm/pix DEM, (c) 1.5-mm/pix Orthophoto, (d) 5.9-mm/pix DEM, (e) 3.5-mm/pix Orthophoto, (f) 14-mm/pix DEM, (g) 4.1-mm/pix Orthophoto, and (h) 16.2-mm/pix DEM

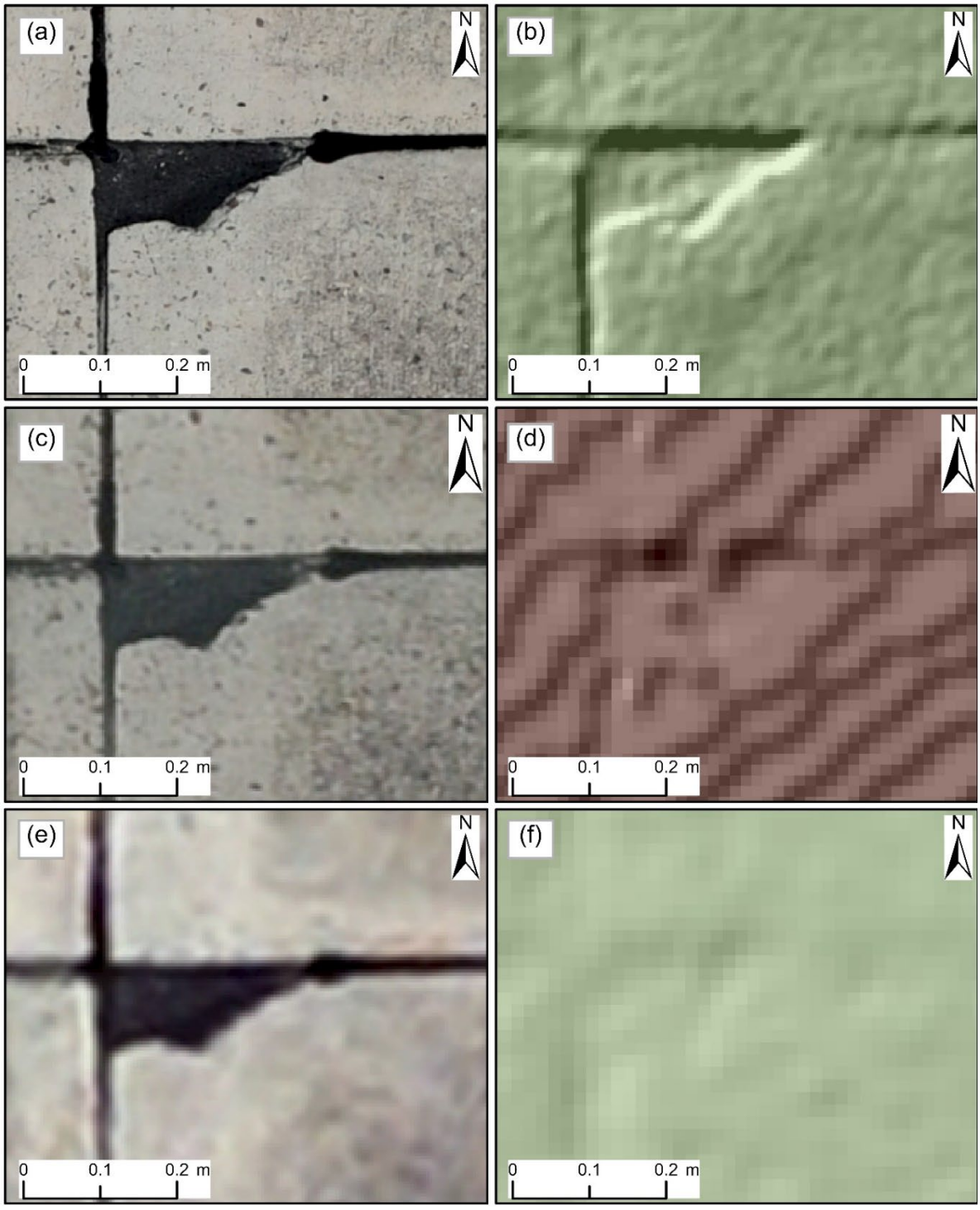

Figure 92. Alkali-Silica Reaction (H) in (a) 1.5-mm/pix Orthophoto, (b) 5.9-mm/pix DEM, (c) 3.5-mm/pix Orthophoto, (d) 14-mm/pix DEM, (e) 4.1-mm/pix Orthophoto, and (f) 16.2-mm/pix DEM

8. PRACTICAL LESSONS FROM FIELD TESTING

8.1 LESSONS ON sUAS PLATFORMS

The research team deployed six different sUAS platforms for data collection at airports in Michigan, Illinois, Iowa, and New Jersey. Some platforms had integrated sensors, and others were used to carry payloads. The sUAS platforms varied in size, weight, and capability. However, all platforms were VTOL multirotor systems, which means they have minimal launch and recovery requirements (i.e., in small areas) and can hover and detect objects from a fixed position and react quickly to changing airport flight operations. The details of the sUAS platforms are provided in Table 19. The flight times are an estimate of practical performance based on flying with the chosen sensor payload and under light wind conditions (< 16 km/h). In contrast, the flight times reported in Table 1 are claims by the manufacturers and are relatively higher than the actual flight times. The sUAS platforms used in this study (Figure 93) were categorized into two classes based on weight and size: (i) relatively larger and heavier sUAS platforms capable of carrying larger, changeable camera payloads such as the Nikon D850 and Sony Rx1R-II; and (ii) smaller and lightweight DJI Mavic drones with integrated sensors.

Table 19. The sUAS Platforms Deployed at Different Airports

sUAS Platform	Type	Sensor	Practical Flight Time (minutes)	Airport Deployed
Bergen Hexacopter	Six rotors, large	Nikon D850 45.7-mp RGB optical, FLIR Vue Pro R 512x640 thermal, Tetracam Micro-MCA6	12	ONZ, TTF, MTO, BNW, PRO
UAVSI Tarot X6	Six rotors, large	Nikon D850 45.7-mp RGB optical	14	ONZ, TTF, WWD
MicroDrones mdMapper1000+	Four rotors, large	Sony RX1R-II 42.4-mp RGB optical	30	TTF, MTO, WWD
DJI Mavic 2 Pro	Four rotors, small	20-mp RGB optical	23	ONZ, TTF, MTO, BNW, PRO, WWD
DJI Mavic 2 Enterprise Advanced	Four rotors, small	48-mp RGB optical Quad Bayer and 512x640 thermal	23	ONZ, TTF, MTO, BNW, PRO, WWD
DJI Mavic 2 Enterprise Dual	Four rotors, small	12-mp RGB optical and FLIR 160x120 thermal	23	TTF

ONZ = Grosse Ile Municipal Airport
TTF = Custer Airport
MTO = Coles County Memorial Airport
FLIR = Forward-looking infrared
PRO = Perry Municipal Airport
WWD = Cape May Airport
BNW = Boone Municipal Airport
mp = Megapixel

8.1.1 Small and Agile Platforms with Integrated Sensors

Three small sUAS platforms were deployed at the data collection sites, all of which included integrated sensors: DJI Mavic 2 Pro, DJI M2EA, and DJI Mavic 2 Enterprise Dual. All three sUAS weighed about 1,100 gm each. They have a maximum expected flight time of 31 minutes, as reported by the manufacturer. However, they were flown back to the original take-off location when the battery had around 30% charge left for safe operation. It usually resulted in around 23 minutes of practical flight time. These sUAS showed better agility and maneuverability compared to the larger platforms. They can also perform better than the larger sUAS in adverse weather conditions; the M2EA and Mavic 2 Pro were deployed safely and successfully at TTF with up to 40 km/h wind gusts. Multiple successful flights were achieved at several airports using these platforms at wind gusts of more than 25 km/h. In addition, DJI provides and maintains flight assistant software for these sUAS, which was found to be reliable and easy to use (DJI Go 4 for the Mavic 2 Pro, DJI Pilot for the M2EA).

Figure 93. Examples of sUAS Platforms and Sensors Deployed
(Clockwise, from top left: Tarot X6 with Nikon D850, mdMapper1000+, Mavic 2 Pro, Nikon D850 camera, M2EA [on top of orange landing pad], Bergen Hexacopter with Nikon D850 ready for deployment)

In addition, the DJI smart controller that comes with M2EA facilitates mission planning, data collection, and collection monitoring, without need for an additional smartphone or tablet computer, although external internet access must be provided to have access to the basemaps (such as existing aerial photos) when in the field. The bright screen and high battery capacity of the controller made it suitable for fast data collection. DJI and third-party flight assistant applications, such as DroneDeploy and Pix4D capture, support continuous data collection with low-battery swap downtime (2–3 minutes). For an example of efficient data collection, in May 2021, the research team collected data over 1,523 m x 30 m (4.6 hectares) on Runway 3/21 at TTF with a more than 2-hour data collection time; the mission was completed within 3 hours and 20 minutes. Based on use during this study, these smaller sUAS have two disadvantages: users cannot mount any

additional significant payloads (such as additional sensors, e.g., optical or thermal cameras), and automated missions are not supported for very low flight altitudes on the mission-planning software provided by the manufacturer. DJI mobile applications for the sUAS used in this study only allow collecting RGB optical data at 15 m or higher elevation and thermal data at 24 m or higher elevation.

8.1.2 Heavier Platforms with Additional Payload Capacities

The research team deployed three relatively large sUAS platforms, weighing 6 kg to 10 kg with batteries on board. These sUAS platforms were mainly used for high-resolution sample unit data collections because of their ability to carry heavier, high-resolution cameras. The newer Tarot X6 North American-made platform from UAVSI (Figure 93, top-left) was used for complete data collection at WWD in August 2021, ONZ in November 2021, and TTF in November 2021. The latter two data collections were not part of the work presented in this report but were conducted for an additional FAA application. The platforms were versatile, and different sensors could be mounted based on the research need. The RGB optical cameras mounted on these platforms were full-frame and higher-resolution devices capable of capturing superior data compared to the smaller platforms' integrated, lower-resolution RGB optical sensors. Thus, these cameras mounted on larger platforms are recommended for higher-resolution data collection needing 2-mm/pix or better resolution RGB imagery with 6-mm/pix or better resolution DEM results for identification and rating of as many pavement distresses as possible.

8.1.3 Recommendations for sUAS Platforms

Small and agile sUAS platforms with integrated sensors are recommended for effective and rapid data collection. These systems are easy to operate and expected to have the following characteristics:

- Practical battery life of more than 20 minutes after keeping 20%–30% for the safe return of the sUAS platform.
- Ability to fly at a wind speed of up to 25 km/h with occasional wind gusts of up to 40 km/h.
- Continuous data collection with flight assistance software that includes automated supervised data collection mission capabilities.

Relatively heavier platforms with the ability to mount sensors are recommended for high-resolution and specific types of data collection that require special sensors. These systems are expected to have the following capabilities:

- Ability to carry additional payloads such as cameras that can weigh up to 1 kg.
- The supported payload should include the ability to carry multiple sensors, with a focus on optical and thermal imaging.
- Support of automated flight plans with flight assistance software.

8.2 LESSONS ON SENSORS

Two main types of sensors were deployed to study their usefulness in detecting and rating airfield pavement distresses: RGB optical sensors for creating orthophotos and DEMs, and longwave thermal infrared sensors collected in stereo data collection mode to create merged thermal image outputs. A multispectral sensor able to collect visible and near-infrared light wavelengths was deployed for an initial demonstration but needs further study to make conclusions. RGB optical sensors were deployed multiple times at different altitudes to obtain different resolutions and to study which resolution could best be used to detect and rate the pavement distresses or damage present at the parts of airports studied for this study. Table 1 shows the sensors, flight altitudes, and output resolutions of all sensors used in this research.

RGB optical sensors were used extensively in this study. The Nikon D840 45.7-mp and Sony RX1R-II 42.4-mp RGB optical sensors are high-resolution, full-frame sensors mounted on larger sUAS platforms that can carry these heavier payloads. Deploying such sensors requires a detailed understanding of the camera's settings, which need to be adjusted based on the light (sunlight and cloud) conditions. The integrated sUAS sensors onboard the three DJI platforms were easy to use but provided relatively fewer visual details of airport pavement than the full-frame sensors due to the higher resolution of the full-frame cameras. For integrated sUAS sensors, this study tested the sensors of the three DJI Mavic platforms that were deployed: 12-mp RGB optical sensor of Mavic 2 Enterprise Dual, 20-mp RGB optical sensor of Mavic 2 Pro, and the 48-mp Quad Bayer RGB optical sensor of M2EA.

Two thermal sensors and one multispectral sensor were also used for this study. Initially, a FLIR Vue Pro R was mounted on a Bergen Hexacopter and deployed at ONZ in December 2020. The FLIR Vue Pro R sensor does not record GPS information along with the thermal image but the thermal images can be processed into usable formats, such as JPG files with per-pixel temperature values. M2EA's thermal sensor has the same resolution as the FLIR Vue Pro R, and the research team extensively used this newly acquired unit throughout this study mainly because of its GPS data collection capabilities, which provided location-tagged thermal images. However, the M2EA was only released in March 2021, and the processing software is not yet mature for its thermal data outputs. A well-established workflow to obtain per-pixel temperature values from the M2EA thermal sensor is being developed by the M2EA user community, as DJI's available software tool for processing M2EA does not yet output data usable for merging geospatial data with actual temperature values. However, the M2EA data area is easily usable for analyzing relative temperature differences in airport pavement. Despite these current limitations, the research team was still able to use the M2EA data to address the utility of thermal cameras to help identify and rate pavement distresses.

These are the primary lessons learned from the deployment of this study's selected sensors:

- Full-frame RGB camera sensors usually provide better visual details in output products with the 42.4- and 45.7-mp systems used in this study, but these sensors are not directly integrated with platforms and additional knowledge and effort are required to use them for data collection.

- The light sensitivity (i.e., ISO), aperture (i.e., F-stop), and shutter speed need to be adjusted on the non-integrated RGB full-frame cameras to capture the best quality images under different light conditions, flight altitudes, and flight speeds. Additional equipment and processing steps are required to capture position information and geotag the collected imagery.

- Quad Bayer sensors do not provide the same visual details as regular sensors with similar resolution. The 20-mp integrated RGB sensor of the Mavic 2 Pro provided better details compared to the M2EA's 48-mp Quad Bayer RGB camera.

- It is challenging to create a thermal orthomosaic image from a non-geotagged image. The FOV of the thermal sensor is narrow, and the presence of a lower number of pixels poses extra difficulty in orthophoto generation. The narrow FOV also greatly increases the required image overlap and, therefore, the total flight time required to create a high-resolution thermal orthomosaic.

- The multispectral sensor deployed at TTF, the Tetracam Micro-MCA6, did not provide additional distress detection and analysis values in the limited testing of this research. Thus, the multispectral data collection was not pursued further for this study but could be worth a more detailed study over more areas, potentially along with hyperspectral sensors.

8.3 LESSONS ON PRACTICAL DATA COLLECTION APPROACH

8.3.1 Minimum Crew Requirement

In most of the sUAS data collection, the research team had more than four members on site. In a feasibility study to determine the minimum crew size required to collect sUAS data successfully from an airport, it was determined that a three-member sUAS crew could successfully collect sUAS data at an airport with low air traffic without interrupting the general flow of data collection. The three-person team consists of one remote pilot in command, one visual observer, and one person responsible for managing data collection logistics activities. Additional activities can include charging the sUAS batteries, taking location-tagged field photos, taking measurements of distresses to compare to the sUAS imaging results, such as the height of shoving or swelling, or placing and removing GCPs. It is also helpful for the crew to include at least one additional sUAS pilot with an additional dedicated observer, if possible, to enable simultaneous data collection at multiple airport locations to expedite data collection. More paired pilot-observer teams could be deployed to quickly complete data collection at multiple locations if resources allowed. Each crew needs to have a dedicated portable aviation radio for efficient, safe operations.

8.3.2 Number and Optimal Location of GCPs

The number and location of GCPs are important to meet data collection and processing needs for detection and rating of distresses. The presence of six or fewer GCPs on a long and narrow runway or taxiway can cause distortion of the orthophoto shape with unexpected spatial deviation. This phenomenon was observed during TTF data collection in March 2021 and during BNW data collection in June 2021. The number of GCPs to put on a data collection site depends on its shape and size and the positional accuracy desired/needed from the sUAS data. The research team

focused on placing GCPs on the four corners of a target area first, followed by placing two GCPs on both sides of the runway or taxiway spaced at around 100 m (Figure 94). For the approximately 1200-m-long by 45-m-wide area of the WWD 10/28 runway, 30 GCPs were used to derive the <2-mm/pix RGB orthophoto and 6-mm/pix or better DEM high-resolution outputs. Priority should be given to placing the GCPs closest to the sample units of greatest interest that will be surveyed with high-resolution sensors; this could be the entirety of the pavement area or some subset. The research team also demonstrated that Propeller AeroPoints™ with built-in location-recording technology (GNSS, such as GPS) can be used effectively multiple times due to their portability and capability of collecting high-resolution (better than 3-cm accuracy with up to 1-cm accuracy) position data within 30 to 45 minutes. See Section 5.1 of this report for information on AeroPoints™ ground accuracy.

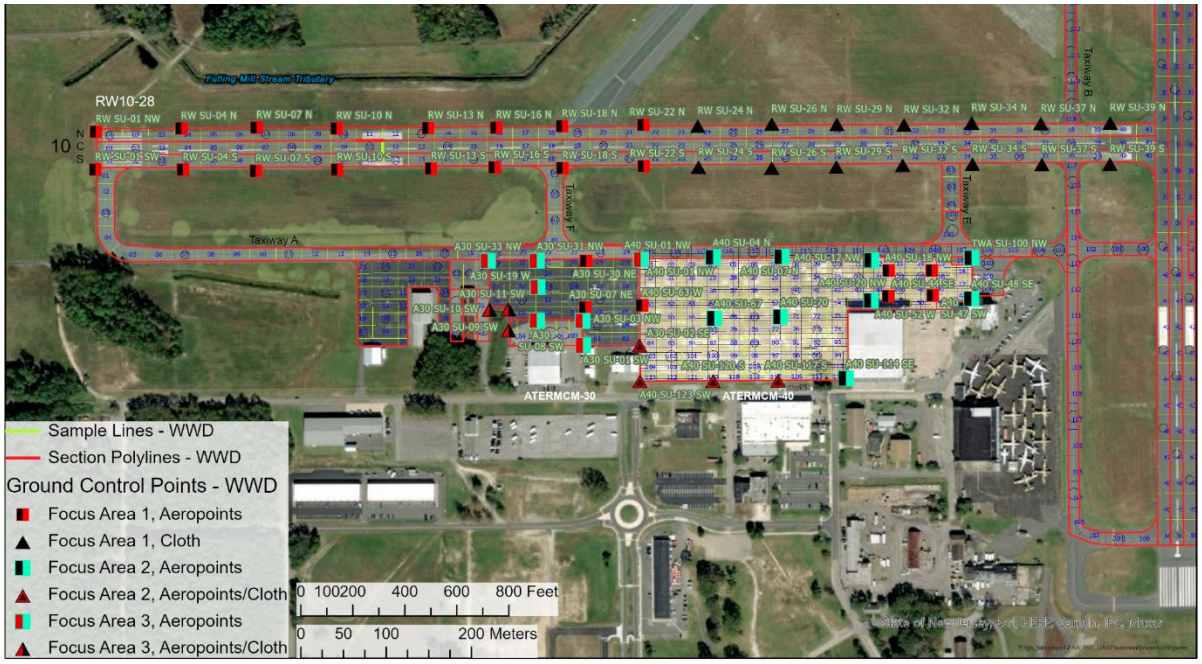

Figure 94. Ground Control Points Locations Planned at WWD Spaced at Approximately 100-m Intervals

8.3.3 Impact of Weather on Data Collection

sUAS data collection generally requires favorable weather for efficient data collection, with no precipitation and reasonably low wind speeds. The research team closely observed weather forecasts starting 10 days ahead of the data collection efforts at each airport site. A final decision on weather conditions was most often made 2 days before data collection, but this decision could still be changed on the day of data collection. Most sUAS cannot collect usable imagery during precipitation, such as rain and snowfall, because it can affect the operation of the platform (i.e., most drones are not waterproof) and the collected imagery (e.g., when moisture on camera lenses makes images unusable for analysis). In addition, wind speed and wind gusts were always strongly considered before data collection. The smaller sUAS can operate effectively at wind speeds up to 40 km/h (~25 mph), while the larger sUAS can successfully collect data up to 24 km/h (~15 mph).

Beyond these speeds, experience from this study shows that the platforms used should not be used for reasons of safety and image quality. It is advisable to proceed with the data collection based on the capabilities of the sUAS platforms and wind speed.

Reasonable illumination by daylight is required to collect quality sUAS imagery (use of artificial illumination to potentially make nighttime RGB imaging possible was not within the scope of this study). Thus, the period of possible data collection in a day depends on the time of the year and the site's geographical location. The research team started collecting data as early as 8:30 a.m. and continued until 7:00 p.m. in the summer (August 2021) at WWD in New Jersey. However, in the fall, the period of available light shortens significantly. A recent field data collection in mid-November at ONZ in Michigan showed that to have sufficient light, data collection could not start before 10:30 a.m. and had to conclude before 3:30 p.m. It is possible to collect data during both cloudy and sunny conditions, with both typically able to provide sufficient illumination. Partly or entirely cloudy conditions are possible too (without fog presence). However, rapid changes in ambient light during an sUAS flight can make the photogrammetric data results inconsistent. Some areas appear darker or brighter than others in the merged orthophoto RGB output. Distress detection is still possible with these "changing light conditions" orthophoto outputs but may require more careful interpretation to understand impacts on how distresses appear. Thus, it is advisable to plan accordingly to obtain adequate light for RGB optical sensors.

8.3.4 Software Updates and Issues with sUAS Platforms

The sUAS are composed of complex technology with many hardware and software components that need to operate properly for safe, efficient, and high-quality data collection. For example, the mdMapper1000+ with Sony RX1R-II 42.4-mp optical RGB camera system proved to be an unexpectedly challenging platform. The research team attempted deployment of this system at airports in Iowa but were unable to have a successful take off due to technical difficulties. The technical difficulties were related to a recent software update that was intended to correct existing known issues, but instead caused the deployment issue. Thus, updating the flight controller software and sUAS platform firmware a week or more prior to data collection and keeping the setup consistent is suggested. The research team also found that the mdMapper system was more sensitive to wind conditions than the other large sUAS (Bergen Hexacopter, Tarot X6) and restricted its use to when winds were below 16 km/h (10 mph). For any platform, test flights are recommended, which would be helpful to identify such issues in the weeks and days before data collection to ensure that imagery will be collected as expected.

A reliability issue was discovered with third-party applications used to control sUAS, such as the DJI Mavic 2 Pro. In some cases during software updates to flight control applications, software that worked for data collection one week might not work the following week. It is strongly recommended to verify that all intended flight control applications work the day before flights occur and to keep the settings consistent until after completing data collection.

The research team also encountered difficulty deploying sUAS at airports that have a requirement for "unlocking geozones" (or geofences) for sUAS takeoff while using flight applications like DJI Go 4, DJI Pilot, and DroneDeploy. The requirement provides considerable safety and security for airports but complicates sUAS-based data collection. Unlocking geozones requires a good internet connection to connect with the flight application server which might not be available in remote

airports. These additional steps add around 15 minutes to the total data collection time. Long-term geozone restrictions, such as class C or class D airspace in towered airports, are simpler to deal with as the request for permission to fly sUAS can be submitted and received a few days prior to the data collection. However, the data collection team encountered two temporarily restricted zones at untowered airports that delayed data collection that day while team members unlocked those zones. Such upcoming issues could be avoided by using the sUAS flight and pilot assistant website and mobile applications such as Aloft.ai, uavforecast.com, and DJI pilot account. However, this process has been evolving rapidly over the past year, often with major changes occurring on a week-to-week basis, thus, close monitoring on those applications and websites are recommended. This can greatly complicate collecting data at airports, especially at locations that do not have a good cellular wireless signal to unlock a geozone. sUAS pilots should ensure that any necessary flight permissions are obtained one or more weeks in advance and linked to necessary accounts. These accounts and pilots must be linked to the sUAS and the applications to be used in the field on the day of the data collection.

8.4 LESSONS ON DATA PROCESSING AND ANALYSIS

8.4.1 Data Processing Framework and Recommendations

The research team collected RGB optical data from all six airports visited in this study. Each data set was imported separately into Agisoft Metashape for processing. The team has worked extensively with Agisoft software, with at least 12 years of experience using the software since it was in beta and knows its capabilities in-depth. Relative to other processing software, Agisoft's tunable processing steps provide more control to the image analyst. The research team has also worked with Pix4D software on occasion for other applications, including helping process thermal imagery.

Using the GCP locations recorded with the AeroPoints™ and Trimble® GeoExplorer® GeoXH 6000 GPS units improved the positional accuracy of the sUAS imagery outputs beyond what can be provided by any onboard GPS. The AeroPoints™ have approximately 3-cm x,y,z accuracy but can be better; at least 45 minutes of data collection on the ground is recommended to achieve this accuracy. The Trimble® GeoExplorer® GeoXH 6000 GPS has approximately 10-cm x,y,z accuracy within 5 minutes of data collection. More expensive and modern GPSs, ideal for achieving survey-grade accuracy in similar rugged field conditions, can achieve approximately 1-cm x,y,z accuracy with as little as 1 minute of data collection.

The images were processed using one or more high-end desktop workstations to create RGB optical orthophotos, DEMs, hillshades, and thermal orthophotos. The DEM is a raster image with each pixel representing the elevation, and the DEM was generated based on the dense cloud created using Agisoft Metashape software as part of the RGB orthophoto production process. The final resolution of the DEM depended on the resolution of the image captured by the optical RGB sensor. Each DEM was imported to ArcGIS Pro to produce a hillshade for easier visualization and interpretation of elevation models. As described by ESRI, a hillshade is derived from the DEM and "produces a grayscale 3D representation of the terrain surface, with the sun's relative position taken into account for shading the image" (ESRI, 2021a). The research team found that it makes DEM data much easier to interpret when overlaid in GIS software with partial transparency over

the DEM, especially for visually identifying areas of greater elevation change in a data collection area.

Each application and platform available for data processing has a different workflow. However, the following steps of the data processing are recommended:

- Medium or high setting for image alignment is recommended.
- Location information of the GCP, if available, must be used.
- A medium setting for dense cloud generation is recommended. However, the high or very high options can be used based on the resolution requirements.
- The DEM and orthophoto output must have a projected coordinate system for accurate viewing and simplified measuring of features; Universal Transverse Mercator or State Plane Coordinate System are the most common with a locally appropriate zone, usually with the NAD83 or WGS84 datum.
- Each processing parameter should be selected based on the number of images to be processed, resolution of the data, estimated time required to complete the processing, and configuration of the computer or cloud-based services being used for the data processing.

8.4.2 Time Required for Data Processing and Analysis

The data processing time for a complete data collection varies based on the resolution of the data, the number of photos in the data set, and the required resolution of the output. An image captured by a Nikon D850 45.7-mp camera contains many more pixels than an image captured by a 12-mp camera; thus, they are expected to have a longer processing time. The number of images dictates the processing time required for images with the same resolution. For example, a data set with 2,938 images required 18 hours and 48 minutes to process, whereas 1,267 images took 7 hours and 40 minutes in a computer equipped with Intel® Xeon® W-2265 Processor (19.25M Cache, 3.50 GHz) with 12 cores and 24 threads, 128 GB DDR4 ECC RAM, and NVIDIA QUADRO RTX 5000 16-GB graphic card with 3,072 CUDA Cores. The export times for these two data sets were also different. It is also worth noting that the configuration of the workstation computer contributes to the data processing time. It is safe to assume that 2,000–3,000 images, each with 45.7-mp resolution, would take at least 24 hours if every step was completed as intended in one of the aforementioned workstations. However, the research team discovered that some processes needed to be redone, so a two-day time frame is assumed to be the shortest achievable processing period for such a large project on one computer, which can be typical for an airport sUAS data collection. Agisoft Metashape, which was used advantageously in this study, allows users to operate multiple computers simultaneously and reduce the processing time significantly. Processing in the cloud was not examined in this study but could help reduce processing speeds and be a possible future resource.

The ability to use sUAS data for airfield pavement distress identification depends on the density and types of distresses present on the sample unit. For example, several PCC sample units at BNW had a few LTD cracks and incidents of joint seal damage. It required an average of 5 to 10 minutes to observe and note the individual distresses visually. On the other hand, the relatively large sample units of WWD PCC sections with patching, ASR, spalling, and LTD cracks took around 40 minutes to 1 hour to annotate and complete. Recording each L&T crack required a significant

amount of time because of their density. Each AC sample unit of WWD took approximately 45 minutes to 1 hour to record all L&T cracks. AC sample units of TTF required approximately 25 minutes as the density of cracks was considerably lower. In addition, such analysis also depends on the experience of the image analysts. For example, ONZ data that were analyzed at the beginning of this research required around 35 minutes for each sample unit. A similar analysis by the same image analyst required 20 to 25 minutes at the end of the study once the analyst was familiar with the analysis and the site.

8.4.3 Overlay of PCI Survey Data with sUAS Data

The existing method of PCI surveys can and do produce geospatial data that show the locations of distresses and airport features, such as sample unit boundaries, concrete slab boundaries, and named locations of runways/taxiways/connectors. New distress data can be recorded in tablets that enable the inspector to record the location, type, and severity of distress data, with existing data such as sample unit locations displayed in the background. For traditional FOG PCI survey, it is not critical that these types of geospatial data have very high, sub-meter, absolute positional accuracy. The same has been generally true for remote sensing products created for airports, such as aerial photography from manned aircraft or orthophotos created from sUAS-enabled photogrammetry. If these products did not align with an accuracy of better than a meter, then this had little to no impact on rating airport pavement condition.

As this research has shown, an important lesson learned is that geospatial data should align relatively accurately to make data easier to compare between different data creators and to compare results over time. For example, Figure 95 shows three different views of FOG (manual) surveys completed for ONZ. On the left is the inspection data as shared, with no imagery background. This is a view that an inspector can also see while recording new PCI data. In the middle is a view of that data when overlaid on an orthoimage created from sUAS collected imagery with approximately 10-cm positional accuracy. The manual inspection geospatial data ranges from 3.1 m to 3.8 m off the location of the sUAS imagery.

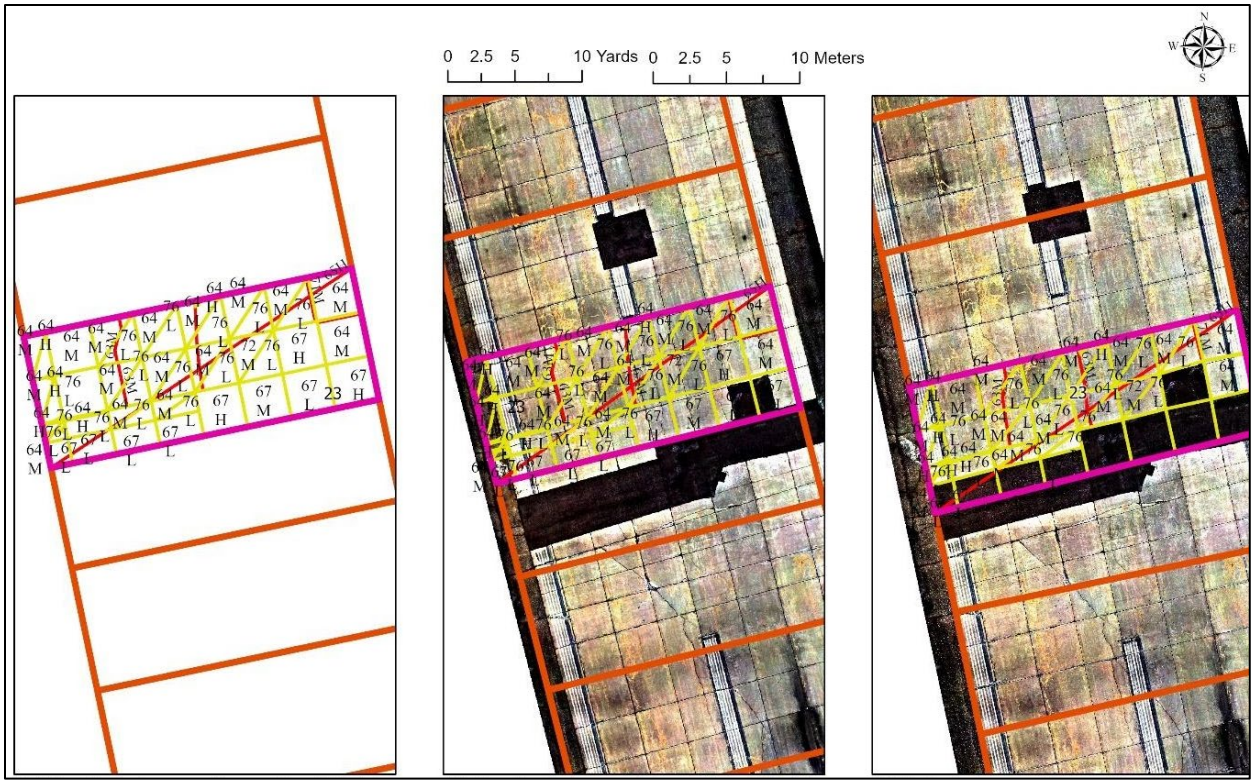

Figure 95. Manual Distress Survey Result (left), Manual Survey Results Overlaid on an RGB Data with Approximately 10-cm Position Accuracy (middle), and Well-Aligned Manual Survey Results

The manual inspection data on the right has gone through a spatial adjustment process to align it with the sUAS imagery that has better positional accuracy. These data are significantly easier to interpret and compare between different sources of imagery. If future imagery is collected with 10-cm or better positional accuracy, this will also align well with historical and future manual or automated inspection data.

A similar issue occurs with sUAS imagery. Depending on the quality of GPS onboard the sUAS, the image processing methods, the use of real-time kinematic (RTK) GPS, and the use of GPS-enabled ground control targets, the absolute positional accuracy of the output products such as orthophotos can vary widely. Figure 96 illustrates this with an example shared by the third-party company that collected data at WWD in May 2021. One image is the 2-mm product, and the other is the 3-mm product. Their detected distress layer is shown on both—it lines up precisely with the 3-mm orthophoto output, but not the 2-mm orthophoto generated and supplied to the research team by the same organization.

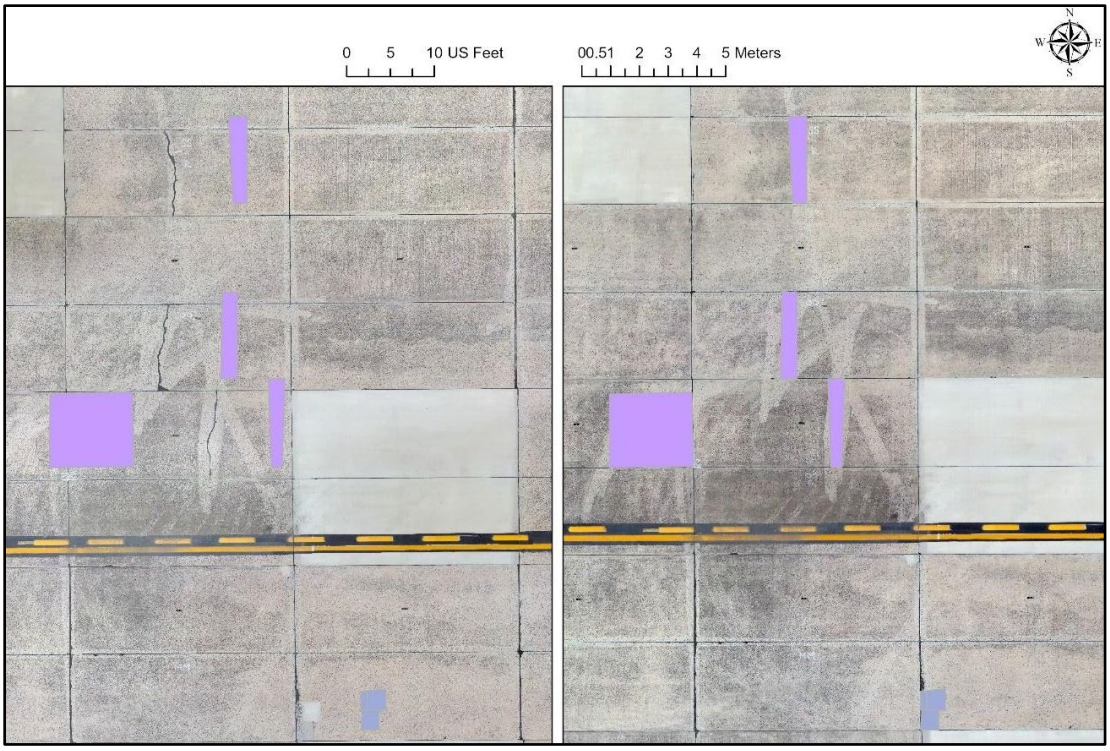

Figure 96. Third-Party Company 2-mm/pix RGB Orthophotos Without GCPs (left) Located 1.8 m Away from 3-mm/pix RGB Orthophoto (right)
(The purple polygons are created based on 3-mm/pix RGB data.)

The 2-mm orthophoto is shifted about 1.8 m west of the 3-mm product; this is most likely because GCPs were not used when collecting imagery via sUAS at their airport surveys, based on the information shared by the third party. This can make it more difficult to know which specific distress is being mapped in each case and also means that imagery collected by other parties or in the future cannot be expected to line up well. Figure 97 shows what should be expected—that manually collected distress data and future automatically detected distress data will align (within 0.5 m or better) with orthophotos output and accurately positioned data that uses 10-cm or better ground control or post-processed kinematic (PPK) or RTK technology. The manually collected FOG distress data did have to be spatially adjusted, but in the future, the UAV-derived orthophoto can be put in the background for field inspection tools so that recorded distress will align with UAV outputs from the start.

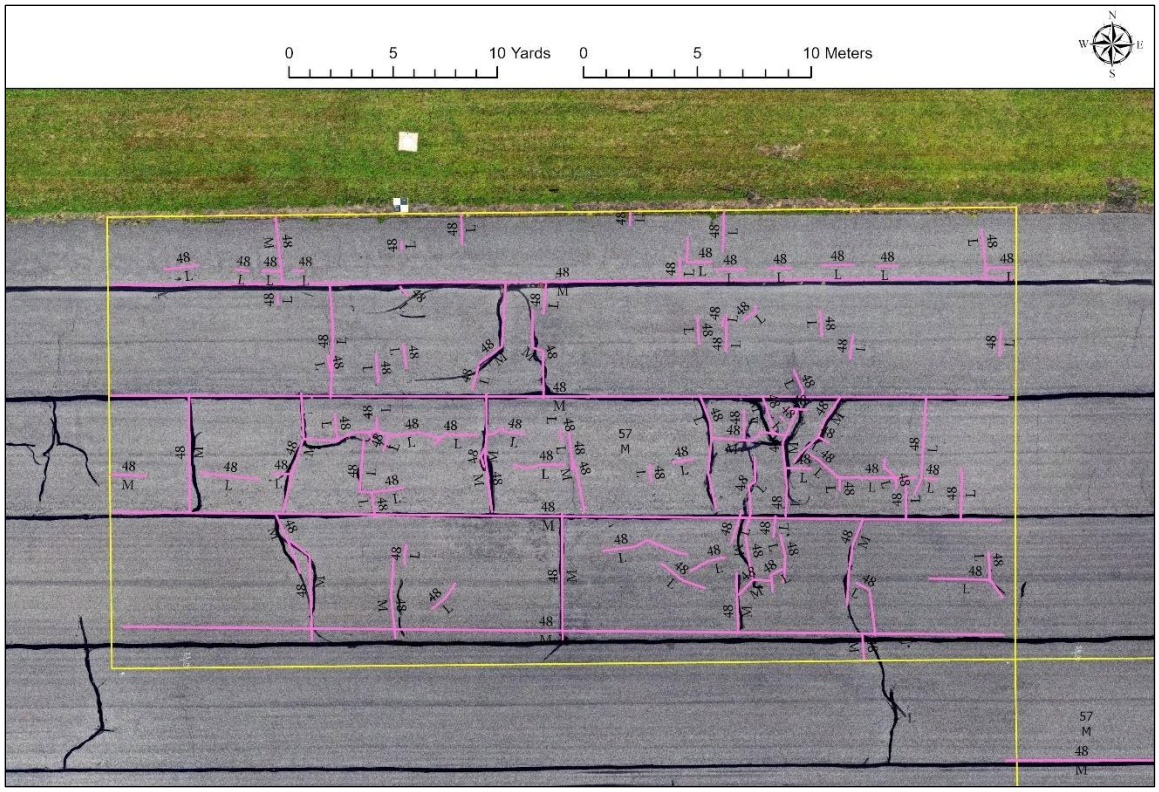

Figure 97. An Example of Recommended Future UAS-assisted PCI Inspections and Geospatial Layers, with Distress Data Well-Aligned with UAS-Derived Output Products

Creating sUAS outputs with high positional accuracy and ensuring that PCI inspection data aligns well with this requires significant time, especially for spatially adjusting existing inspection Geographic Information System (GIS) data. However, it is assumed that aligning the future inspection data and sUAS outputs is well worth the effort. On a practical basis, it is recommended that sUAS imagery outputs (RGB orthophotos, DEMs, and hillshades) should have at least 0.5-m positional accuracy. Positional accuracy of 10 cm or better is highly recommended. This can be accomplished using ground control targets such as the GPS-enabled Propeller AeroPoints™, or traditional cloth or plastic targets whose locations are recorded with a 10-cm or better accuracy GPS unit. If RTK positioning can provide this accuracy with few or no GCPs, this would be acceptable as well; however, RTK positioning was not explored in this research study.

Field demonstration in Michigan showed that as few as 10 GCPs can work for some single-runway or single-taxiway data collections. At WWD, 60 different locations were used (some locations collected more than once over multiple days) to ensure high positional accuracy for each geospatial output. While one person is assigned responsibility for collecting this GCP positioning data, other crew members can focus on sUAS data collection. With a dedicated person, this can be accomplished in two hours or less at a two-runway untowered airport such as WWD. The amount of time depends on the type of GPS unit used, if more than one unit is available, or if multiple GPS-enabled GCPs such as AeroPoints™ are available and can be left to collect data while other survey activities take place. One option that can be used by surveyors is to use temporary paint markings on the ground and collect GPS data (using AeroPoints™ or other GPS-enabled GCP

units) over the course of the data collection. This avoids any potential issues of moving AeroPoints™ or GPS units during drone surveying, especially if multiple days are required to complete surveys. In addition, placing the AeroPoints™, then collecting the sUAS data, followed by moving the AeroPoints™ to a different location is another solution. A similar approach was followed at TTF where 10 AeroPoints™ were used three times to increase the number of GCPs. It was also observed that placing AeroPoints™ for 30 minutes can provide location information with very high accuracy. Until RTK technology is evaluated further, it is recommended to use GCPs for all sUAS airport surveys going forward.

8.5 LESSONS LEARNED ON USEFUL DATA TYPE AND RESOLUTION

Three types of sensors (RGB optical, thermal, and multispectral) were deployed at six airports in Michigan, Illinois, Iowa, and New Jersey to collect four types of data: RGB optical orthophoto, DEM, thermal, and multispectral. The demonstration of a multispectral imaging system was limited to one data collection effort at one airport, TTF, and the resulting images did not provide any useful details beyond the other two sensors. Additional testing could reveal further value in multispectral and potentially hyperspectral, UAS-collected data products. This section focuses on the value of the RGB optical and thermal sensor data that the research team explored in more detail.

8.5.1 Red, Green, and Blue Optical Data

RGB optical orthophotos with resolutions ranging from 0.8 mm/pix to 21 mm/pix were viewed using ArcGIS Pro to determine their usefulness in airfield pavement distress detection and rating. ASTM D5340-20 lists 16 PCC pavement distresses, and 14 were available in this study's sUAS data collection sites (blowup and pumping were not available) (ASTM International, 2020). The analysis showed that the RGB optical orthophotos of 3.3-mm/pix or better resolution are sufficient to detect 13 out of 14 PCC pavement distresses, with one or more severity level(s) observed in this study. Faulting could not be detected in the surveyed locations. Eight AC pavement distresses occurred at TTF and MTO out of the 17 distresses listed by ASTM D5340 (ASTM International, 2020). The analysis showed block cracking, alligator cracking, patching, and L&T cracks could be identified with RGB orthophotos. The details of these AC and PCC pavement distress identifications are illustrated in the result and discussion sections of Section 4 to Section 7 in this report.

8.5.2 Digital Elevation Model Data

DEMs are two-dimensional data products where each cell of the data represents the elevation value for an area. The DEM is produced during the SfM and 3D processing in Agisoft Metashape. An intermediate step is required to produce the DEM in Agisoft Metashape during RGB orthophoto generation. This study demonstrated that pavement distresses with elevation change could be detected and measured using the DEM data. Using the high-resolution DEMs of at least 6.0 mm/pix or better (higher), as shown in Figure 68, can confirm suspected and known locations of faulting in PCC pavement, and depression and shoving in AC pavement. There is a scope of automatic faulting detection using DEM. It could be done by tracking elevation changes automatically in numerous locations on a sample unit and finding sharp elevation changes. In addition, the presence of the faulting on the PCC pavement showed a significant elevation

difference, which could be used to confirm the suspected location of faulting in a slab (Figure 17 and Figure 59). Figure 98 illustrates the usefulness of high-resolution DEM data in detecting and verifying a change in elevation that indicates the presence of a distress. The two slabs where faulting exists at their edges show height differences of approximately 10 mm, as shown in parts Figure 17 (a) and (b); where there is no faulting, a rapid elevation drop is not present, as shown in Figure 17 (c) and (d). The usefulness of DEM data in the automated detection of elevation-based distresses without prior knowledge of their presence could be a topic for future research.

With this high-resolution DEM data, it is also possible to "drape" the orthophoto imagery over the DEM in GIS software to display how elevation changes of just a few centimeters can be captured through the sUAS surveys. Figure 98 shows an oblique 3D view of a 2.5-mm resolution orthophoto, draped over a 10-mm resolution DEM collected in May 2021 at ONZ. A 5-cm difference exists between the highest point of the asphalt patch and the surrounding edges of the concrete slabs, which can be visualized in the GIS software (e.g., ArcGIS Pro) that was used to create Figure 98. Interpreters can view this draped data in GIS software to visually confirm the presence of 3D distresses.

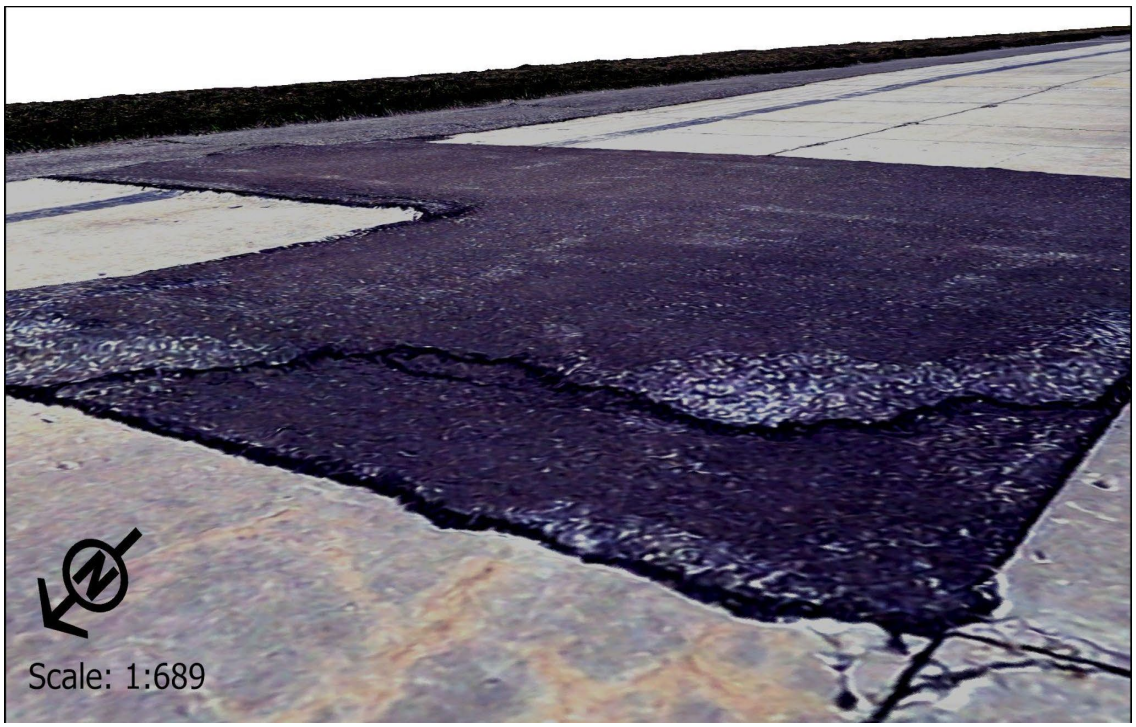

Figure 98. Example of Draping an sUAS-Derived Orthophoto Over a DEM Showing Elevation Differences for an Area of Patching on an Airport Runway

8.5.3 Thermal Data

In this study, the analysis of thermal data has been more limited than RGB orthophoto and DEM analysis (see discussion in Section 2 on thermal sensors), but it has shown promising performance in detecting L&T cracks in AC pavement and LTD cracks and spalling in PCC pavement (Figures 99 and 100). The L&T cracks of AC pavement underneath the pavement markings, and those with

a recent overlay of a concrete layer, showed significantly different heat signatures than other sections of the AC pavement. Further investigation of the value of thermal data for distress detection, potentially in a dedicated study, is recommended.

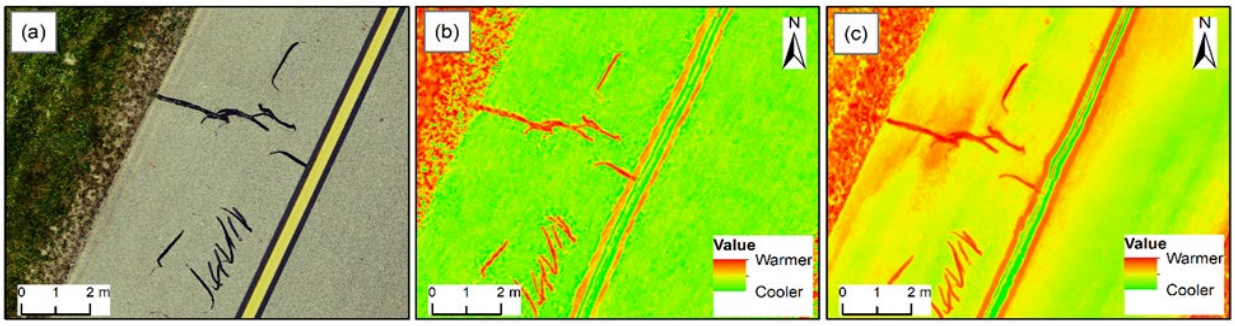

Figure 99. Sealed L&T Cracks on AC Pavement in Taxiway A Sample Unit 23 at TTF: (a) 1.5-mm/pix Orthophoto, (b) 31-mm/pix Thermal, and (c) 14-mm/pix Thermal

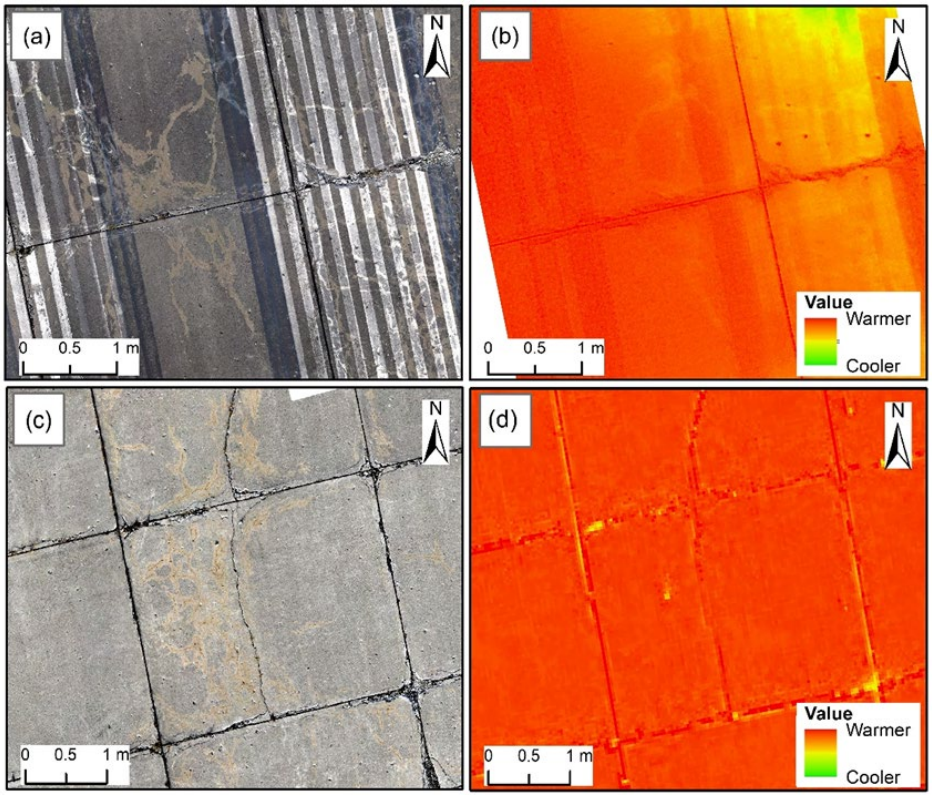

Figure 100. Longitudinal, Transverse, and Diagonal Cracks and D-cracks in PCC Pavement on Runway 17/35 at ONZ: (a) 1.5-mm/pix Orthophoto of Sample Unit 5, (b) 8-mm/pix Thermal of Sample Unit 5, (c) 1.5-mm/pix Orthophoto of Sample Unit 23, and (d) 31-mm/pix Thermal of Sample Unit 23

8.5.4 Different Data Types and Resolutions for Different Distresses

Based on the usefulness of these data types, Tables 20 and 21 provide a summary of different data resolutions and types that worked well for different distress identifications and ratings by an image analyst.

In addition, the following data types are recommended based on the allowable budget and time for future sUAS data collection:

- RGB optical sensors are recommended if the deployment of only a single sensor is possible. RGB optical and DEM data are adequate to detect the majority of airfield pavement distresses outlined in ASTM D5340.
- If budget and time permit, thermal, multispectral, and other sensors could be deployed to address specific project needs, with thermal appearing the most promising so far for helping with distress detection.

This study evaluated a wide range of RGB optical, DEM, and thermal photos with different resolutions. Each data resolution was also studied for its capabilities in detecting and rating airfield pavement distresses. The following resolutions are recommended based on the comparisons presented in this report:

- Any sUAS producing an RGB optical orthophoto with resolutions smaller than 5 mm/pix can detect and rate at least some distresses. Resolutions smaller than 2 mm/pix produce the best data for identifying and rating the largest number of distresses.
- Any sUAS producing a DEM and thermal orthophoto with resolutions smaller than 20 mm/pix and 30 mm/pix, respectively, are likely to be useful for distress detection and rating for at least some distress types, as listed above.
- Resolutions for a combination of 1.5-mm/pix or smaller RGB optical orthophoto and 6.0-mm/pix or smaller DEM are highly recommended in terms of data collection and processing time with visual details to detect and rate the largest number of distresses.

Table 20. Distresses and Resolutions for PCC

Distress Name (PAVER™ Distress Number)	Severity	Distress Detected and Severity Rating (mm/pix)		Airport(s) with Distress
		Orthophoto	DEM	
Blowup (61)				Data not available
Corner breaks (62)	L	2.5	ND	ONZ, BNW, PRO, MTO, WWD
	M, H	21	ND	
LTD cracks (63)	L	7.3	ND	ONZ, BNW, PRO, MTO, WWD
	M	21	ND	
	H*	21		
Durability cracking (64)	L	7.3	ND	ONZ
	M	21	10	
	H	21	29.1	
Joint seal damage (65)	L	ND	ND	BNW, PRO, MTO, WWD
	M	2.5	ND	BNW, PRO, WWD
	H	7.3	6	ONZ, BNW, PRO
Small patching (66)	L	3.3	ND	BNW, PRO, WWD
	M	4.5	6	BNW, PRO, WWD
	H*	4.5	6	PRO
Large patching (67)	L	21	ND	ONZ, BNW, PRO, WWD
	M, H	21	29	ONZ, WWD
Pop-outs (68)	N/A	3.3	6	BNW
Pumping (69)	N/A			Data not available
Scaling (70)	L			Data not available
	M, H*	21	10	ONZ
Settlement or faulting (71)	L	ND	ND	ONZ, PRO, WWD
	M, H*	ND	3	ONZ, PRO, WWD
Shattered slab (72)	L	ND	ND	
	M, H	21	10	ONZ, PRO
Shrinkage cracks (73)	N/A**	2.5	ND	MTO, WWD
Joints spalling (74)	L**	2.5	ND	MTO, BNW, PRO, WWD
	M**, H	2.5	6	
Corner spalling (75)	L**, M**	3.3	ND	MTO, BNW, PRO, WWD
	H	3.3	10	PRO
Alkali-Silica Reaction (76)	L**	7.3	ND	ONZ, BNW, PRO, WWD
	M**, H	7.3	6	ONZ, BNW, PRO, WWD

L = Low, M = Medium, H = High
N/A = Not applicable
ND = Not detected
*Based on the detection of lower severity
**Detection not always possible or misidentified as other distresses

Table 21. Distresses and Resolutions for AC

Distress Name (PAVER™ Distress Number)	Severity	Distress Detected and Severity Rating (mm/pix)		Distresses Available
		Orthophoto	DEM	
Alligator cracking (41)	L	3.5	5.9	WWD
	M, H			Data not available
Block cracking (43)	L	7.3	9.2	MTO, WWD
	M, H	7.3	19.6	
Corrugation (44)	N/A			Data not available
Depression (45)	L	ND	ND	WWD
	M	ND	6	TTF, WWD
	H	4.1	16	WWD
Jet blast erosion (46)	N/A			Data not available
Joint reflection cracking (47)	N/A			Data not available
L&T cracking (48)	L	7.3	9.2	TTF, MTO, WWD
	M, H	7.3	19.6	
Oil spillage (49)				Data not available
Patching (50)	L, M, H	4.1	16.2	WWD
Polish aggregate (51)				Data not available
Raveling (52)	L, M, H*	1.5	ND	TTF, WWD
Rutting (53)	N/A			Data not available
Shoving (54)	L	ND	5.9	WWD
	M	2.5	10	MTO, WWD
Slippage cracking (55)				Data not available
Swell (56)	L, M	ND	ND	TTF, WWD
	H			Data not available
Weathering (57)	L, M, H	ND	ND	TTF, MTO, WWD

L = Low, M = Medium, H = High
N/A = Not applicable
ND = Not detected
Data not available means that distress or a particular severity rating was not present.
*Based on the detection of lower severity

8.6 DIFFERENT CATEGORIES OF DISTRESSES

Based on the sUAS data visual analysis at all six airports, the distress detection and rating could be divided into three categories: detectable, detectable with previous PCI data, and undetectable (Table 22).

Table 22. Different Types of Distresses

Type	PCC Pavement Distresses	AC Pavement Distresses
Detectable	Corner breaks (LMH), LTD cracks (LMH), Durability cracking (LMH), Joint seal damage (MH), Small patching (LMH), Large patching (LMH), Pop-outs, Scaling (MH), Shattered slab (LMH), Shrinkage cracks, Joints spalling (MH), Corner spalling (MH), Alkali-silica reaction (MH)	Alligator cracking (LMH), L&T cracking (LMH), Block cracking (LMH), Patching (LMH), Raveling (H)
Detectable with previous PCI data	Faulting (LMH), Joints spalling (LM), Corner spalling (LM), Alkali-silica reaction (LM)	Raveling (MH), Depression (LMH), Shoving (LMH)
Undetectable	Joint seal damage (L), Alkali-silica reaction (L)	Swell (LM), Weathering (LMH)

L = Low, M = Medium, H = High

8.6.1 Detectable

Detectable distresses do not need any additional information apart from the sUAS data to be detected. Their location can be identified by visually observing the sUAS data, mainly RGB optical orthophotos. Alligator cracking (LMH), L&T cracking (LMH), block cracking (LMH), patching (LMH), and raveling (M) are detectable AC pavement distresses in this category. However, detecting raveling (M) is not always possible. Low-severity alligator cracking present at two airports was detected; thus, it is safe to assume that medium- and high-severity alligator cracking can also be detected. Corner breaks (LMH), LTD cracks (LMH), durability cracking (LMH), joint seal damage (MH), small patching (LMH), large patching (LMH), pop-outs, scaling (MH), shattered slab (LMH), shrinkage cracks, joints spalling (MH), corner spalling (MH), and ASR (MH) in PCC pavement are also in this category. Detection of shrinkage cracks is not always possible with the tested technologies; they can often be submillimeter in size. New digital cameras with 100-mp or greater resolution that are becoming available could help with detection and rating of very small distresses in the future. Joint spalling and corner spalling can also be identified as ASR or vice versa.

8.6.2 Detectable with Previous PCI Data

Some distresses require previous PCI data to be available to help identify and rate them accurately. The most common distresses in this category are those associated with vertical height differences. Depression and shoving of AC pavement and faulting of PCC pavement show pavement surface movement vertically. An area with shoving goes up, depression goes down, and faulting exhibits elevation difference between adjacent slabs. The research team found the DEM outputs for detecting these distresses of high value, including when visualized with the aid of a 35% transparent hillshade draped over the DEM in GIS software, such as ESRI ArcMap and ArcGIS

Pro. This should be possible with other GIS software, such as QGIS, as well, but these products were not tested in this study. It is not yet feasible to run a stack profile algorithm of ArcGIS Pro in every part of the sample units to identify the mentioned distresses using a DEM. Thus, the possible location of these distresses can be nominated citing a previous PCI inspection report. The presence of faulting can be confirmed by running a stack profile algorithm in those nominated locations. There are often visual similarities in low- and medium-severity joint spalling, corner spalling, and ASR. In some cases, it is hard to distinguish them by physically looking at the pavement, and additional laboratory testing is required for accurate identification. Previous PCI inspection results can assist in accurately identifying these distresses. Low- and medium-severity raveling detection is challenging as it does not produce easily viewable differences in even the highest resolution orthophotos and DEMs the research team has produced so far. Historical PCI inspection data can assist in confirming the locations as well.

8.6.3 Undetectable in this Study

The distresses in this category were seldom identified consistently or could not be identified using even the highest-resolution sUAS data created in this study. Low-severity joint seal damage cannot be identified by viewing it in the field or on an sUAS image. According to the *Concrete Surfaced Airfields Paver™ Distress Identification Manual* (U.S. Army Corps of Engineers-Construction Engineering Research Laboratory, 2009), the presence of low-severity joint seal damage can be confirmed by inserting a knife blade between the sealer and joint face without resistance. Thus, these distresses are categorized as undetectable via sUAS. In some cases, low-severity ASR, swell, and all-severity weathering showed no detectable traits that could be used for these distress detections.

9. CONCLUSIONS

The research team successfully collected small unmanned aircraft systems (sUAS) data from a total of six airports in Michigan, Illinois, Iowa, and New Jersey. Different data types were processed and analyzed to assess their usefulness in airfield pavement distress detection and rating. Available airfield distresses previously recorded as being present at the test airports were assessed with visual interpretation in Geographic Information System (GIS) software with several different resolutions of red, green, and blue (RGB) optical orthophoto and Digital Elevation Model (DEM) data to identify their presence in the sUAS outputs. Potentially detectable distresses were also studied using thermal data.

The research team's analysis showed that visual and thermal data could be used to identify many airport Portland cement concrete (PCC) and asphalt concrete (AC) pavement distresses. Higher-resolution (more than 5 mm/pix) RGB orthophotos can be used to effectively identify many distresses, while lower-resolution data sets are useful for identifying a limited number of distresses. The DEM derived using RGB optical data were mainly useful in confirming the suspected location of the pavement distresses with elevation differences, such as faulting, shoving, depression, and medium- and high-severity crack-based distresses. The 1.5-mm/pix orthophotos and 6.0-mm/pix DEMs derived via photogrammetry from sUAS-collected images with a 45.7-megapixel (mp) resolution full-frame camera were the best outputs for identifying and rating the most distresses.

Thermal data were shown to be useful for identifying certain pavement distresses that exhibit a different thermal profile compared to intact concrete or asphalt pavement. High-accuracy (< 10 cm) positioning data for ground control points (GCPs) are valuable for accurately orienting orthophotos, creating high-quality DEM outputs, and for accurately aligning output products and traditional Pavement Condition Index (PCI) survey data for distress evaluation. This also allows for the layering/stacking of various data sets and makes it easier to compare data sets between years and different data collectors. Thermal data also make it easier to track distress changes over time.

This research also established guidelines for sUAS operations for pavement inspection, such as deployment of smaller sUAS for fast RGB data collection, deployment of a larger platform for very high-resolution data collection, the data collection team consisting of a minimum of three people, and the use of GCPs to ensure high-quality orthophoto. In addition, this research study found that sUAS data are sufficient to detect and rate several AC and PCC airfield pavement distresses. However, the current technology does not yet fully offer the capability to detect and rate some low-severity distresses (alkali-silica reaction, corner spalling, joint spalling, joint seal damage, depression, raveling, swell, and weathering). In the future, more sUAS platforms and sensors can be evaluated and tools for automated pavement inspection can be developed using sUAS data.

10. REFERENCES

Airsight. (2020a). *Airfield pavement inspections using drones, Hamburg Finkenwerder aerodrome*. https://www.airsight.de/projects/item/airfield-pavement-inspections-using-drones/

Airsight, (2020b). *Runway pavement inspections using airsight drone, Paris Charles De Gaulle Airport*. https://www.airsight.de/projects/item/runway-pavement-inspections-using-airsight-drone/

ASTM International, (2020). *Standard test method for airport pavement condition index surveys* (ASTM D5340-20). https://doi.org/10.1520/D5340-20

Brooks, C., Dobson, R., Banach, D., Oommen, T., Zhang, K., Mukherjee, A., Havens, T. C., Ahlborn, T., Escobar-Wolf, R., Bhat, C. G., Zhao, S., Lyu, Q., & Marion, N. (2018). *Implementation of unmanned aerial vehicles (UAVs) for assessment of transportation infrastructure—Phase II* (SPR-1674). Michigan Department of Transportation. https://rosap.ntl.bts.gov/view/dot/36994

Brooks, C., Dobson, R. J., Banach, D. M., Dean, D., Oommen, T., Wolf, R. E., Havens, T. C., Ahlborn, T. M., & Hart, B. (2015). Evaluating the use of unmanned aerial vehicles for transportation purposes: [parts A-D]. *Michigan Connected and Automated Vehicle Working Group*. https://rosap.ntl.bts.gov/view/dot/28859.

Escobar-Wolf, R., Oommen, T., Brooks, C. N., Dobson, R. J., & Ahlborn, T. M. (2018). Unmanned aerial vehicle (UAV)-based assessment of concrete bridge deck delamination using thermal and visible camera sensors: A preliminary analysis. *Research in Nondestructive Evaluation, 29*(4), 183–198. https://doi.org/10.1080/09349847.2017.1304597

ESRI. (2021a). *Hillshade function*. ArcGIS Pro. https://pro.arcgis.com/en/pro-app/2.7/help/analysis/raster-functions/hillshade-function.htm

ESRI. (2021b). *Stack profile (3D analyst)*. ArcGIS Pro. https://pro.arcgis.com/en/pro-app/latest/tool-reference/3d-analyst/stack-profile.htm

Federal Aviation Administration (FAA). (2014). *Guidelines and procedures for maintenance of airport pavements* (Advisory Circular (AC) 150/5380-6C). https://www.faa.gov/documentLibrary/media/Advisory_Circular/150-5380-6C.pdf

FAA. (2016). Airspace classification, operating requirements, and flight restrictions. In *Remote Pilot—Small Unmanned Aircraft Systems Study Guide* (FAA-G-8082-22). FAA Flight Standards Service, Washington, DC, United States. pp. 5–13. https://www.faa.gov/regulations_policies/handbooks_manuals/aviation/media/remote_pilot_study_guide.pdf

FAA. (2021). FAA PAVEAIR [Database]. https://faapaveair.faa.gov/

FLIR. (2020). FLIR Vue Pro Thermal Camera for Drones | FLIR Systems. https://www.flir.com/products/vue-pro/ (accessed 11.13.20).

GSMArena. (2019). Quad Bayer Sensors: What they are and what they are not. https://www.gsmarena.com/quad_bayer_sensors_explained-news-37459.php

Inzerillo, L., Di Mino, G., & Roberts, R. (2018). Image-based 3D reconstruction using traditional and UAV datasets for analysis of road pavement distress. *Automation in Construction*, *96*, 457–469. https://doi.org/10.1016/j.autcon.2018.10.010

Peshkin, D., Dzwilewski, P.-P. F., Potvin, K., Gauthier, K., Wade, M., Risner, E., Robinson, R., Snyder, C., Cardwell, M., & Feighan, K. (2019.) *Guidelines for collecting, applying, and maintaining pavement condition data at airport* (ACRP Research Report 203). Airport Cooperative Research Program, The National Academies Press. https://doi.org/10.17226/25566

Romero-Chambi, E., Villarroel-Quezada, S., Atencio, E., & La Rivera, F. M. (2020). Analysis of optimal flight parameters of unmanned aerial vehicles (UAVs) for detecting potholes in pavements. *Applied Science, 10*(12), 4157. https://doi.org/10.3390/APP10124157

Sourav, M. A. A., Ceylan, H., Brooks, C., Peshkin, D., Kim, S., Dobson, R., Cook, C., & Brouillette, O. (2022). *Small unmanned aircraft system for pavement inspection: Task 4—Execute the field demonstration plan and analyze the collected data* (DOT/FAA/TC-22/35). https://doi.org/10.21949/1524511

Sourav, M. A. A., Ceylan, H., Kim, S., Brooks, C., Peshkin, D., Dobson, R., Brynick, M., & DiPilato, M. (2022, May 31–June 3). Small uncrewed aircraft systems-based orthophoto and digital elevation model creation and accuracy evaluation for airfield portland cement concrete pavement distress detection and rating. In H. Wei (Ed.), *International Conference on Transportation and Development 2022: Other modes—Rail, Transit, and Aviation*, Seattle, WA, United States, 168–180. https://doi.org/10.1061/9780784484371.016

Sourav, M. A. A., Mahedi, M., Ceylan, H., Kim, S., Brooks, C., Peshkin, D., Dobson, R., & Brynick, M. (2022). Evaluation of small uncrewed aircraft systems data in airfield pavement crack detection and rating. *Transportation Research Record: Journal of the Transportation Research Board*, *2677*(1), 653–668. https://doi.org/10.1177/03611981221101030

Tan, Y., & Li, Y., (2019). UAV photogrammetry-based 3D road distress detection. *International Journal of Geo-Information, 8*(9), 409. https://doi.org/10.3390/ijgi8090409

U.S. Army Corps of Engineers-Construction Engineering Research Laboratory. (2009). *Concrete surfaced airfields—Paver™ distress identification manual*. https://www.faa.gov/documentLibrary/media/Advisory_Circular/Concrete-Surfaced-Airfields-Distress-Manual.pdf

Vidyadharan, A., Carter, T., Ceylan, H., Bloebaum, C., Gopalakrishnan, K., & Kim, S. (2017, August 27–30). Civil infrastructure health monitoring and management using unmanned aerial systems [Paper]. *International Conference on Highway Pavements and Airfield Technology 2017*, Philadelphia, PA, United States. https://doi.org/10.1061/9780784480946.019

APPENDIX A—LITERATURE REVIEW

A.1 INTRODUCTION

The U.S. Federal Aviation Administration (FAA) airport pavement design procedure is based on a minimum of 20 years of design life, considering regular maintenance and repair works. Over time, pavements deteriorate due to climatic/environmental factors, traffic loading, differential subgrade movements, and maintenance practices. In order to reach 20 years of life or more, airport pavements require routine maintenance, upgrading, and rehabilitation. The most effective way to preserve airport pavement is to establish and implement a maintenance program, and Airport Improvement Program (AIP) grants require many airports to develop and sustain an effective maintenance program. The FAA also encourages airports not requiring a maintenance program to establish one to preserve their airport pavement areas. A maintenance program allows systematic and engineered approaches to protecting the airport pavements along with the performance assessment, modeling, performance prediction, budgeting, and cost analyses of alternative rehabilitation options. However, airport pavement maintenance programs need to be updated regularly through pavement inspections.

According to the FAA, the early detection and repair of distresses are essential aspects of preserving airport pavements. If pavements are not routinely maintained during the early stages of deterioration, severe distresses requiring costly and extensive repair works will develop. This is especially important because approximately 70% of AIP grants allocated each year are invested in airfield pavements. While pavement distresses caused by environmental conditions cannot be prevented, early and routine maintenance work can minimize the deterioration. Only a strong and frequent pavement inspection program can reveal the distresses early, allowing enough time to undertake the corrective measures. Thus, the failure of airfield pavements can be linked to inadequate maintenance characterized by the absence of a robust inspection program that is linked to an asset management program. The airport authorities should adopt effective and timely pavement inspection techniques to ensure the structural integrity, riding quality, and safety of the airport users.

The current practice for airport pavement inspections relies on visual surveys and manual interpretation of reports and sketches prepared by inspectors in the field to quantify pavement conditions using the Pavement Condition Index (PCI) method as outlined in ASTM International D5340-12 (2018) *Standard Test Method for Airport Pavement Condition Index Surveys*. The procedure is time-consuming and costly, thus the assessment of a pavement branch (i.e., apron, taxiway, and runway) is completed by selecting and inspecting the sample units within a pavement section. The overall PCI of a pavement section is based on the inspection results of selected sample units rather than a complete inspection of 100% of the pavement.

Recently, the use of small unmanned aircraft systems (sUAS) has attracted attention as an option for performing cost-effective and efficient pavement inspections, among many other applications (Vidyadharan et al., 2017). The FAA Airport Technology Research and Development Branch (ATR) is currently researching how to enable safe, reliable, and effective integration of sUAS-mounted sensor technologies into an airport environment. In recent years, several attempts have been made both by the industry and airport operators to use sUAS for conducting various types of pavement imaging and inspection of airports. These activities have included proof-of-concept

demonstrations involving various types of sUAS platforms, sensors, and procedures under previous and newer sUAS regulations. Peshkin et al. (2019) noted that sUAS could survey a runway faster than on-the-ground crews, helpful for meeting more frequent inspection needs, providing imagery with 0.1-in. (2.5-mm) resolution, mapping cracks, identifying patches needing maintenance, and evaluating entire runways rather than just sample areas. As such, the FAA ATR plans to develop procedures and technical specifications for sUAS platform(s) and sensor(s) that could be used to supplement the traditional airport Pavement Management Program (PMP) inspections.

The primary objectives of this research project are to develop recommended processes and procedures for using sUAS to complement current methods of airport PMP inspection methods, and technical evaluations for various types of sUAS and sUAS-mounted sensor technology(s) that will lead to recommended specifications enabling consistently safe, reliable, and effective sUAS-assisted airport PMP inspections. The processes and procedures developed will be standard, time-effective, and repeatable for collecting, analyzing, maintaining, and reporting airport pavement data collected by sUAS-mounted sensors. The recommended technical specifications will address performance and other required criteria for various types of sUAS platforms and mounted sensors utilized to supplement airport PMP inspections.

This is a comprehensive review of (1) FAA guidance on airport pavement inspections; (2) current and emerging sUAS technologies including platforms, sensor technologies, mapping, and analysis software; and (3) implementation and lessons learned from sUAS applications by airport authorities and surface transportation agencies (i.e., state highway agencies and local road agencies).

A.2 FAA GUIDANCE ON AIRPORT PAVEMENT INSPECTIONS

The FAA offers several Advisory Circulars to provide efficient airport operations, airworthiness regulations, training standards, operational standards, assessments of facilities, certifications, and maintenance and rehabilitation activities. The active FAA Advisory Circulars related to airport pavements are listed in Table A-1.

Managing airports involves good decision making about preserving, maintaining, rehabilitating, and reconstructing airfield pavements within budget and time constraints. An efficient airport pavement inspection technique could help the airports in timely and economic decision making. A condition assessment is essential for mapping airfield pavement performance to ensure both the safe and economic operation of the aircraft. The FAA Advisory Circulars related to airport pavement distress assessment are summarized in the following sections.

The U.S. Army Corps of Engineers developed the PCI to describe airport pavement conditions through visual surveys, which was further adopted by ASTM International as a standard method (ASTM D5340). The procedure has been verified and widely adopted by the U.S. Naval Facilities Engineering Command and the FAA. The PCI is a numerical indicator rating the pavement surface conditions. The PCI allows the assessment of a variety of airport pavements, including asphalt-surfaced pavements, concrete pavements, and porous friction courses based on the distresses observed on the pavement surface. The distresses are an indicator of structural integrity and

operational conditions. In general, the PCI provides a rational basis for determining the maintenance and repair needs of pavements. Regular monitoring of pavement PCI facilitates the determination of the rate of pavement deterioration, which could play a significant role in the early decision of rehabilitation requirements. In addition, the use of PCI provides feedback on pavement performance required for the validation and improvement of current pavement design methods and maintenance techniques. However, the structural capacity, smoothness, and skid resistance of the pavements cannot be evaluated through the PCI.

Table A-1. The Active FAA Advisory Circulars Related to Airport Pavements

Document Number	Advisory Circular
150/5380-6C	Guidelines and Procedures for Maintenance of Airport Pavements
150/5320-12C	Measurement, Construction, and Maintenance of Skid Resistant Airport Pavement Surfaces
150/5200-18C	Airport Safety Self-Inspection
150/5380-7B	Airport Pavement Management Program (PMP)
150/5100-13C	Development of State Aviation Standards for Airport Pavement Construction
150/5320-17A	Airfield Pavement Surface Evaluation and Rating Manuals
150/5370-17	Airside Use of Heated Pavement Systems
150/5320-6F	Airport Pavement Design and Evaluation
150/5370-11B	Use of Nondestructive Testing in the Evaluation of Airport Pavements
150/5380-9	Guidelines and Procedures for Measuring Airfield Pavement Roughness
150/5335-5C	Standardized Method of Reporting Airport Pavement Strength – PCN
150/5370-16	Rapid Construction of Rigid (Portland Cement Concrete) Airfield Pavements
150/5370-13A	Off-Peak Construction of Airport Pavements Using Hot-Mix Asphalt
150/5000-15B	Announcement of Availability of Airport-Related Research and Development Products
150/5340-1M	Standards for Airport Markings
150/5370-10H	Standard Specifications for Construction of Airports
150/5370-14B	Hot Mix Asphalt Paving Handbook
150/5390-2C	Heliport Design
150/5370-12B	Quality Management for Federally Funded Airport Construction Projects
150/5220-9A	Aircraft Arresting Systems

A.2.1 Summary of the Test Method

The pavement is divided into branches, and each branch is divided into sections. Each section is further divided into sample units. The pavement sample units are visually inspected for the type and severity of distresses. Once the pavement distresses are documented, the PCI is calculated for each of the sample units. As a PCI function, pavement condition descriptions, also known as pavement condition ratings, are provided, and followed. Figure A-1 shows examples of PCI rating scales. Based on the PCI rating scale, a numerical rating between 0 and 100 is given in the PCI system, with 0 being the worst possible condition and 100 being the best possible condition. Based on the PCI of the inspected sample units, an average PCI of the pavement section is determined.

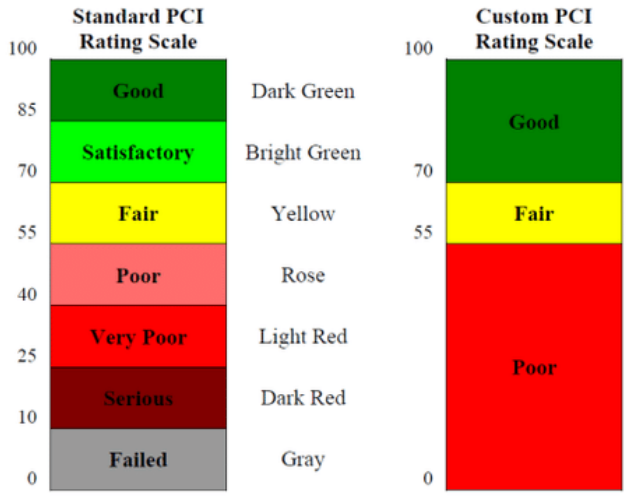

Figure A-1. Pavement Condition Index (PCI) Rating Scales (ASTM D5340)

The identification of sample units is a crucial aspect of the determination of PCI. The sample units are the recognized areas in pavement branches with different uses, such as the airport plan layout, aprons, taxiways, and runways. If the focused airfield pavement is asphalt concrete (AC) and/or porous friction surface, the sample units should cover 5,000 ft^2 ($\pm$2,000 ft^2) (465 m^2 [$\pm$185 m^2]) of contiguous pavement surface if the pavement area is not evenly divided by 5,000. For Portland Cement Concrete (PCC) airfield pavements, it is required to assess 20 ($\pm$8) continuous slabs when the total number of slabs in the pavement section is not divisible by 20. ASTM D5340 recommends subdividing the PCC slabs into 25-ft- (7.6-m-) long imaginary slabs when the joint spacing is greater than 25 ft (7.6 m). The joints of the imaginary slabs are assumed to be in perfect condition. It is also essential to accurately relocate the sample units for future verification of distress results and future inspection, and to track condition changes over time.

To obtain a statistically satisfactory estimate (95% confidence) of the PCI of a pavement section, the minimum number of sample units to survey is calculated as follows:

$$n = \frac{Ns^2}{\left(\left(\frac{e^2}{4}\right)(N-1) + s^2\right)}$$

Where:
n = minimum number of sample units by rounding to the next highest whole number.
N = total number of sample units in the section.
s = standard deviation of the PCI from one sample unit to another. When performing the initial inspection, the standard deviation is assumed to be 10 for AC pavements and 15 for PCC pavements.
e = acceptable error in estimating the section PCI. Commonly, e = $\pm$5 PCI points.
If it is critical to achieving a 95% confidence level, the adequacy of the number of sample units must be confirmed. In the previous equation, the number of sample units was estimated based on an assumed standard deviation. The actual standard deviation (s) can be calculated as follows:

$$s = \sqrt{\sum_{i=1}^{n} \frac{(PCI_i - PCI_f)^2}{(n-1)}}$$

Where:
PCI_i = PCI of surveyed sample unit i.
PCI_f = mean PCI of surveyed sample units.
n = the total number of sample units surveyed.

It is recommended to revise the minimum number of sample units based on the actual calculated standard deviation. If the revised number of sample units is higher than the sample units already surveyed, additional sample units will be surveyed. These sample units should be evenly distributed across the pavement section. The process is repeated to check, verify, and revise the required minimum number of sample units. Once the required number of sample units is decided, the spacing interval of the sample units is determined by systematic random sampling. The sample units are equally spaced throughout the section, with the first unit selected at random. The spacing interval of the sample units is calculated as follows:

$$i = \frac{N}{n}$$

Where:
i = spacing interval of sample units rounded to the next whole number.
N = total number of sample units in the section.
n = number of sample units to be inspected.

A.2.2 Inspection Procedure

ASTM D5340 provides guidelines for the inspection and identification of pavement distresses for PCI determination. It is recommended to inspect each sample unit individually, with survey details on the number and types of sample units, size of the sample units, branch and pavement section numbers, sketches, and orientations. The distress inspection is performed by walking over the sample units and measuring and documenting every distress severity level. Depending on the distress type, the severity may be reported either in the number of occurrences, linear feet, or square feet. The process is repeated for each of the sample units inspected. For PCC surfaces, the number of slabs in each sample unit is recorded along with a distress survey summary.

A.2.3 Pavement Condition Index Calculation for AC and Porous Friction Surfaces

ASTM D5340 lists 17 distresses associated with AC surfaces: alligator cracking, bleeding, block cracking, corrugation, depression, jet blast, joint reflection cracking, longitudinal/transverse cracking, oil spillage, patching, polished aggregate, weathering/raveling, rutting, shoving, slippage cracking, swelling, and weathering. Once the individual distress type and severity are quantified, the total severity and the percent density associated with the sample unit are calculated. The

distress densities of the sample units are implemented to calculate the deduct value (DV). An example of this relationship is shown in Figure A-2.

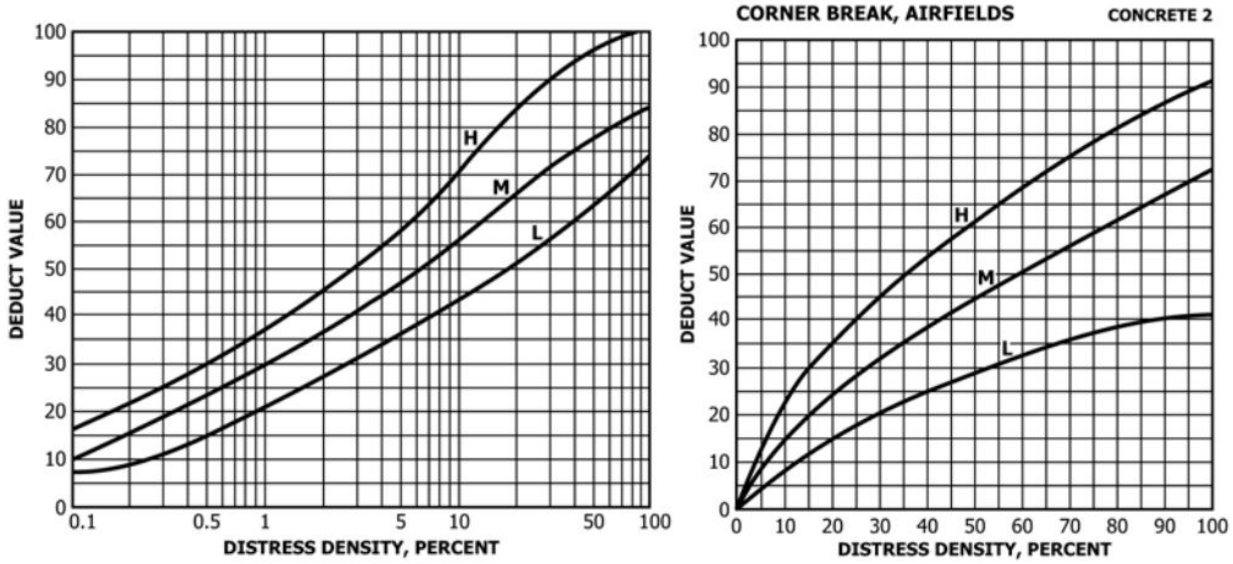

Figure A-2. Distress Density and Deduct Value Relationship: (a) Alligator Crack for AC Surfaces, and (b) Corner Break for PC Surfaces
(Note: H, M, and L represent high, medium, and low severity, respectively [ASTM D5340])

If more than one individual DV is greater than five, the maximum corrected deduct value (CDV) must be calculated. To determine the CDV, the allowable number of deducts (m) is calculated following the chart provided in Figure A-3. Next, the number of individual DVs is reduced to the m largest DVs, including the fractional part. If less than m DVs are available, all the DVs are used. The sum of TDV is calculated, and the number of individual DVs greater than 5 (q) is determined.

The CDV is calculated from the TDV and q values following the specific charts designated for AC surfaces. The correlation chart for calculating CDV from total DV and q values for AC surfaces is provided in Figure A-3. The q value denotes the number of entries with DV more than 5. Once the CDV is determined, the process is repeated by reducing the smallest individual DV greater than 5 to 5 until the q value becomes 1. For the calculation of PCI, the maximum CDV value is selected. Finally, the PCI is calculated by using the maximum CDV value as follows:

$$PCI = 100 - \max CDV$$

However, PCI correction is required if there is a distress with multiple severities, such as low, medium, and high severities. The distress percentages are added together for two severity cases, and the PCI is calculated based on the total distress percentage. The PCI calculated from the total distress percentages should be lower than the PCI calculated for individual percent distresses. If not, the PCI calculated from individual percent distresses is considered. If there are three severity cases, the PCI is calculated based on a set of percentage distress combinations (i.e., low and medium, medium and high, low and high, low, medium, and high), and the highest value PCI is reported.

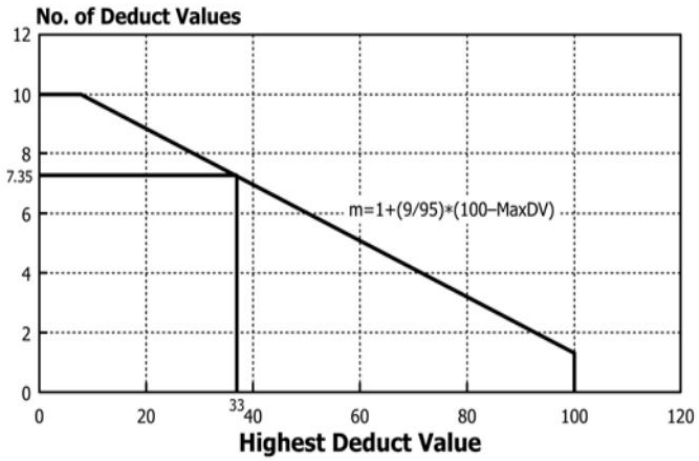

Figure A-3. Chart for Calculating the Maximum Allowable Number of Deducts (m) (ASTM D5340)

A.2.4 The PCI Calculation for PCC Surfaces

For PCC surfaces, the distresses of interest are blowup, corner break, linear cracking, durability cracking, joint seal damage, small patch, patching/utility cut, pop-outs, pumping, scaling, faulting, shattered slab, shrinkage cracking, joint spalling, corner spalling, and alkali-silica reaction (ASR). The total number of slabs with each unique combination of distress type and severity is determined. The density of each distress is calculated as the percentage of the total number of slabs with that specific variety of distress and severity. Using the derived distress density, the DV values are calculated following the same procedure applied for AC surfaces (Figure A-4) but using specific charts for PCC surfaces (Figure A-5).

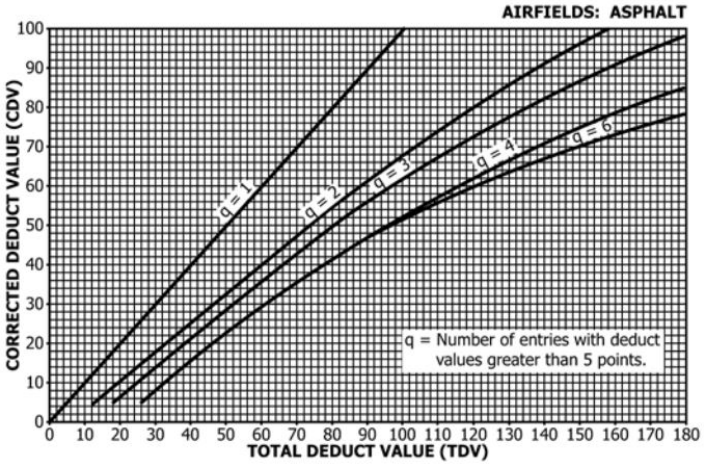

Figure A-4. Correlation Between TDV and CDV for AC Surfaces (ASTM D5340)

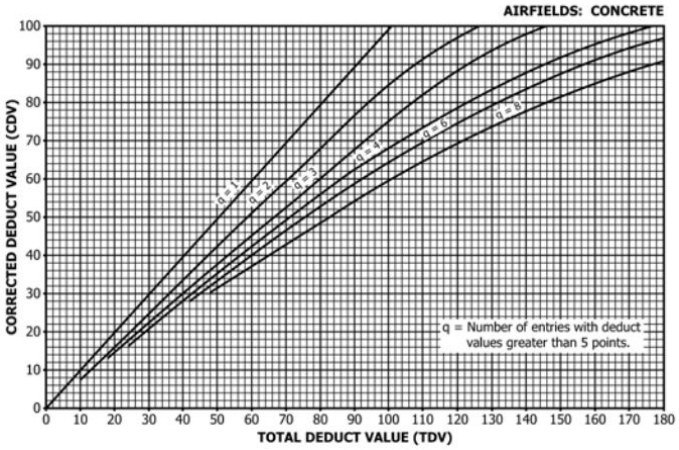

Figure A-5. Correlation Between TDV and CDV for PCC Surfaces (ASTM D5340)

Once the DV values are determined, the m value is calculated. The same procedure is also applied for the determination of total DV (TDV) and q value. The CDV is calculated from the TDV and q values following the specific charts designated for PCC surfaces. The correlation chart for calculating CDV from TDV and q values for AC surfaces is provided in Figure A-4. Once the CDV is calculated, the smallest DV greater than 5 is replaced by 5, and the whole procedure is repeated. It is required to repeat the iteration process until "q" becomes equal to unity. Next, the maximum CDV value calculated throughout the iteration procedure is determined and implemented for the PCI determination of the analyzed PCC pavement surface.

For the random selection of sample units, the PCI of the section is calculated as the area-weighted PCI of the surveyed sample units as follows:

$$PCI_r = \frac{\sum_{i=1}^{n} PCI_{ri} A_{ri}}{\sum_{i=1}^{n} A_{ri}}$$

Where:
PCI_r = area-weighted PCI of randomly surveyed sample units.
PCI_{ri} = PCI of random sample unit i.
A_{ri} = area of random sample unit i.
n = number of random sample units surveyed.

If there are any additional units, the PCI is also calculated for the additional units (PCI_a) separately following the technique as mentioned above. Once the PCI values for both the randomly selected and additional sample units are determined, the PCI of the pavement section is calculated as follows:

$$PCI_s = \frac{PCI_r(A - \sum_{i=1}^{m} A_{ai}) + PCI_a(A - \sum_{i=1}^{m} A_{ai})}{A}$$

Where:
PCI_a = area-weighted PCI of additional sample units.
A_{ai} = area of additional sample unit i.

A = area of the section.
m = number of additional sample units surveyed.
PCI_s = area-weighted PCI of the pavement section.
Finally, the condition rating of the section is determined using section PCI and the condition rating scale as provided in Figure A-1.

A.2.5 Reporting

The standard method ASTM D5340 recommends developing a summary report for each section. The summary lists section location, size, total number of sample units, sample units inspected, PCIs obtained, average PCI for the section, and section condition ratings.

A.2.6 Precision and Bias

Even though ASTM D5340 is widely implemented in pavement surface condition assessment, the standard method does not provide any precision estimate and/or bias from statistical design tests. This is because of the subjective nature of the process, dependent as it is on the experience of the inspector. However, the statement is subjected to change in the next 5 years, as indicated in ASTM D5340. Currently, the standard assumes that the inspector is able to identify the distresses accurately 95% of the time. Measurements are accurate if the remeasurements are within 10% of initial linear measurements and within 20% of area measurements.

A.3 CURRENT AND EMERGING SMALL UNMANNED AIRCRAFT SYSTEM (sUAS) TECHNOLOGIES

The use of sUAS could offer a safe, efficient, economical, and timely assessment of airport pavements, facilitating the sensible management of repair and rehabilitation projects. sUAS are commonly referred to as drones; however, the use of remotely piloted aircraft and UAV (Unmanned Aircraft Vehicles) is also widespread. Historically, sUAS were employed and operated primarily for military purposes, but today they are widely available for commercial and recreational purposes. In 2016, global sales of sUAS increased by 2.2 million, with revenue exceeding $4.5 billion (Glaser, 2017). Hundreds of manufacturers are producing sUAS. In the United States alone, 2.4 million sUAS were sold during 2016 (Current Landscape of Unmanned Aircraft Systems at Airports, 2019). As of July 2018, about a million recreational sUAS and 200,000 commercial sUAS were registered with the FAA (FAA, 2018). It is reasonable to project that the use of sUAS will increase considerably in the future, accompanied by technological advancements, and enhanced capabilities.

A.3.1. Components of Unmanned Aircraft Systems

sUAS platforms vary widely in size, weight, speed, range, endurance, and application (Armstrong, 2010). According to the FAA, any sUAS weighing between 0.55 lb to 55 lb (0.25 to 25 kg) is defined as an (sUAS). The sUAS platforms could be even smaller in the form of micro UAS. In general, sUAS platforms operate below 400 feet above ground level (AGL), at less than 100 mph, and do not extend Beyond Visual Line of Sight (BVLOS) to follow standard FAA commercial

sUAS operation rules known as Part 107 (FAA, 2020). All the sUAS have the following four main components:

- Unmanned Aircraft: The actual unmanned aircraft system commonly referred to as UA
- Pilot and Crew: Includes mission commanders, visual observers, pilot, and the sensors and payload operators
- Data Collection and Control: Includes any satellite, radio, Wi-Fi, and ground communication used in controlling UA and data recovery purposes
- Launch and Recovery: Includes launch and recovery equipment, flight terminals, and payloads

A.3.1.1 Unmanned Aircraft

A.3.1.1.1 Types of Unmanned Aircraft

sUAS platforms are commonly available in three types: (1) rotorcraft, (2) fixed-wing, and (3) tethered (Booz Allen Hamilton Inc., 2019), with some systems now combining aspects of these types. For rotorcraft, or rotary-wing, the lifting surfaces rotate; whereas, for fixed-wing types, the lifting surfaces are stationary. The fixed-wing sUAS platforms can generally fly with greater range and flight duration. However, the fixed-wing sUAS generally require advanced launch and recovery systems, such as a catapult, runway, and capture net. Conversely, the rotorcrafts require minimum launch and recovery requirements and can hover and detect objects from a fixed position. The tethered sUAS platforms use a permanent link, such as a wire or cable, for power supply and ground communication. Like rotorcraft, the tethered systems use aerostats/blimps, quadcopters, or other multirotors and can hover at a fixed position. Thus, tethered systems have the highest endurance, requiring minimum operation area. However, tethered sUAS platforms have altitude restrictions depending on the wire length.

According to Prather (2019), sUAS platforms commonly used by airports are sUAS operating below 400 feet AGL and at speeds slower than 100 mph. Mission demand, payloads, capacity, endurance, and flight time requirements are the major factors determining the selection of sUAS platforms. For maximum endurance, a fixed-wing sUAS with an internal combustion engine could be used. If the mission requires hovering over a restricted working area, a vertical takeoff and landing (VTOL) could be used; most of these systems are rotorcraft but some hybrid rotor and fixed-wing systems are available. Table A-2 provides the typical characteristics of sUAS platforms, as summarized by Prather (2019).

Table A-2. Typical Characteristics of sUAS. Adopted from Prather (2019)

Characteristics	sUAS	Fixed-Wing sUAS	VTOL sUAS	Electric sUAS	Internal Combustion sUAS
Cruise speed (knots)	28.5	34.9	21.8	25.3	42.2
Maximum speed (knots)	49.1	62.1	3.53	44	71
Endurance (hours)	2.2	3.6	0.9	1.1	7.4
Range (status mile)	112.9	175.7	44.9	42.3	408.5
Payload capacity, (lb/kg)	6.8/3.1	6.8/3.1	6.9/3.1	5.2/2.4	13.1/5.9

VTOL = Vertical takeoff and landing

A.3.1.1.2 Propulsion

Batteries power most of today's sUAS platforms. However, battery-powered sUAS platforms have limited endurance and operational durations. In general, battery-powered, fixed-wing sUAS have higher endurance than rotorcrafts. For greater endurance, sUAS are available with multiple power sources such as battery, fuel, and tether. sUAS with various power options are larger because fuel and combustion engines add to payloads. Moreover, these sUAS platforms require enhanced launch and recovery systems.

A.3.1.1.3 Payloads

According to Prather (2019), sUAS payloads are often divided into three categories: (a) still imagers, (b) full-motion video, and (c) other payloads. Still imagers could be commercial-off-the-shelf (COTS) digital cameras or specialized spectral imagers, both of which can take multiple images per second at a given point. Stable platforms such as rotorcrafts are most suited for still imagers (most still imagers can also take video). Metadata, including GPS x,y,z coordinates, and image information, such as time, date, and shutter speed, are also collected along with the images. When the still imager captures greater than 15 frames per second, it is considered a full-motion video (FMV). FMV is capable of capturing real-time motion and has been found useful in monitoring animal and people movements. However, FMV resolution is usually lower compared to that of still imagers. The sUAS could also be equipped with other payloads such as thermal cameras, radars, Light Detection and Ranging (LiDAR) sensors, multispectral/hyperspectral cameras, sampling devices, and ground penetrating radar (GPR). The requirements of payloads are more specific to the purpose of the mission intended for a particular task.

A.3.1.2 Pilot and Crew

The sUAS platforms are maneuvered and controlled in a predetermined route with remote pilots. The crew requirements are dependent on mission objective, sUAS type, launch and recovery methods, sensor requirements, and sensor operation criteria. Depending on installed sensors' complexities, sensor operator(s) could be required to operate, collect data, and manipulate the sUAS payloads efficiently. Part 107 commercial sUAS operation rules require a certified pilot and recommend at least one visual observer. Fixed-wing sUAS platforms often require additional personnel for the successful launching and recovery of the unit.

A.3.1.3 Data Link and Control Methods

In compliance with the flight mission, the data link and control methods of sUAS could be one of four types: (a) autonomous, (b) automated, (c) semi-automated, and (d) remotely piloted. While autonomous, automated, and semi-automated methods are used most often for military purposes, the remotely piloted control systems are more suited for sUAS platforms. In a remotely piloted control system, the operator directly controls the maneuvering and the flight path of the sUAS. A handheld console with joysticks, throttle, roll, aircraft pitch, and yaw are typically used to control the sUAS. Depending on the aircraft specification, additional controls could include gears, brakes, flaps, and so on. The most recent sUAS platform could have smartphone-enabled controls, allowing both semi-automated and remotely piloted operation of sUAS. Pre-selected autonomous missions can now also be accomplished through commercially available sUAS.

A.3.1.4 Launch and Recovery

The launch and recovery of sUAS could range from very simple to more complex. The launching of sUAS could be vertical lift, handheld launch, catapult launch, or vehicle launch. The recovery system includes a handheld, vertical landing, belly landing, or surface landing. The launch and recovery systems of an sUAS platform rely on platform type, manufacturer specification, and mission objectives. Rotorcraft generally have the simplest launch and recovery.

A.3.2 SENSORS FOR UNMANNED AIRCRAFT SYSTEM

The sUAS platforms can be equipped with several types of sensors simultaneously or one at a time, depending on the platform's specifications and mission requirements. An overview of the typical sensors used in sUAS platforms is summarized from Prather (2019) as follows:

A.3.2.1 Red Green Blue (RGB)/High-Resolution Video/Photography

RGB or "natural color" cameras are the most widely used sensors in sUAS platforms. These cameras can be used for photogrammetry, monitoring, and recording high-resolution images and videos. Proper lighting is required for RGB cameras, restricting their use to during daylight hours. In addition, the spectral bands of RGB cameras might not be adequate for complex analysis and precise detection, depending on the feature of interest. The sUAS platforms equipped with RGB cameras must be operated at lower altitudes when a higher resolution is desired with the same camera. Low flying altitude requires many images or videos to cover a targeted area, likely requiring multiple flights, longer flying time, long processing time, and enhanced data storage facilities. The primary outputs of RGB cameras are in the forms of images and videos. Many off-the-shelf software systems are available to recognize the RGB camera file types for use with close-range photogrammetric processing to create three-dimensional (3D) geospatial outputs. Thus, the RGB camera images could be used in measurement, planning, and comparative analysis. RGB cameras are most widely implemented in monitoring construction progress and pavement deterioration over time.

A.3.2.2 Thermal Camera

Thermal cameras are useful for measuring and identifying thermal variations in materials that might not be visible with RGB cameras, including indicators of sub-surface problems. For instance, delamination, loss of fines, and joint seal damage would have distinct thermal signatures compared to unaffected pavement areas. While RGB cameras are often unable to address these anomalies, temperature profile (typically lower temperature) obtained by thermal cameras could be useful in identifying these distresses. Because they use radiation emitted from the surface of the object, they can also be used at night. Thus, thermal cameras can offer extended hours of operation. Thermal cameras have various applications, including bridge and pavement monitoring for structural integrity, construction inspection, wildlife management, and land management. Thermal sensors provide heat-based images and videos of the targeted objects, which could be analyzed by implementing several off-the-shelf software applications.

A.3.2.3 Multispectral/Hyperspectral Camera

These cameras detect specific objects with a given color and shape using many visible and near-infrared light bands. Hyperspectral cameras produce data sets in a 3D hypercube format in which two dimensions present spatial coordinates (e.g., x, y), while the third dimension contains the spectral information. Depending on the camera specification, hyperspectral images can contain 100 to 200 spectral bands in each image pixel, while COTS multispectral cameras typically have 4 to 14 bands.

A.3.2.4 Light Detection and Ranging

LiDAR can provide high-resolution maps and has a broad application for collecting 3D point cloud data, geomatics, surveying, and so on. In general, LiDAR is employed when the elevation, height, or depth is the parameter of interest. Using laser light, LiDAR can collect 100 to 500 points per meter of resolution and can collect data at night since this is an active (not passive) sensor. Thus, the user can produce 3D models, surface modes, and orthomosaic images using the high-resolution data. LiDAR is one of the most expensive sensors available to use in sUAS platforms.

A.4 IMPLEMENTATION OF sUAS

In the past decade, the use of sUAS in highway, bridge, and airport pavement inspections has increased significantly. Several state highway agencies in the United States, including Michigan, Minnesota, Ohio, Utah, Indiana, Idaho, Oregon, Kentucky, and New Jersey, are actively evaluating and implementing use of sUAS platforms in managing their transportation infrastructure assets. Potential applications for sUAS technologies in state departments of transportation (DOTs) and local road agencies include real-time monitoring, data collection, and inspections (Brooks et al., 2015; FHWA, 2018a, 2018b). Various sensors enable sUAS platforms to provide images, accurate measurements, and condition data on highways, bridges, and local roads. The sUAS platforms can have immediate access to locations that are not easily accessible to ground crews. This can include performing a regular inspection practice of high mast poles or bridges or irregular surveillance required under emergency conditions. sUAS platforms can provide fast operation, accessibility, and a unique view of circumstances, providing useful information for timely decision making.

A.4.1 USE OF sUAS BY SURFACE TRANSPORTATION AGENCIES

A survey conducted by the University of Massachusetts Amherst indicated that 33 DOTs in the United States are planning or showing interest in employing sUAS in various applications (Ni & Plotnikov, 2016). The following sections summarize case examples of sUAS by state DOTs. Based on the case studies, the potential applications of sUAS platforms for highway agencies were identified and are summarized in Table A-3.

A.4.1.1 Ohio Department of Transportation: sUAS Platforms for Traffic Monitoring and Inspection

The Ohio Department of Transportation (ODOT) is using sUAS for construction monitoring, promotional videos, traffic monitoring, and truck counting (FHWA, 2018b). They use the Da-Jiang Innovations (DJI) Matrice 210 Real-time kinematic (RTK), equipped with a camera capable of 30× zoom. A machine-learning algorithm is used to identify the vehicle types and travel directions. Thus, the system allows the quantification of traffic traveled in each direction. If a tethered platform was used, a 9-hour continuous operation could be enabled (FHWA 2018b). Figure A-6 shows the use of sUAS platform in traffic monitoring and truck counting by ODOT.

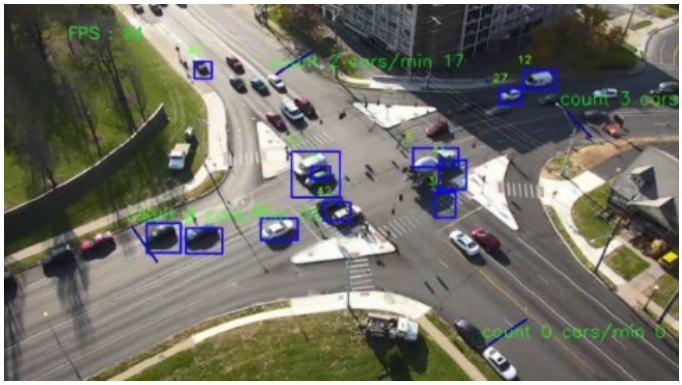

Figure A-6. Use of sUAS For Traffic Monitoring and Truck Counting by Ohio DOT (FHWA, 2018b)

A.4.1.2 New Jersey Department of Transportation: Use of sUAS for High-Mast Light Pole Inspections

The New Jersey Department of Transportation (NJDOT) started its sUAS program in 2016 and used it to inspect high-mast light poles (FHWA, 2018b). The plan was to examine 250 poles and, at the end of the program, 241 poles were inspected successfully (Figure A-7). NJDOT reported reduced lane closures and increased safety for both workers and the traveling public. NJDOT also reported a cost saving of 15% by using sUAS compared to conventional inspection methods. Using sUAS, it was possible to inspect six to seven poles per day, compared to traditional methodologies where only one or two poles were inspected per day.

Figure A-7. Image of sUAS for High-Mast Lighting Pole Inspection by NJDOT (FHWA, 2018b)

A4.1.3 North Carolina DOT: sUAS Platforms for Collision Reconstruction

The North Carolina Department of Transportation (NCDOT) is using sUAS platforms in vehicle collision reconstruction. North Carolina law requires photographing or scanning evidence after a collision (Figure A-8). Typically, total station and laser scanning are employed to gather the evidence, requiring lane closures and longer inspection times. NCDOT showed that the collision evidence collection is faster, accurate, and reliable when sUAS was coupled with advanced image processing tools. Employing sUAS allowed NCDOT to start clearing the scene within 25 minutes of a collision, whereas it would take more than 2 hours with conventional methods.

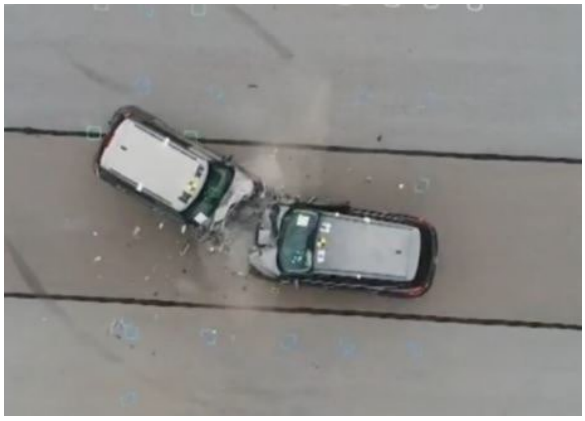

Figure A-8. Image of Vehicle Collision Acquired by NCDOT from sUAS Recorded Slow-Motion Video (FHWA, 2018b)

A.4.1.4 Utah DOT: Use of sUAS for Improving Construction Process

The Utah Department of Transportation (UDOT) used sUAS platforms to inspect and ensure the quality of construction projects. The sUAS point cloud was combined with LiDAR data to produce hybrid 3D models, allowing enhanced data collection at a lower cost (Figure A-9). Using sUAS, UDOT completed a project 25 days ahead of schedule, with about 2.6% cost savings.

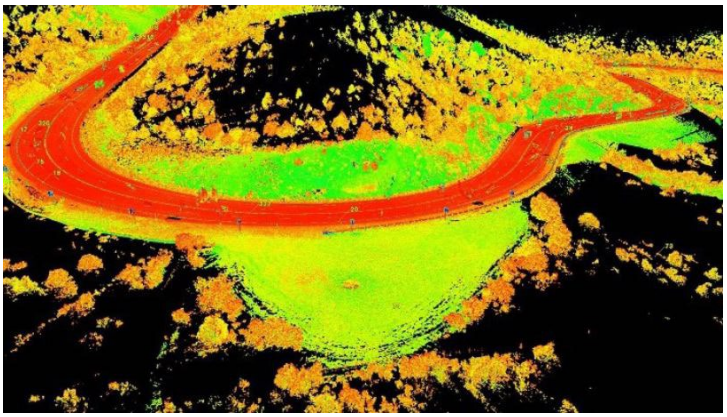

Figure A-9. Hybrid 3D Point Cloud Created by UDOT Using sUAS (FHWA, 2018b)

A.4.1.5 Minnesota DOT: Underbridge Inspection Using sUAS

Since 2015, the Minnesota Department of Transportation (MnDOT) has been using sUAS for bridge inspection (FHWA, 2018a). MnDOT's sUAS capabilities are object sensing; 360-degree camera; and photo, video, and thermal imaging. The sUAS system uses a confinement cage to protect the system, as shown in Figure A-10. MnDOT reported a 40% cost savings by using sUAS for the structural inspection of bridges compared to conventional inspection methods. The report also indicates that close attention should be given to coordinate with the FAA and Aeronautics Office by providing the intended purpose and documentation for sUAS applications. The report also notes that inspection by sUAS does not need to entirely replace current inspection practices, and that further studies are required for future advancement.

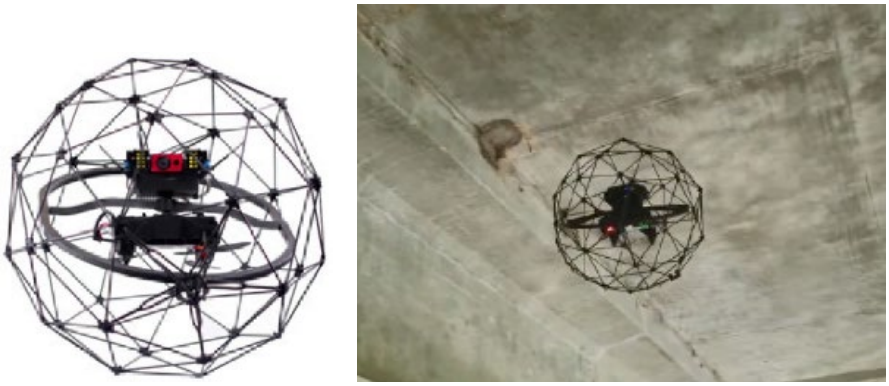

Figure A-10. Images of sUAS With Confinement Tested by MnDOT (FHWA, 2018a)

A.4.1.6 Michigan DOT: Use of sUAS for Construction Monitoring and Structural Inspection

The Michigan Department of Transportation (MDOT) has used sUAS equipped with thermal cameras and LiDAR sensors (Brooks et al., 2018, 2015). The thermal camera images were used for structural inspection of bridges and to identify potential deterioration such as the locations and sizes of subsurface delaminations in concrete bridge decks (Figure A-11, right side). LiDAR data were used to generate 3D cloud data for modeling facilities and construction sites. sUAS video

data were used for creating quantitative traffic data. Photogrammetric data were used to automatically detect spalls (potholes) in bridge decks.

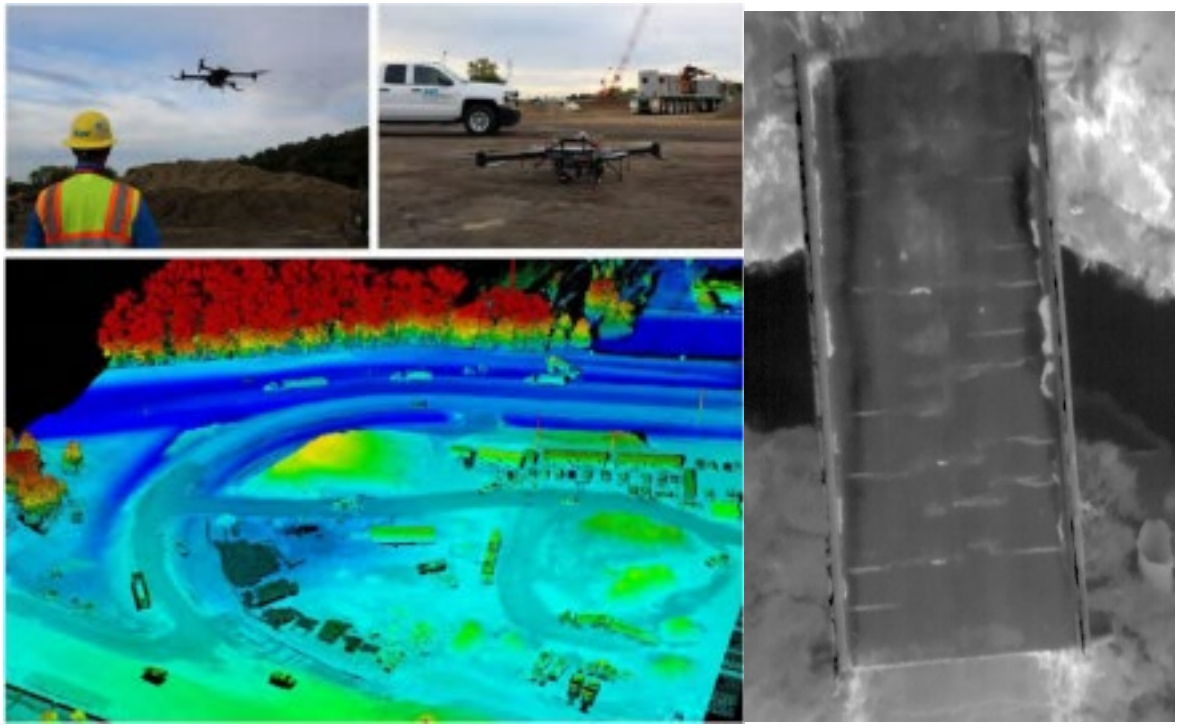

Figure A-11. Images of sUAS with LiDAR to Provide a 3D Model of the Construction Site and Thermal Imaging System for Bridge Condition Inspection (Brooks et al., 2018)

A.4.1.7 South Dakota DOT: The Use of sUAS in Unpaved Roads

In association with the South Dakota Department of Transportation (SDDOT), South Dakota State University investigated the use of sUAS with a photogrammetric mapping center to evaluate the surface condition of unpaved roads (Zhang, 2008). The mission was operated with an automated flight control system following a pre-programmed flight path. The sUAS platform was equipped with GPS, geomagnetic sensors, a UEye 2220C video camera, and an OptiLogic RS-232 laser range finder. The collected images were analyzed to produce orthoimage and digital 3D models, which provided standard guidelines for unpaved pavement condition assessment using sUAS platforms. Team member, Dr. Colin Brooks, built on this initial work to create a commercially ready Automated Unpaved Road Assessment (AURA) system (Dobson et al., 2014; MTRI, 2020).

Table A-3. Potential Applications of sUAS for Highways and Local Roads
(Adopted from Banks et al. (2018) and Booz Allen Hamilton (2019))

sUAS Use	Purpose	Outcomes/Improvements
Construction Management	The use of sUAS for construction monitoring for planning and safety purposes can include surveying, documenting progress, project-scoping, calculating the required material for the construction, work zone traffic monitoring, and positioning workers.	Worker safety can be improved, and communication between various crews involved in construction can be facilitated. More accurate estimations of required materials and faster communication can save money and time during construction.
Damage Assessment	Use of sUAS to assess the damage due to natural events such as storms, floods, hurricanes, avalanches, and earthquakes.	After a natural event, DOTs can use sUAS platforms to get to locations that crews cannot easily access.
Emergency Response	Use of sUAS to supplement on-site emergency personnel, augment existing capabilities, or provide new capabilities such as mobile lighting, surveillance, or appropriate resource allocation. Thermal sensors could also provide surveillance at night.	As a new solution in responding to emergencies, sUAS platforms can offer mobile and indefinite lighting sources to improve crew visibility and illumination at night. Crews can quickly mobilize sUAS surveillance platforms to understand the scope of the emergency and allocate appropriate resources.
Facility Inspection	Inspection of the storage facilities, buildings, entrances, and other on-site infrastructure. Gather an understanding of facility assets to assess and prioritize needs.	Depending on the facility inspected, sUAS-collected data can improve the understanding of the current conditions. For example, 3D models of facilities can be recorded and used as a reference for making modifications, or thermal imaging can be used to improve energy efficiency in buildings.
Pavement Inspection	Inspection of roads, highways, and rest areas to meet any DOT-mandated condition levels.	Data collected can be referenced and analyzed to understand pavement condition and support infrastructure decision making.
Perimeter Monitoring	Use of sUAS to monitor and scan the perimeter of a DOT property. Constant surveillance and sweeps or hotspot monitoring can be accomplished depending on the DOT need.	Improved surveillance of DOT property through thermal or visual live-feed or recorded video. This can improve upon fixed HD cameras by adding the flexibility to maneuver and capture blind spots.

Table A-3. Potential Applications of sUAS for Highways and Local Roads (Continued)
(Adopted from Banks et al., (2018) and Booz Allen Hamilton, (2019))

sUAS Use	Purpose	Outcomes/Improvements
Bridge Inspection	Deployment of sUAS to provide quantitative data on distresses such as spalls and delamination. Creating as-built 3D models of bridges and providing visual documentation of hard-to-access locations.	Location-specific bridge defect information can help bridge asset management and improve the safety of bridge inspection processes.
Traffic Control	Use of sUAS to monitor traffic during regular hours, maintenance operations, and after a collision.	DOTs can collect real-time information that helps with decision making for traffic control, designing detours, and gathering evidence.

A.4.2 Use of sUAS by Airport Authorities

A.4.2.1 Pavement Inspection

Airport pavement assessment is an essential component of the airport PMP to ensure serviceability; life-cycle cost minimization; and longevity of airport areas, including runways, taxiways, hangars, and aprons. Conventional airport pavement inspection methods can require closing the pavement section completely while inspecting. An inspector walks over the pavements to visually identify and note the distresses following the procedure designated in ASTM D5340. However, Peshkin et al. (2019) indicated that several asphalt and concrete pavement distresses could be identified by implementing sUAS platforms, advanced sensors, and computer vision. Among the 17 asphalt pavement distresses, 7 distresses (i.e., alligator cracking, bleeding, block cracking, joint reflection cracking, longitudinal and transverse cracking, patching, and slippage cracking) with the corresponding severity levels (i.e., low, medium, and high) are identifiable from sUAS imaging. Asphalt pavement distresses, including shoving and swelling with medium and high severity, are also distinguishable from sUAS image analysis. However, the detection of other asphalt distresses such as corrugation, depression, jet blast erosion, oil spillage, rutting, and weathering are challenging from sUAS imaging.

In concrete pavements, longitudinal, transverse, and diagonal cracks; blowups; corner breaks; joint seal damage; patching; pop-outs; pumping; shatter slabs; and spalling with low, medium, and high severities are recognizable by sUAS-enabled inspection (Peshkin et al., 2019). Concrete distresses, including scaling, settlement, and ASR with high severity, are identifiable from sUAS imaging. However, it has been reported that the sUAS imaging might not be useful in identifying durability and shrinkage cracking associated with the concrete pavements. Peshkin et al. (2019) also compared identifiable pavement distresses between the inspection methods, including conventional surveys, laser imaging, LiDAR, and sUAS. The comparisons showed that sUAS imaging has advantages over laser imaging and terrestrial LiDAR in detecting asphalt pavement bleeding, patching, and swelling. For concrete pavements, sUAS was useful in identifying longitudinal, transverse, and diagonal cracks and patching. For convenience, Tables A-4 and A-5

provide comparisons between different inspection methods. According to Hubbard et al. (2017), an airport runway inspection could be completed in 30 minutes using sUAS platforms, while the conventional inspection methods require 6 to 8 hours.

Table A-4. Inspection Capabilities of Different Methods in Identifying Concrete Pavement Distress (Adopted from Peshkin et al. (2019))

Distress	Manual	Laser Imaging	LiDAR	UAS Imaging
Blowup	☒ Low Severity ☒ Medium Severity ☒ High Severity	☒ Low Severity ☒ Medium Severity ☒ High Severity	☒ Low Severity ☒ Medium Severity ☒ High Severity	☒ Low Severity ☒ Medium Severity ☒ High Severity
Corner breaks	☒ Low Severity ☒ Medium Severity ☒ High Severity	☒ Low Severity ☒ Medium Severity ☒ High Severity	☒ Low Severity[1] ☒ Medium Severity ☒ High Severity	☒ Low Severity[1] ☒ Medium Severity[1] ☒ High Severity
Longitudinal, transverse, and diagonal cracks	☒ Low Severity ☒ Medium Severity ☒ High Severity	☒ Low Severity ☒ Medium Severity ☒ High Severity	☒ Low Severity[1] ☒ Medium Severity ☐ High Severity	☒ Low Severity[1] ☒ Medium Severity[1] ☒ High Severity
Durability cracking	☒ Low Severity ☒ Medium Severity ☒ High Severity	☐ Low Severity ☒ Medium Severity ☒ High Severity	☐ Low Severity ☐ Medium Severity ☒ High Severity	☐ Low Severity ☐ Medium Severity ☐ High Severity
Joint seal damage	☒ Low Severity ☒ Medium Severity ☒ High Severity	☒ Low Severity[2] ☒ Medium Severity[2] ☒ High Severity[2]	☒ Low Severity[2] ☒ Medium Severity[2] ☒ High Severity[2]	☒ Low Severity[2] ☒ Medium Severity[2] ☒ High Severity[2]
Patching	☒ Low Severity ☒ Medium Severity ☒ High Severity	☒ Low Severity ☒ Medium Severity ☒ High Severity	☐ Low Severity ☐ Medium Severity ☒ High Severity	☒ Low Severity[3] ☒ Medium Severity[3] ☒ High Severity
Pop-outs	☒ Severity N/A	☒ Severity N/A	☒ Severity N/A	☒ Severity N/A
Pumping	☒ Severity N/A	☒ Severity N/A[4]	☒ Severity N/A[4]	☒ Severity N/A[4]
Scaling	☒ Low Severity ☒ Medium Severity ☒ High Severity	☐ Low Severity ☒ Medium Severity ☒ High Severity	☐ Low Severity ☐ Medium Severity ☒ High Severity	☐ Low Severity ☐ Medium Severity ☒ High Severity
Settlement	☒ Low Severity ☒ Medium Severity ☒ High Severity	☒ Low Severity ☒ Medium Severity ☒ High Severity	☐ Low Severity ☐ Medium Severity ☒ High Severity	☐ Low Severity ☐ Medium Severity ☒ High Severity
Shattered slab	☒ Low Severity ☒ Medium Severity ☒ High Severity	☒ Low Severity ☒ Medium Severity ☒ High Severity	☒ Low Severity ☒ Medium Severity ☒ High Severity	☒ Low Severity[1] ☒ Medium Severity[1] ☒ High Severity
Shrinkage cracking	☒ Severity N/A	☒ Severity N/A[5]	☐ Severity N/A	☐ Severity N/A
Spalling	☒ Low Severity ☒ Medium Severity ☒ High Severity	☒ Low Severity ☒ Medium Severity ☒ High Severity	☒ Low Severity[1] ☒ Medium Severity ☒ High Severity	☒ Low Severity[1] ☒ Medium Severity[1] ☒ High Severity
Alkali-silica reactivity (ASR)	☒ Low Severity ☒ Medium Severity ☒ High Severity	☐ Low Severity ☒ Medium Severity ☒ High Severity	☐ Low Severity ☐ Medium Severity ☒ High Severity	☐ Low Severity ☐ Medium Severity ☒ High Severity

[1]Data collection method applicable if cracks have been sealed.
[2]Data collection method applicable if damage is from extrusion, vegetation growth, or sliver spalls.
[3]Data collection method applicable depending where there are color differences between patch material and original concrete.
[4]Data collection method may be applicable depending on extent of pumping.
[5]Data collection method may be applicable depending on characteristic of shrinkage cracking.

Table A-5. Inspection Capabilities of Different Methods in Identifying Asphalt Pavement Distress (Adopted from Peshkin et al. (2019))

Distress	Manual	Laser Imaging	LiDAR	UAS Imaging
Alligator cracking	☒ Low Severity ☒ Medium Severity ☒ High Severity	☒ Low Severity[1] ☒ Medium Severity ☒ High Severity	☒ Low Severity[2] ☒ Medium Severity ☒ High Severity	☒ Low Severity[2] ☒ Medium Severity ☒ High Severity
Bleeding	☒ Severity N/A	☒ Severity N/A[3]	☐ Severity N/A	☒ Severity N/A[3]
Block cracking	☒ Low Severity ☒ Medium Severity ☒ High Severity	☒ Low Severity[4] ☒ Medium Severity[4] ☒ High Severity[4]	☒ Low Severity[2] ☒ Medium Severity ☒ High Severity	☒ Low Severity[2] ☒ Medium Severity ☒ High Severity
Corrugation	☒ Low Severity ☒ Medium Severity ☒ High Severity	☐ Low Severity ☐ Medium Severity ☐ High Severity	☒ Low Severity ☒ Medium Severity ☒ High Severity	☐ Low Severity ☐ Medium Severity ☐ High Severity
Depression	☒ Low Severity ☒ Medium Severity ☒ High Severity	☐ Low Severity ☐ Medium Severity ☐ High Severity	☒ Low Severity ☒ Medium Severity ☒ High Severity	☐ Low Severity ☐ Medium Severity ☐ High Severity
Jet blast erosion	☒ Severity N/A	☐ Severity N/A	☐ Severity N/A	☐ Severity N/A
Joint reflection cracking	☒ Low Severity ☒ Medium Severity ☒ High Severity	☒ Low Severity ☒ Medium Severity ☒ High Severity	☒ Low Severity[2] ☒ Medium Severity ☒ High Severity	☒ Low Severity[2] ☒ Medium Severity ☒ High Severity
Longitudinal and transverse cracking	☒ Low Severity ☒ Medium Severity ☒ High Severity	☒ Low Severity ☒ Medium Severity ☒ High Severity	☒ Low Severity[2] ☒ Medium Severity ☒ High Severity	☒ Low Severity[2] ☒ Medium Severity ☒ High Severity
Oil spillage	☒ Severity N/A	☐ Severity N/A	☐ Severity N/A	☐ Severity N/A
Patching and utility cut patching	☒ Low Severity ☒ Medium Severity ☒ High Severity	☒ Low Severity ☒ Medium Severity ☒ High Severity	☐ Low Severity ☐ Medium Severity ☒ High Severity	☒ Low Severity[5] ☒ Medium Severity[5] ☒ High Severity
Polished aggregate	☒ Severity N/A	☐ Severity N/A	☐ Severity N/A	☐ Severity N/A
Raveling	☒ Low Severity ☒ Medium Severity ☒ High Severity	☐ Low Severity ☒ Medium Severity ☒ High Severity	☐ Low Severity ☒ Medium Severity ☒ High Severity	☐ Low Severity ☐ Medium Severity ☐ High Severity
Rutting	☒ Low Severity ☒ Medium Severity ☒ High Severity	☒ Low Severity ☒ Medium Severity ☒ High Severity	☒ Low Severity ☒ Medium Severity ☒ High Severity	☐ Low Severity ☐ Medium Severity ☐ High Severity
Shoving	☒ Low Severity ☒ Medium Severity ☒ High Severity	☒ Low Severity ☒ Medium Severity ☒ High Severity	☒ Low Severity ☒ Medium Severity ☒ High Severity	☐ Low Severity ☒ Medium Severity ☒ High Severity
Slippage cracking	☒ Severity N/A	☒ Severity N/A	☒ Severity N/A	☒ Severity N/A
Swelling	☒ Low Severity ☒ Medium Severity ☒ High Severity	☐ Low Severity ☐ Medium Severity ☐ High Severity	☒ Low Severity ☒ Medium Severity ☒ High Severity	☐ Low Severity ☒ Medium Severity ☒ High Severity
Weathering	☒ Low Severity ☒ Medium Severity ☒ High Severity	☐ Low Severity ☐ Medium Severity ☐ High Severity	☐ Low Severity ☐ Medium Severity ☐ High Severity	☐ Low Severity ☐ Medium Severity ☐ High Severity

[1]Data collection method applicable if wheelpath location is known.
[2]Data collection method applicable if cracks have been sealed.
[3]Data collection method applicable if bleeding is not scattered and uniformly distributed.
[4]Full extent of block cracking may be difficult to document without image stitching.
[5]Data collection method applicable where there are color differences between patch material and original asphalt.

Booz Allen Hamilton (2019) investigated the runways, taxiways, aprons, parking, public roads, and access roads at Front Range Airport, Colorado, using sUAS platforms. The mission was conducted at an elevation of 196 ft (60 m) AGL to acquire high-quality images with a resolution of 1.3 cm/pixel. For the taxiways, sUAS were flown above 50 ft (15 m) AGL. Figure A-12 shows the flight map of this case study indicating flight parameters, altitude, flight paths, direction, and flight numbers. As part of the investigation, high-resolution images were acquired using a Sony R10C 20.1-megapixel (mp) camera. In addition, orthomosaics, contour, 3D models, and 3D point clouds were produced based on the sUAS-based sensors. This study provided invaluable experience on the operation of sUAS in towered airports, concluding that communication is the key to the successful implication of sUAS in pavement assessment in such airports.

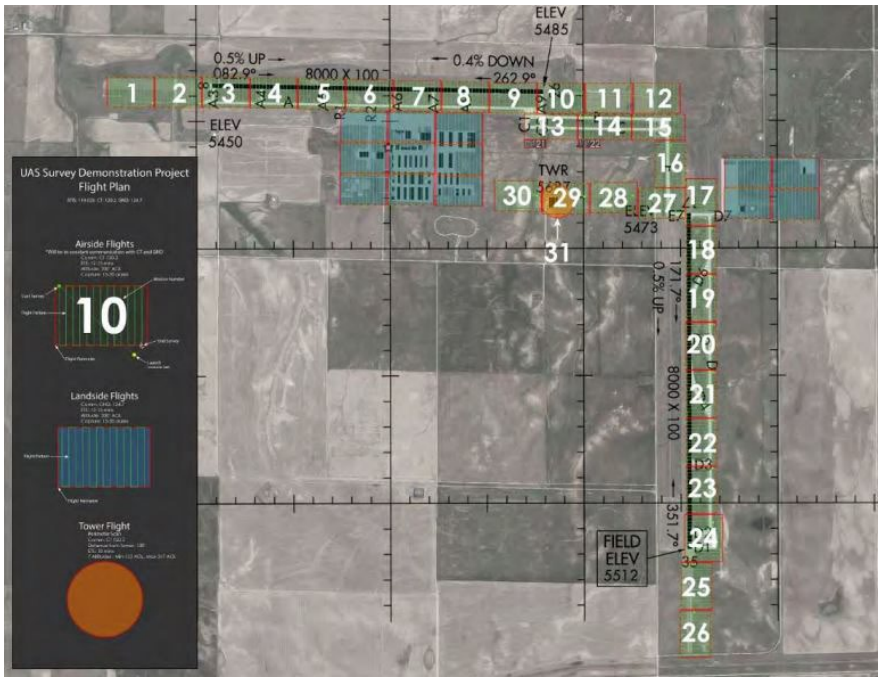

Figure A-12. Flight Map for the Investigation of Front Range Airport, Colorado (Adopted from Booz Allen Hamilton (2019))

Another effort on sUAS-aided airport runway inspection was taken by Booz Allen Hamilton at Johnston Regional Airport, North Carolina, which has Class G airspace. The sUAS platform was equipped with a high-resolution camera to capture images of 1.3 cm/pixel. The mission was accomplished by flying the sUAS platform at 197 ft (60 m) AGL. A reference map was produced and followed, identifying the flying parameters required for convenient image collection. The high-resolution images were employed to detect pavement deterioration and the identification of wildlife in the airport periphery. Thus, the sUAS platform was also equipped with a thermal camera. For the pavement distress analyses, 3D models and orthomosaics were created from the sUAS captured images.

In another event, the Booz Allen Hamilton team implemented sUAS in inspecting the runway, hangars, and drainage canal in Sebring Regional Airport, Florida. The mission was accomplished by flying the sUAS at an altitude of 196 ft (60 m) AGL. To accommodate the airport authorities'

requirements, the sUAS was equipped with LiDAR for 3D mapping. The collected data were also utilized to create point cloud and elevation maps. In addition, the use of tethered sUAS at dark was demonstrated as part of emergency response.

A.4.2.2 Airport Wildlife Management

Wildlife management in airports is a core component of airport operations. In each year, wildlife strikes cause more than $1.3 billion worldwide (Begier, 2014). Wildlife assessment in airports includes identifying the species, their habitat, food sources, and the control methods. Various sUAS platforms could be employed for these purposes, proving to be more effective than in-person inspection. The sUAS platforms equipped with sonic devices could be useful in discouraging birds on airfields.

Savannah/Hilton Head International Airport, Georgia, uses sUAS to monitor the perimeter fencing, pavement inspection, and wildlife management (Wysocky, 2018).T The incorporation of sUAS has been very useful in monitoring the airport's hard-to-access fencing through the swamps. In these places, in-person inspection is challenging since vehicles can often get stuck in muddy swamps. Flying sUAS over the swamp was the most effective option to identify unwanted bird nesting and wildlife migration, and to evaluate drainage for this airport.

A.4.2.3 Airport Security

Airport security is crucial because even the smallest airport can access the nation's airspace and the busiest and largest airports. To ensure airport security, routine surveillance of the airport perimeter and fences is required. However, some airports encompass a vast acreage, including remote, inaccessible terrain where in-person inspection is difficult. For these airports, sUAS is the appropriate tool to ensure faster and more comprehensive examinations. sUAS could be deployed to check the fence quality, inspect locks, and prevent trespassing in airport areas. The basic sUAS-aided surveillance consists of video monitoring, while the most robust unit could equip thermal cameras, automated video detections, and alert systems. In Europe, several airports, including Luton, Stansted, Heathrow, and Gatwick, are using sUAS for their security inspections (Hubbard et al., 2017).

A.5 SUMMARY OF LITERATURE REVIEW

In the airport PMP, the inspection of pavement areas is probably the most crucial aspect of airfield pavement maintenance and repair works. The FAA urges airport authorities to undertake corrective measures as quickly as possible even though the distresses are at an early stage and could be considered minor. Delayed attention to minor distresses could lead to major pavement failures, requiring extensive repair works, resources, and labor, along with traffic closure, loss in operation, and higher maintenance costs. Early detection of airport pavement distresses allows adequate time for corrective works, which would increase the service life of airport pavements, reduce maintenance costs, and improve both user safety and travel security. For the early detection of distresses, frequent inspections of the airfield pavements are required. In addition, timely assessments enable the airport authorities to model and predict pavement performance, and to evaluate the effectiveness of maintenance initiatives.

According to the FAA, the airfield pavements must be inspected every 3 years when a detailed PCI survey is performed. Otherwise, yearly inspections of airfield pavements are required. However, the traditional inspection methods for airport pavements are labor-intensive, time-consuming, and costly to the airport authorities. Therefore, as part of the standard practice, sample units in airfield pavement branches are selected, inspected, and considered to be representative of the entire pavement sections. The assessment of airfield pavements based on the sample units might not always represent the whole pavement, requiring inspection of additional sample units.

The literature review revealed that the deployment of sUAS could result in a faster and more frequent inspection of airport pavements at a lower cost. In addition, sUAS could allow the inspection of the entire pavement sections, thus providing a comprehensive assessment of airfield pavement conditions. Moreover, sUAS-enabled inspections could ensure adequate data acquisition, as required for realistic pavement condition prediction and prudent resource allocation for maintenance works. Several transportation agencies are successfully implementing sUAS platforms with different sensor arrangements in various applications with a focus on infrastructure inspection, such as bridges, highways, light poles, and unpaved roads. In the past decade, technological advancements have allowed significant progress in sUAS capabilities and sensor accuracy. Powerful computers, computational efficacy, and robust software packages are also available for accurate and realistic interpretations of sUAS data. Therefore, a number of sUAS platforms and sensors could be practically implemented to complement the current airport pavement inspection method depending on the mission objectives, distress severity levels, and the required accuracy of measurements.

A.6 REFERENCES

Armstrong, A. J. (2010). Development of A Methodology for Deriving Safety Metrics for UAV Operational Safety Performance Measurement. The University of York.

ASTM International. (2018). *Standard test method for airport pavement condition index surveys,* (ASTM D5340). https://doi.org/10.1520/D5340-12R18

Banks, E., Cook, S. J., Fredrick, G., Gill, S., Gray, J., Larue, T., Milton, J., Tootle, A., & Wheeler, P. (2018). *Successful approaches for the use of unmanned aerial system by surface transportation agencies.* American Association of State Highway and Transportation Officials. https://trid.trb.org/view/1723536

Begier, M. J., (2014). Strike, snarge and safety - reporting wildlife strikes to aviation, in: Airports Conference. Hershey, PA.

Booz Allen Hamilton Inc. (2019). *Airports and unmanned aircraft systems, volume 3: Potential use of sUAS by airport operators.* National Academies of Sciences, Engineering, and Medicine. https://doi.org/10.17226/25607

Brooks, C., Dobson, R., Banach, D., Oommen, T., Zhang, K., Mukherjee, A., Havens, T., Ahlborn, T., Escobar-Wolf, R., Bhat, C., Zhao, S., Lyu, Q., & Marion, N. (2018). *Implementation of Unmanned aerial vehicles (UAVs) for assessment of transportation infrastructure-Phase II.* https://rosap.ntl.bts.gov/view/dot/36994

Brooks, C., Dobson, R. J., Banach, D. M., Dean, D., Oommen, T., Wolf, R. E., Havens, T. C., Ahlborn, T. M., & Hart, B. (2015). *Evaluating the use of unmanned aerial vehicles for transportation purposes: [parts A-D].* Michigan Connected and Automated Vehicle Working Group. https://rosap.ntl.bts.gov/view/dot/28859.

Current Landscape of Unmanned Aircraft Systems at Airports. (2019). The National Academies Press. https://doi.org/10.17226/25659

Dobson, R. J., Colling, T., Brooks, C., Roussi, C., Watkins, M. K., & Dean, D. (2014). Collecting decision support system data through remote sensing of unpaved roads. *Journal of the Transportation Research Board,* 2433(1), 108–115. https://doi.org/10.3141/2433-12

FAA. (2018). Drone Advisory Committee. Washington D.C. https://www.federalregister.gov/documents/2018/07/03/2018-14394/july-17-2018-drone-advisory-committee-dac-meeting

Federal Highway Administration (FHWA). (2018a). *Unmanned Aircraft Systems (UAS): Complete Summit Workbook.*

FHWA. (2018b). *Use of Unmanned Aircraft Systems (sUAS) by State DOTs*.

Glaser, A. (2017). DJI is running away with the drone market - Vox. https://www.vox.com/2017/4/14/14690576/drone-market-share-growth-charts-dji-forecast

Hubbard, S., Pak, A., Gu, Y., & Jin, Y. (2017). sUAS to support airport safety and operations: Opportunities and challenges. *Journal of Unmanned Vehicle Systems,* 6(1). https://doi.org/10.1139/juvs-2016-0020

Michigan Tech Research Institute (MTRI). (2020). *Unpaved Roads Assessment.* https://www.mtu.edu/mtri/research/project-areas/transportation/infrastructure/unpaved-roads/

Ni, D., & Plotnikov, M. (2016). *The State of the Practice of sUAS Systems in Transportation.*

Prather, C. D. (2019). *Current Landscape of Unmanned Aircraft Systems at Airports, Current Landscape of Unmanned Aircraft Systems at Airports.* The National Academies Press. https://doi.org/10.17226/25659

Peshkin, D., Dzwilewski, P.-P. F., Potvin, K., Gauthier, K., Wade, M., Risner, E., Robinson, R., Snyder, C., Cardwell, M., & Feighan, K. (2019.) *Guidelines for collecting, applying, and maintaining pavement condition data at airport* (ACRP Research Report 203). Airport Cooperative Research Program, The National Academies Press. https://doi.org/10.17226/25566

Vidyadharan, A., Carter, T., Ceylan, H., Bloebaum, C., Gopalakrishnan, K., & Kim, S. (2017, August 27–30). *Civil infrastructure health monitoring and management using unmanned aerial systems* [Paper]. International Conference on Highway Pavements and Airfield Technology 2017, Philadelphia, PA, United States. https://doi.org/10.1061/9780784480946.019

Wysocky, K. (2018). Savannah/Hilton Head Int'l prepares to integrate drones into airport & airfield operations. *Airport Improvement Magazine.*

Zhang, C. (2008). An UAV-based photogrammetric mapping system for road condition assessment. *International Archives of the . Photogrammetry, Remote Sensing And Spatial Information Sciences*, 37, 627-632.

APPENDIX B—SMALL UNMANNED AIRCRAFT SYSTEM DATA COLLECTION PLAN FOR CAPE MAY AIRPORT, LOWER TOWNSHIP, NEW JERSEY, IN AUGUST 2021

B.1 SMALL UNMANNED AIRCRAFT SYSTEM REQUIRED

- DJI Mavic 2 Pro with integrated 20-mp camera (2 systems) with spare batteries [charged]
    - Controller [charged]
    - Integrated Controller [charged]
    - Spare 4G Pixel phone as a backup controller [charged]
- DJI Mavic 2 Enterprise Advanced with integrated dual 48-mp camera and 640x512 thermal camera (2 systems: one from MTRI, one from Iowa State)
    - 7 batteries from MTRI, 6 batteries from Iowa State [charged]
    - Smart Controller for each drone [charged]
- Bergen Hexacopter with spare batteries [charged]
    - Controller [charged]
    - FPV screen [charged]
    - Optical Camera (Nikon D850 45.7 mp) [batteries charged]
- mdMapper1000+ with spare batteries [charged]
    - Controller [charged]
    - Optical camera (Sony RX1R-II 42.4 mp) [batteries charged]
- Tarot X6 V2.2 with spare batteries [charged]
    - Controller [charged]
    - Optical Camera (Nikon D850 45.7 mp) [batteries charged]
    - Herelink video transmission system [batteries charged]

B.2 OTHER EQUIPMENT

- Propeller Aeropoint electronic Global Positioning System (GPS)-based ground control targets (20)
- Micro SD cards/spare micro-SD cards with SD card adapter + full-sized SD cards [past data stored/removed]
- 2xPortable 1 TB SSD
- 256 GB Pendrive
- Folding take-off pad
- Generator and Gas can
- Rugged Olympus Tough TG-5 GPS Camera (12 mp) (for geolocated field photos) (2) [charged]
- Sony Alpha Camera (16 mp) for field photos (With zoom lens) (1) [charged]
- MTRI flight logging form (at least 2 copies), pre-filled out with information for documenting flight details
- Sporty's® SP-400 (2) and Yaesu FTA 750L (1) aviation radios, tuned to Cape May Airport (WWD), Cape May, NJ Unicom frequency **122.7** for the entire time the team is on site at WWD
    - Two aviation radios are for two sUAS flight sub teams each consisting of one pilot and one observer. The third one is for the person(s) placing ground control points (GCPs) or moving on the airfield so that they can operate in separate parts of the

airport, completing needed tasks more quickly while staying safe and aware of manned and unmanned aircraft operations on or near WWD.

- MTRI anemometer (for wind speed checking)
- MTRI iPad Mini with GeoPDF airport map that includes recommended GCP locations to assist with placing GCPs
- Clipboard
- Field books/personal notebook
- Pens and pencils
- Measuring tape
- Ruler (30 cm)
- Tools and tape
- Appropriate clothing and protective eyewear
- Steel/composite toe boots/shoes
- Facemasks (see COVID-19 portion of the safety plan)
- First aid kit(s) – at least 1
- Car emergency visibility lights
- Traffic cones
- Fire extinguisher
- Personal water

All batteries will be charged and equipment will be packed the day prior to travel to Cape May, NJ.

B.3 AIRPORT CONTACT INFORMATION

The senior airport manager of WWD is **Thomas Berry**, who has agreed to our sUAS field deployment. The general phone number for the airport is (609) 886-8652.

Airport webpage: http://www.capemayairport.com/

SkyVector webpage about WWD: https://skyvector.com/airport/WWD/Cape-May-County-Airport

B.4 FOCUS AREAS FOR DATA COLLECTION

The focus will be on Runway 10/28 and the full apron at WWD. The runway has six different asphalt overlay over asphalt concrete (AAC) pavement sections. The plan is to collect data from three of them: RW1028CM10N, RW1028CM10C, and RW1028CM10S. The dimensions of Runway 10/28 are 1,523.39 m x 45.72 m. Each test section of the runway is 1,242.06 m long and 15.24 m wide.

According to a PCI inspection survey conducted by Applied Research Associates, Inc. (ARA) in 2019, the area-weighted average PCIs for RW1028CM10N, RW1028CM10C, and RW1028CM10S were 67, 71, and 50, respectively, as shown in Table B-1. The PCI survey also

noted that the focus areas of the runway had joint reflection cracking (L), L&T cracking (LM), rutting (LM), depression (M), patching (L), and weathering (L).

The aprons consist of six sections of AC and one section of PCC pavements. The branch had a total area of 73,719.68 m^2, and the area-weighted average PCI was 62 (Fair). However, the plan is to collect sUAS data from section 30 with AC pavement and section 40 with PCC pavement. The PCC pavement of the apron showed a wide variety of distresses that include corner break (L), corner spalling (LMH), corrugation (L), faulting (LM), joint seal damage (LM), joint spall (LMH), large patch (LMH), LTD cracks (LMH), pop-outs, and small patch (LMH). The dominant PCC pavement distresses are corner spall, D-crack, faulting, joint spall, large patch, small patch, shrinkage crack, and LTD crack (Table B-1). The PCI value for the PCC section of the apron in 2019 was 58, whereas section 30 with AC pavement had a PCI value of 72. Section 30 had L&T cracking (LM), raveling (L), and weathering (L) throughout the whole pavement. The following inspection report was directly provided by FAA.

Table B-1. PCI Survey Result of the Data Collection Area

Branch ID	Section ID	Surface Type	2019 PCI	Area m^2	Distresses
ATERM CM	30	AC	72	30,280	L&T cracking (LM), raveling (L), weathering (L)
	40	PCC	58	73,720	Corner break (L), corner spalling (LMH), corrugation (L), faulting (LM), joint seal damage (LM), joint spall (LMH), large patch (LMH), LTD cracks (LMH), pop-outs, and small patch (LMH)
RW102 8CM	10C	AAC	71	18,929	Joint reflection cracking (L), L&T cracking (LM), weathering (L)
	10N	AAC	67	18,929	L&T cracking (L), rutting (L), weathering (L), patching (L)
	10S	AAC	50	18,929	L&T cracking (LM), rutting (LM), weathering (L), patching (L)

L = Low Severity, M = Medium Severity, H = High Severity
AC = Asphalt Concrete Pavement
PCC = Portland Cement Concrete Pavement
AAC = Asphalt Overlay over Asphalt Concrete Pavement
L&T cracking = Longitudinal and Transverse cracking
LTD cracking = Longitudinal, Transverse, and Diagonal Cracking

B.4.1 High-Resolution Data Collection Sample Units

Nine sample units were selected for high-resolution data collection. These sample units have AC, AAC, and PCC pavements, with most of the airfield pavement distresses found at WWD. Three AAC sample units from Runway 10/28, three AC sample units from Apron 30, and three PCC sample units from Apron 40 were selected, as shown in Figure B-1. The runway sample units are

noted to have L&T cracking, weathering, and depression. Conversely, L&T cracking and swell and shoving, due to movement of PCC pavements, were exhibited on the Apron 30 sample units. The four selected PCC sample units had LTD cracks, joint spalling, shrinkage crack, joint seal damage, small patching, large patching, and scaling. The sample units will also have higher priority in PCI data collection by Applied Pavement Technology, Inc. (APTech). They have been marked as level 1 or high-priority sample areas. Table B-2 provides a detail of the PCI data-collection sample units and their priority level.

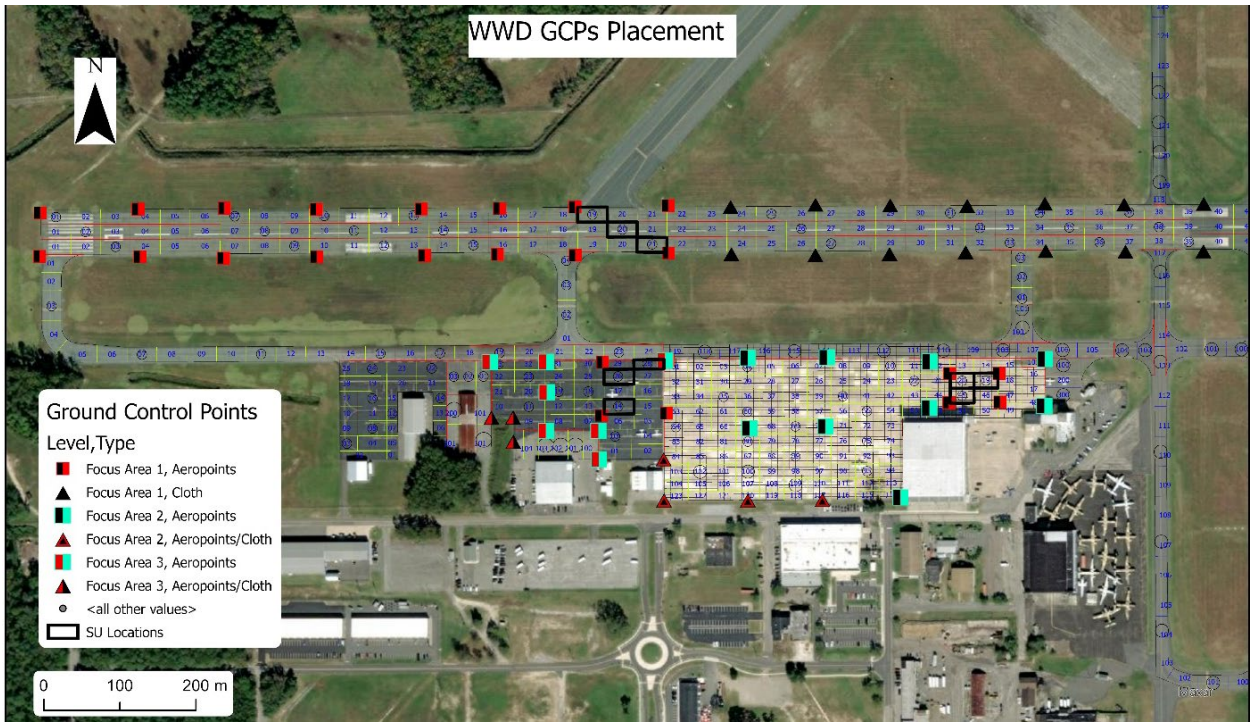

Figure B-1. Overview of WWD and Sampling Focus Areas, Including Recommended Locations for GCPs

B.5 OBJECTIVES FOR UPCOMING AUGUST 2021 UAS DATA COLLECTION

Bergen Hexacopter or Tarot X6

The Bergen Hexacopter or Tarot X6 with Nikon D850 will be flown at 18.3 m AGL to collect optical imagery of Runway 10/28 section 10 and Aprons 30 and 40. At 7.4 m, the RGB optical imagery will be 1.49-mm resolution. In addition, the same system will be flown at 9.1 m over the selected sample units to collect very high-resolution optical RGB data. Because of the closeness of the selected sample units, they will be covered in three manual flights: one for runway sample units, one for AC sections of the aprons' sample units, and one for the PCC sections of the aprons' sample units. Each flight will require 3 to 10 minutes to complete, depending on how far apart the paired sample units are. At 9.14 m, the RGB optical imagery will be 0.75-mm resolution. The Tarot X6 flight will be operated using the software that comes with the Pixhawk controller. Conversely, manual control is preferred because of the small areas planned for data collection and because the older Bergen flight control hardware and software is not compatible with current mission-planning applications.

Table B-2. Data Collection Priority Level

Priority Level	Airfield	Pavement Type	Section	Sample Unit
1	RW1028	AAC	CM10N	19
			CM10C	20
			CM10S	21
	ATERM	AC	CM30	14, 26, 28
	ATERM	PCC	CM40	19, 20, 45
2	RW1028	AAC	CM10N	1, 7, 10, 13, 25, 31, 34, 37
			CM10C	2, 8, 11, 14, 26, 32, 35, 38
			CM10S	3, 9, 12, 15, 27, 33, 36, 39
	ATERM	AC	CM30	3, 11, 18, 19, 23, 33
		PCC	CM40	4, 10, 22, 35, 40, 55, 60, 64, 69, 75, 80, 89, 95, 100, 102, 109

mdMapper1000+

The team also has a German-made mdMapper1000+ UAS, purchased in 2020, that is focused on photogrammetric optical data collection for helping map defects on bridge decks and measuring 3D rates of construction progress. This system has been flown at 18.29 m AGL with lesser winds and turbulence at Custer Airport, Monroe, Michigan (TTF) and Coles County Memorial Airport, Mattoon, Illinois (MTO). The mdMapper1000+ is currently configured to collect data with a 42.4-mp Sony RX1R-II. At 18.29 m, the optical imagery will have a 2.3-mm resolution.

Mavic 2 Pro

Optical imagery is planned to be collected at 15.24 m AGL with the Mavic 2 Pro 20 mp for Runway 10/28 section 10 and apron Sections 30 and 40 as a backup data set. MTRI is planning to bring 2 Mavic 2 Pro sUAS with additional batteries. At least seven pre-planned missions are likely to be needed to cover the focus areas. The flight plans for these missions are created with the Pix4D Capture or DroneDeploy android app, which has been successfully used in mission planning for previous data collection in this research. An 80% forward overlap and a 70% side overlap are being used, standard for most of the missions where close-range photogrammetry software will be used to create orthophotos and digital elevation model (DEM) outputs. These overlap settings were used successfully for creating outputs for different flights at TTF; Grosse Ile Municipal Airport, Grosse Ile Township, Michigan (ONZ); MTO; Boone Municipal Airport, Boone, Iowa (BNW); and Perry Municipal Airport, Perry, Iowa (PRO). Figures B-2, B-3, and B-4 show drafts of the pre-planned runway mission at 15.24 m based on using the Mavic 2 Pro sUAS. The details of the flight plans are provided in Table B-3.

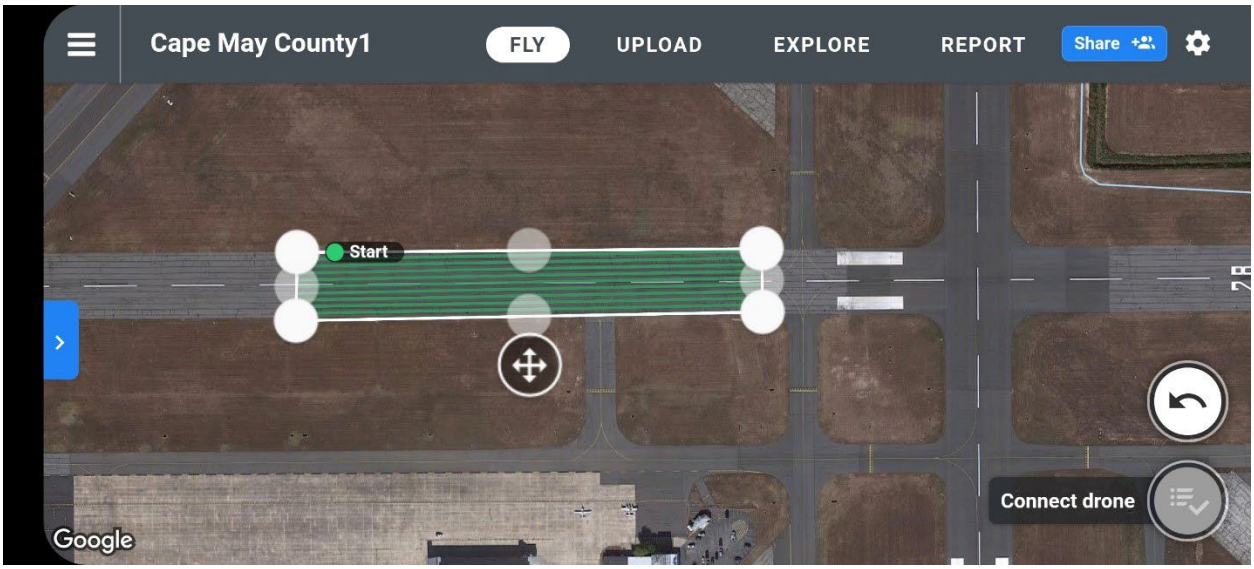

Figure B-2. Mavic 2 Pro Flight Plan for Runway 10/28

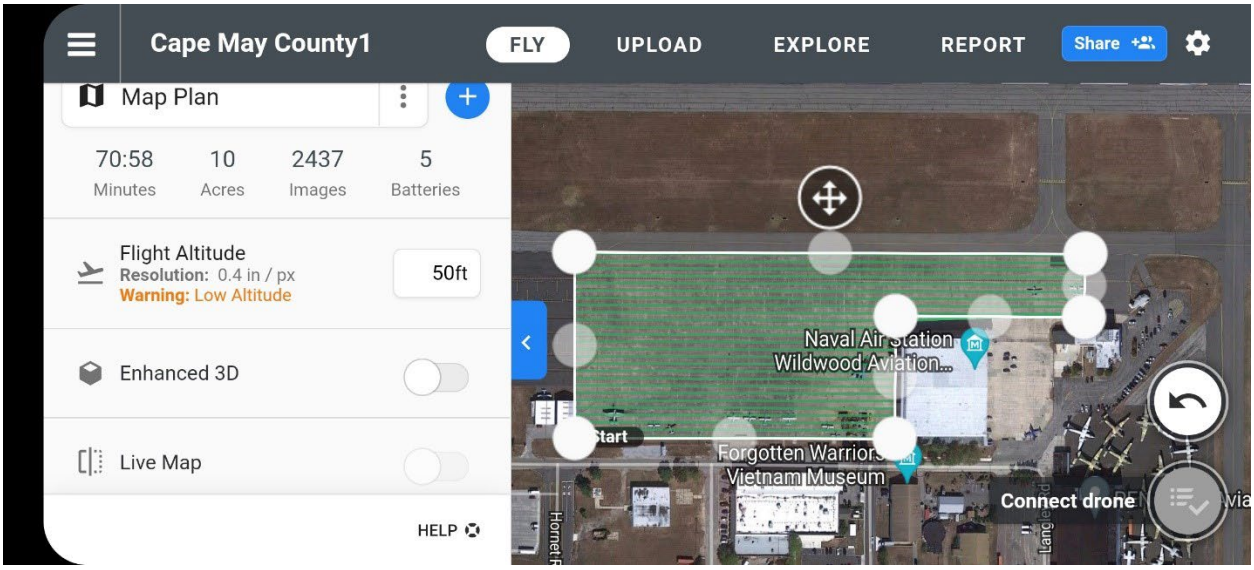

Figure B-3. Mavic 2 Pro Flight Plan for Apron Section 40

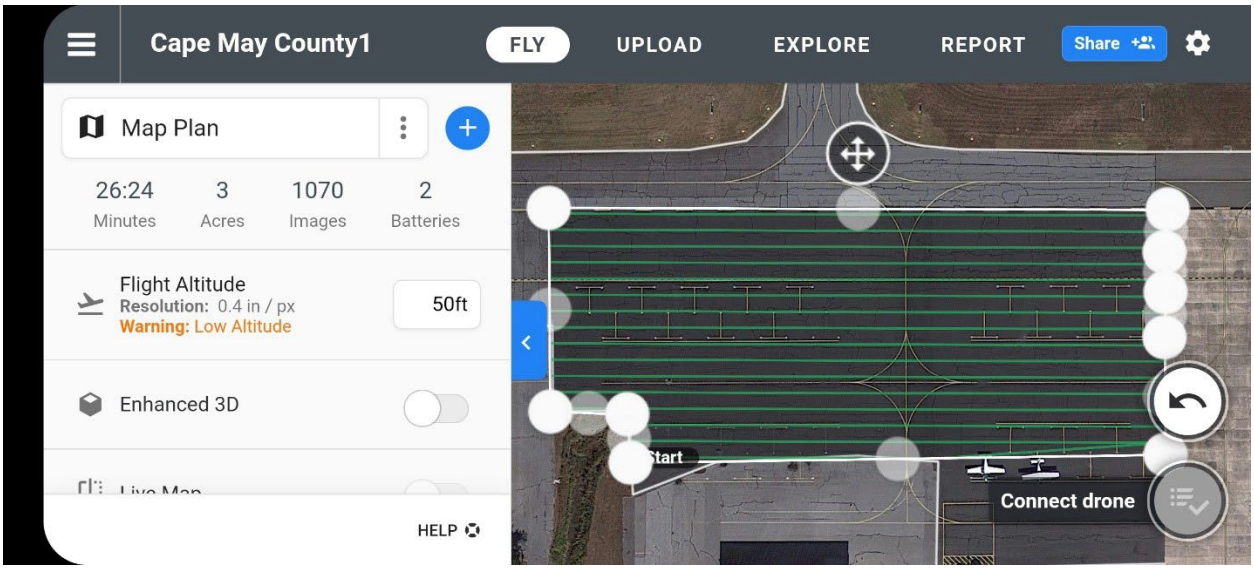

Figure B-4. Mavic 2 Pro Flight Plan for Apron Section 30

Table B-3. Planned Sensors and Flying Heights for All sUAS

Date	Target Area	sUAS Platform	Sensors	AGL m	Resolution mm/pix
8/24	Sample Units	Bergen Hexacopter or Tarot X6	45.7-mp optical RGB Nikon D850	9.14	0.75
		mdMapper1000+	42.4-mp optical RGB Sony RX1R-II	18.29	2.3
8/24, to 8/26	RW1028CM10N, RW1028CM10C, RW1028CM10S, TWECM10, TWECM20, ATERMCM30, and ATERMCM40	Bergen Hexacopter or Tarot X6	45.7-mp optical RGB Nikon D850	18.29	1.49
		Mavic 2 Enterprise advanced	640x512 stereo thermal	24.38	3.1
		Mavic 2 Pro	20-mp optical RGB	15.24	3.7

Mavic 2 Pro RGB optical data will be collected as a backup if required.

Mavic 2 Enterprise Advanced

Thermal imagery will be collected over Runway 10/28 section 10 and Apron Sections 30 and 40. Two M2EA units will be available, one with seven batteries and one with six batteries. Batteries can be recharged during the day with an available generator. The average flight time is estimated at 20 minutes per battery. The stereo thermal data are from 24.38 m AGL. The preplanned flights are shown in Figures B-5 and B-6.

Figure B-5. Flight Plan for Stereo Thermal Data Collection with Mavic 2 Enterprise Advanced Over Part of Runway 10/28

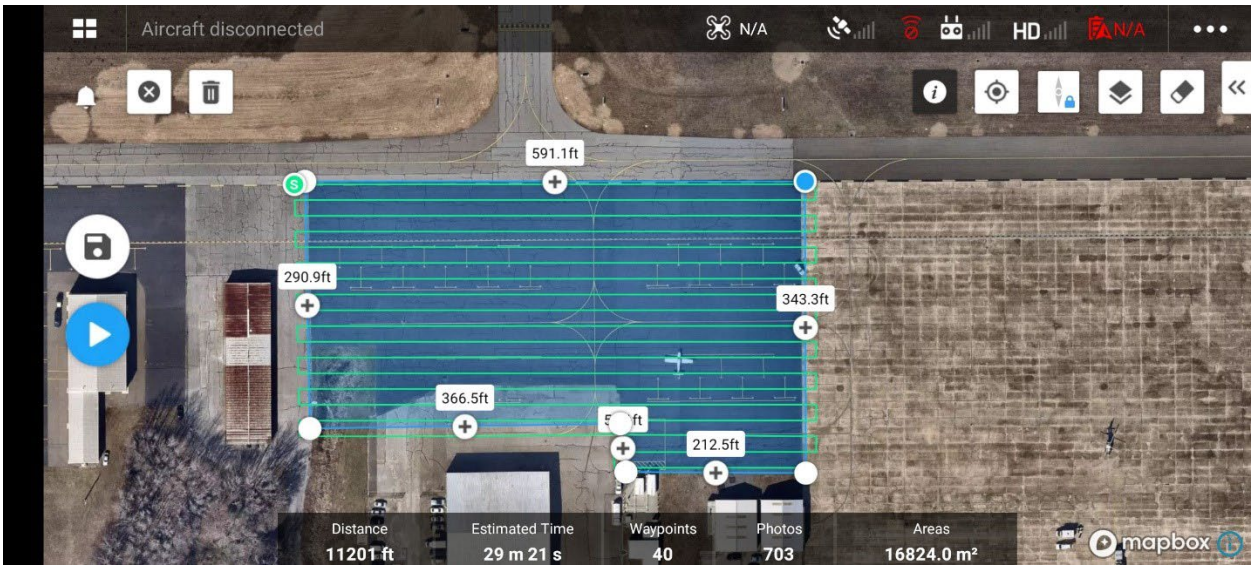

Figure B-6. Flight Plan for Stereo Thermal Data Collection with Mavic 2 Enterprise Advanced Over Apron 30

B.6 PILOTS AND SUPPORT TEAM

The research team has four research staff available for flying the sUAS, all of whom have a current Part 107 Unmanned Pilot's Certificate. Other team members can help with GCP GPS data collection and capturing pavement distress images. The standard procedure is to have at least two staff members for each sUAS flight, one sUAS pilot and one safety observer. In simultaneous data

collection, each sUAS pilot will have a dedicated field observer. WWD is a class G airspace. Therefore, none of the sUAS pilots will need any approval for flying sUAS under 121.92 AGL.

The research team will travel to Cape May, New Jersey, from Iowa, Michigan, and Illinois on August 22 and 23, 2021. The research team will take part in any training or paperwork that needs to be completed before entering the airfield or driving personnel vehicles. Once the research team is on the airfield, the GCPs will be placed, followed by focusing on collecting data from the sample units by the remote pilot in command. This will be followed by data collection over the other parts of the airfield by different pilots. The main objective for the day is to collect the high-resolution sample unit data first. If time allows, as much data as possible from Runway 10/28 and Aprons 30 and 40 will be collected on the same day. The remaining data will be collected on August 25 and 26, 2021. The data-collection team will have their aviation radio on at all times for data collection on Unicom frequency 122.7 used for WWD. Communications via the radio should be in the form of **"Cape May. [Announcement]. Cape May."**

Windows of moving vehicles will be kept open, with car radios off, to listen for unexpected aircraft when driving on runways and taxiways. The team will minimize time on runways by having non-data collection activities, such as data-collection conversations, battery charging, and checking data collection outside the Runway Safety Area. A representative Runway Safety Area of 76.2 m from the runway centerline and 304.8 m from the runway ends is being used, so the team will stay outside these areas when not collecting data. The team will keep 76.2 m horizontally from any moving aircraft and will not operate sUAS if wind gusts exceed 24 kph and temperatures are above 37.78 degrees Celsius. A hand-held anemometer will be used to measure wind speed before each mission.

Following is the planned data collection timeline:

August 23, 2021

8:30 AM – 5:00 PM: PCI data collection by APTech
5:00 PM – 5:30 PM: PCI data collection conclusions

August 24, 2021

8:30 AM – 9:00 AM: Paperwork, training, and stand-up meeting lead by the remote pilot in command
8:30 AM – 5:00 PM: PCI data collection by APTech
9:00 AM – 9:30 AM: Aeropoints and GCPs based on the ground control placement map
9:30 AM – 5:00 PM:

- Remote pilot in command with Bergen Hexacopter or Tarot X6 data collection
  - Sample Units
    - Bergen Hexacopter or Tarot X6 at 9.14 m AGL
      - Estimated Total Time: 30 mins or 20 mins
    - mdMapper1000+ at 18.29 m AGL
      - Estimated Total Time: 15 mins
  - Runway 10/28 Section 10

        - Bergen Hexacopter or Tarot X6 at 18.28 m
            - Estimated Total Time: 2.9 hours or 3.3 hours
- Pilot 2 and Pilot 3
    - Runway 10/28 Section 10
        - Mavic 2 Pro at 15.24 m
            - Estimated Total Time: 2 hours
        - Mavic 2 Enterprise Advanced at 18.38 m stereo thermal data
            - Estimated Total Time: 3 hours

5:00 PM – 5:30 PM: GCP collection and PCI and sUAS data collection conclusions

August 25, 2021

8:30 AM – 9:00 AM: Paperwork, training, and stand-up meeting lead by the remote pilot in command
8:30 AM – 5:00 PM: PCI data collection by APTech
9:00 AM – 9:30 AM: Aeropoints and GCPs based on the ground control placement map

9:30 AM – 5:00 PM:

- Remote pilot in command with Bergen Hexacopter or Tarot X6 data collection.
    - Any remaining data from 8/24
    - Apron Section 30
        - Bergen Hexacopter or Tarot X6 at 18.29 m
            - Estimated Total Time: 1.4 hours or 1.2 hours
    - Apron Section 40
        - Bergen Hexacopter or Tarot X6 at 18.29 m
            - Estimated Total Time: 2.2 hours or 2 hours
- Pilot 2 and Pilot 3
    - Any remaining data from 8/24
    - Apron Section 30
        - Mavic 2 Pro at 15.24 m
            - Estimated Total Time: 0.5 hour
        - Mavic 2 Enterprise Advanced at 18.29 m stereo thermal data
            - Estimated Total Time: 1 hour
    - Complete Apron Section 40
        - Mavic 2 Pro at 15.24 m
            - Estimated Total Time: 1.8 hours
        - Mavic 2 Enterprise Advanced at18.29 m stereo thermal data
            - Estimated Total Time: 2.5 hours

5:00 PM – 5:30 PM: GCP collection and PCI and sUAS data collection

August 26, 2021

8:30 AM – 9:00 AM: Paperwork, training, and stand-up meeting led by the remote pilot in command
9:00 AM – 9:30 AM: Aeropoints and GCPs based on the ground control placement map
9:30 AM – 5:00 PM:

- Remote pilot in command with Bergen Hexacopter or Tarot X6 data collection.
    - Any remaining data from 8/24 and 8/25
- Pilot 2 and Pilot 3
    - Any remaining data from 8/24 and 8/2

5:00 PM – 5:30 PM: GCP collection and data collection conclusions

August 27, 2021
Back-up date.

The data-collection schedule is developed based on the weather condition shown on the forecast. The weather forecast shows mostly sunny or sunny on August 24 to 26, 2021 (Figure B7). However, the data-collection team will closely monitor.

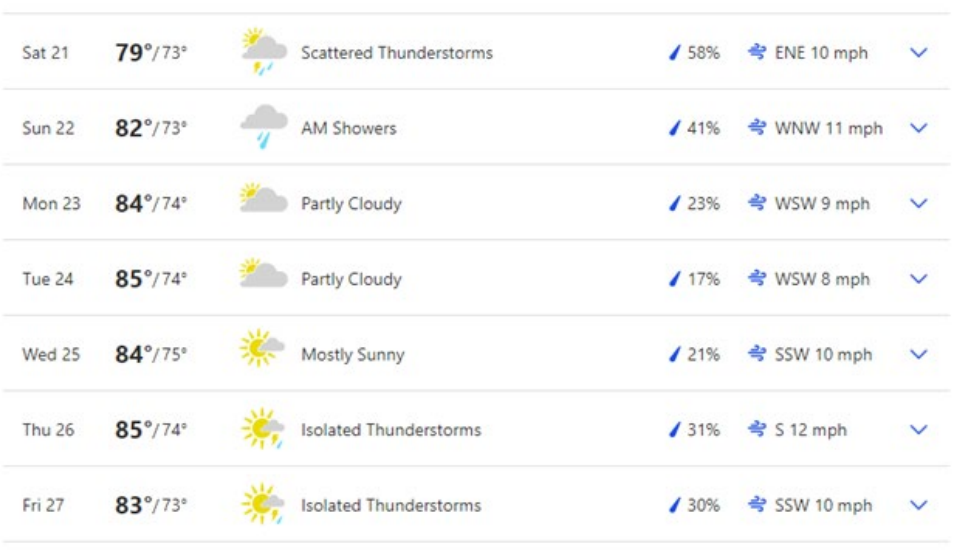

Figure B-7. Weather Forecast for Cape May, New Jersey (as of August 16, 2021)

All missions will be documented by a photographer designated for each mission. One team member is not flying the sUAS or acting as an observer (this is usually one of the GCP data collection team members). A separate safety plan has also been completed and shared and will be reviewed no later than 3 days ahead of the deployment date if any final modifications are needed.

APPENDIX C—AIRPORT CONDITION SURVEY SAFETY PLAN FOR CAPE MAY AIRPORT (WWD), NEW JERSEY IN AUGUST 2021

This safety plan was developed for safe data collection from WWD. This document was developed along with the data collection plan provided in Appendix B. Figure C-1 to C-3 show the travel plans for the research team whereas Figure C-4 and C-5 highlight WWD layout.

Data Collection Date: August 23 and 26, 2021

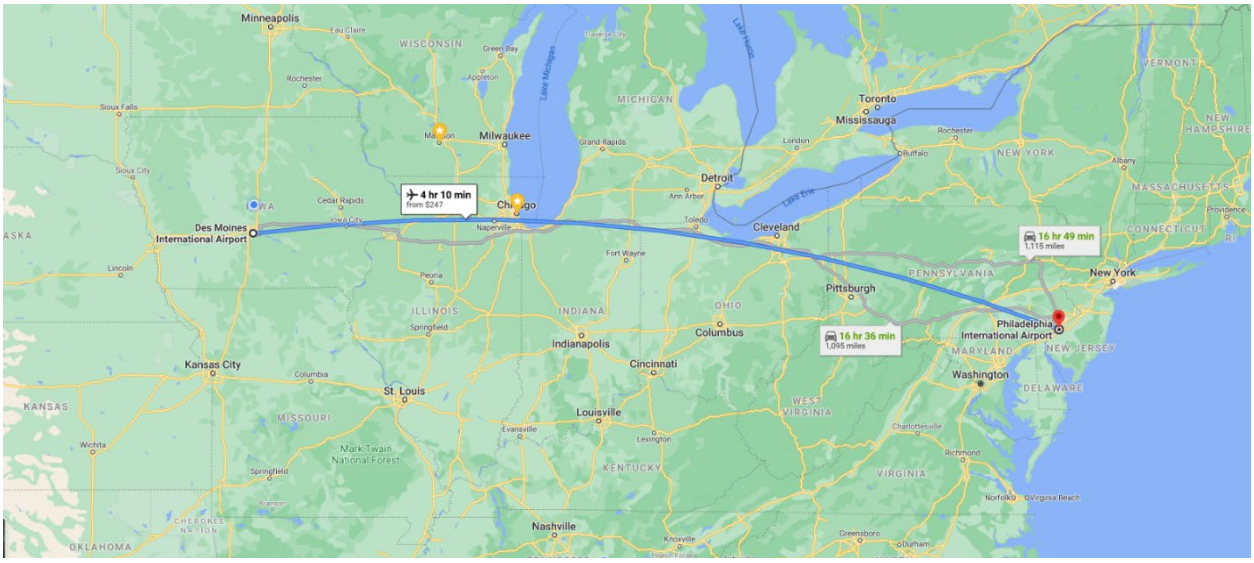

Figure C-1. Air Travel from Des Moines, IA to Philadelphia, PA

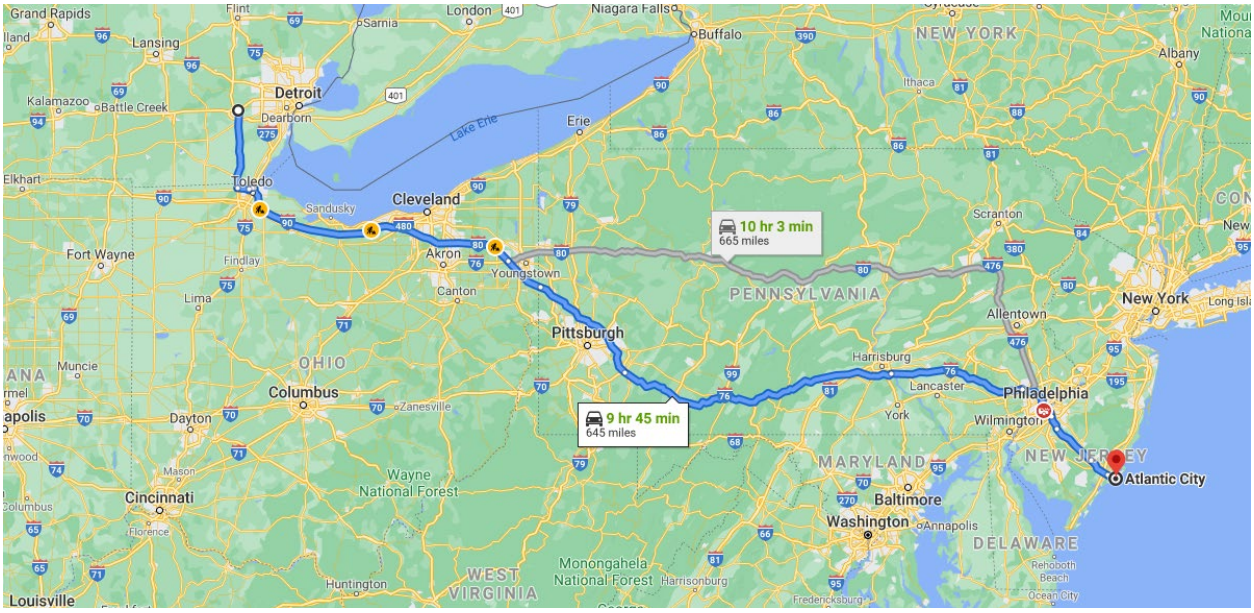

Figure C-2. Travel from Ann Arbor, MI to Atlantic City, NJ

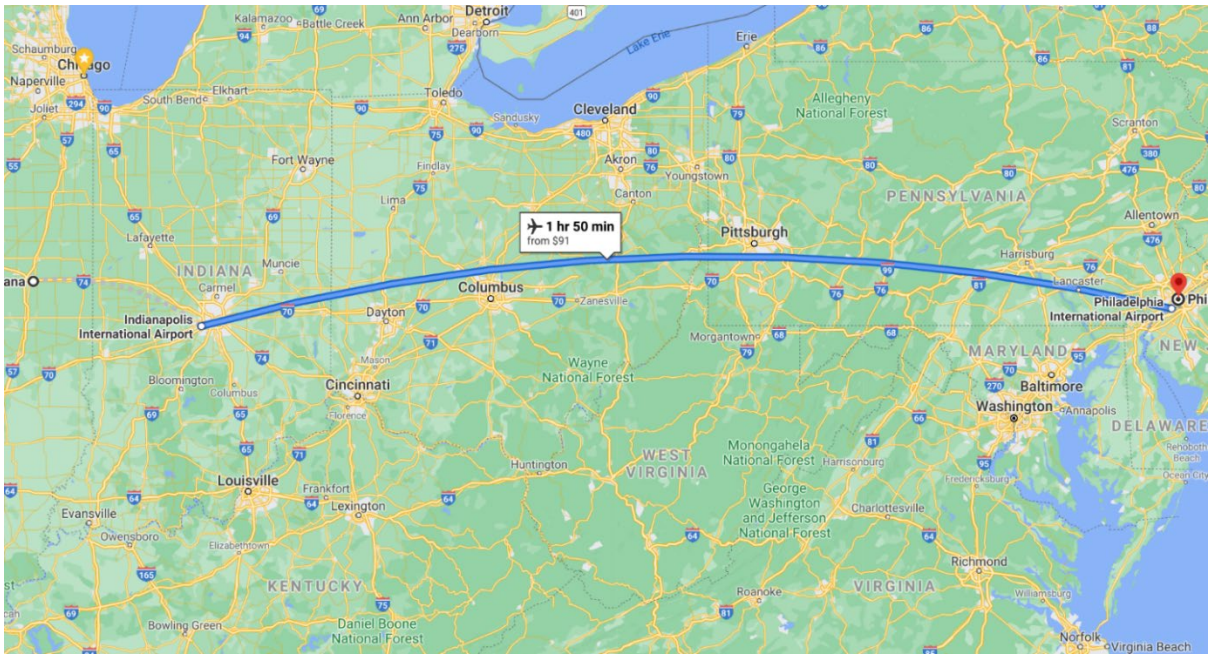

Figure C-3. Travel From Indianapolis, IN to Philadelphia, PA

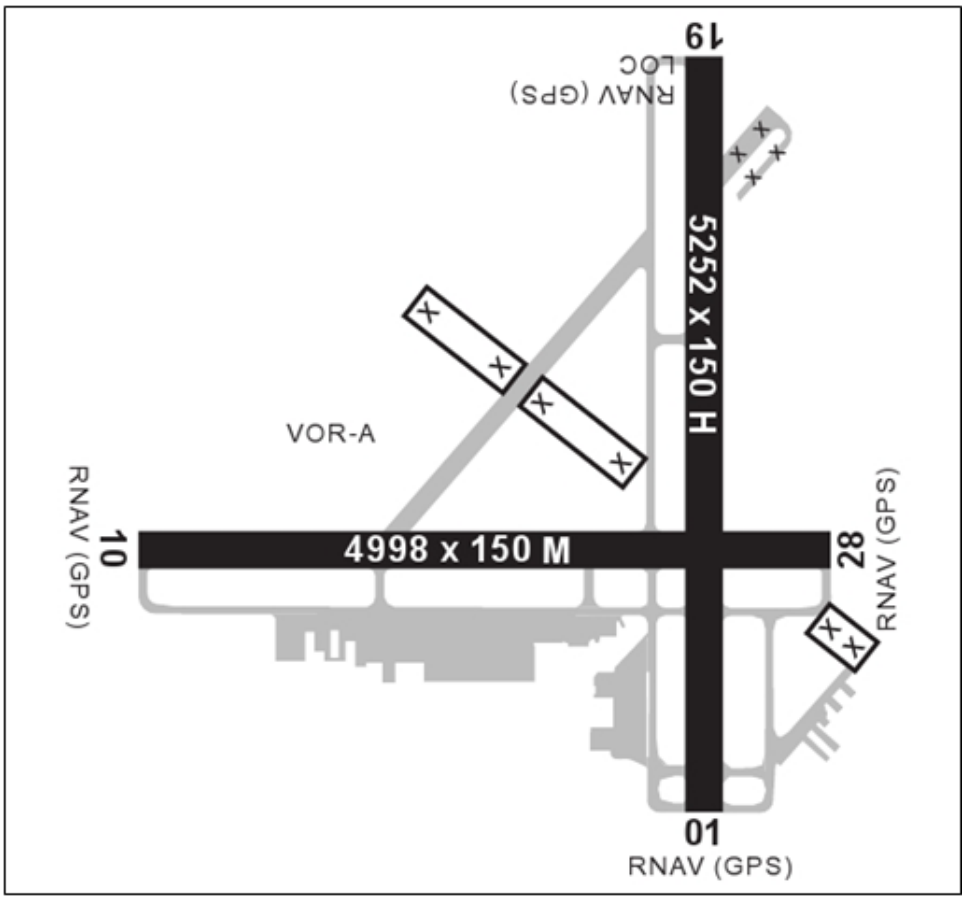

Figure C-4. Airport Diagram of Cape May Airport (WWD), Cape May, NJ

Figure C-5. View of the Cape May Airport (WWD), Cape May, NJ

C.1 SAFETY INFORMATION

For any safety questions during field data collection, please contact:

- Halil Ceylan, Iowa State University (ISU) (Project PI and Lead).
- Colin Brooks, MTRI (MTRI Project Lead) (Also a backup pilot, ground control collector)
- Richard Dobson (Lead Pilot-in-command)

Other participants are:

- Abdullah Sourav, ISU (drone pilot)
- Chris Cook, MTRI (road and drone safety observer, backup pilot)
- Olivia Brouillette, ISU (undergraduate research assistant intern)
- Abby Jenkins, MTRI ((ground control data collector, backup road and drone safety observer)
- David Peshkin, APTech (APTech project lead)
- Trent Montgomery, APTech (PCI inspector)
- Katie Gauthier, APTech (PCI inspector)

Proposed schedule

- ISU team will depart Ames, Iowa, in the morning on August 23, arriving in Atlantic City by evening on the same day. The airport of departure is Des Moines International Airport (DSM), and airport of arrival is Philadelphia International Airport (PHL).
- MTRI team will depart Ann Arbor, Michigan, at 8 am on August 23, arriving in Atlantic City approximately 10 pm on August 23 (travel time to Atlantic City, New Jersey, from MTRI is approximately 10 hours minus the time change).
- The PCI inspectors of APTech. will depart Urbana, Illinois, on August 22, arriving in Cape May by evening on the same day. The APTech project lead will travel to Cape May on August 23.
- The data collection team will commute from Atlantic City, New Jersey, to WWD each day.
- The PCI survey will be conducted from August 23 to 25.
- The sUAS data collection team will survey the airport on August 24 to 26, as needed.
- Return to Ames, Iowa, on August 27.
- Return to Ann Arbor, Michigan, on August 27.
- Return to Urbana, Illinois, on August 25 and 26.

C.2 FIELD SITE

Cape May Airport (WWD) is in Cape May, New Jersey. The senior airport manager of WWD is **Thomas Berry**, who has agreed to sUAS field deployment. The general phone number for the airport is (609) 886-8652.

C.3 AIRPORT SAFETY

At all times on the fieldwork site, crew members must have on a hard hat and reflective vest. Driving vehicles must have yellow caution lights present.

- A stand-up safety briefing will be held at the beginning of any data collection days. After data collection, input will be sought from team members on any safety concerns that come up.
- All crew members on the field site must wear protective clothing (steel-toe or composite-toe boots, high-vis vest, glasses) at all times.
- Drone pilots MUST have an undistracted spotter watching for vehicle and air traffic and for the safety of the pilot. The spotter will control an aviation radio and have the option of sharing control with an additional team member.
- Testing will operate on a give-way basis to any air traffic at the airport. If manned aircraft are preparing to take off or approach for a landing along the runway or taxiway being surveyed by sUAS, operations will cease (land sUAS) and continue after the aircraft have finished their take-off or landing procedures.
- There will be two sUAS data collection teams, with Rick Dobson (Michigan Tech) and Abdullah Sourav (Iowa State) as the lead pilots for each team. Each team will have their own Sporty's® 400/ YEASU Spirit aviation radio, which will be on at all times while performing data collection operations (including setup and takedown time) on **Unicom frequency 122.7 used for WWD.**
- Aeropoint GCPs will be placed at the beginning of data collection each day, with Abby Jenkins and Colin Brooks assigned to this task. Additional traditional cloth targets will be placed at the beginning of the first day and have their locations recorded with a decimeter-resolution GPS. Both sets of targets will be placed off the runway and aprons.
- Windows of moving vehicles will be kept open, with car radios off, to enable listening for unexpected aircraft when driving on runways and taxiways.
- **Always be conscious of the presence of moving traffic or aircraft. Due to the presence of restricted airspace, pilots and spotters must be conscious of potential aircraft moving through the survey area.**
- If one member is taking measurements of any kind in an area with traffic or other safety risks, another crewmember must spot.
- Only stand on runways or taxiways during data collection, if needed.
- Do not stand in open traffic lanes present at the airport. If walking along an open stretch of roadway, walk against the flow.
- As noted in the Data Collection Plan, the team will minimize time on runways by having non-data collection activities such as data collection conversations, battery charging, and checking data collection outside of the Runway Safety Area. A representative Runway Safety Area located 76.2 m from the runway centerline and 304.8 m from the ends of the runway will be used, so crewmembers must stay outside these areas when not completing data collection. Crewmembers must keep 76.2 m horizontally from any moving aircraft.

C.4. sUAV SAFETY

The pilot in command (PIC), Rick Dobson, will brief all participants a day prior to field collections on where the sUAV will be operating, safe places and minimum distance to stand or work while the sUAS is taking off/landing and collecting data, and general safety procedures. Under Part 107, any individual without a Remote Pilots Certificate may not operate a drone unless being directly supervised by a person with a remote pilot's license. Only certified Part 107 pilots will fly.

- Remain a safe distance from and do not stand directly below a flying sUAS.
- DO NOT attempt to distract the pilot or designated spotters while the sUAS are being operated unless it is an immediate emergency.
- All sUAS operations MUST have a designated spotter.
- If any low-flying aircraft are spotted and heading towards the sUAS flight path, all operations must immediately end until safe passage of the manned aircraft.
- Listen to the PIC at all times.
- The field team will have a small fire extinguisher on hand at the place of sUAS operation in case of a battery fire.

C.5. FIRST AID AND MEDICAL

- First aid kit will be on site with the field crew for all site visits.
- Emergency number is 911.
- Nearest hospital location to study site: Cape Regional Medical Center, Cape May Court House, New Jersey (15.5 km, 17 minutes).
- 218 N Main St, Cape May Court House, New Jersey 08210.
- MTRI phone number: (734) 913-6870, Lisa Phillips (Office Manager, MTRI safety lead). Any workplace injury must be reported to Lisa, and appropriate forms must be filled out if medical care is sought due to any workplace injuries.
- ISU phone number: (515) 294-8213, Paul Kremer (Manager Research, CCEE, ISU). Any workplace injury must be reported to Mr. Kremer if medical care is sought due to any workplace injuries.
- APTech. phone number: (217) 398-3977, APTech headquarters in Urbana, Illinois.

C.6. COVID-19 SAFETY

- **Notes:** Most states have lifted COVID-19 restrictions. More information on New Jersey COVID-19 guidance is available at: https://covid19.nj.gov/.
- ISU's COVID-19 Safety Plan
    - The COVID-19 guidelines have been updated for regent institutions in Iowa on May 20, 2021. Mask use continues to be encouraged for those who have not been vaccinated, and optional for those who have been vaccinated.
    - Travelers have been encouraged to adhere to CDC guidance for domestic travel.
    - The team will follow the rules outlined by the Iowa State University Transportation Services while operating the vehicle and properly clean inside the vehicle while returning.
    - All details are available at the following web addresses:

        - COVID-19 guideline update for regent institutions in Iowa: https://www.iowaregents.edu/news/board-news/statement-from-president-mike-richards-lifting-regents-state-of-emergency
        - ISU safety and health policy resources: https://web.iastate.edu/safety/
        - ISU safety policy on COVID-19: https://web.iastate.edu/safety/updates/covid19
        - ISU gathering and events policy: https://web.iastate.edu/safety/updates/covid19/events-gatherings
        - ISU Civil, Construction, and Environmental Engineering (CCEE) safety resources: https://www.ccee.iastate.edu/safety/
        - ISU CCEE research and instructional labs and fieldwork safety policies: https://www.ccee.iastate.edu/files/2019/07/CCEE-Laboratory-Policies-and-Guidelines-CCEE-Safety-and-Health-Committee-and-EHS-Reviewed-and-Approved-2.23.18-3.pdf
- MTRI's COVID-19 Safety Plans
    - MTRI's COVID-19 safety plans have been as follows, and unvaccinated participants are expected to follow them closely:
        - Field crew will stay at least 6 ft apart and wear face coverings when within 10 ft of other people.
        - Field crew travel with hand sanitizer and use it at the beginning and end of the day, and at all breaks.
        - Field equipment will be individually assigned as much as possible (for example, whoever starts with a particular sUAS will use that one throughout the day) and will be disinfected with Lysol®-type wipes when possible.
    - Multiple workers are allowed to travel within the same vehicle when the University's Health and Safety Level is at Level 2.
    - As of 6/9/2021, the University is at Level 2. (https://www.mtu.edu/flex/operations/levels/).
    - Note that there is a cleaning protocol for the MTRI Durango that MUST be followed – laminated copies can be found inside the Durango.
    - Work is to comply with the Michigan Tech COVID-19 Fieldwork protocol and safety checklist found at the locations shown below:
        - COVID-19 Research FAQs: https://www.mtu.edu/research/covid-19/faqs.html
        - Current campus health and safety level: https://www.mtu.edu/flex/operations/levels/
        - Research Pandemic Checklist: Research Pandemic Checklist - Google Docs
    - Now that the University is back at Level 2, travel authorization is obtained through the normal channel of submitting a signed MTRI Travel Authorization Form to the MTRI Co-Directors for their approval, with a cc: to Office Manager/Facility Security Officer, Lisa Phillips. That permission is being obtained for this data collection.

- COVID-19 safety guidelines of Illinois
    - https://coronavirus.illinois.gov/

Note: All website links provided above are accessible during this data collection plan development. However, all websites are not expected to be maintained and updated by the authority in future as the COVID-19 situation is expected to be changed.

APPENDIX D—PAVEMENT CONDITION INDEX DATA COLLECTION PLAN

Applied Pavement Technology, Inc., Field Data Collection and Safety Plan
Custer Airport: January 18–19, 2021
Grosse Ile Municipal Airport: January 19–20, 2021

Applied Pavement Technology, Inc. Survey Team	• Katie Gauthier, P.E. • Trent Montgomery
Schedule	• January 18, 2021: Drive from Champaign-Urbana, Illinois, to Monroe, Michigan • January 18, 2021: Begin data collection at Custer Airport (TTF) • January 19, 2021: Complete data collection at TTF (if necessary), travel to Grosse Ile Municipal Airport (ONZ), and begin data collection • January 20, 2021: Complete data collection at ONZ and return to Champaign-Urbana, Illinois (trip may be extended one day more if additional inspection time is needed)
Airport Contacts TTF and ONZ	TTF: Dan Diesing, (734) 384-9616 ONZ: Michael Duker, (734) 675-0155 Both airports have been contacted, are aware of the schedule and planned activities, and have given permission for the field crew to be on site to perform the described data collection.
Safety Plan	• Inspectors will follow the safety procedures of operating on an active airfield. • ANSI Type II reflective vests will be worn at all times. • Inspectors will work in a group of two. • The vehicles will have a working strobe beacon while on airfields. • All site rules and driving speed limits will be followed. • Crews will monitor UNICOM radio frequencies and use situational awareness to track and react to any aircraft. • The crew will give way to all aircraft movements. • Runway inspection work will be coordinated around aircraft movements. • Inspectors will wear multiple layers of warm clothing. • Inspectors will take breaks to allow them to warm up when needed. • Inspectors will wear proper closed-toed footwear. • Inspectors will remain on paved surfaces when possible. • Inspectors will wear earplugs when aircraft operations are ongoing.

<table>
<tr><td>COVID-19 safety</td><td>See attached APTech COVID-19 Health and Safety Guidelines and Protocols for Fieldwork document. This has been shared with both airport managers.
No meetings are anticipated, but any interactions can occur outside, with all parties wearing masks and maintaining physical distance greater than 6 ft.</td></tr>
<tr><td>Operational Plan for Data Collection</td><td>The crew is performing a visual pavement condition survey within select branches and sections at each airport. The following sample units will be inspected:
<table>
<tr><th colspan="3">TTF</th><th colspan="3">ONZ</th></tr>
<tr><th>Surface</th><th>Section</th><th>Sample Unit</th><th>Surface</th><th>Section</th><th>Sample Unit</th></tr>
<tr><td rowspan="8">A01MN</td><td rowspan="8">10</td><td>1</td><td rowspan="16">RW1735 GI</td><td rowspan="8">10</td><td>03</td></tr>
<tr><td>8</td><td>05</td></tr>
<tr><td>11</td><td>08</td></tr>
<tr><td>17</td><td>12</td></tr>
<tr><td>21</td><td>14</td></tr>
<tr><td>27</td><td>17</td></tr>
<tr><td>30</td><td>20</td></tr>
<tr><td>35</td><td rowspan="15">20</td><td>05</td></tr>
<tr><td rowspan="14">RW321 MN</td><td rowspan="14">10</td><td>3</td><td>14</td></tr>
<tr><td>13</td><td>23</td></tr>
<tr><td>16</td><td>31</td></tr>
<tr><td>23</td><td>40</td></tr>
<tr><td>33</td><td>49</td></tr>
<tr><td>43</td><td>58</td></tr>
<tr><td>53</td><td>67</td></tr>
<tr><td>63</td><td>76</td></tr>
<tr><td>73</td><td>85</td></tr>
<tr><td>83</td><td>94</td></tr>
<tr><td>93</td><td>103</td></tr>
<tr><td rowspan="7">TWAMN</td><td rowspan="7">10</td><td>7</td><td>112</td></tr>
<tr><td>16</td><td colspan="3" rowspan="6"></td></tr>
<tr><td>23</td></tr>
<tr><td>25</td></tr>
<tr><td>29</td></tr>
<tr><td>35</td></tr>
<tr><td>41</td></tr>
</table>
Each crew member will use a handheld tablet computer equipped with a GPS unit to locate and map distresses in each sample unit. The crew will also be taking photographs to document general conditions and specific distresses.</td></tr>
</table>

APPENDIX E—AIRFIELD PAVEMENT DISTRESSES

Key to airport distress types for both asphalt and concrete runways, from the Concrete Surfaced Airfields PAVER Distress Identification Manual (USACE, 2009a) and Asphalt Surfaced Airfields PAVER Distress Identification Manual (USACE, 2009b).

Table E-1. Airfield Pavement Distresses

Asphalt surface		Concrete surface	
Distress type	Distress ID	Distress type	Distress ID
Alligator or Fatigue Cracking	41	Blowup	61
Bleeding	42	Corner break	62
Block Cracking	43	Cracks	63
Corrugation	44	Durability (“D”) Cracking	64
Depression	45	Joint Seal Damage	65
Jet Blast Erosion	46	Patching, Small	66
Joint Reflection Cracking	47	Patching, Large	67
Long and Trans Cracking	48	Pop-outs	68
Oil Spillage	49	Pumping	69
Patching and Utility Cut Patch	50	Scaling	70
Polished Aggregate	51	Settlement or Faulting	71
Raveling	52	Shattered Slab	72
Rutting	53	Shrinkage Cracks	73
Shoving	54	Spalling (Joint)	74
Slippage Cracking	55	Spalling (Corner)	75
Swell	56	Alkali-Silica Reaction	76
Weathering	57		

REFERENCES:

U.S. Army Corps of Engineers (USACE)-Construction Engineering Research Laboratory. (2009a). *Asphalt surfaced airfields—Paver™ distress identification manual*. https://www.faa.gov/documentLibrary/media/Advisory_Circular/Asphalt-Surfaced-Airfields-Distress-Manual.pdf

U.S. Army Corps of Engineers-Construction Engineering Research Laboratory. (2009b). *Concrete surfaced airfields—Paver™ distress identification manual*. https://www.faa.gov/documentLibrary/media/Advisory_Circular/Concrete-Surfaced-Airfields-Distress-Manual.pdf

APPENDIX F— DRAFT GUIDE RECOMMENDING MINIMUM TECHNICAL SPECIFICATIONS AND STANDARD PROCESSES AND PROCEDURES

DRAFT ENGINEERING BRIEF #001

Memorandum

Date: 2/3/2022

To: Mike DiPilato and Matthew Brynick, Technical Points of Contact (POCs)
Federal Aviation Administration (FAA) Airport Technology
William J. Hughes Technical Center, Atlantic City International Airport, New Jersey 08405

From: Halil Ceylan, Ph.D. (Principal Investigator)
Colin N. Brooks, Ph.D. (Co-Principal Investigator)
David G. Peshkin, P.E. (Co-Principal Investigator)
Sunghwan Kim, Ph.D., P.E. (Co-Principal Investigator)

Prepared by: Abdullah Sourav, ABE (Research Assistant)
Halil Ceylan, Ph.D. (Principal Investigator)
Colin N. Brooks, Ph.D. (Co-Principal Investigator)
David G. Peshkin, P.E. (Co-Principal Investigator)
Sunghwan Kim, Ph.D., P.E. (Co-Principal Investigator)

Subject: Draft engineering brief #001, Draft content for a guide recommending minimum technical specifications and standard processes and procedures

This draft Engineering Brief (EB) provides information about the recommended technical specifications for small unmanned aircraft system (sUAS) platforms, sUAS sensors, data types, and data resolutions for airfield pavement distress inspection and rating. It also recommends standard processes and procedures for sUAS data collection, processing, and analysis.

Attachment

Draft Content for a Guide Recommending Minimum Technical Specifications and Standard Processes and Procedures

F.1 PURPOSE

This Engineering Brief (EB) provides information about the recommended technical specifications for small unmanned aircraft system (sUAS) platforms, sUAS sensors, data types, and data resolutions for airfield pavement distress inspection and rating. It also recommends standard processes and procedures of sUAS data collection, processing, and analysis. These recommendations are based on the capabilities of current sUAS technologies and should be updated in the future as these develop.

F.2 BACKGROUND

Early detection and repair of airfield pavement distresses are essential aspects of preserving airport pavements for the full spans of their design periods and maintaining their structural integrity, ride quality, and safety. Routine maintenance and early preservation can minimize pavement deterioration, but only an effective, consistent, and frequently used pavement inspection program can reveal distresses early enough to allow sufficient time to undertake effective corrective measures. ASTM D5340-20 version defines and describes distresses for asphalt and concrete airfield pavements, along with the severity ratings of each distress. The identification and severity assessment of these distresses are the basis for reporting the airfield pavement condition index (PCI), as described in the ASTM standard. Current airfield pavement inspections rely heavily on visual surveys and interpretation of reports and maps prepared by airfield pavement inspectors in the field.

The U.S. Federal Aviation Administration (FAA) defines sUAS as UASs that are under 55 lb (25 kg). sUAS can provide images, three-dimensional information, accurate measurements, and condition data on highways, bridges, and local roads. In the past decade, their use in infrastructure health-monitoring has increased significantly, with the most common use being in construction work progress and highway and bridge inspections. In recent years, various studies have been conducted for pavement distress detection and mapping using alternate data collection methodologies, including sUAS.

There are two primary hardware components of the sUAS for pavement monitoring applications: the sUAS platform and the data collection sensor(s) carried by the platform. The sUAS platforms are commonly available in three types: (1) rotorcraft, (2) fixed-wing, and (3) tethered variants (primarily of rotorcraft). Some platforms also combine the features of these three types. Each platform offers some advantages for specific tasks. Each category's sUAS varies widely in size, weight, speed, range, endurance, payload capacity, and application. Rotorcrafts are the most commonly used sUAS platform for data collection due to their highly adaptable launch and recovery systems, with the capability to hover and collect data from various positions. The sUAS platforms either have or are designed to carry one or more imaging, photogrammetry, thermal, Light Detection and Ranging (LiDAR), and multi/hyperspectral sensors for data collection from different elevations, among others. The optical imaging sensors (common red, green, blue [RGB] natural color optical cameras) used for close-range photogrammetry appear to be the most common. Minimum technical specifications of these sUAS platforms and sensors are provided in this EB along with recommended standard processes and procedures.

F.3 APPLICATION

This EB will be applied to recommend the minimum technical specifications for various types of sUAS and sUAS-mounted sensor technologies to consistently conduct safe, reliable, and effective sUAS airport PMP inspections.

F.4 DESCRIPTION

This EB provides guidance to airfield pavement inspection entities about the use of sUAS to detect and rate airfield pavement distresses.

F.5 EFFECTIVE DATE

To be determined by the FAA.

F.6 MINIMUM TECHNICAL SPECIFICATIONS AND STANDARD PROCESSES AND PROCEDURES

F.6.1 SPECIFICATION OF sUAS

Small and agile sUAS platforms with integrated sensors are recommended for effective and rapid data collection. These systems are easy to operate and expected to have the following characteristics:

A. Practical battery life of more than 20 minutes after keeping 20–30% for the safe return of the sUAS platform.
B. Ability to fly at a wind speed of up to 25 kph/15 mph with occasional wind gusts of up to 40 kph/25 mph.
C. Continuous data collection with flight assistance software that includes automated supervised data collection mission capabilities.

Heavier platforms with the ability to mount sensors are recommended for high-resolution and any specific types of data collection needing special sensors. These systems are expected to have the following specifications:

A. Ability to carry additional payloads such as cameras that can weigh up to 1 kg/2.2 lb.
B. The supported payload should include the ability to carry multiple sensors.
C. Support of automated flight plans with flight assistance software.

F.6.2 SPECIFICATION OF DATA TYPE

RGB optical, Digital Elevation Model (DEM), and stereo thermal data have been demonstrated to have value in airfield distress detection and rating in FAA-sponsored applied research. Table F-1 shows the capability of RGB optical and DEM data for Portland Cement Concrete (PCC) and Asphalt Concrete (AC) pavement distress detection. The RGB optical data and DEM are most valuable when used together for distress detection. The DEM should be viewed with a hillshade model to enhance the evaluation of distresses that typically feature elevation changes, such as faulting. The stereo thermal data are also valuable for detecting crack-based distresses as cracks tend to display different temperatures than the surrounding pavement, whether sealed or unsealed.

Table F-1. Airfield Pavement Distresses Detectable in RGB Optical and DEM Data

Type	Portland Cement Concrete (PCC) Pavement Distresses	Asphalt Concrete (AC) Pavement Distresses
Distresses tested for detection from FAA research	Corner break, LTD cracks, Durability cracking, Joint seal damage, Small patching, Large patching, Pop-outs, Scaling, Faulting, Shattered slab, Shrinkage cracks, Joint spalling, Corner spalling, Alkali-silica reaction (14 available at tested FAA research sites)	Alligator cracking, L&T cracking, Block cracking, Depression, Patching, Raveling, Shoving, Swell, Weathering (9 available at tested sites)
RGB Optical data	Corner break, LTD cracks, Durability cracking, Joint seal damage, Small patching, Large patching, Pop-outs, Scaling, Shattered slab, Shrinkage cracks, Joint spalling, Corner spalling, Alkali-silica reaction (13/14 detectable)	Alligator cracking, L&T cracking, Block cracking, Patching, Raveling, Shoving (6/9 detectable)
DEM	Corner break, LTD cracks, Durability cracking, Joint seal damage, Pop-outs, Scaling, Faulting, Shattered slab, Joint spalling, Corner spalling, Alkali-silica reaction (11/14 detectable)	Alligator cracking, L&T cracking, Block cracking, Depression, Patching, Shoving (6/9 detectable)

Based on the capability, the following sensor types are recommended:

A. RGB optical sensors are recommended if the deployment of only a single sensor is possible. RGB optical and DEM data are adequate to detect the majority of airfield pavement distresses outlined in ASTM D5340.
B. If budget and time permit, thermal, multispectral, and other sensors could be deployed to address specific project needs.

F.6.3 RECOMMENDED RESOLUTIONS

A. Any sUAS system producing an RGB optical orthophoto with resolutions smaller than 5 mm/pix can detect and rate at least some distresses. Resolutions smaller than 2 mm/pix produce the best data for identifying and rating the largest number of distresses.
B. Any sUAS system producing a DEM and stereo thermal orthophoto with resolutions smaller than 20 mm/pix and 30 mm/pix, respectively, are likely to be useful for distress detection and rating for at least some distress types, as listed above.
C. Resolutions of 1.5 mm/pix or smaller RGB optical orthophoto and 6.0 mm/pix or better DEM combination are highly recommended in terms of data collection and processing time with visual details to detect and rate the largest number of distresses.

F.6.4 STANDARD PROCESSES AND PROCEDURES

The recommended standard process and procedures of sUAS data collection, processing, and analysis are provided below:

F.6.4.1 Planning and Preparation

A. Acquire permissions from the airport authority, FAA, and any other relevant entities.
B. Review any long-term or temporary airspace restrictions and prepare ahead of time to fly within some restricted airspace such as areas covered by the automated LAANC permission process.
C. Identify region(s) of interest and focus area(s) (Runway, Taxiway, and Apron).
D. Outline sUAS data collection plan and safety plan. Data collection plans should focus on safe and rapid data collection. Safety plans should emphasize clear communications between data collection teams, airport personnel, and approaching manned aircraft.
E. Develop a Ground Control Point (GCP) map based on the shape and size of the data collection area. The recommended distance between any two GCPs is less than 100 m/328 ft. Positional accuracies for GCPs should be 20 cm/8 in. or better. Real-time Kinematic (RTK) capabilities onboard sUAS could reduce the need for GCPs, but some are still likely to be needed.
F. Plan mission(s) on flight planning assistance software before the data collection day.
G. All sUAS platforms, sensors, controllers, batteries, communication devices, GCPs, and all other necessary devices must be charged and prepared at least one day prior to the data collection.
H. sUAS firmware and any other software should be updated at least a week before the data collection and not changed, if possible, ahead of the data collection. Test flights prior to deployment are recommended following any firmware update or when using a newly acquired sUAS system.

F.6.4.2 Data Collection

A. A stand-up safety briefing should be held at the beginning of data collection days where any team member can bring up safety issues, and the safety plan should be reviewed.
B. All crew members on the field site must wear protective clothing appropriate to the airport environment at all times. A high-visibility safety vest and protective eyewear are the minimum; some airport environments may require hard-toed boots and safety helmets as well.
C. sUAS pilots must have an undistracted spotter with aviation radio watching for vehicle and air traffic and for the safety of the pilot.
D. sUAS should be operated on a give-way basis to any air traffic at the airport.
E. Each data collection team must have an aviation radio on the Unicom frequency of the airport. Announcements should be made before sUAS flights start and after they are completed. An example format is "[Airport name], drone survey crew operating at/over [Runway/Taxiway/Apron] [Number], [Airport name]," e.g., "Grosse Ile, drone survey crew operating over Runway 17/35, Grosse Ile" and "Grosse Ile, drone survey crew completed operations over Runway 17/35, Grosse Ile."
F. GCPs should be put down at the beginning of each day of data collection before sUAS data collections start.
G. Windows of moving vehicles must be kept open, with car radios off, to enable listening for unexpected aircraft when driving on runways and taxiways.
H. Only stand on runways or taxiways during data collection if needed.
I. Do not stand in open traffic lanes present at the airport. If walking along an open stretch of runway, taxiway, or apron, walk against the flow of the traffic.

F.6.4.3 Data Processing

sUAS data can be processed using different close-range photogrammetry applications (Agisoft Metashape, Pix4D, Drone2Map, OpenDroneMap, DroneMapper), some of which are desktop-focused applications and some of which have online platforms or are only online. Each application and platform has a different workflow. However, the following steps of the data processing are recommended:

A. Medium or high setting for image alignment is recommended.
B. Location information of the GCP, if available, must be used.
C. A medium setting for dense cloud generation is recommended. However, the high or very high options can be used based on the resolution requirements.
D. The DEM and orthophoto output must have a projected coordinate system for accurate viewing and simplified measuring of features; Universal Transverse Mercator or State Plane Coordinate System are the most common with a locally appropriate zone, usually with the NAD83 or WGS84 datum.
E. Each processing parameter should be selected based on the number of images to be processed, resolution of the data, estimated time required to complete the processing, and configuration of the computer or cloud-based services being used for the data processing.

F.6.4.4 Data Analysis and PCI Value Calculation

A. All sUAS data available to the image analyst should be used to identify the distresses.
B. If available, the most recent PCI inspection should be used to help understand what distresses are likely to be present.
C. Use of a GIS layer such as a shapefile to identify the sample units is recommended.
D. One GIS layer for each individual distress should be avoided. It is highly recommended to use one line feature GIS layer and one polygon feature to record distress locations and types for all distresses at an airport based on image analysis. These layers could be divided into major sub-areas (e.g., runways, aprons) for convenience.
E. Each identified distress must contain name, severity, area, location, and other necessary information. Some distresses may be possible to identify with automated techniques, but these should be well-documented as being accurate.
F. The GIS layers of distresses should be stored and shared to permit reuse in the future, such as comparison with future surveys.
G. The distresses on a single sample unit should be summarized before they are used for PCI value calculation.
H. PCI calculation software or services such as FAA PAVEAIR or PAVER™ are highly recommended for accurate calculation.

F.6.5 sUAS-BASED INSPECTION INTEGRATION IN PAVEMENT MANAGEMENT PROGRAM

Routine airfield pavement inspection is an essential part of an airfield Pavement Management Program (PMP). The FAA requires an annual pavement condition inspection unless a PCI survey following ASTM standards is used, in which case the interval of airfield inspection can increase to 3 years. A PCI survey can detect and rate all airfield pavement distresses identified in ASTM. In contrast, an sUAS-based inspection can perform very well for detecting and rating many but not all distresses. The distresses that can be both detected and rated using sUAS data are L&T cracks, alligator cracking, and block cracking of AC pavement and corner break; and LTD cracks, D cracking, small patching, large patching, pop-outs, scaling, and shattered slabs of PCC pavement. The number of accurately detectable distresses that can be detected but not necessarily rated is even higher, as shown in Table F-1.

Apart from detection and rating of the airfield pavement distress, sUAS-based survey provides some additional advantages over PCI surveys, which are:

A. 100% surveys through imaging all airport pavement areas rather than the representative sampling used in PCI surveys.
B. A true quantity of the distresses present on the complete airfield pavement as a result of 100% data collection with sUAS.
C. A permanent and accurate location-based photographic record that can be compared to future sUAS photographic imaging surveys, rather than summary statistics or graphic representations.
D. Use of the photographic record for verification of distresses identified in PCI inspection.

E. Ability to apply distinctions of severity level more accurately based on measured dimensions (area, quantity, or length/width), especially for small patching and large patching, and cracking severities.
F. The potential for lower data collection time to collect the same level of details.

Considering the above-mentioned advantages, ***PCI inspection with 5-year interval could be recommended with an sUAS inspection in the third year***, given that:

A. The PCI values are dominated by the distresses accurately detected and rated in sUAS data (L&T cracks, alligator cracking, and block cracking of AC pavement and corner break; and LTD cracks, D cracking, small patching, large patching, pop-outs, scaling, and shattered slabs of PCC pavement).
B. There is absence of materials-related distresses that have the potential to be misidentified with other distresses, like spalling and ASR in PCC pavement.
C. If a drone vendor and an experienced engineer/person with adequate knowledge on standard procedure and processes of airfield distress detection together recommend the sUAS-based survey for one or more distresses based on their judgment.

In addition, sUAS-based inspection can complement (PCI and sUAS-based survey conducted at the same time) the current PCI survey, if time and resources permit. It could be beneficial for an overall pavement condition assessment, keeping a permanent record, and verification of the detection and rating of the distresses. PCI surveys could focus on the most challenging distresses that currently require direct observation, such as detecting likely ASR areas. sUAS data collection could focus on distresses that are time-consuming to identify and where sUAS images and DEM data can make them easier to detect and rate.

F.7 REFERENCES

The following publications form a part of this specification to the extent referenced. The publications are referred to within the text by the basic designation only.

ASTM International (ASTM)

ASTM 150/5380-7B	Airport Pavement Management Program (PMP)
ASTM D5340-20	Standard Test Method for Airport Pavement Condition Index Surveys
ASTM D5340-12	Standard Test Method for Airport Pavement Condition Index Surveys

APPENDIX G—SMALL UNMANNED AIRCRAFT SYSTEM-BASED PAVEMENT CONDITION INDEX INSPECTION DETAILS

All small unmanned aircraft system (sUAS)-based Pavement Condition Index (PCI) inspection results and details are provided in this chapter. The Federal Aviation Administration (FAA) PAVEAIR website was used to calculate the PCI values. For AC pavement PCI calculation, the measurements were directly added to the portal. For Portland cement concrete (PCC) pavement, the number of slabs impacted by a specific distress were used to calculate the affected area which were the input to the FAA PAVEAIR system. In the case of Grosse Ile Municipal Airport (ONZ) in Grosse Ile, Michigan, not all slabs had equal size, thus, areas were calculated directly.

Table G-1. Airfield Pavement Distresses

Asphalt surface		Concrete surface	
Distress type	Distress ID	Distress type	Distress ID
Alligator Or Fatigue Cracking	41	Blowup	61
Bleeding	42	Corner break	62
Block Cracking	43	Cracks	63
Corrugation	44	Durability (“D”) Cracking	64
Depression	45	Joint Seal Damage	65
Jet Blast Erosion	46	Patching, Small	66
Joint Reflection Cracking	47	Patching, Large	67
Long & Trans Cracking	48	Pop-outs	68
Oil Spillage	49	Pumping	69
Patching And Utility Cut Patch	50	Scaling	70
Polished Aggregate	51	Settlement or Faulting	71
Raveling	52	Shattered Slab	72
Rutting	53	Shrinkage Cracks	73
Shoving	54	Spalling (Joint)	74
Slippage Cracking	55	Spalling (Corner)	75
Swell	56	Alkali-Silica Reaction	76
Weathering	57		

Table G-2. The PCI Details of ONZ Airport

Section ID	Section PCI	Sample Number	Sample PCI	Distress	Severity	Number of Distresses	Number of Slabs Affected	Affected Slab Area (sq feet)	sUAS FAA PAVEAIR Quantity Area (sq feet)	Paver Quantity	Units	sUAS PCI
10	34	03	32	62	H	1	1	100	100	1	Slabs	36
				63	L	1	1	100	200	1	Slabs	
				65	H	1	24	2,250	2,250	1	Samples	
				71	L	1	1	100		1	Slabs	
				76	L	24	24	2,250	1,650	12	Slabs	
					M	17	12	1,050	650	12	Slabs	
		05	34	63	L	8	6	598	600	6	Slabs	37
				65	H	1	24	2,240	2,250	1	Samples	
				70	M	1	1	102	100	1	Slabs	
				71	M	2	2	196	200	2	Slabs	
				76	L	24	24	2,241	1,900	20	Slabs	
					M	5	4	299	350	4	Slabs	
		08	19	63	L	6	5	532	900	5	Slabs	31
					M	7	7	730	200	7	Slabs	
				65	H	1	24	2,320	2,250	1	Samples	
				76	L	23	23	2,263	1,200	12	Slabs	
					M	15	12	1,082	750	12	Slabs	
		12	41	63	L	7	6	631	600	5	Slabs	41
				65	H	1	24	2,276	2,250	1	Samples	
				76	L	24	24	2,277	1,350	17	Slabs	
					M	10	7	610	700	7	Slabs	
		14	40	63	L	12	7	699	600	7	Slabs	49
				65	H	1	24	2,245	2,250	1	Samples	
				70	L				100		Slabs	
				76	L	24	24	2,245	1,850	17	Slabs	

Section ID	Section PCI	Sample Number	Sample PCI	Distress	Severity	Number of Distresses	Number of Slabs Affected	Affected Slab Area (sq feet)	sUAS FAA PAVEAIR Quantity Area (sq feet)	Paver Quantity	Units	sUAS PCI
10	34	14	40		M	9	7	597	200	7	Slabs	
		17	31	63	L	14	10	1,047	1,000	10	Slabs	44
					M	2	2	210	100	2	Slabs	
				65	H	1	24	2,349	2,250	1	Samples	
				71	L	2	2	205		2	Slabs	
					M	1	1	108	100	1	Slabs	
				76	L	24	24	2,349	1,850	21	Slabs	
					M	3	3	319	100	3	Slabs	
		20	36	63	L	12	7	693	700	7	Slabs	46
					M	1	1	102		1	Slabs	
				65	H	1	24	2,222	2,250	1	Samples	
				71	L	3	3	296		3	Slabs	
				76	L	24	24	2,223	1,850	20	Slabs	
					M	6	4	355	300	4	Slabs	
20	33	05	20	63	L	3	3	300	900	3	Slabs	17
					M	2	2	200		2	Slabs	
				64	H	2	2	150	200	6	Slabs	
					L	6	6	600	1,050	16	Slabs	
					M	17	17	1,600	200	2	Slabs	
				65	H	1	24	2,250	2,250	1	Samples	
				76	L	12	12	1,200	1,650	12	Slabs	
					M	1	1	100	100	1	Slabs	
		14	26	63	L				300		Slabs	21

Section ID	Section PCI	Sample Number	Sample PCI	Distress	Severity	Number of Distresses	Number of Slabs Affected	Affected Slab Area (sq feet)	sUAS FAA PAVEAIR Quantity Area (sq feet)	Paver Quantity	Units	sUAS PCI
20	33			64	H	3	2	100	100	2	Slabs	
					L	4	4	350	100	3	Slabs	
					M	16	16	1,500	1,550	15	Slabs	
				65	H	1	24	2,250	2,250	1	Samples	
				76	L	24	24	2,250	1,900	24	Slabs	
					M				300	24	Slabs	
		23	3	63	M	4	4	400	300	4	Slabs	4
					L				100			
				64	H	9	5	350	550	5	Slabs	
					M	17	17	1,550	1,100	13	Slabs	
				65	H	1	24	2,250	2,250	1	Samples	
				67	H	3	3	300	300	3	Slabs	
					L	5	5	450	450	5	Slabs	
					M	1	1	100	100	1	Slabs	
				71	L	1	1	100		1	Slabs	
					M	1	1	100	100	1	Slabs	
				72	M	1	1	100	100	1	Slabs	
				76	M				100			
					L	15	15	1,350	1,100	14	Slabs	
		31	28	63	L	2	2	200	400	1	Slabs	13
					M	2	2	200	200	2	Slabs	
				64	H	2	1	100	350	1	Slabs	
					L	4	4	350	700	4	Slabs	
					M	20	20	1,900	1,200	19	Slabs	
				65	H	1	24	2,250	2,250	1	Samples	
				76	L	12	12	1,100	1,550	12	Slabs	

Section ID	Section PCI	Sample Number	Sample PCI	Distress	Severity	Number of Distresses	Number of Slabs Affected	Affected Slab Area (sq feet)	sUAS FAA PAVEAIR Quantity Area (sq feet)	Paver Quantity	Units	sUAS PCI
20	33	40	38	64	L	5	5	496	1,000	5	Slabs	39
					M	19	19	1,715	1,250	19	Slabs	
				65	H	1	24	2,211	2,250	1	Samples	
				76	L	13	13	1,139	1,350	13	Slabs	
		49	29	62	M	1	1	100	100	1	Slabs	28
				63	L				100			
					M	2	2	200	100	2	Slabs	
				64	L	8	8	800	1,050	5	Slabs	
					M	16	16	1,450	1,200	16	Slabs	
				65	H	1	24	2,250	2,250	1	Samples	
				71	M	1	1	100	100	1	Slabs	
				76	L	6	6	600	1,250	3	Slabs	
		58	50	64	L	14	14	1,400	1,400	14	Slabs	51
					M	10	10	850	850	10	Slabs	
				65	H	1	24	2,250	2,250	1	Samples	
				64	H				50			
		67	46	64	L	6	6	600	950	6	Slabs	39
					H				50			
					M	18	18	1,650	1,250	18	Slabs	
				65	M	1	24	2,250	2,250	1	Samples	
				76	L				300	1	Samples	
		76	46	64	L	7	7	700	500	7	Slabs	46
					M	17	17	1,550	1,750	17	Slabs	
				65	H	1	24	2,250	2,250	1	Samples	
		85	46	64	L	6	6	600	400	6	Slabs	46

Section ID	Section PCI	Sample Number	Sample PCI	Distress	Severity	Number of Distresses	Number of Slabs Affected	Affected Slab Area (sq feet)	sUAS FAA PAVEAIR Quantity Area (sq feet)	Paver Quantity	Units	sUAS PCI
20	33				M	18	18	1,650	1,850	18	Slabs	
				65	H	1	24	2,250	2,250	1	Samples	
		94	42	64	L	10	10	1,000	300	10	Slabs	41
					M	14	14	1,250	1,950	14	Slabs	
				65	H	1	24	2,250	2,250	1	Samples	
				76	L	6	6	600	200	6	Slabs	
		103	34	62	L	1	1	50		1	Slabs	40
				64	H	1	1	100		1	Slabs	
					L	12	12	750	500	11	Slabs	
					M	19	19	1,125	1,750	19	Slabs	
				65	H	1	32	2,250	2,250	1	Samples	
				71	L	2	2	100		2	Slabs	
				76	L	12	10	750	950	12	Slabs	
		112	17	64	H	13	6	550	600	6	Slabs	15
					L	16	16	1,500	650	10	Slabs	
					M	9	8	750	1,000	7	Slabs	
				65	H	1	24	2,250	2,250	1	Samples	
				76	L	6	6	550	500	6	Slabs	
					M	1	1	100		1	Slabs	

Table G-3. The PCI Details of TTF Airport

Branch	Section	Section PCI	Sample Number	Sample PCI	Distress	Severity	Quantity	sUAS FAA PAVEAIR Quantity	PAVER Quantity	Units	sUAS PCI
RW32 1MN	10	74	03	66	48	L	86	149	86	Ft	76
						M	218	134	218	Ft	
					57	L	5,000		5,000	SqFt	
			13	80	48	L	82	93	82	Ft	86
						M	39	32	39	Ft	
					57	L	5,000		5,000	SqFt	
			16	69	48	L	103	111.2	103	Ft	83
						M	99	54.8	99	Ft	
					56	L	104		104	SqFt	
					57	L	5,000		5,000	SqFt	
			23	90	48	L	36	52.87	36	Ft	94
					57	L	5,000		5,000	SqFt	
			33	70	48	L	211	360	211	Ft	76
						M	163	38	163	Ft	
					57	L	5,000		5,000	SqFt	
			43	71	48	L	106	153	106	Ft	83
						M	137	60	137	Ft	
					57	L	5,000		5,000	SqFt	
			53	70	48	L	174	161	174	Ft	79
						M	136	99	136	Ft	
					56	L	8		8	SqFt	
					57	L	5,000		5,000	SqFt	
			63	67	48	L	99	74	99	Ft	73
						M	203	201	203	Ft	
					57	L	5,000		5,000	SqFt	
			73	77	48	L	200	181	200	Ft	83

Branch	Section	Section PCI	Sample Number	Sample PCI	Distress	Severity	Quantity	sUAS FAA PAVEAIR Quantity	PAVER Quantity	Units	sUAS PCI
RW32 1MN	10	74				M	61	42	61	Ft	83
					57	L	5,000		5,000	SqFt	
			83	75	48	L	206	243	206	Ft	81
						M	93	35	93	Ft	
					57	L	5,000		5,000	SqFt	
			93	74	48	L	160	181	160	Ft	83
						M	102	51	102	Ft	
					57	L	5,000		5,000	SqFt	
TWA MN	10	63	07	56	48	L	113	85	113	Ft	71
						M	200	206	200	Ft	
					52	L	139		139	SqFt	
						M	25		25	SqFt	
					57	M	4,350		4,350	SqFt	
			16	65	48	L	82	29	82	Ft	76
						M	125	162	125	Ft	
					52	L	178		178	SqFt	
					57	M	4,375		4,375	SqFt	
			23	65	48	L	162	105	162	Ft	76
						M	125	125	125	Ft	
					52	L	95		95	SqFt	
					57	M	4,375		4,375	SqFt	
			25	66	48	L	56	34	56	Ft	78
						M	133	133	133	Ft	
					52	L	252		252	SqFt	
					57	M	4,375		4,375	SqFt	
			29	65	48	L	98	98	98	Ft	73
						M	161	156	161	Ft	

Branch	Section	Section PCI	Sample Number	Sample PCI	Distress	Severity	Quantity	sUAS FAA PAVEAIR Quantity	PAVER Quantity	Units	sUAS PCI
TWA MN	10	63			52	L	64		64	SqFt	73
					57	M	4,375		4,375	SqFt	
			35	63	48	L	174	197	174	Ft	75
						M	170	131	170	Ft	
					52	L	166		166	SqFt	
					57	M	4,375		4,375	SqFt	
			41	63	48	L	257	225	257	Ft	71
						M	171	198	171	Ft	
					52	L	24		24	SqFt	
					57	M	4,375		4,375	SqFt	

Table G-4. The PCI Details of AC Pavement of MTO Airport

Branch	Section	Section PCI	Sample Number	Sample PCI	Distress	Severity	PAVER Quantity	sUAS FAA PAVEAIR Quantity	Units	sUAS PCI
DMTO	1	26	01	26	41	L	380	470	SqFt	28
					43	M		4,800	SqFt	
					48	H	48	47	Ft	
						L	567		Ft	
						M	788		Ft	
					57	M	5,000		SqFt	
			02	26	41	L	315	300	SqFt	31
					43	M		4,800	SqFt	
					48	H	45	45	Ft	
						L	629		Ft	
						M	838		Ft	
					57	M	5,000		SqFt	

Branch	Section	Section PCI	Sample Number	Sample PCI	Distress	Severity	PAVER Quantity	sUAS FAA PAVEAIR Quantity	Units	sUAS PCI
DMTO	1	26	04	27	41	L	242	470	SqFt	30
					43	M		4,800	SqFt	
					48	H	21	20	Ft	
						L	891		Ft	
						M	705		Ft	
					57	M	5,000		SqFt	
			06	26	41	L	296	450	SqFt	28
					43	M		4,800	SqFt	
					48	H	50	52	Ft	
						L	813		Ft	
						M	703		Ft	
					57	M	5,000		SqFt	
D3MTO	1	16	02	16	41	L	196	282	SqFt	34
					43	M		4,006		
					48	H	50	49	Ft	
						L	675		Ft	
						M	719		Ft	
					52	M	5,000		SqFt	
RMTO	3	57	01	57	45	L	8		SqFt	61
					48	L	1,013	1,003	Ft	
					54	L	150	120	SqFt	
					57	M	5,000		SqFt	
			04	57	48	L	1,091	1,001	Ft	66
						M	1		Ft	
					57	M	5,000		SqFt	

Table G-5. The PCI Details of PCC Pavement of MTO Airport

Branch	Section ID	Section PCI	Sample Number	Sample PCI	Distress	Severity	Quantity	Number of Slabs Affected	PAVER Quantity	sUAS Paver Quantity	PAVER Units	sUAS PCI
DMTO	4	40	01	40	63	L	130.79	7	6	1	Slabs	42
						M	143.62	7	7	9	Slabs	
					65	L	1.00	1	20		Slabs	
					72	M	504.00	1	1	1	Slabs	
					73	NA	16.38	3	3		Slabs	
					75	L	0.12	1	1		Slabs	
DMTO	5	84	01	69	63	M	40.88	2	2	2	Slabs	75
					65	L	1.00	1	18		Slabs	
					73	NA	8.39	3	3		Slabs	
					74	L	0.05	1	1		Slabs	
						M	0.55	1	1	1	Slabs	
			02	98	65	L	1.00	1	18		Slabs	100

Table G-5. The PCI Details of PRO Airport

Section ID	Section PCI	Sample Number	Sample PCI	Distress	Severity	Number of Distresses	Number of Slabs Affected	Paver Quantity	sUAS FAA PAVEAIR Quantity	PAVER Units	sUAS PCI
03	14	02	9	63	L	7	5	2	6	Slabs	6
					M	6	5	3	5	Slabs	
				65	L	1	1	12		Slabs	
				72	M	2	2	2	2	Slabs	
				73	NA	1	1	0		Slabs	
				75	L	2	2	2		Slabs	
				76	L	9	7	2	3	Slabs	
					M	17	8	6	7	Slabs	

Section ID	Section PCI	Sample Number	Sample PCI	Distress	Severity	Number of Distresses	Number of Slabs Affected	Paver Quantity	sUAS FAA PAVEAIR Quantity	PAVER Units	sUAS PCI
03	14	03	13	63	L	8	5	4	3	Slabs	9
					M	6	5	4	4	Slabs	
				65	L	1	1	12		Slabs	
				72	M	1	1	1		Slabs	
				73	NA	1	1	1		Slabs	
				74	M	3	3	1	3	Slabs	
					H	2	2	2	3	Slabs	
				75	L	1	1	1	3	Slabs	
					M	2	2	2	1	Slabs	
				76	L	1	1	0		Slabs	
					M	2	2	1		Slabs	
					H	1	1	0	1	Slabs	
		04	3	63	L	4	2	0	1	Slabs	5
					M	12	8	6	6	Slabs	
				65	M	1	1	12		Slabs	
				71	L	2	2	1		Slabs	
				72	M	2	2	2		Slabs	
					H	2	2	2		Slabs	
				73	NA	1	1	1		Slabs	
				74	L	1	1	1	1	Slabs	
					M	1	1	1	1	Slabs	
				75	L	5	3	3	2	Slabs	
					M	4	3	2	2	Slabs	
				76	M	1	1	1		Slabs	
					H	3	3	0	3	Slabs	
		06	20	62	L	2	2	1		Slabs	15
				63	L	8	4	2	3	Slabs	

Section ID	Section PCI	Sample Number	Sample PCI	Distress	Severity	Number of Distresses	Number of Slabs Affected	Paver Quantity	sUAS FAA PAVEAIR Quantity	PAVER Units	sUAS PCI
03	14	06			M	4	4	3	4	Slabs	15
				65	L	1	1	16		Slabs	
				72	M	2	2	2		Slabs	
				73	NA	2	1	1		Slabs	
				74	L	1	1	1		Slabs	
				74	M				1	Slabs	
				75	L	8	6	2	3	Slabs	
					M	4	4	4	3	Slabs	
					H	1	1	1		Slabs	
				76	L	1	1	0	1	Slabs	
					M	6	4	2	4	Slabs	
		09	18	63	L	8	6	4	4	Slabs	8
					M	4	3	2	2	Slabs	
				65	L	1	1	16		Slabs	
				72	M	1	1	1	1	Slabs	
				73	NA	8	4	2		Slabs	
				74	H	3	2	2	2	Slabs	
				75	L	4	4	2	2	Slabs	
					M	2	2	2	4	Slabs	
					H	1	1	1		Slabs	
				76	L	7	3	0	3	Slabs	
					M	16	8	7	7	Slabs	
		11	16	63	L	10	6	2	2	Slabs	
					M	9	8	5	7	Slabs	
				65	M	1	1	17		Slabs	
				66	L	2	2	1	2	Slabs	
				72	M	2	2	2		Slabs	

Section ID	Section PCI	Sample Number	Sample PCI	Distress	Severity	Number of Distresses	Number of Slabs Affected	Paver Quantity	sUAS FAA PAVEAIR Quantity	PAVER Units	sUAS PCI
03	14			73	NA	13	9	6		Slabs	14
				74	L				2	Slabs	
				74	M	2	2	1	1	Slabs	
				75	L	8	6	4	2	Slabs	
					M	5	3	1	3	Slabs	
				76	L	3	3	3		Slabs	
					M	3	1	0	1	Slabs	
					H	2	1	1	1	Slabs	
01	25	04	18	62	M	3	3	3	3	Slabs	42
				63	L	1	1	1	1	Slabs	
					M	2	2	2	1	Slabs	
				65	H	1	1	24	24	Slabs	
				66	H	1	1	1		Slabs	
				71	L	11	9	4		Slabs	
					M	9	7	2		Slabs	
					H	7	6	6		Slabs	
				75	L	2	2	2	2	Slabs	
					M	2	2	2	1	Slabs	
				76	L	14	11	8	1	Slabs	
					M	3	3	3	3	Slabs	
		07	30	63	L	1	1	1	1	Slabs	66
				65	H	1	1	24	24	Slabs	
				67	L	1	1	1	1	Slabs	
				71	L	3	3	1		Slabs	
					M	6	5	4		Slabs	
					H	4	4	4		Slabs	
				74	L	4	3	3	3	Slabs	

Section ID	Section PCI	Sample Number	Sample PCI	Distress	Severity	Number of Distresses	Number of Slabs Affected	Paver Quantity	sUAS FAA PAVEAIR Quantity	PAVER Units	sUAS PCI
01	25			75	M	1	1	1	1	Slabs	66
					H	1	1	1	1	Slabs	
				76	L	13	6	6	3	Slabs	
		11	51	63	M	1	1	1		Slabs	62
				65	H	1	1	24	24	Slabs	
				71	L	7	7	5		Slabs	
					M	3	2	2		Slabs	
				73	NA	1	1	1		Slabs	
				75	L	1	1	1	1	Slabs	
					M	5	5	5	3	Slabs	
				76	L				2	Slabs	
				76	L	5	3	3	2	Slabs	
		15		62	M	2	2	2	3	Slabs	
					H	1	1	1		Slabs	
				63	L	5	5	3	8	Slabs	
					M	17	8	4	6	Slabs	
				65	H	1	1	24	24	Slabs	
				66	H	1	1	1		Slabs	
				67	L	1	1	0	1	Slabs	
				71	L	3	3	0		Slabs	
					M	5	4	2		Slabs	
					H	5	5	3		Slabs	
				72	M	4	4	4	4	Slabs	
				74	L				1	Slabs	
				75	L	1	1	1		Slabs	
					M	3	3	3	3	Slabs	
					H	2	2	2		Slabs	

Section ID	Section PCI	Sample Number	Sample PCI	Distress	Severity	Number of Distresses	Number of Slabs Affected	Paver Quantity	sUAS FAA PAVEAIR Quantity	PAVER Units	sUAS PCI
01	25	15	14	76	L	11	6	6	5	Slabs	15
					M	2	2	2	2	Slabs	
		18	14	62	L	1	1	1		Slabs	39
					M	2	2	1	2	Slabs	
				63	L	1	1	0		Slabs	
					M	1	1	0		Slabs	
				65	H	1	1	24	24	Slabs	
				66	L	3	3	3	2	Slabs	
					H	1	1	1		Slabs	
				67	L	1	1	1	1	Slabs	
				71	L	2	2	0		Slabs	
					M	4	4	3		Slabs	
					H	5	5	5		Slabs	
				72	M	1	1	1		Slabs	
				74	M	1	1	1	1	Slabs	
				75	L	6	4	2	2	Slabs	
					M	7	7	6	6	Slabs	
				76	L	23	15	14	4	Slabs	
					M	4	4	4	5	Slabs	
		22	19	62	M	1	1	1	1	Slabs	45
				63	L	1	1	1	1	Slabs	
					M	17	11	10		Slabs	
				65	H	1	1	24	24	Slabs	
				66	L	1	1	0	13	Slabs	
				67	L	3	3	3	3	Slabs	
				71	L	3	3	1		Slabs	
					M	6	6	5		Slabs	

Section ID	Section PCI	Sample Number	Sample PCI	Distress	Severity	Number of Distresses	Number of Slabs Affected	Paver Quantity	sUAS FAA PAVEAIR Quantity	PAVER Units	sUAS PCI
01	25	22	19		H	1	1	1		Slabs	45
				72	M	1	1	1	1	Slabs	
				73	NA	1	1	1		Slabs	
				75	L	4	4	3	1	Slabs	
					M	4	4	4	3	Slabs	
				76	L	5	4	3	1	Slabs	
					M	1	1	1		Slabs	
		25	29	62	L				1		33
				63	L	1	1	1	1	Slabs	
				65	H	1	1	24	24	Slabs	
				66	L	4	4	4	2	Slabs	
					M	1	1	1	1	Slabs	
				67	M				1	Slabs	
					L	1	1	1	1	Slabs	
				71	L	11	9	8		Slabs	
					M	2	2	2		Slabs	
				74	L	1	1	1		Slabs	
					M	2	2	2	3	Slabs	
					H	1	1	1		Slabs	
				75	L	13	10	5	3	Slabs	
					M	6	6	6	5	Slabs	
					H	2	2	2	1	Slabs	
				76	L	11	8	4		Slabs	
					M	8	7	7		Slabs	
		28	28	62	L	1	1	1		Slabs	41
					M	1	1	1		Slabs	
				63	L	1	1	1		Slabs	

Section ID	Section PCI	Sample Number	Sample PCI	Distress	Severity	Number of Distresses	Number of Slabs Affected	Paver Quantity	sUAS FAA PAVEAIR Quantity	PAVER Units	sUAS PCI
01	25	28	28		M				1	Slabs	41
				65	H	1	1	24	24	Slabs	
				66	L	3	3	3	4	Slabs	
					M	1	1	1		Slabs	
				67	L				1	Slabs	
				71	L	8	7	5		Slabs	
					M	3	3	3		Slabs	
				74	M	2	2	2	3	Slabs	
					H	2	2	2	2	Slabs	
				75	L	5	5	3	2	Slabs	
					M	12	7	6	6	Slabs	
					H	1	1	1		Slabs	
				76	L	6	5	3	2	Slabs	
					M	2	2	2	1	Slabs	

Table G-6. The PCI Details of PCC Pavement of WWD Airport

Section ID	Section PCI	Sample Number	Sample PCI	Distress	Severity	Number of Distresses	Number of Slabs Affected	PAVER Quantity	sUAS FAA PAVEAIR Quantity	PAVER Units	sUAS PCI
40		4	56	66	L	7	6	6	6	Slabs	78
				67	L	2	2	2	2	Slabs	
				73		7	7	7	3	Slabs	
				74	L	1	1	1	1	Slabs	
				75	L	3	3	3	3	Slabs	
				75	M	1	1	1		Slabs	
				76	L	2	2	1		Slabs	
				76	M	1	1	1		Slabs	
		10	65	63	L	1	1	1	1	Slabs	71
				63	M	1	1	1	1	Slabs	
				66	L	2	2	2	1	Slabs	
				67	L	4	3	3	4	Slabs	
				73		1	1	1	1	Slabs	
				74	M	2	1	1		Slabs	
				75	L	2	2	1	2	Slabs	
				75	M	2	2	2		Slabs	
		19	31	63	L				1	Slabs	
				63	M	5	4	4	3	Slabs	
				66	L	15	9	8	8	Slabs	
				66	M	1	1	1	1	Slabs	
				67	L	5	5	5	6	Slabs	
				71	L	4	3	3		Slabs	
				73		1	1	1	1	Slabs	
				75	L	4	4	3	3	Slabs	
				75	M	4	3	3	2	Slabs	

Section ID	Section PCI	Sample Number	Sample PCI	Distress	Severity	Number of Distresses	Number of Slabs Affected	PAVER Quantity	sUAS FAA PAVEAIR Quantity	PAVER Units	sUAS PCI
40	47	19	31	75	H	3	2	2	2	Slabs	45
				76	L	2	2	2		Slabs	
				76	M	2	2	2		Slabs	
		20	34	63	L	2	2	2		Slabs	
				63	M	1	1	1		Slabs	
				66	L	10	8	8		Slabs	
				67	L	7	6	6		Slabs	
				71	L	3	3	3		Slabs	
				73		2	2	2		Slabs	
				74	L	2	1	1		Slabs	
				74	M	1	1	1		Slabs	
				75	M	1	1	1		Slabs	
				75	H	1	1	1		Slabs	
				76	L	15	8	4		Slabs	
				76	M	9	5	5		Slabs	
		22	51	63	L	1	1	1	1	Slabs	61
				66	L	6	6	5	5	Slabs	
				66	M	2	2	2	3	Slabs	
				66	H	1	1	1		Slabs	
				67	L	8	8	8	7	Slabs	
				73	L	1	1	1	1	Slabs	
				75	L	5	5	5	2	Slabs	
				75	M	1	1	1		Slabs	
				76	L	2	2	2	1	Slabs	
		35	48	63	L	1	1	1		Slabs	
				66	L	8	6	6		Slabs	
				71	L	4	4	3		Slabs	

Section ID	Section PCI	Sample Number	Sample PCI	Distress	Severity	Number of Distresses	Number of Slabs Affected	PAVER Quantity	sUAS FAA PAVEAIR Quantity	PAVER Units	sUAS PCI
40	47	35	48	71	M	1	1	1		Slabs	
				73		6	6	6		Slabs	
				74	L	2	2	2		Slabs	
				74	M	2	2	2		Slabs	
				75	M	1	1	1		Slabs	
				76	L	5	3	3		Slabs	
				76	M	1	1	1		Slabs	
		40	49	63	L	1	1	1	1	Slabs	59
				63	M	1	1	1	1	Slabs	
				65	L	1	1	20	1	Slabs	
				66	L	14	11	11	8	Slabs	
				67	L	2	2	2	4	Slabs	
				73	L	1	1	1		Slabs	
				74	L	1	1	1	2	Slabs	
				74	M	2	2	2	1	Slabs	
				75	L	4	4	4		Slabs	
				75	M				2		
				76	L	2	2	2		Slabs	
				76	M	1	1	1		Slabs	
		45	48	63	L	2	2	2	2	Slabs	57
				65	L	1	1	20		Slabs	
				66	L	8	7	7	4	Slabs	
				66	M	1	1	1	2	Slabs	
				67	L	4	4	4	6	Slabs	
				71	L	2	2	2		Slabs	
				74	L	4	3	3	3	Slabs	
				75	L	4	4	4	3	Slabs	

Section ID	Section PCI	Sample Number	Sample PCI	Distress	Severity	Number of Distresses	Number of Slabs Affected	PAVER Quantity	sUAS FAA PAVEAIR Quantity	PAVER Units	sUAS PCI
40	47			76	L	1	1	1		Slabs	57
				76	M	1	1	1		Slabs	
		55	63	63	L	4	3	3	3	Slabs	60
				66	L	11	9	8	8	Slabs	
				66	M	1	1	1	1	Slabs	
				67	L	1	1	1	3	Slabs	
				73	N/A	5	4	4	4	Slabs	
				74	L	1	1		1		
				74	M	1	1	1		Slabs	
				75	L	1	1	1	2	Slabs	
				75	M	2	2	2	1	Slabs	
		60	60	66	L	8	5	5	4	Slabs	81
				66	M				1	Slabs	
				67	L	1	1	1	2	Slabs	
				73	N/A	9	9	9	5	Slabs	
				76	L	6	4	4	2	Slabs	
				76	M	2	2	2	1	Slabs	
		64	51	66	L	3	3	3	3	Slabs	49
				73		1	1	1		Slabs	
				74	L	1	1	1	1	Slabs	
				76	L	21	13	6	10	Slabs	
				76	M	7	7	7	6	Slabs	
		69	71	66	L	3	3	3	3	Slabs	83
				71	L	1	1	1		Slabs	
				73	N/A	12	12	12	11	Slabs	
				74	L	1	1	1		Slabs	
				75	L				2	Slabs	

Section ID	Section PCI	Sample Number	Sample PCI	Distress	Severity	Number of Distresses	Number of Slabs Affected	PAVER Quantity	sUAS FAA PAVEAIR Quantity	PAVER Units	sUAS PCI
40	47	69	71	75	M	3	3	3	1	Slabs	83
				76	L	3	3	3		Slabs	
		75	61	63	M	1	1	1	1	Slabs	73
				66	L	4	4	4	5	Slabs	
				66	M	1	1	1		Slabs	
				73	N/A	4	4	4	1	Slabs	
				75	L	1	1	1	2	Slabs	
				76	L	2	1		1		
				76	M	2	2	2		Slabs	
		80	40	66	L	8	7	6	7	Slabs	43
				66	M	4	4	4	2	Slabs	
				67	L	1	1	1	3	Slabs	
				73		2	2	1		Slabs	
				75	L	1	1	1	1	Slabs	
				76	L	6	5		3		
				76	M	11	9	11	7	Slabs	
		89	46	63	M	1	1	1	1	Slabs	51
				66	L	7	5	5	2	Slabs	
				67	L	5	4	4	6	Slabs	
				67	M	1	1	1	1	Slabs	
				73	N/A	14	14	12	10	Slabs	
				75	L	1	1	1	1	Slabs	
				76	L	9	5	3	3	Slabs	
				76	M	2	2	2	1	Slabs	
		95	29	63	M	5	5	5		Slabs	
				63	H	1	1	1		Slabs	
				65	L	1	1	20		Slabs	

Section ID	Section PCI	Sample Number	Sample PCI	Distress	Severity	Number of Distresses	Number of Slabs Affected	PAVER Quantity	sUAS FAA PAVEAIR Quantity	PAVER Units	sUAS PCI
40	47	95	29	66	L	6	4	4		Slabs	
				67	L	6	3	2		Slabs	
				67	M	1	1	1		Slabs	
				73	N/A	1	1	1		Slabs	
				75	L	2	2	2		Slabs	
				76	L	7	3				
				76	M	8	3	3		Slabs	
		100	19	63	L				2		37
				63	M	1	1	1		Slabs	
				66	L	18	10	10	7	Slabs	
				67	L	23	15	11	15	Slabs	
				67	M	4	4	4	4	Slabs	
				71	L	2	2	2		Slabs	
				73	N/A	5	5	3	2	Slabs	
				74	L	2	1	1		Slabs	
				74	M				1		
				75	M	1	1	1		Slabs	
				76	L	31	15		7		
				76	M	11	10	18	7	Slabs	
		102	38	63	L	3	3	3	2	Slabs	35
				63	M	1	1	1	1	Slabs	
				66	L	8	7	7	7	Slabs	
				67	L	10	7	6	10	Slabs	
				67	M	1	1	1	1	Slabs	
				73	N/A	6	6	6	2	Slabs	
				74	L	2	2	2	3	Slabs	
				74	M	2	1	1	2	Slabs	

Section ID	Section PCI	Sample Number	Sample PCI	Distress	Severity	Number of Distresses	Number of Slabs Affected	PAVER Quantity	sUAS FAA PAVEAIR Quantity	PAVER Units	sUAS PCI
40	47	102	38	75	L	2	2	2		Slabs	35
				76	L	12	7	5	2	Slabs	
				76	M	3	3	3	3	Slabs	
		109	20	63	M	1	1	1		Slabs	
				66	L	13	8	7		Slabs	
				66	M	1	1				
				67	L	20	11	9		Slabs	
				67	M	1	1	1		Slabs	
				73	N/A	1	1	1		Slabs	
				74	M	1	1	1		Slabs	
				76	L	23	10	4		Slabs	
				76	M	16	8	7		Slabs	
				76	H	1	1	1		Slabs	

Table G-7. The PCI Details of AC Pavement of WWD Airport

Section ID	Section PCI	Sample ID	Sample PCI	Distress	Severity	PAVER Quantity	sUAS FAA PAVEAIR Quantity	PAVER Units	sUAS PCI
30	49	3	48	48	L	298.5		Ft	
				48	M	281.4		Ft	
				52	L	4,283.0		SqFt	
				52	M	1,017.0		SqFt	
		11	48	48	L	541.1	386.0	Ft	
				48	M	387.2	357.0	Ft	
				52	L	5,050.0	5,050.0	SqFt	52.0
		14	56	48	L	806.8	608.0	Ft	
				48	M	95.7	78.0	Ft	
				52	L	5,000.0	5,000.0	SqFt	59.0
		18	46	48	L	626.7	738.0	Ft	
				48	M	129.5		Ft	
				52	L	3,850.0	4,456.0	SqFt	
				52	M	1,150.0	544.0	SqFt	48.0
		19	53	48	L	627.7	597.0	Ft	
				48	M	207.6	125.0	Ft	
				52	L	5,000.0	5,000.0	SqFt	56.0
		23	50	48	L	646.3	575.0	Ft	
				48	M	268.0	107.0	Ft	
				52	L	5,000.0	5,000.0	SqFt	57.0
		26	54	42			2,043.0	SqFt	
				48	L	872.8	316.0	Ft	
				48	M	117.8	15.0	Ft	
				52	L	5,000.0	5,000.0	SqFt	52.0

Section ID	Section PCI	Sample ID	Sample PCI	Distress	Severity	PAVER Quantity	sUAS FAA PAVEAIR Quantity	PAVER Units	sUAS PCI
30	49	28	37	42	L		491.0	SqFt	45.0
				48	L	397.9	340.0	Ft	
				48	M	16.7	5.0	Ft	
				52	L	2,704.0	3,442.0	SqFt	
				52	M	1,034.0	1,558.0	SqFt	
				52	H	62.0		SqFt	
				54	L	264.0	250.0	SqFt	
		33	43	48	L	162.9	106.0	Ft	49.0
				48	M	166.1	157.0	Ft	
				52	L	1,969.0	3,726.0	SqFt	
				52	M	1,071.0	1,274.0	SqFt	
10C	56	2	47	41	L	30.0		SqFt	64.0
				48	L	172.5	110.0	Ft	
				48	M	405.6	384.0	Ft	
				57	M	4,810.0		SqFt	
				57	H	190.0		SqFt	
		8	56	48	L	253.2	199.0	Ft	63.0
				48	M	423.0	395.6	Ft	
				57	M	5,000.0		SqFt	
		11	57	48	L	204.2	134.4	Ft	64.0
				48	M	399.5	370.7	Ft	
				57	M	5,000.0		SqFt	
		14	55	48	L	195.8	137.8	Ft	61.0
				48	M	465.7	441.1	Ft	
				57	M	5,000.0		SqFt	
		20	57	48	L	252.4	176.4	Ft	59.0

Section ID	Section PCI	Sample ID	Sample PCI	Distress	Severity	PAVER Quantity	sUAS FAA PAVEAIR Quantity	PAVER Units	sUAS PCI
				48	M	291.0	266.6	Ft	59.0
				57	M	4,779.9		SqFt	
				57	H	220.1		SqFt	
		26	65	48	L	297.6	166.7	Ft	
				48	M	188.5	211.2	Ft	
				57	M	5,000.0		SqFt	72.0
		32	58	48	L	210.0	94.9	Ft	
				48	M	377.8	333.6	Ft	
				57	M	5,000.0		SqFt	66.0
		35	58	48	L	201.5	194.5	Ft	
				48	M	382.3	259.1	Ft	
				57	M	5,000.0		SqFt	69.0
		38	54	48	L	184.6	187.1	Ft	
				48	M	490.0	424.2	Ft	
				57	M	5,000.0		SqFt	62.0
10N	46	1	49	48	L	188.8	131.3	Ft	
				48	M	492.8	454.9	Ft	
				57	M	4,936.0		SqFt	
				57	H	64.0		SqFt	61.0
		7	51	48	L	259.2	201.0	Ft	
				48	M	574.6	464.8	Ft	
				57	M	5,000.0		SqFt	60.0
		10	51	48	L	304.8	186.7	Ft	
				48	M	580.6	542.7	Ft	
				57	M	5,000.0		SqFt	57.0
		13	53	48	L	174.6	79.3	Ft	61.0

Section ID	Section PCI	Sample ID	Sample PCI	Distress	Severity	PAVER Quantity	sUAS FAA PAVEAIR Quantity	PAVER Units	sUAS PCI
10N	46	13	53	48	M	515.2	495.8	Ft	61.0
				57	M	5,000.0		SqFt	
		19	46	48	L	168.4	91.5	Ft	59.0
				48	M	576.1	538.0	Ft	
				57	M	4,832.0		SqFt	
				57	H	168.0		SqFt	
		25	42	45	H	1.5	1.5	SqFt	48.0
				48	L	83.5	55.8	Ft	
				48	M	630.2	615.3	Ft	
				50	M	11.7	11.0	SqFt	
				57	M	4,988.3		SqFt	
		31	40	41	H	4.8	5.0	SqFt	48.0
				48	L	103.9	69.7	Ft	
				48	M	692.2	603.8	Ft	
				50	H	10.7	11.0	SqFt	
				57	M	4,989.3		SqFt	
		34	42	48	L	140.9	78.1	Ft	54.0
				48	M	626.7	567.4	Ft	
				50	L	49.1	50.0	SqFt	
				50	H	8.6	10.0	SqFt	
				57	M	4,941.4		SqFt	
		37	40	45	M	1.0	1.0	SqFt	49.0
				48	L	164.8	59.6	Ft	
				48	M	640.1	567.3	Ft	
				50	H	12.5	11.0	SqFt	
				57	M	4,987.5		SqFt	

Section ID	Section PCI	Sample ID	Sample PCI	Distress	Severity	PAVER Quantity	sUAS FAA PAVEAIR Quantity	PAVER Units	sUAS PCI
10S	49	3	49	48	L	172.6	70.7	Ft	56.0
				48	M	455.7	499.5	Ft	
				48	H	31.3	37.7	Ft	
				56	L	5.1		SqFt	
				57	M	5,000.0		SqFt	
		9	50	48	L	171.8	97.1	Ft	57.0
				48	M	464.5	454.5	Ft	
				48	H	18.3	19.4	Ft	
				57	M	5,000.0		SqFt	
		12	48	48	L	266.6	263.9	Ft	56.0
				48	M	516.7	428.0	Ft	
				50	M		17.0	SqFt	
				52	H	2.6		SqFt	
				57	M	4,997.4		SqFt	
		15	52	48	L	216.6	219.7	Ft	61.0
				48	M	532.7	449.5	Ft	
				57	M	5,000.0		SqFt	
		21	46	45	H	22.5	20.0	SqFt	55.0
				48	L	186.0	214.1	Ft	
				48	M	590.1	468.0	Ft	
				57	M	5,000.0		SqFt	
		27	50	48	L	238.5	162.9	Ft	56.0
				48	M	606.9	580.6	Ft	
				57	M	5,000.0		SqFt	
		33	46	45	L	9.0		SqFt	57.0
				48	L	217.5	177.5	Ft	

Section ID	Section PCI	Sample ID	Sample PCI	Distress	Severity	PAVER Quantity	sUAS FAA PAVEAIR Quantity	PAVER Units	sUAS PCI
10S	49			48	M	584.2	531.2	Ft	57.0
				57	M	4,991.2		SqFt	
				57	H	8.8		SqFt	
		36	44	48	L	319.5	158.5	Ft	
				48	M	540.3	499.8	Ft	
				50	L	45.8	42.0	SqFt	
				50	H	6.4	5.0	SqFt	
				57	M	4,947.8		SqFt	53.0
		39	58	48	L	83.8	53.3	Ft	
				48	M	296.5	255.4	Ft	
				57	L	2,700.0		SqFt	
				57	M	2,300.0		SqFt	72.0